University of California
Santa Barbara

Aspects of Black Holes in Higher Dimensions

A dissertation submitted in partial satisfaction
of the requirements for the degree

Doctor of Philosophy
in
Physics

by

Gavin S. Hartnett

Committee in charge:

Professor Gary T. Horowitz, Chair
Professor Donald Marolf
Professor Harry Nelson

June 2015

The Dissertation of Gavin S. Hartnett is approved.

Professor Donald Marolf

Professor Harry Nelson

Professor Gary T. Horowitz, Committee Chair

May 2015

Aspects of Black Holes in Higher Dimensions

by

Gavin S. Hartnett

This thesis is dedicated to the memory of Matthew Anderson.

Acknowledgements

First and foremost, I owe a great deal of thanks to my excellent adviser, Gary Horowitz. My early trajectory in graduate school was atypical and far from geodesic, and I am very indebted to Gary for taking a chance with me. Throughout my time as Gary's student he has displayed what I have now come to realize are very characteristic qualities of patience, clarity of thinking, and kindness. I can only apsire to one day be as good of a teacher and adviser as he was to me. I am proud to call myself a Horographer! [1]

I would also like to thank Professors David Berenstein, Don Marolf and Joseph Polchinski for being excellent teachers and for always being happy to answer my many questions. Together with Gary, they managed to create a high energy/gravitation group with an atmosphere that was a wonderful combination of intellectually vibrant and extremely friendly. I would also like to thank Don Marolf and Harry Nelson for serving as my committee. Harry and Omer Blaes also derserve a separate thanks for being great Vice Chairs during my tenure as the head TA, and I am particularly grateful to them for always being on my side, even when I had stepped on some tenured toes.

Jorge Santos deserves a tremendous thank you for his immeasurable help throughout my Ph.D. Jorge taught me much about numerics, black hole perturbation theory, and Euclidean Quantum Gravity, and he suggested many fascinating projects to me. We also collaborated on many projects together, and Jorge would often joke that I was his first gradute student, a designation I am happy to accept. I also think of Jorge as a great friend, and I wish to thank him for his seemingly

[1] Also known as a Horowitz-Holographer.

unbounded curiosity and enthusiasm which permeated our discussions and collaborations and made Jorge great fun to be around. I don't think I've enjoyed discussing physics with anyone as much as I have with Jorge.

Oscar Dias is another great friend and mentor (*and future boss!*) who deserves thanks for the wonderful collaborations we have had. He also deserves thanks for the moniker "Gabirro" I adopted during the so-called Latin-Gang Collaboration [4]. Andrea Puhm deserves special thanks for her patience throughout many long discussions on the intricacies of brane polarization and the Klebanov-Strassler solution.

Next comes the many graduate students I am indebted to. I owe a tremendous deal to Benson Way for helping me understand numerics and holographic superconductors during the early period of my time as Gary's student. I also could not understate how helpful Sebastian Fischetti has been, being always happy to explain a wide host of concepts to me. He has also helped me sharpen and hone my ideas by patiently listening to them and being a critical skeptic to his core. Will Kelly also deserves special thanks for many wonderful conversations over the years.

I also wish to acknowledge the many helpful and stimulating conversations with my excellent colleagues Ahmed Almheiri, Curtis Asplund, Eric Dzienkowski, Netta Engelhardt, Ben Michel, Eric Mintun, and Teddy Parker. As a young and inexperienced graduate student, I beneffited from patient older students who explained and taught me many things. Yoni BenTov deserves thanks for his indispensable help as I learned QFT, and Idse Heemskerk, Jamie Sully, and Erik Perkins for their help as I learned string theory, and Ian Morrison for his help

explaining QFT in de Sitter space.

Lastly, I couldn't have done this without the support of my family and friends. Ted White deserves thanks as a poor experimentalist who has patiently sat through many aggregate hours of my attempts to explain string theory and quantum gravity to him, and I am grateful to have had Patrick Reilly as my friend on the Outside, who reminded me time and time again of the wider world beyond graduate school. And I am terribly grateful to my family, in particular my sister and mother, for their continuous love and support.

Permissions and Attributions

1. The content of chapter 2 is a result of a collaboration with Jorge Santos, and has previously appeared in the journal Physical Review D [5]. It is reproduced here with permission from the publisher, the American Physical Society: `http://journals.aps.org/copyrightFAQ.html#thesis`. See `http://publish.aps.org/info/terms.html` for the official copyright transfer agreement.

2. The content of chapter 3 is a result of a collaboration with Oscar Dias and Jorge Santos, and has previously appeared in the journal of Classical and Quantum Gravity [3]. It is reproduced here with the permission of the IOP Science `http://iopscience.iop.org/page/copyright`

3. The content of chapter 5 is a result of a collaboration with Gary Horowitz, and has previously appeared in the Journal of High Energy Physics [6]. It is reproduced here with the permission of the International School of Advanced Studies (SISSA), Trieste, Italy. `http://www.//jhep.sissa.it/jhep/help/JHEP/CR_OA.pdf`

4. The content of chapter 6 is a result of a collaboration with Vitor Cardoso, Oscar Dias, Luis Lehner, and Jorge Santos, and has previously appeared in the Journal of High Energy Physics [4]. It is reproduced here with the permission of the International School of Advanced Studies (SISSA), Trieste, Italy. `http://www.//jhep.sissa.it/jhep/help/JHEP/CR_OA.pdf`

5. The content of chapter 8 is a result of a collaboration with Gary Horowitz, and has previously appeared in the Journal of Classical and Quantum Gravity [2]. It is reproduced here with the permission of IOP Science `http://iopscience.iop.org/page/copyright`

6. The content of chapter 9 has previously appeared in the Journal of High Energy Physics [1]. It is reproduced here with the permission of the International School of Advanced Studies (SISSA), Trieste, Italy. `http://www.jhep.sissa.it/jhep/help/JHEP/CR_OA.pdf`

Curriculum Vitæ

Gavin S. Hartnett

Education

2015	Ph.D. in Physics (Expected), University of California, Santa Barbara.
2012	M.A. in Physics, University of California, Santa Barbara.
2009	B.Sc. (Summa cum Laude), Physics and Mathematics, Syracuse University

Publications

[1] **"Localised Anti-Branes in Flux Backgrounds"**
G. S. Hartnett.
JHEP **1506**, 007 (2015) [arXiv:1501.06568 [hep-th]]

[2] **"A No Black Hole Theorem"**
G. S. Hartnett, G. T. Horowitz and K. Maeda.
Class. Quant. Grav. **32**, no. 5, 055011 (2015) [arXiv:1410.1875 [hep-th]]

[3] **"Quasinormal modes of asymptotically flat rotating black holes"**
O. J. C. Dias, G. S. Hartnett and J. E. Santos.
Class. Quant. Grav. **31**, no. 24, 245011 (2014) [arXiv:1402.7047 [hep-th]]

[4] **"Holographic thermalization, quasinormal modes and superradiance in Kerr-AdS"**
V. Cardoso, O. J. C. Dias, G. S. Hartnett, L. Lehner and J. E. Santos.
JHEP **1404**, 183 (2014) [arXiv:1312.5323 [hep-th]]

[5] **"Non-Axisymmetric Instability of Rotating Black Holes in Higher Dimensions"**
G. S. Hartnett and J. E. Santos.
Phys. Rev. D **88**, 041505 (2013) [arXiv:1306.4318 [gr-qc]]

[6] **"Geons and Spin-2 Condensates in the AdS Soliton"**
G. S. Hartnett and G. T. Horowitz.
JHEP **1301**, 010 (2013) [arXiv:1210.1606 [hep-th]]

Abstract

Aspects of Black Holes in Higher Dimensions

by

Gavin S. Hartnett

This thesis is divided into three Parts. In Part I the general theory of black holes in higher dimensions is discussed. In addition to an introductory essay, two studies of linear perturbations of Myers-Perry black holes are presented. These black holes are the higher dimensional generalization of the Kerr black hole, and their analysis reveals numerous instabilities. Threshold unstable modes provide the connection between the Myers-Perry black holes and novel stationary black hole solutions such as black rings or black Saturns, as well as other non-stationary solutions known as single Killing vector field black holes.

In Part II gauge/gravity duality is briefly reviewed and two aspects are studied in detail. First, the problem of finding a holographic dual to a superconductor with d-wave order parameter is investigated, and second, we examine the problem of holographic thermalization in field theories dual to rotating black holes.

Lastly, in Part III the role of de Sitter solutions in string theory is discussed. A recent puzzle surrounding the fate of the de Sitter landscape is reviewed, and it is shown how the study of black holes in certain flux backgrounds can provide insight into this puzzle. We then present a theorem ruling out the addition of black holes to a certain class of flux backgrounds. Finally, a study is presented which shows that black holes can be added to the flux backgrounds relevant for

the de Sitter landscape in string theory, thereby providing strong evidence for the resolution of the puzzle.

Contents

Part I

Black Holes in Higher Dimensions

Chapter 1

Introduction

It has been my pleasure to work on a wide variety of problems throughout my graduate career, ranging from black hole instabilities, holographic models of superconductors, general relativity in the limit of large dimensions, and the de Sitter landscape in string theory. That such a diverse collection of topics belongs in a single thesis is a consequence of the remarkable directions the fields of high energy physics and gravitation have taken in recent years. As a result, this Thesis is naturally divided into 3 Parts. Part I concerns the study of black holes in higher dimensions, Part II the gauge/gravity duality, and Part III the de Sitter landscape in string theory. In this section a brief introduction to the study of black holes in higher dimensions will be presented. Given that there is ample evidence that the world around us is four dimensional (3 space + 1 time), it is eminently reasonable to ask "why study higher dimensions?" This introduction therefore begins by answering this question.

One of the most common answers is that higher dimensions (10, or 11, de-

pending on the solution) are predicted by string theory, the most successful and popular theory of quantum gravity. It could well be that our universe is truly 10- or 11-dimensional, with the extra dimensions curled up to be very small. Another popular way to account for the extra dimensions in string theory is to suppose that the Standard Model fields are constrained to lie on a lower dimensional brane. Regardless of the mechanism, the study of black holes in higher dimensions is partially motivated by string phenomenology, which is the study of how exactly string theory can explain and predict physics in the real world. Beyond this motivation, even if it turns out that our universe is not governed by string theory, string theory has already allowed significant advances in our understanding of quantum gravity and quantum field theory, and has also provided important insights into real world condensed matter systems. The most prominent example of such an advance is the AdS/CFT duality and its generalization, the gauge/gravity duality. The study of black holes is crucially important for understanding both string theory in general, as well as the gauge/gravity duality, and therefore even if a given higher dimensional black hole is almost certainly not realizable in nature, its study can lead to important insights into these other areas.

Another answer, independent of string theory, the gauge/gravity duality, or other putative models of quantum gravity, is that classical gravity has no "knobs" to turn. In order to gain a better understanding of a particular theory, it is useful for it to possess parameters that can be varied or used to construct controlled expansions. In this sense, the dimension D of a theory can be thought of as a parameter to be varied to gain insight into the nature of the theory, in much the same way that the rank of the gauge group of a Yang-Mills theory can be used.

This perspective is developed further below in Sec. 1.3. A related answer is that in attempting to gain an understanding of a particular theory, is often helpful to have the freedom to consider different but related theories as a way to separate salient from minor features in a given problem. As an example, in the canonical textbook on quantum field theory in curved space [7], Birrell and Davies find it convenient to introduce Hawking Radiation first in two dimensions, and a major advance in the study of black hole evaporation came from a 2D model which allowed many explicit calculations that would be much harder to do in four dimensions [8].

1.1 A Beastiary of Black Holes

Although there is a rich body of mathematical results concerning black holes in general relativity, and despite the fact that important advances in our understanding of black holes are being made even today, almost 50 years after the term black hole was first coined, there is a strong sense in which black holes have an appealing simplicity. Perhaps this is captured most eloquently by Chandrasekhar: "The black holes of nature are the most perfect macroscopic objects there are in the universe: the only elements in their construction are our concepts of space and time." An important property obeyed by black holes in this regard is that they "have no hair".[1] The unique stationary black hole solution to 4-dimensional Einstein gravity is the Kerr solution describing a charged and rotating black hole, and this solution is fully specified by three global charges–mass, angular momentum, and charge.

[1] Actually, black holes can have hair, but not in 4D Einstein-Maxwell theory, the usual subject of the no hair theorems.

Does this aspect of gravity remain true in higher dimensions? Restricting to the case of vacuum, source-less solutions, there is indeed a natural generalization of the Kerr solution to higher dimensions, found by Myers and Perry. This solution describes a stationary black hole with $\lfloor (D-1)/2 \rfloor$ angular momentum parameters (there are multiple angular momenta in $D > 4$ because as the dimension increases beyond 4 there are multiple orthogonal planes that the black hole can rotate in). Remarkably, there are other, completely novel solutions possible in $D > 4$! The first such solution to be discovered was the rotating black ring of Emparan and Reall in $D = 5$ [9]. A black hole horizon is a $(D-1)$-dimensional null hypersurface, with a $(D-2)$-dimensional spatial cross section. For $D = 4$ the Kerr solution has spatial horizon topology S^2, i.e. that of a sphere. In $D = 5$ the Myers-Perry solution is the natural generalization, having spatial horizon topology S^3. The black ring however, has topology $S^2 \times S^1$! In fact, there are even more exotic solutions beyond the black ring. There are black Saturns, bicycling rings and in fact a whole infinite family of such solutions with novel topologies! Gravity in higher dimensions therefore appears to allow for a much richer set of solutions. Moreover, these solutions are interconnected with one another in a way made clear through the study of linear perturbations.

1.2 Quasinormal Modes and Linear Mode Analysis

Much of this Thesis (in particular Chapters 2, 3, 6) concern the linear mode analysis of black holes in higher dimensions. It is therefore prudent to provide

a brief introduction to the subject of quasinormal modes before turning to the question of how linear instabilities provide the connections between various black hole solutions. Before progressing it is worth mentioning the excellent review article [10] which does great justice to the subject of black hole quasinormal modes.

The concept of a normal mode is very common in physics. The normal mode characterizes how an object "rings". Normal modes represent an idealization as they do not incorporate dissipation; in the real world however, bells ring only for a finite time. Quasinormal modes are then the generalization of normal modes to include modes with complex frequencies, with the imaginary part determining the exponential decay (or growth, in the event of an instability) of the mode.

Quasinormal modes of black holes are the modes of linear perturbations of the black hole spacetime. As a concrete example, consider the case of a free Klein-Gordon scalar field on the Schwarzschild background. Often we are most interested in linear metric perturbations, but a free scalar field is simpler to consider and retains the essential features of the problem. The equation of motion is $\Box\phi = 0$, which for a generic perturbation is a complicated PDE in 4 dimensions, even for this very simple example. There are many ways to study this equation. One such way is to view it as an initial value problem, with initial data given on some initial time surface and then evolved forward in time using the equation of motion. The problem is also amenable to a spectral analysis, wherein the function ϕ is decomposed into a set of mode functions. The PDE may be separated using spherical harmonics and complex exponentials, as in $\phi(t, r, \Omega) = \psi(r)e^{-i\omega t}Y(\Omega)$, resulting in a single ODE for the radial profile function $\psi(r)$. This equation is then a boundary value problem, with the boundaries being the horizon and asymptotic

infinity. The boundary conditions are determined by demanding that the field be purely outgoing at infinity (i.e. there is no energy travelling into the spacetime), and that it be purely ingoing at the horizon (i.e. there is no energy exiting the horizon). A solution to the equation satisfying these boundary conditions only exists for a countably infinite set of complex frequencies ω, known as the quasinormal mode frequencies. Quasinormal modes are naturally interpreted as the "sound" of a black hole. These modes govern the decay of a perturbation, and after a short time the perturbation will be dominated by the mode with least negative imaginary part, (i.e. the lowest lying one).

For bona fide quasinormal modes, $\mathrm{Im}(\omega) < 0$, so that the perturbation will decay. For the case of Kerr in $D = 4$, all quasinormal frequencies lie in the lower half complex plane, and therefore the Kerr black hole is linearly mode stable. In higher dimensions, it so happens that many, if not all, of the exotic solutions are believed to be unstable, that is, they possess frequencies for which $\mathrm{Im}(\omega) > 0$.

The existence of an unstable mode implies that small perturbations will not remain small, and will in fact grow exponentially. The implication of this growth depends on the problem at hand. As a mode changes from being stable to unstable, it crosses a threshold point where $\mathrm{Im}(\omega) = 0$. If the real part also vanishes, that is, $\omega = 0$, then this mode is correctly interpreted as the linearization of a new branch of stationary solutions splitting off of the background branch of solutions. The new branch will correspond to a black hole with a deformed horizon. As an example, for sufficiently rapid rotation Myers-Perry black holes possess instabilities which pinch the horizon in various locations depending on the instability. The first mode to go unstable as the rotation increases from zero pinches the black hole at the

north and south poles. At the threshold points, these modes correspond to the joining of the Myers-Perry branch with branches in which the horizon is non-uniform, or "lumpy". As one moves further down these so-called lumpy branches of solutions, the lumps on the black hole grow pronounced, and the pinching more severe, and there is a topology changing transition leading to the novel solutions discussed above. For the case of the pinching occurring at the poles, the lumpiness will eventually become so pronounced that the solution will join the black ring branch of solutions through a topology-changing transition. It is believed that other instabilities will connect the other novel solutions, for example black Saturns, etc, in exactly the same manner. In some cases these connections between different branches of solutions is somewhat speculative, and in others, most notably the case of Kaluza-Klein gravity in $D = 5$, the connections have been studied extensively with combined analytic and numerical analyses.

If $\mathrm{Re}(\omega) \neq 0$ at the threshold, as happens for superradiant instabilities which carry momentum around a circular direction, then the interpretation of the unstable mode becomes more complicated. In general, there is no new branch of solutions as the backreaction of the perturbation will be necessarily time dependent. However, if $\mathrm{Re}(\omega) = m\Omega_H$, with Ω_H the angular velocity of the horizon, and m the angular quantum number, then although the perturbation breaks both time translation invariance and axisymmetry, the mode preserves a very special linear combination of the two symmetries, the generator of the Killing horizon. In particular, $K = \partial_t + \Omega_H \partial_\phi$ will remain an unbroken symmetry of the perturbation, where t, ϕ are the time and azimuthal coordinates. In this special case, the threshold perturbation corresponds to the linearization of a new solution which preserves

this symmetry. These solutions are known as single Killing field black holes, and have been much less studied than stationary black hole solutions. They are somewhat exotic, as rotating non-axisymmetric solutions must radiate, and only with a kind of reflecting boundary condition is the outgoing radiation able to be balanced with the reflected radiation. Miraculously, these boundary conditions are naturally enforced by requiring that the spacetime be asymptotically AdS. Therefore, these superradiant instabilities and their associated novel 1 Killing Field Theory black hole solutions should have an interesting interpretation in terms of the dual field theory.

Before moving on to another interesting aspect of the study of black holes in higher dimensions, a few comments are in order regarding the limitations of quasinormal modes. Typically when a linear mode analysis is preformed, as is done in the case of quasinormal modes, the idea is that a generic perturbation can be decomposed as an infinite superposition of modes which can be be individually solved for. This is not the case for black hole quasinormal modes, however. They are known to be incomplete, that is they do not form a complete basis of functions for generic perturbations. In fact, for asymptotically flat black holes stable quasinormal modes exhibit divergent behaviour at asymptotic infinity. As a result of these limitations, the response of a black hole to generic perturbations is unable to be expressed entirely using quasinormal modes, although for certain timescales the response is dominated by quasinormal mode ringing. A second, somewhat related issue is that quasinormal modes do not provide a comprehensive delineation between stable and unstable solutions. Certainly a solution with an exponentially growing mode should be regarded as unstable, but the converse is not necessarily

true. If there are no exponentially growing modes, the system could still be unstable because not all instabilities are mode instabilities, and also because generic perturbations cannot be expressed entirely of quasinormal modes. It may become clear to the reader at this point that a precise definition of instability has not been given, and this has been by design. Exponentially growing modes are in many ways to most violent form of instability, but there are other more benign instabilities. An interesting recent example concerns the Aretakis instability of extremal black hole horizons [11], wherein the unstable behaviour is polynomial growth in time, and moreover this growth is restricted to the horizon. Instances such as these are a refinement beyond the linear quasinormal mode stability discussed in this thesis, and shall not be considered here further.

1.3 The Large D-Limit

Now that we have unburdened ourselves from thinking about only four-dimensions, what dimension should we focus on? 5? 6? 7? It is rare to see analysis beyond $D = 11$, as this is the largest dimension in which a supersymmetric theory of gravity can be constructed. In this section we will be interested in the case $D = \infty$! More precisely, the large-D limit of general relativity will be introduced wherein the number of dimensions is taken large and used as an expansion parameter, much akin to the more familiar large-N expansion of $SU(N)$ gauge theories. Although it may seem preposterous to study a theory in the limit of large dimensions, there are good reasons for doing so. The Einstein equations are notoriously complicated, and precious few exact, analytical results exist. If the equations admit a sensible

expansion in $1/D$, then perhaps the large-D limit can provide a calculational tool to learn about physics in more modest numbers of dimensions, such as $D = 10$.

A program to develop the Large-D limit was recently initiated by Emparan and collaborates. There are a number of interesting features of this limit. The exponential in D fall off of black hole warp functions (for example $f = 1 - \frac{r_0^{D-3}}{r^{D-3}}$ is the warp factor for Schwarzschild-Tangherlini) means that in the limit of large-D, the spacetime outside a black hole is negligibly curved, and the black hole can be replaced by a hole cut out of the spacetime with particular boundary conditions if the horizon radius is held constant as the limit of large D is taken. Furthermore, the ratio of volume of a unit cube and sphere in D dimensions vanishes exponentially fast in the limit $D \to \infty$, and therefore black holes have finite radius but zero area.

The large-D expansion has been successfully used to analytically approximate solutions to a wide range of problems. In this brief review attention will be restricted to the calculation of quasinormal modes. Preliminary investigations into the quasinormal modes of black holes in the large-D limit revealed a fascinating universality. For a wide range of black holes, the quasinormal mode spectrum was found to be universal to leading order in $1/D$ [12]. Moreover, as $D \to \infty$, $|\omega| \to \infty$ also, with the frequencies moving downward in the lower half complex plane. In Sec. 3, we present work in which a second class of quasinormal modes were discovered in the large-D limit for the case of D-dimensional Schwarzschild, i.e. zero rotation. These frequencies do not scale with D, i.e. $\omega \sim D^0$, and moreover these modes are *not* universal; they encode the details of the horizon geometry. These are in some sense the most important quasinormal frequencies

because they have finite lifetime, $\mathrm{Im}(\omega^{-1}) \sim D^0$ as opposed to the vanishing lifetime of the scaling modes in the large D limit.

The existence of these modes has important implications for the solution space of black holes in large-D. Investigations of $D = 5$ revealed an interesting zoology of novel black hole solutions which are related via linear instabilities. These novel solutions are believed to exist in all $D > 5$, and therefore the instabilities which interconnect them should as well. Evidence in support of this is presented in Sec.'s 2, 3, where it is shown that the instabilities persist in each dimension studied (as high as $D = 15$), and moreover, important features such as the critical rotation speed seem to converge to a fixed, finite value in the limit of large D. This informs us that the instabilities are connected to the non-scaling modes found for zero rotation. Thus we see that the non-scaling modes are intimately related to the continued existence of the novel black hole solutions in higher D; if there were no scaling modes and all the quasinormal frequencies of D-dimensional Schwarzschild obeyed $|\omega| \sim D^{-\alpha}$, for some $\alpha > 0$, then as the rotation increased the frequencies would have to travel infinitely far in the complex plane in order to become the threshold unstable modes which connect, for example, the Myers-Perry and black ring solutions. [2]

The remainder of this Part is organized as follows. In 2 a study is presented in

[2]The existence of the non-scaling modes is important for instabilities which occur at finite rotation in the large D limit. It is worth pointing out that for certain configurations of the angular momenta parameters, there is no extremal bound and the black holes can rotate arbitrarily fast, which may lead one to wonder if the instabilities occur at faster and faster speeds as D increases. There well may instabilities of this sort, however, for generic configurations in which all the angular momenta are turned on, there is an extremal bound, and moreover this bound asymptotes to a constant as $D \to \infty$. Therefore, we can conclude that there exist instabilities which must occur at finite rotation, and hence the necessity of the non-scaling quasinormal modes at zero rotation.

which a non-axisymmetric instability of a rotating black hole in higher dimensions is discovered and analyzed. In 3 an comprehensive study of quasinormal modes of black holes in higher dimensions is presented, and the non-scaling quasinormal modes are presented for the first time.

Chapter 2

Non-Axisymmetric Instability of Rotating Black Holes in Higher Dimensions

Introduction: Black holes in four spacetime dimensions are remarkably featureless. The Kerr metric is the unique stationary and axisymmetric solution to the vacuum Einstein equations, and is completely characterized by just two parameters, its mass and angular momentum [13]. In contrast, General Relativity in higher dimensions allows for a fantastic diversity of different asymptotically flat black objects. In addition to black holes of spherical topology, there are also black rings [9], black Saturns [14], systems of bicycling black rings [15], and so on [1]. In fact, it has been shown [17] that in marked contrast to the uniqueness of the Kerr metric in four dimensions, in higher dimensions there are many black holes of a

[1] For a recent and comprehensive review, see [16].

given mass and set of angular momenta. Perhaps more exotically, in [18], it has been argued that an *infinite* number of black holes can exist with the same set of conserved asymptotic charges! Understanding the phase space of black hole solutions, as well as their stability, is currently a very active program of research.

In this Letter we report progress in this direction by studying the classical stability of Myers-Perry (MP) black holes, which are the generalization of the Kerr solution to higher dimensions [19]. In D spacetime dimensions these solutions are characterized by their mass and $\lfloor (D-1)/2 \rfloor$ angular momenta parameters. The properties of these solutions strongly depends on both the dimension of spacetime as well as the angular momenta. For example, for $D \geq 6$, when none of the angular momenta vanish there is an extremal limit and the black hole cannot be made to rotate arbitrarily fast, just as in four dimensions. However, when at least one of the angular momenta vanishes, there is no extremal limit and the remaining angular momenta can be taken to be arbitrarily large.

The lack of an extremal limit suggests that these black holes might be unstable. Emparan and Myers [20] showed that in the limit where n angular momenta are taken to be arbitrarily large, the horizon 'pancakes' out to have topology $\mathbb{R}^{2n} \times S^{D-2n-2}$. Black holes with this horizon shape are known as black branes, and were famously shown to be unstable by Gregory and Laflamme [21]. Therefore, Emparan and Myers conjectured that MP black holes should also be unstable, at least in certain fast-spinning regions of the parameter space. Although the comparison to the Gregory-Laflamme instability was made in the limit of infinite rotation, it was expected that the instability would set for finite, sufficiently rapid rotation.

Since this conjecture, there has been much work on investigating the stability of MP black holes in various dimensions and for various configurations of the angular momenta parameters. One of the most studied cases has been in odd dimensions with all the angular momenta equal. This is because in this limit the metric becomes cohomogeneity-1, which is to say that it depends non-trivially only on the radial coordinate, and therefore the linearized Einstein equations form a coupled system of ODE's. For generic rotations, the perturbation equations necessarily involve PDE's, greatly complicating the stability analysis. The fact that there exists a cohomogeneity-1 MP metric is rather remarkable, as the only other case in which the linearized Einstein equations are known to separate on a rotating black hole background is Kerr, as shown by Teukolsky [22].

Although the perturbation equations become more tractable for equal angular momenta, in this case the spins cannot be made arbitrarily large, and a priori it is not clear whether the black hole would be able to rotate at a sufficiently rapid speed to become unstable. A precise definition of sufficiently rapid was given in [23], who formulated an ultraspinning condition based upon black hole thermodynamics. In odd $D \geq 7$ this ultraspinning condition can be satisfied for the equal angular momenta case, and therefore these black holes might be unstable. Indeed, it was found that very near extremality these black holes were unstable to perturbations that do not break rotational symmetries.[2] It is expected that this instability persists for all odd $D \geq 7$.

No instability was found in $D = 5$, and in fact this was not unexpected since

[2]This instability was first found in $D = 9$ [23], but upon further investigation (motivated by the study of the relationship of near-horizon instabilities to instabilities of the full geometry in Ref. [24]) the instability was found to also exist in $D = 7$.

the ultraspinning condition is only possible in $D \geq 7$. Further evidence for stability in $D = 5$ for the case of equal angular momenta came from the linear perturbative analysis of Ref. [25]. The study of axisymmetric perturbations has been extended to configurations with a single non-vanishing spin [26], and more general configurations [27]. Instabilities have been found in all $D \geq 6$. These instabilities are very important for the phase diagram of black holes in higher dimensions, because at the threshold of instability, the perturbations are time-independent and therefore correspond to a new family of stationary, axisymmetric black holes branching off of the MP family.

Thus far the discussion has been restricted to axisymmetric perturbations. Of course a full analysis of the stability of any physical system should include all possible perturbations; therefore we now turn to discuss non-axisymmetric perturbations. In an impressive series of numerical simulations, it was found that singly-spinning MP black holes were unstable to non-axisymmetric instabilities, first in $D = 5$ [28], and then in $D = 6, 7, 8$ [29]. These results strongly suggest that black holes might be much more sensitive to non-axisymmetric perturbations than to axisymmetric perturbations, since $D = 5$ black holes are stable to axisymmetric perturbations, but unstable to non-axisymmetric ones. It might therefore be expected that in higher D non-axisymmetric instabilities set in for smaller spins than the axisymmetric ones.

The above results motivated the work presented here. We study non-axisymmetric perturbations of higher dimensional black holes. We restrict our attention to the equal angular momenta case (and therefore odd D), due to the simplification that occurs when the metric is cohomogeneity-1. We find that in odd $D \geq 7$,

equal angular momenta MP black holes are unstable to non-axisymmetric perturbations, and that these instabilities set in for much smaller rotations than the previously discovered axisymmetric ultraspinning instabilities [23]. Our analysis explores the full spectra of scalar-gravitational perturbations, in particular its quasi-normal mode frequencies. We studied the cases of $D = 5, 7, 9, 11, 13, 15$, and found instabilities for $D \geq 7$. We expect these instabilities to persist for all higher odd D.

Methodology and Results: The equal angular momenta Myers-Perry black hole line element is

$$\begin{aligned} \bar{ds}^2 &= -f(r)^2 dt^2 + g(r)^2 dr^2 \\ &+ h(r)^2 [d\psi + A_a dx^a - \Omega(r) dt]^2 + r^2 \hat{g}_{ab} dx^a dx^b. \end{aligned} \tag{2.1}$$

Here f, g, h, Ω are functions of r which can be found in Ref. [23], and $x^a, \hat{g}_{ab}$ are the coordinates and Fubini-Study metric on $\mathbb{CP}^N$, respectively. N is related to the spacetime dimension D by $D = 2N+3$, while A_a is related to the Kähler form J by $dA = 2J$. In this equal angular momenta case the above metric functions depend on two dimensionful parameters, which we take to be the horizon radius r_+, and the spin parameter a. When $a \to 0$, this reduces to the higher-dimensional Schwarzschild metric, with the S^{2N+1} metric expressed as the Hopf fibration. The presence of the $\mathbb{CP}^N$ factor is what facilitates the separability of the equations into ODE's, rather than PDE's. That this manifold only exists for integer N explains why the separability only happens in odd spacetime dimension. Extremality is

reached at $a = a_{\rm ext}$, the value of which can also be found in Ref. [23].

We studied linear perturbations of this background:

$$g_{\mu\nu} = \bar{g}_{\mu\nu} + h_{\mu\nu}, \tag{2.2}$$

where barred quantities refer to the MP background. We then solved the linearized vacuum Einstein equations, which after imposing the traceless and transverse gauge conditions become

$$(\Delta_L h)_{\mu\nu} \equiv -\bar{\nabla}^\rho \bar{\nabla}_\rho h_{\mu\nu} - 2\bar{R}_{\mu\rho\nu\sigma} h^{\rho\sigma} = 0. \tag{2.3}$$

We further used the stationarity and axisymmetry of the background metric to decompose the time and azimuthal dependence as $h_{\mu\nu} \propto e^{-i(\omega t - m\psi)}$. Here ω is a complex number which will be determined numerically, and m is restricted to be an integer. The azimuthal coordinate is ψ, and therefore perturbations with $m = 0$ are axisymmetric, whilst those with $m \neq 0$ are non-axisymmetric. Lastly, following [23], we separated the angular dependence of the perturbation $h_{\mu\nu}$ through the use of charged scalar harmonics on $\mathbb{CP}^N$. As this decomposition is beyond the scope of this article, and results in numerous lengthy equations, we refer the reader to the original article for details [23]. Each such charged scalar harmonic can be classified by two integers (κ, m), with $\kappa \geq 0$. We also mention that mode stability for tensor perturbations was shown in [30], for both axisymmetric and non-axisymmetric modes. The vector case remains to be investigated.

Our strategy was to look for exponentially growing solutions to the above equations. These are modes with $\mathrm{Im}(\omega) > 0$. Threshold unstable modes have

$\mathrm{Im}(\omega) = 0$, and the spin at which this happens is labelled a_{crit}. The absence of exponentially growing modes does not establish stability, but the existence of one clearly does imply an instability. We used the physically relevant boundary conditions of ingoing waves at the horizon, and outgoing near infinity. This choice corresponds to studying the quasi-normal mode spectrum of these black holes [3]. With the decomposition of perturbations described above, the problem has now been reduced to a quadratic Sturm-Liouville eigenvalue problem for ω in a coupled system of ODE's. We used a numerical scheme based on spectral methods to solve these equations, see Ref. [23] for more details [4].

Our results are as follows. In $D = 5$, we find no instability, which is consistent with Ref. [25], who also studied the equal angular momenta case. It is also consistent with Ref. [28], who found an instability, but only for singly-spinning black holes. For $D = 7, 9, 11, 13, 15$, we find numerous bar-mode instabilities. In Fig. 2.1 we plot $\mathrm{Im}(\omega)$ for the $(\kappa, m) = (0, 2)$ mode, which is the first mode to go unstable as the spin in increased. We refer to this mode as the dominantly unstable mode, as it sets in before any others, and is the mode with the largest growth rate. For completeness we also show in Fig. 2.2 the real part of the dominant mode, as a function of a/r_+. Our results indicate that a_{crit}/r_+ saturates as a function of D, which suggests a possibly analytic understanding in a $1/D$ expansion as in [32].

We expect that the unstable modes we find will persist for all odd $D \geq 7$. In all dimensions studied, the dominant instability was due to the $(\kappa, m) = (0, 2)$

[3] For a review of quasi-normal modes, see Ref. [10].

[4] Actually, Ref. [23] used an identical numerical scheme, but applied it to a slightly different problem, the study of the Gregory-Laflamme instability for the black string constructed out of these MP black holes.

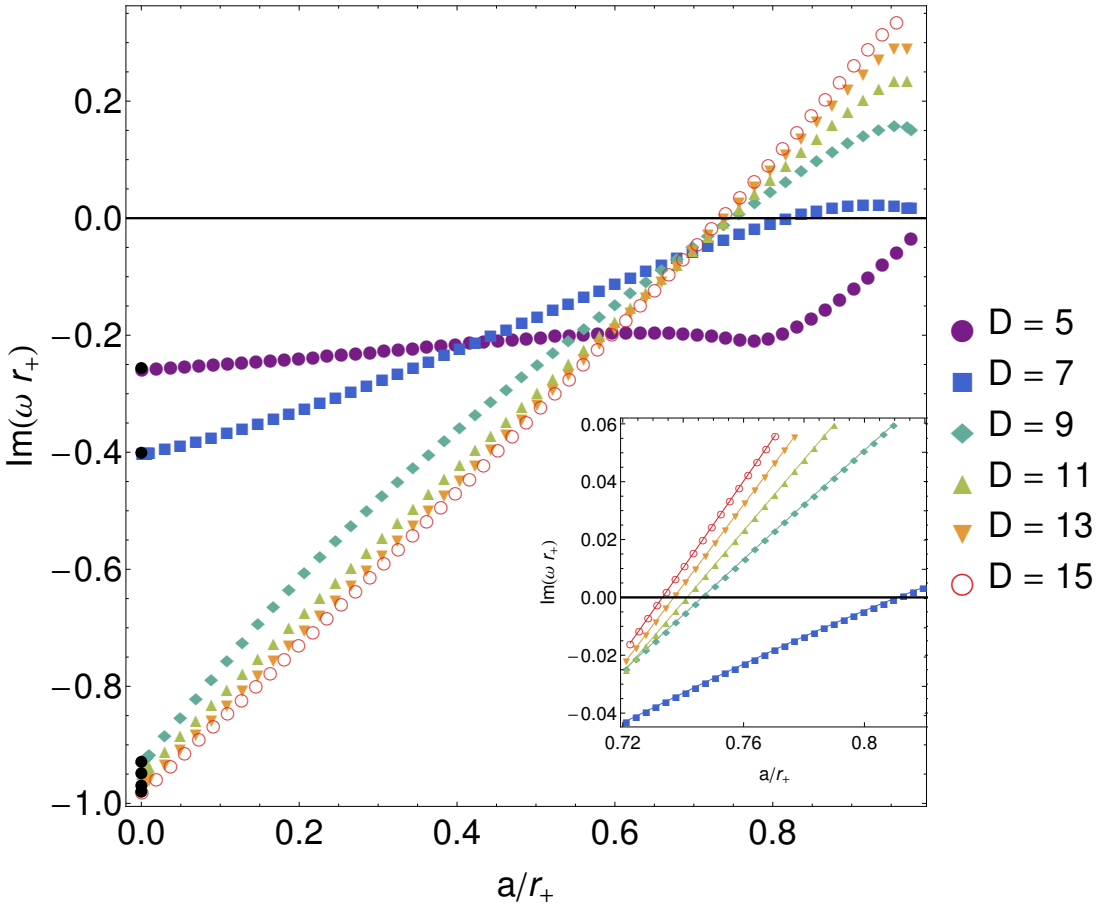

Figure 2.1: Plot of $\mathrm{Im}(\omega)$ for for the dominantly unstable mode, $(\kappa, m) = (0, 2)$. The black points at $a = 0$ were computed using a different code based upon the gauge invariant formalism of Ref [31]. Note that as D increases the critical spin for which $\mathrm{Im}(\omega) = 0$ decreases. For $D = 5$, $\mathrm{Im}(\omega) \to 0^-$ as $a/a_{\mathrm{ext}} \to 1$, and we find no instability. The inset plot zooms the region where $\mathrm{Im}(\omega)$ becomes positive.

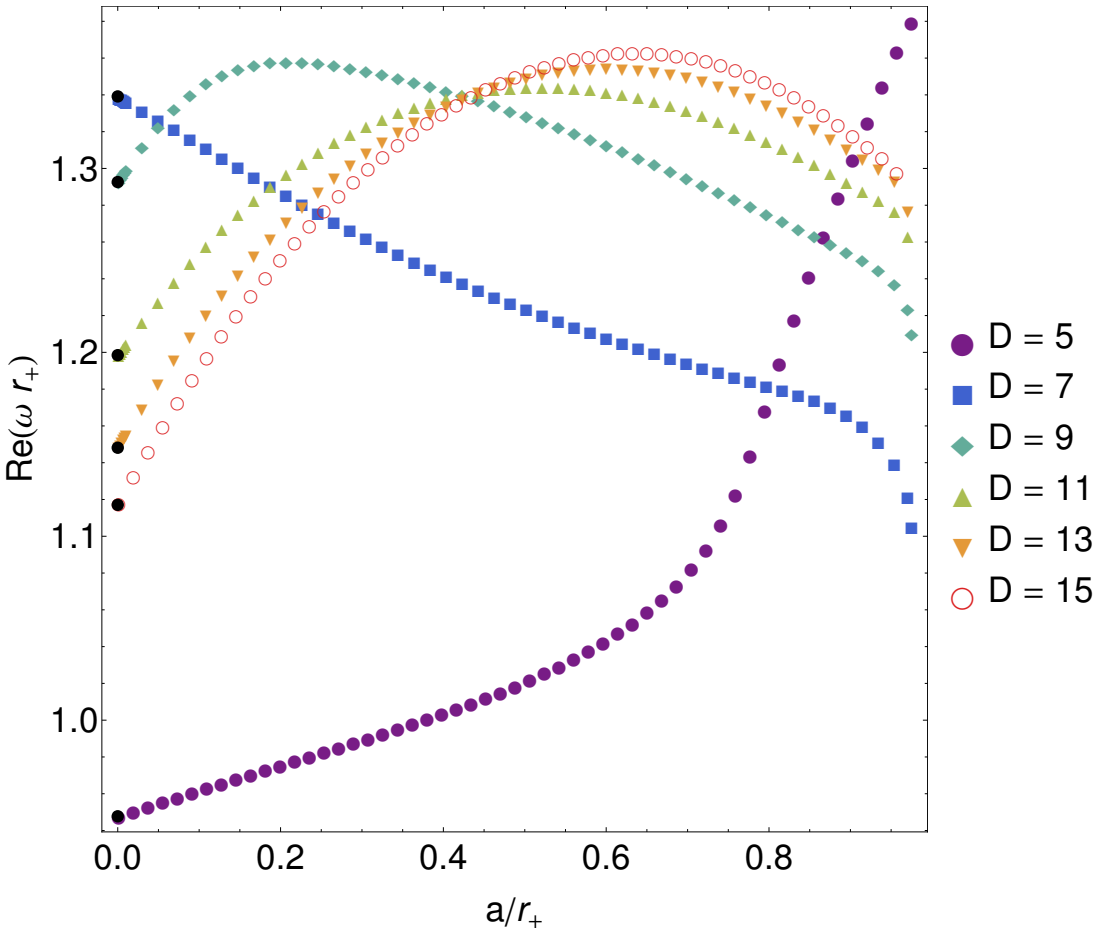

Figure 2.2: Plot of $\mathrm{Re}(\omega)$ for for the dominantly unstable mode, $(\kappa, m) = (0, 2)$. The black points at $a = 0$ were computed using a different code based upon the gauge invariant formalism of Ref [31].

mode. We also found instabilities for $(0, m)$ modes with $m > 2$ as well as for $(1, m)$ modes with $m \geq 1$, but these have a larger value of $a_{\rm crit}$ [5] In Table 2.1 we tabulate the critical spin at which the bar mode and axisymmetric instabilities first set in. The bar mode instabilities set in for much smaller rotation speeds, and are therefore the dominant instabilities of these black holes.

We computed several checks on our results. First, we computed the Schwarzschild quasi-normal modes using the gauge-invariant formalism of Ref. [31] and found that our results reproduced this spectrum as $a \to 0$. We also computed the axisymmetric $(2, 0)$ mode that was first found to be unstable, and compared our result with Ref. [23], who only calculated this mode for $\mathrm{Im}(\omega) > 0$. It was expected that as a was increased from zero, ω would in general be complex, reach $\omega = 0$ at $a_{\rm crit}$, and then become purely imaginary. However, we find that this mode is always purely imaginary, taking the form $\mathrm{Im}(\omega) = i\, K(a)$ where $K(a)$ is a real function that is negative for $a < a_{\rm crit}$, zero at $a_{\rm crit}$, and positive for $a > a_{\rm crit}$. For $a > a_{\rm crit}$, our results agreed with Ref. [23].

Discussion: While a thorough investigation of the linear mode stability is still far from complete for the full MP family, it is nearly finished in the equal angular momenta sector. Scalar perturbations have been examined here in the non-axisymmetric case, and in Ref. [23] for the axisymmetric one. Tensor perturbations of both types were studied in [30]. Only vector perturbations remain to be analyzed, although it is expected that the dominantly unstable modes will be

[5] This is in contrast to the phenomenon of superradiance in AdS space, where larger m modes become unstable before smaller m modes, first conjectured in [33], and later explicitly checked in [34] using the Teukoslky formalism.

D	$1 - a_{\rm crit}/a_{\rm ext}$ (NA)	$1 - a_{\rm crit}/a_{\rm ext}$ (A)
7	0.1891	2.339×10^{-5}
9	0.2537	2.116×10^{-3}
11	0.2587	7.854×10^{-3}
13	0.2631	1.504×10^{-2}
15	0.2669	2.232×10^{-2}

Table 2.1: Critical rotations for non-axisymmetric (NA) and axisymmetric (A) ultraspinning instabilities. The critical rotation is defined to be the largest rotation such that there are no instabilties for the sector of perturbations in question (axisymmetric or non-axisymmetric). The values for the (A) sector were first presented in [23] and [24]. Note that the bar mode instability sets in for *much* smaller spins.

scalars. Thus it is likely that we have found the dominant instabilities for these black holes, and it is then natural to inquire about the endpoint of this instability.

Of course, this question deserves a full non-linear numerical treatment, but our results provide some insights. Due to the fact that these perturbations break axisymmetry, the black hole will radiate angular momentum and energy, and in doing so spin down until it reaches a stable spin. In order for the black hole to be able to radiate, the loss of angular momentum and energy must be consistent with Hawking's Area Law, $\delta A \geq 0$. This condition was shown to be equivalent to the superradiant bound $\mathrm{Re}(\omega) - m\Omega_H < 0$ [29], and indeed, we find that only after this condition is satisfied are there modes with $\mathrm{Im}(\omega) > 0$. Therefore, for initial spins slightly larger than the critical values, it is expected that the black holes will simply radiate until they reach a stable configuration.

However, for initial spins much larger than the critical value it will take the black holes some finite amount of time to radiate away their excess angular momentum, and during this time the horizon will be rapidly deformed by the growing perturbation. An exciting possible outcome of this scenario would be that

the time scale for the growth of the perturbation might exceed the time scale for radiation, and that the black hole might actually fragment into a multiple black hole configuration. If the fragmentation is sufficiently violent, these black holes could fly apart and escape to infinity. Otherwise, they would continue to radiate away energy and angular momentum and would eventually inspiral and merge into a single, non-axisymmetric black hole. This black hole would itself continue to radiate until it settled down to axisymmetric and stationary state. This is a fascinating, but speculative possibility for the endpoint of the instability that would necessarily violate the cosmic censorship.

This bar mode instability has implications for the stability of some of the more novel black hole solutions that branch off from the MP family. The points in the black hole phase diagram where these solutions join with the MP black holes correspond to the existence of axisymmetric perturbations with $\omega = 0$. As the spins for which these modes exist are all much greater than the smallest non-axisymmetric $a_{\rm crit}$ we find, our results suggest that these new solutions will be unstable at least near the branching point, and perhaps more generally.

A curious feature of our solutions concerned the existence of purely imaginary frequencies ω. As noted earlier, the $(2, 0)$ unstable mode was found to be purely imaginary for any a. We also found that the $a \to 0$ limit of the $(1, m)$ unstable modes were purely imaginary. In $D = 4$, purely imaginary frequencies have special status, and some of them are associated with changes in the algebraic classification of the spacetime. The important role that these purely imaginary modes had in determining the stability of the black hole, and in connecting the MP family to new stationary axisymmetric families suggested that there might be a connection

with changes in algebraic classifications. However, it has recently been shown that there are no algebraically special modes of Schwarzschild in $D \geq 5$ [35], and therefore it appears unlikely that any special geometrical significance can be assigned to these modes.

In summary, we have found a new, non-axisymmetric instability of a certain class of higher dimensional rotating black holes. These black holes were previously found to be unstable to axisymmetric perturbations, and the instabilities we find occur for much slower rotation speeds. We expect that the instability we find with the smallest $a_{\rm crit}$ corresponds to the dominant instability of equal angular momenta Myers-Perry black holes. We discussed two possible endpoints of this instability, either spinning down through gravitational radiation, or through a more complicated process involving black hole fragmentation as an intermediate step.

Acknowledgements

It is a pleasure to thank Gary Horowitz, Óscar Dias, and Harvey Reall for helpful discussions throughout this project. This work was supported in part by the National Science Foundation under Grant No. PHY12-05500.

Chapter 3

Quasinormal modes of asymptotically flat rotating black holes

3.1 Introduction

The understanding of asymptotically flat higher-dimensional black holes (BHs) in classical general relativity has seen remarkable progress in recent years (see [36] for an excellent review on the subject). We have learned that BHs in $d \geq 5$ space-time dimensions have markedly different properties from their four-dimensional counterparts: several asymptotically flat higher-dimensional BHs exist for the same set of asymptotic charges [37], horizons can have distinct topologies [37, 38], solutions with disconnected horizons exist [14], and cosmic censorship does not

hold in $d \geq 5$[1] [39], to name but a few. Given the plethora of higher-dimensional BHs and the intricate nature of the phase space of BH solutions, it is interesting to study their stability. This paper addresses this question for a specific class of higher-dimensional BHs.

The most general exact solution known in closed form for an arbitrary number of dimensions is the Myers-Perry BH (MP BH) [19]. In many ways, this is the natural generalization of the Kerr solution to higher dimensions. The spatial cross section of the horizon has topology S^{d-2}, and it is uniquely characterized by its mass and $\lfloor (d-1)/2 \rfloor$ angular momenta. The properties of these solutions strongly depend on the spacetime dimension, as well as the angular momenta. In $d \geq 6$, if all angular momenta are non-vanishing, there is an extremal limit, meaning that all angular momenta are bounded above. If, on the other hand, at least one of the angular momenta vanishes, there is no upper bound on any of the remaining angular momenta and MP BHs are allowed to rotate arbitrarily fast. This fact was picked out by Emparan and Myers in [20], who conjectured rapidly spinning MP BHs to be unstable. When $\tilde{n}$ of the angular momenta are taken to be arbitrarily large, the horizon "pancakes" out near the poles, and acquires an almost exact $\mathbb{R}^{2\tilde{n}} \times S^{d-2\tilde{n}-2}$ topology, i.e. they look like black branes. Since black branes are known to be unstable [21, 39], they conjectured these highly deformed BHs to be unstable as well. The argument given above, strictly speaking, only works if the rotation parameters are taken to be infinitely large. However, Emparan and Myers went beyond this and estimated the rotation for which the instability

[1] Strictly speaking, a black string is not asymptotically flat. To date, there is no proof that a violation of cosmic censorship occurs for asymptotically flat BHs in $d \geq 5$, even though very thin black rings provide an excellent candidate for such a phenomenon.

should appear for singly spinning BHs. In order to do this, they used two distinct arguments that each give different estimates. In the first argument, the critical rotation was estimated by the condition that thermodynamic quantities, such as the temperature, behave similarly to those of a black brane. The other argument directly compares the entropy of a singly spinning BH to that of two disjoint BHs with the same total energy and angular momentum. The latter process necessarily breaks the rotation symmetry of the original BH. The critical rotation extracted from the former argument is systematically larger than that of the latter. Moreover, the first argument only applies to $d \geq 6$, whereas the second gives a positive result for $d \geq 5$. The first type of instability was coined the ultraspinning instability, and the second, rotational symmetry-breaking instability was dubbed the $m-$bar or bar-mode instability.

It took six years to know whether this conjecture was correct, and to detail its properties. In [26, 40] it was shown that singly spinning MP BHs in $d \geq 6$ are unstable to perturbations that do not break rotational symmetry, and in [28, 29] it was found that, at the full non-linear level, MP BHs are also unstable to perturbations that do break rotational symmetry, but this time for $d \geq 5$. The rotation required to herald the second type of instability was found to be much smaller than the first, in agreement with the conjecture of [20]. None of these results shed any light on what happens in the general case, where all angular momenta are non-vanishing. The arguments given by Emparan and Myers are also much weaker in this case, because there is an upper bound on the angular momenta and the horizons cannot get very distorted. The reason why singly spinning BHs were easier to study is related to the fact that they preserve a

much larger symmetry group than the general case. There is however, one case that is amenable to a more systematic study, and that has an upper bound on the rotation. In odd spacetime dimensions, the equal angular momenta (EAM) MP solution exhibits a large symmetry group that can be employed to reduce the study of general linearized perturbations to a system of coupled ordinary differential equations. This was used in [23] to show that equal angular momenta MP solutions in odd $d \geq 7$ have ultraspinning instabilities [2], very much like the singly spinning case. It was further shown in [27], that the ultraspinning instability found in the equal angular momenta MP is connected to the one found in the singly spinning MP. More recently, in [5], the $m-$bar instability was also shown to exist in equal angular momenta MP BHs.

However, to date, the study of quasinormal modes (QNMs) of higher-dimensional rotating BHs in asymptotically flat space is very meager. The main reason for this is the absence of a master equation that governs how generic gravitational perturbations propagate on such backgrounds. For the Kerr geometry such equation exists, the Teukolsy equation [22]. Partial progress was made for the $d = 5$ equal angular momenta MP, where a clever decomposition was used [25]. Moreover, certain simple gravitational perturbations of higher-dimensional BHs have been studied [42, 30], but only for very special perturbation sectors where no instabilities were found. Another approach, pursued in [24], focused the study of near horizon geometries and their stability properties. The idea is simple: the authors prove that, for certain matter fields, and for axisymmetric perturbations, an instability of the near horizon geometry implies an instability of the full ex-

[2]This instability was first found in $d \geq 9$ [23]. However, upon further investigation requested by the authors of Ref. [41], the instability was found to also exist in $d = 7$.

tremal geometry. However, it is much easier to study the stability of near horizon geometries, which often exhibit a large isometry group that reduces the problem to an algebraic calculation. Nevertheless, none of the studies described above gave a complete description of the behavior of QNMs in higher-dimensional rotating backgrounds, since their main goal was to study stability of such geometries. This article is entirely devoted to complete that gap, and presents a first exhaustive study of QNMs of the most representative cases of higher-dimensional asymptotically flat rotating BHs. Furthermore, the instability found in [28, 29] has never been reproduced with a linear calculation, which we attempt in this manuscript.

Although in this paper we are mostly interested in the QNMs of rotating BHs, we begin by reviewing QNMs of the Schwarzschild-Tangherlini BH (henceforth referred to as simply Schwarzschild). There are two motivations for doing so. First, the rotating BHs considered in later sections reduce to Schwarzschild in the zero rotation limit, and in this limit the QNMs of these rotating BHs should reduce to those of Schwarzschild. A second motivation for studying Schwarzschild is the recent interest in studying general relativity in the large-d limit [12, 43, 32]. This is a very interesting limit to consider. The equations simplify drastically, and yet enough structure is preserved such that the physics does not become trivial. For example, the physical picture associated with the infinite-d limit is that the space outside a BH is completely flat, BHs have zero cross-section, and can be modelled as dust. From this picture one might conclude that the infinite-d limit is too strong to be useful, and that it has erased all the interesting features of BHs. However, this is certainly not the case, and our analysis of Schwarzschild QNMs and their connection with instabilities of rotating BHs adds to the interesting

results of the infinite-d limit.

We conclude this section with a brief outline of the paper. In Section 3.2 we introduce the general metric of MP BHs, showing that under appropriate limits it reduces to the Schwarzschild, singly spinning MP and equal angular momenta MP BHs. In Section 3.3 we briefly review the Kodama-Ishibashi formalism, and present the QNMs of the Schwarzschild BH as a function of the spacetime dimension d. Section 3.4 studies generic gravitational perturbations, including scalar, vector and tensor-type perturbations, of the equal angular momenta MP BH and in Section 3.5 we present gravitational QNMs of the singly spinning MP BH. We then conclude in Section 3.6.

Note added. As this work was nearing completion, we learned from Emparan, Suzuki, and Tanabe of their recent work [44] studying the (in)stability of odd-dimensional rotating black holes with equal angular momenta in the large dimension limit. When a comparison is possible, our numerical results agree with the analytical findings of [44].

3.2 General Myers-Perry black holes

3.2.1 Most general Myers-Perry family

In this section we present the general MP solution [19], for general $d \geq 4$, and as a function of their mass M and $\lfloor (d-1)/2 \rfloor$ rotation parameters $\{a_i\}$. Its line

element, in Boyer-Lindquist coordinates, takes the following form

$$ds^2 = -dt^2 + \frac{r_0^{d-3}}{U(r,\mu_1,\ldots,\mu_{\tilde{N}})}\left(dt - \sum_{i=1}^{\tilde{N}} a_i \mu_i^2\, d\varphi_i\right)^2 + \sum_{i=1}^{\tilde{N}} \mu_i^2 (r^2+a_i^2) d\varphi_i^2 + \frac{U(r,\mu_1,\ldots,\mu_{\tilde{N}})\, dr^2}{F(r) - r_0^{d-3}} + \sum_{i=1}^{\tilde{N}+\varepsilon} (r^2+a_i^2) d\mu_i^2 \quad (3.1)$$

where

$$U(r,\mu_1,\ldots,\mu_{\tilde{N}}) = r^{\varepsilon} \sum_{i=1}^{\tilde{N}+\epsilon} \frac{\mu_i^2}{r^2+a_i^2} \prod_{j=1}^{\tilde{N}} (r^2+a_j^2)\,, \quad \text{and} \quad F(r) = r^{\varepsilon-2} \prod_{j=1}^{\tilde{N}} (r^2+a_j^2)\,. \quad (3.2)$$

We have also defined $d = 2\tilde{N}+1+\varepsilon$ (where $\varepsilon = 1$ for even d, and $\varepsilon = 0$ otherwise) and for even d, $a_{N+1} = 0$. Finally, the coordinates μ_i are not independent, and must satisfy

$$\sum_{i=1}^{\tilde{N}+\epsilon} \mu_i^2 = 1\,. \quad (3.3)$$

The energy and angular momenta of this solution can be readily computed using Komar integrals, and yield:

$$M = \frac{(d-2)\,\omega_{d-2}}{16\pi G_d}\, r_0^{d-3}\,, \quad \text{and} \quad J_i = \frac{2}{d-2} M\, a_i\,, \quad (3.4)$$

where ω_{d-2} is the area of a $(d-2)$ round sphere with unit radius and G_d is the $d-$dimensional Newton's constant. The event horizon, located at $r = r_+$, is defined as the largest real root of $F(r) - r_0^{d-3}$.

Finally, for the sake of completeness, we also present the remaining thermo-

dynamic quantities, such as the entropy S_H, Hawking temperature T and angular velocities Ω_i:

$$S_H = \frac{\omega_{d-2}}{4\, r_+^{1-\varepsilon}\, G_d} \prod_{i=1}^{\tilde{N}} (r_+^2 + a_i^2)\,, \quad T = \frac{r_+}{2\pi} \left[\sum_{i=1}^{\tilde{N}} \frac{1}{r_+^2 + a_i^2} - \frac{1}{(1+\varepsilon) r_+^2} \right] \quad \text{and} \quad \Omega_i = \frac{a_i}{r_+^2 + a_i^2}\,. \tag{3.5}$$

It is clear from the line element (3.1) that, unless $d = 4$ or $d = 5$, studying a generic gravitational perturbation of a general MP solution in a given dimension, will necessarily involve solving PDEs in more than two variables. This makes the problem quite difficult to study. For this reason, we focus on particular configurations of the angular momenta parameters that result in solutions with enhanced symmetry, which we describe next.

3.2.2 Schwarzschild, singly spinning and equal angular momenta MP black holes

The simplest solution corresponds to the case where all of the angular momenta are set to zero. This is the Schwarzschild-Tangherlini solution first presented in [45], and whose line element is given by

$$ds^2 = -f(r)dt^2 + \frac{dr^2}{f(r)} + r^2 d\Omega_{d-2}^2, \qquad f(r) = 1 - \frac{r_0^{d-3}}{r^{d-3}}, \tag{3.6}$$

where $d\Omega_n^2$ is the line element of an $n-$dimensional unit round sphere. The spatial symmetry group of Schwarzschild is enhanced to $SO(d-1)$, which we will use in Section 3.3.

Another simplifying limit occurs if we set all but one angular momenta to zero. This BH is often denominated singly spinning MP BH. In this case, the line element (3.1) reduces to:

$$ds^2 = \frac{(1-\widetilde{x}^2)}{\Sigma}\left[d\phi\left(a^2+r^2\right)-adt\right]^2 - \frac{\Delta}{\Sigma}\left[dt - ad\phi\left(1-\widetilde{x}^2\right)\right]^2 + \frac{\Sigma}{\Delta}dr^2 + \frac{\Sigma}{1-\widetilde{x}^2}d\widetilde{x}^2 + r^2\widetilde{x}^2\, d\Omega^2_{(d-4)}\,, \tag{3.7}$$

where

$$\Delta = r^2 + a^2 - \frac{r_0^{d-3}}{r^{d-5}}\,, \qquad \Sigma = r^2 + a^2\widetilde{x}^2 \qquad \text{and} \qquad \widetilde{x} = \cos\theta \in (0,1)\,. \tag{3.8}$$

The symmetry group is now enhanced to $SO(d-3)$, which means that generic perturbations will reduce to a set of coupled PDEs in two variables, $r, \widetilde{x}$ (after Fourier mode decomposition both in time and rotational angle ϕ). This line element, in many ways, is the simplest generalization of the Kerr BH to higher dimensions. Note that in this case, the temperature defined in Eq. (3.5) cannot be made zero for $d \geq 6$, and as such no upper bound on the rotation exists. For the special case of $d = 5$, there is an upper bound on the rotation, corresponding to $a = r_0$, but this corresponds to a naked singularity, i.e. $r_+ = 0$. Despite the many efforts over the past years, no decoupled equation describing how gravitational perturbations propagate on the singly spinning MP BH has been found, see for instance [46] for a recent effort in this direction. We shall proceed in Section 3.5 by considering the full PDE problem.

A even more drastic simplification, which is less obvious, occurs when all the angular momenta are equal, i.e. $a_i = a$, and when d is odd, as was first noted in

[47]. In this case the general line element (3.1), reduces to

$$ds^2 = -\frac{p(\hat{r})}{h(\hat{r})}dt^2 + \frac{d\hat{r}^2}{p(\hat{r})} + \hat{r}^2\left[h(\hat{r})^2\left(d\psi + A_a dx^a - u(\hat{r})dt\right)^2 + \hat{g}_{ab}dx^a dx^b\right] \quad (3.9)$$

where $d = 2N + 3$, and the metric functions are defined as follows:

$$p(\hat{r}) = 1 - \frac{r_0^{2N}}{\hat{r}^{2N}} + \frac{r_0^{2N}a^2}{\hat{r}^{2(N+1)}}, \quad u(\hat{r}) = \frac{r_0^{2N}a}{\hat{r}^{2(N+1)}h(\hat{r})} \quad \text{and} \quad h(\hat{r}) = 1 + \frac{r_0^{2N}a^2}{\hat{r}^{2(N+1)}}\,. \quad (3.10)$$

Here $\hat{g}_{ab}$ is the Fubini-Study metric on $\mathbb{CP}^N$ and A is related to its Kähler form by $J = dA/2$. Some comments concerning this line element are in order. First, we note that the radial coordinate $\hat{r}$ is related to the general Boyer-Lindquist coordinate as $\hat{r}^2 = r^2 + a^2$. Second, this line element has a much larger isometry group than the singly spinning MP solution, namely $\mathbb{R} \times U(1) \times SU(N + 1)$. Finally, in passing from Eq. (3.1) to Eq. (3.9) we have used the fact that any round S^{2N+1} sphere can be written as a Hopt fibration over $\mathbb{CP}^N$, i.e.

$$d\Omega_{2N+1}^2 = (d\psi + A_a dx^a)^2 + \hat{g}_{ab}dx^a dx^b\,. \quad (3.11)$$

These equal angular momenta BHs cannot rotate arbitrarily fast, and in fact have an extremal bound,

$$a_{\text{ext}} = \sqrt{\frac{N}{N+1}}r_+. \quad (3.12)$$

A remarkable property about the line element (3.9) is that it is cohomogeneity-one, which is to say that it only depends non-trivially on one coordinate, namely $\hat{r}$. Its large symmetry group will allow us to study generic gravitational perturbations by studying a system of coupled ODEs. This procedure was first used in [23],[30],

and shall be reviewed in Section 3.4.

3.3 Schwarzschild black holes

In this section we review gravitational perturbations of Schwarzschild and study the QNM spectrum in the limit of large dimensions.

3.3.1 Review of the Kodama-Ishibashi formalism

Here we briefly review the Kodama-Ishibashi (KI) master variable formalism [31], which has proven to be an invaluable tool for the study of the linear stability of BH spacetimes. The KI formalism exists for spacetimes for which the line element can be written as

$$ds^2 = h_{AB}(y)dy^A dy^B + r^2(y)\hat{g}_{ab}dx^a dx^b. \tag{3.13}$$

Here h_{AB} is the Lorentzian metric of a two-dimensional orbit spacetime, and $\hat{g}_{ab}$ is the metric for a $n = d-2$ dimensional Euclidean signature space which (in our study) is restricted to be maximally symmetric with constant sectional curvature, normalized to be 0 or ± 1. In what follows, we will restrict ourselves to Schwarzschild BHs, for which the line element is given by (3.6).

We wish to consider linearized gravitational perturbations of this spacetime. Although a general metric perturbation will depend on all the coordinates, the angular and time dependence can be separated out using spherical tensor harmonics on S^{d-2} and complex exponentials of the form $e^{-i\omega t}$. The linearized Einstein

equations then become a system of ordinary differential equations. Three types of harmonic tensors will be needed to construct the most generic perturbation: scalar, vector, and tensor. The scalar harmonics S are both the most familiar and the simplest, and satisfy

$$(\hat{\nabla}^2 + \lambda_S)S = 0, \tag{3.14}$$

where the requirement of regularity quantizes the eigenvalue as $\lambda_S = \widetilde{\ell}_S(\widetilde{\ell}_S+n-1)$, $\widetilde{\ell}_S = 0, 1, 2, ..$, and $\hat{\nabla}_a$ is the covariant derivative on the n-sphere. Less familiar are vector V and tensor T harmonics which satisfy similar equations:

$$(\hat{\nabla}^2 + \lambda_V)V_a = 0, \qquad \hat{\nabla}^a V_a = 0\,; \tag{3.15}$$

$$(\hat{\nabla}^2 + \lambda_T)T_{ab} = 0, \qquad \hat{\nabla}^a T_{ab} = 0, \qquad \hat{g}^{ab}T_{ab} = 0, \qquad T_{ab} = T_{(ab)}. \tag{3.16}$$

The eigenvalues of these regular harmonics are quantized as $\lambda_V = \widetilde{\ell}_V(\widetilde{\ell}_V+n-1)-1$, $\widetilde{\ell}_V = 1, 2, ..$, and $\lambda_T = \widetilde{\ell}_T(\widetilde{\ell}_T+n-1)-2$, $\widetilde{\ell}_T = 1, 2, ..$ [3]. In terms of these harmonics, the most general metric perturbation can be constructed from superpositions of scalar, vector, and tensor perturbations, which take the form

$$\delta g_{AB} = f^{(S)}_{AB}S, \quad \delta g_{Aa} = r f^{(S)}_{A} S_a, \quad \delta g_{ab} = r^2(H^{(S)}_T S_{ab} + H_L \hat{g}_{ab} S) \qquad \text{(scalar)}, \tag{3.17}$$

[3] Gravitational scalar perturbations with $\widetilde{\ell}_S = 0, 1$ or vector perturbations with $\widetilde{\ell}_V = 1$ do not represent local degrees of freedom. Scalar perturbations with $\widetilde{\ell}_S = 0$ or vector perturbations with $\widetilde{\ell}_V = 1$ describe simply a variation of the mass and angular momentum parameters of the solution, respectively, and $\widetilde{\ell}_S = 1$ corresponds to a pure gauge mode [31, 35]. We do not consider these special modes further.

$$\delta g_{AB} = 0, \quad \delta g_{Aa} = r f_A^{(V)} V_a, \quad \delta g_{ab} = r^2 H_T^{(V)} V_{ab} \qquad \text{(vector)}, \tag{3.18}$$

$$\delta g_{AB} = 0, \quad \delta g_{Aa} = 0, \quad \delta g_{ab} = r^2 H_T^{(T)} T_{ab} \qquad \text{(tensor)}. \tag{3.19}$$

In the above, S_a, S_{ab}, and V_{ab} are derived harmonics which can be written as derivatives of the more fundamental harmonic. For example, $S_a = -\lambda_S^{-1/2}\hat{\nabla}_a S$ is a scalar-derived vector harmonic. We refer the reader to the original paper for more details. The functions f_{AB}, f_A are functions of the orbit coordinates (t, r) only, and the time dependence can be trivially separated into Fourier modes, as in $f_{AB} \propto e^{-i\omega t}$, as mentioned above.

With this parametrization, the linearized equations become a system of ODE's. At this point the gauge redundancy has not been taken into account, and in fact the above decomposition is not gauge invariant; under a linearized gauge transformation, many of the above functions will shift. Kodama and Ishibashi were able to combine the perturbation functions for each of the sectors into a single function called the master variable which is a gauge invariant quantity [4]. A differential map acting on this master variable reconstructs the metric perturbation in a given gauge. The remarkable end result is that one can study gravitational perturbations of Schwarzschild by simply solving a Schrödinger equation for each sector. The master equations are of the form:

$$-f\partial_r(f\partial_r\phi_I) + (V_I - \omega^2)\phi_I = 0, \tag{3.20}$$

[4]The tensor sector is trivially put into master variable form, since there is only one perturbation function and it is already gauge invariant.

where I is an index that runs over scalar, vector, or tensor perturbations and ϕ_I is the master variable. The expressions for the potentials V_I are rather lengthy and we will not reproduce them here; they can be found in the original Kodama Ishibashi paper [31]. QNMs are then solutions to these equations with appropriate boundary conditions: the perturbations should be ingoing at the horizon and outgoing at infinity.

3.3.2 Gravitational QNMs of Schwarzschild in higher dimensions

The QNM spectrum of the four dimensional Schwarzschild BH has been well understood for many years, and there are also many studies of the spectrum in higher dimensions. For a detailed review, see [10]. Here, we are interested in the the spectrum not at any one particular value of d, but as a function of d. In particular, we are interested in the behaviour of the frequencies as d tends toward infinity. Although Schwarzschild BHs exist for integer $d \geq 4$, we will find it useful to consider d a continuous parameter and to study the spectrum as d increases. The Kodama-Ishibashi (KI) equations were derived analytically for arbitrary integer d, and we will simply use these equations but allow d to vary continuously. Here a comment is in order. Considered as a function of d, the potentials are not analytic, and one should use care in considering the QNM frequencies as continuous functions of d. Our main motivation for considering non-integer d is twofold: it will make clearer the pattern of the QNM behavior as d is increased, and it will allow us to use a certain powerful numerical method which utilizes a continuous parameter. Of course, when d is an integer, we will

check that our results for the continuous-d code agree with the results of the integer-d code.

As mentioned above, the KI formalism allows the complicated equations for gravitational perturbations to be reduced to simple Schrödinger-type ODE's. A simple Frobenius analysis yields the following behaviour near the two boundaries (here we suppress the I-index),

$$\phi = \quad e^{i\omega r_\star}\phi_\infty^{\rm out} + e^{-i\omega r_\star}\phi_\infty^{\rm in} \qquad \text{(infinity)}, \tag{3.21}$$

$$\phi = \quad e^{i\omega r_\star}\phi_{\rm hor}^{\rm out} + e^{-i\omega r_\star}\phi_{\rm hor}^{\rm in} \qquad \text{(horizon)}, \tag{3.22}$$

where $r_\star = \int dr/f$ is the usual tortoise coordinate, and the functions $\phi_{\rm hor/\infty}^{\rm in/out}$ are regular and non-zero at the relevant boundary. The boundary conditions appropriate for QNMs are such that the perturbation is ingoing at the BH horizon and outgoing at infinity. These conditions can be easily formulated in Eddington-Finkelstein coordinates, and they amount to setting $\phi_\infty^{\rm in} = \phi_{\rm hor}^{\rm out} = 0$. It is useful to define a new function $\widetilde{\phi}$ with this asymptotic behaviour stripped off [5],

$$\phi = \left(1 - \frac{r_0}{r}\right)^{-\frac{i\omega r_0}{d-3}} e^{i\omega r}\widetilde{\phi}, \tag{3.23}$$

which is then regular and finite at either boundary when the above conditions are imposed.

We then solved these equations numerically for the new $\widetilde{\phi}_I$ variables using the following scheme: introduce a compactified radial coordinate $r = r_0/z$, where $z \in [0,1]$, with $z = 0$ corresponding to infinity, and $z = 1$ corresponding to the horizon.

[5] The case $d = 4$ is special and has a slightly different fall-off near infinity.

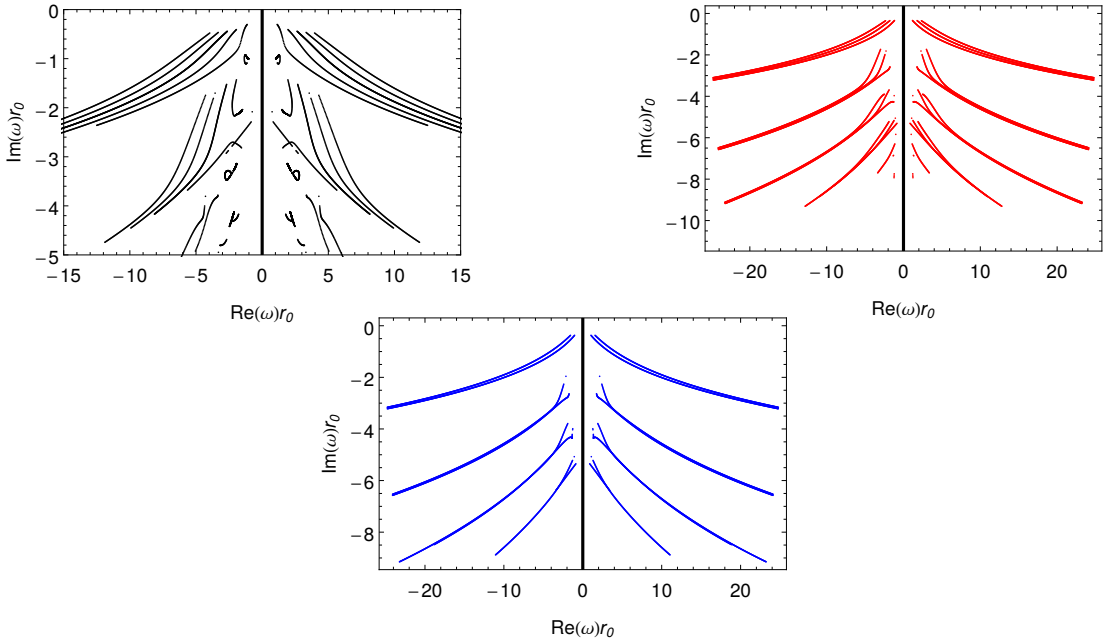

Figure 3.1: **Schwarzschild**. The complex QNM frequencies for scalar (*top left*), vector (*top right*), and tensor (*bottom*) perturbations. In these plots, the dimension ranges from $d = 6$ to $d = 100$. For the scalar plot, $\widetilde{\ell}_S = 2, 3, 4, 5, 6$ modes are displayed, while for vectors $\widetilde{\ell}_V = 2, 3, 4$, and for tensors $\widetilde{\ell}_T = 1, 2$. As d is increased the QNM's generally move to larger values of $|\omega r_0|$ in the lower half of the complex plane, although there are some interesting exceptions to this rule. These plots are meant to give the reader a rough sense of the behaviour of the QNM frequencies as d is increased; more quantitative and focused analyses follow below.

This interval is then discretized using a Chebyshev grid. The QNMs were then solved for using one of two methods. The first relies on converting the equations into an eigenvalue problem for the frequencies ω, which can then be solved using Mathematica's built-in routine Eigensystem. More details of this method and the discretization scheme can be found in [23]. The second method is based on an application of the Newton-Raphson root-finding algorithm, and is detailed in [4]. The strength of the first method is that it gives many QNMs simultaneously,

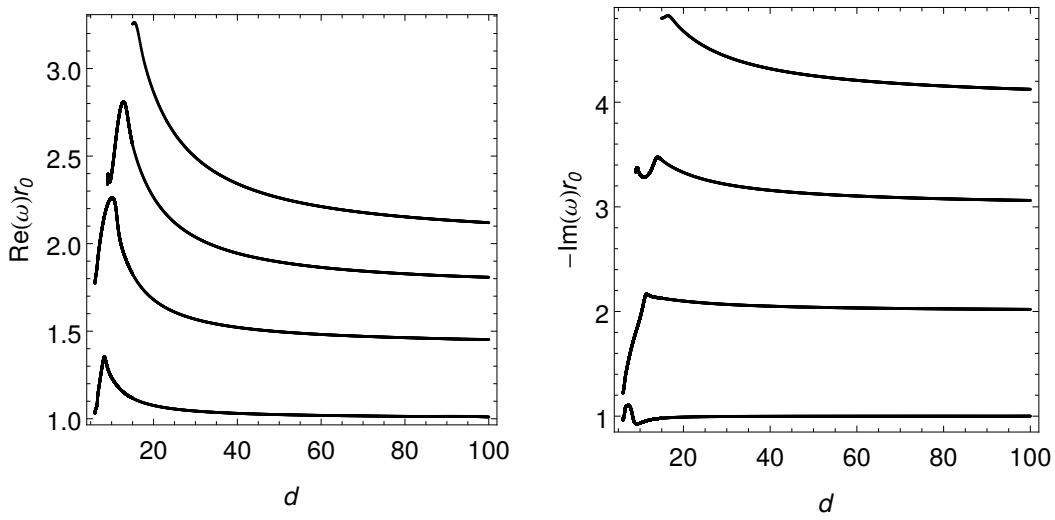

Figure 3.2: **Schwarzschild**. The real and imaginary parts of the saturating scalar QNM's for $\widetilde{\ell}_S = 2, 3, 4, 5$. Higher $\widetilde{\ell}_S$ curves lie above lower ℓ_S curves.

allowing for easy determination of the spectra. The second method can only be used to compute a single mode at a time, and only when a seed is known that is sufficiently close to the true answer. However, this method is much quicker as both the size of the grid and numerical precision increases, and can be used to push the numerics to extreme regions of the parameter space. For example, using the Newton-Raphson method, dimensions as large as $d = 100$ were attainable, which is quite remarkable considering the steepness of the warp function $f(r) = 1 - (r_0/r)^{d-3}$ near the horizon.

We are now ready to present our results. In Fig. 3.1 we display the QNM frequencies for scalar, vector, and tensor perturbations. We will analyse these results in more detail below, but two interesting features are immediately obvious. The first is that many of the modes scale with d, so that both their decay rate $\mathrm{Im}(\omega)$ and oscillation frequency $\mathrm{Re}(\omega)$ increase in magnitude as the dimension is

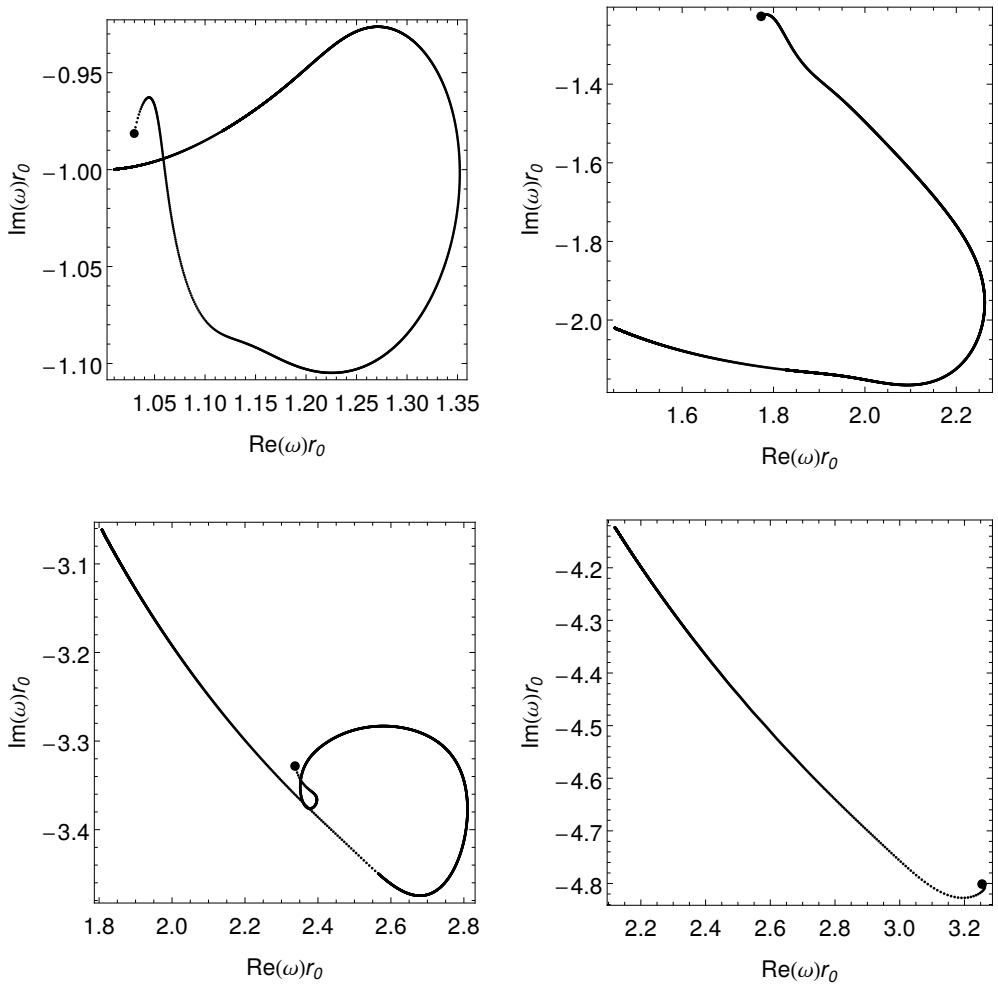

Figure 3.3: **Schwarzschild**. The saturating scalar QNM's in the complex ω plane for $\widetilde{\ell}_S = 2$ (top left), $\widetilde{\ell}_S = 3$ (top right), $\widetilde{\ell}_S = 4$ (bottom left), $\widetilde{\ell}_S = 5$ (bottom right). The curves begin at $d = 6, 6, 9, 15$ (large dots) for $\widetilde{\ell}_S = 2, 3, 4, 5$, respectively, and d increases along the curve, reaching $d = 100$ at the other endpoint.

increased. The second is that many of the curves seem to lie on top one another. The curves that scale together have different angular quantum numbers $\widetilde{\ell}$. Evidently in the large-d limit, the difference between these QNMs with $\widetilde{\ell} \sim \mathcal{O}(d^0)$ goes to zero.

A perhaps less obvious feature is arguably the most interesting: in the scalar

plot there are QNM curves that do not scale with d, and in fact seem to not stray too far from their low-d values. We dub these modes *saturating modes*, and will study them in detail below. Let us also mention that saturating modes also exist for vectors, but they cannot be seen from the above plots because they are purely imaginary [6]. We found no saturating modes for tensors.

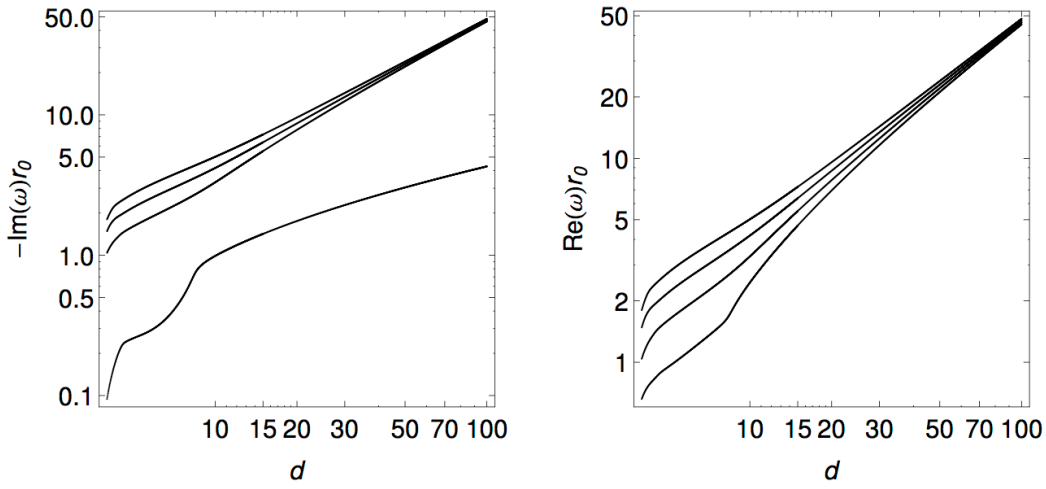

Figure 3.4: **Schwarzschild**. Plot of non-saturating scalar modes for $\widetilde{\ell}_S = 2, 3, 4, 5$. For both plots the curves appear in terms of increasing $\widetilde{\ell}_S$, from bottom to top.

[6]Throughout this paper we will encounter purely imaginary modes, and therefore two comments concerning them are in order. Firstly, in $d = 4$ there is a very interesting relationship between purely imaginary modes and algebraically special perturbations–a relationship which, unfortunately, does not appear to extend to higher dimensions [35]. Secondly, in $d = 4$ it is known that there is a branch cut for the Green's function and certain homogeneous solutions of the perturbation equations [10]. The branch cut is realised in our numerics as many spurious purely imaginary or almost purely imaginary modes which pollute the data. To isolate the QNMs from the numerical manifestation of the branch cut, we can utilise two techniques. The first is to vary the number of grid points, which typically causes the spurious modes to jump around and thereby be identified. The second technique is to use the results of the following sections and add a small amount of rotation. If the purely imaginary mode is legitimate, it will connect to a QNM of the slowly rotating BH. We do not know of studies on branch cuts in higher dimensions or rotating BHs, which would certainly be interesting to investigate.

Scalar modes

Amongst the three sectors, the scalar potential is the most complicated, and it is presumably this structure which allows for the interesting behaviour observed as d is varied. We start by presenting our scalar results for the saturating QNMs. In Fig. 3.2, we display the real and imaginary part of the saturating modes for $\widetilde{\ell}_S = 2, 3, 4, 5$. These modes are clearly saturating to finite values as $d \to \infty$. In Fig. 3.3 we plot these saturating QNM's in the complex plane. In all cases the curves begin at the large dot and execute interesting trajectories as d increases. The values of the saturating modes for $d = 100$ are likely close to their limiting values, and are:

$$(\widetilde{\ell}_S, \omega r_0) \simeq (2, 1.01{-}1.00i), \quad (3, 1.45{-}2.02i), \quad (4, 1.81{-}3.06i), \quad (5, 2.12{-}4.12i). \tag{3.24}$$

One would expect a simple analytic formula to describe these results. It is not obvious how the real part is changing as a function of $\widetilde{\ell}_S$, but the imaginary part seems to obey the simple relation $\lim_{d\to\infty} \mathrm{Im}(\omega) = -(\widetilde{\ell}_S - 1)$. The error of the numerical data from these values is consistent with the corrections being $\mathcal{O}(d^{-1})$ [7].

In addition to the saturating modes, there are also modes which scale with d and that we might call *non-saturating* or *scaling modes*. Indeed, as can be seen from Fig. 3.1, many QNMs scale the same way in the large-d limit. In Fig. 3.4 we plot one such group of scaling QNMs. For these curves we can extract their

[7] After the first version of this article appeared, we learned that an analytic formula had been derived by Ref. [44] who found: $\omega r_0 = \pm\sqrt{\widetilde{\ell}_S - 1} - i(\widetilde{\ell}_S - 1)$ at leading order, agreeing remarkably well with our numerical results.

dependence on d. It is power law with roughly the dependence

$$\mathrm{Im}(\omega\, r_0) \sim d^{1/2}, \qquad \mathrm{Re}(\omega\, r_0) \sim d. \tag{3.25}$$

We stress that these results pertain just to the group of modes plotted, and it could well be the case that there are many different scalings. It is harder to extract the power laws of the other groups of scaling modes as they enter the scaling regime at larger d's than the group displayed.

Vector modes

We now turn to discuss the vector modes. We again find both saturating and scaling modes. Interestingly, the saturating vector modes are purely imaginary. These are plotted in Fig. 3.5. The values of the saturating vector modes for

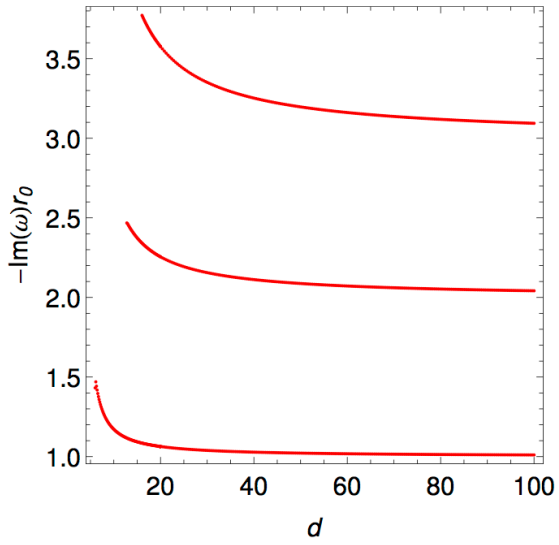

Figure 3.5: **Schwarzschild**. The imaginary part of the saturating vector QNM's for $\widetilde{\ell}_V = 2, 3, 4$. Higher $\widetilde{\ell}_V$ curves lie above lower $\widetilde{\ell}_V$ curves.

$d = 100$ are:

$$(\widetilde{\ell}_V, \omega r_0) \simeq (2, -1.01i), \quad (3, -2.04i), \quad (4, -3.09i). \tag{3.26}$$

As before, the data suggests a simple formula for the saturating QNM in the $d \to \infty$ limit: $\lim_{d\to\infty} \omega = -(\widetilde{\ell}_V - 1)$ [8]. For reference, we also quote the value of the lowest lying purely imaginary mode in $d = 5$, namely $\omega r_0 = -1.50i$. [9]

Turning to the modes that scale with d, we can make the same plot as in the scalar case, plotting QNM's of different $\widetilde{\ell}_V$ that seem to scale the same way. The results are plotted in Fig. 3.6. These modes also have the same scaling (3.25) as in the scalar case, namely $\mathrm{Im}(\omega r_0) \sim d^{1/2}$, and $\mathrm{Re}(\omega r_0) \sim d$.

Tensor modes

For the tensor modes, we observe no saturating modes. A few of the lowest-lying scaling modes are plotted in Fig. 3.7. Once again, these modes have the same scaling (3.25) as in the scalar and vector cases, i.e. $\mathrm{Im}(\omega r_0) \sim d^{1/2}$, and $\mathrm{Re}(\omega r_0) \sim d$.

[8] This agrees exactly with the leading order expression derived in Ref. [44].

[9] Previous literature on QNMs did not find purely imaginary modes in $d = 5$. Our numerical method is however more robust than those used in the past to study QNMs. Indeed, we use a Chebyshev differentiation scheme with (crucially) quadruple precision which directly integrates the perturbation equations and exhibits exponential convergence as the number of grid points is changed. So, varying this number of grid points, we are able to resolve the branch cut along the negative imaginary axis and we manage to single out the physical modes that do not change as the grid changes. As a further test we look to the eigenfunction of the modes: the physical mode eigenfunctions are clearly distinct from any other wave function along the poles that are associated with the branch cut.

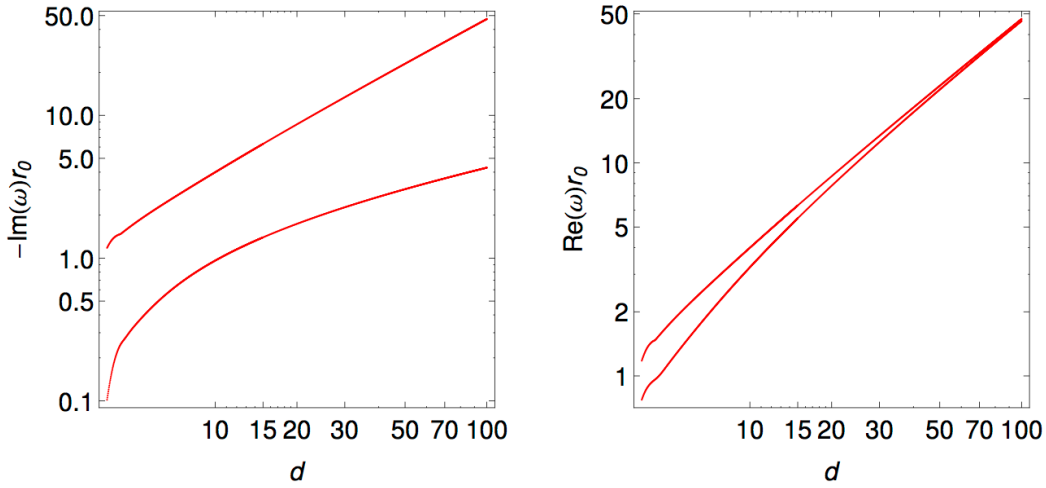

Figure 3.6: **Schwarzschild**. Plot of non-saturating vector modes for $\widetilde{\ell}_V = 2, 3$. For both plots the curves appear in terms of increasing $\widetilde{\ell}_V$, from bottom to top.

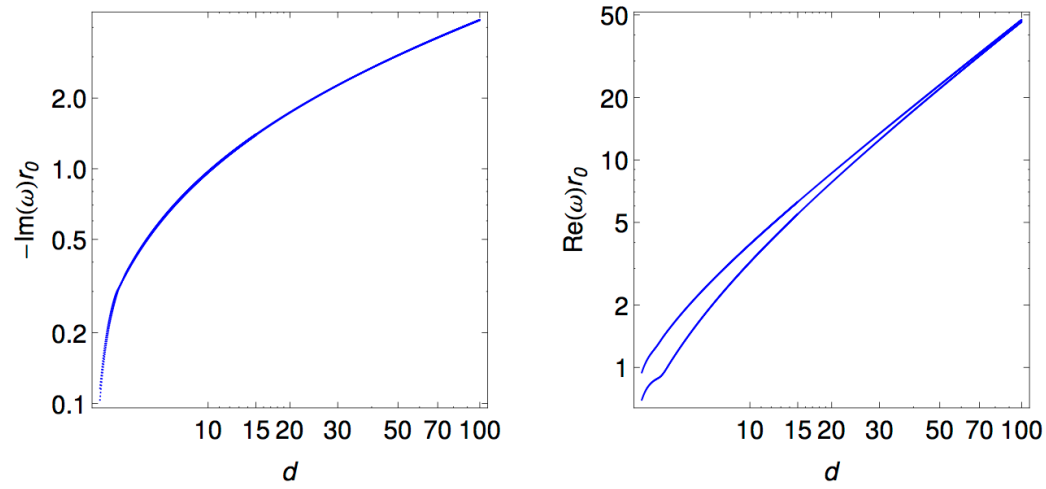

Figure 3.7: **Schwarzschild**. Plot of non-saturating tensor modes for $\widetilde{\ell}_T = 1, 2$. For both plots the curves appear in terms of increasing $\widetilde{\ell}_T$, from bottom to top. For the imaginary plot, the two curves are so close as to be indistinguishable.

Discussion of results

The physics of the saturating modes is very interesting. In terms of the Schwarzschild time t, the modes that scale with d decay increasingly rapidly as d increases, whilst the saturating modes have a finite decay rate even in the infinite-d limit. Thus, for phenomena for which t is the relevant time, the QNM mode spectra consists only of the saturating modes and all the others become irrelevant. This is a particularly sharp characterization of the way in which the large-d limit simplifies the physics.

Another important feature of the saturating modes is that they are localized near the horizon. In Fig. 3.8 we plot the real and imaginary parts of the scalar gauge invariant wavefunction $\widetilde{\phi}_S$ for $\widetilde{\ell}_S = 2$ and various d. It is clear that as d is increased, the wavefunction becomes increasingly localized around $z = 1$, which corresponds to the horizon. The near-horizon geometry was shown to take the form of the direct product of a 2d string BH and a sphere [43],

$$ds^2 = \frac{4r_0^2}{\tilde{n}^2}\Big(-\tanh^2\rho d\hat{t}^2 + d\rho^2\Big) + r_0^2 d\Omega^2_{\tilde{n}+1}, \tag{3.27}$$

where $\tilde{n} = d-3$ and the time coordinate of the near-horizon geometry is related to the usual time via $\hat{t} = \tilde{n}t/(2r_0)$. In terms of this time coordinate, the saturating modes do not decay or oscillate in the infinite-d limit,

$$\exp(-i\omega t) = \exp(-2i\omega r_0\hat{t}/\tilde{n}) \sim 1. \tag{3.28}$$

Ref. [43] argued that modes with $\omega \sim \mathcal{O}(d^0)$ could be said to decouple from

the asymptotic region, and the localization of the wavefunctions of these modes confirms this.

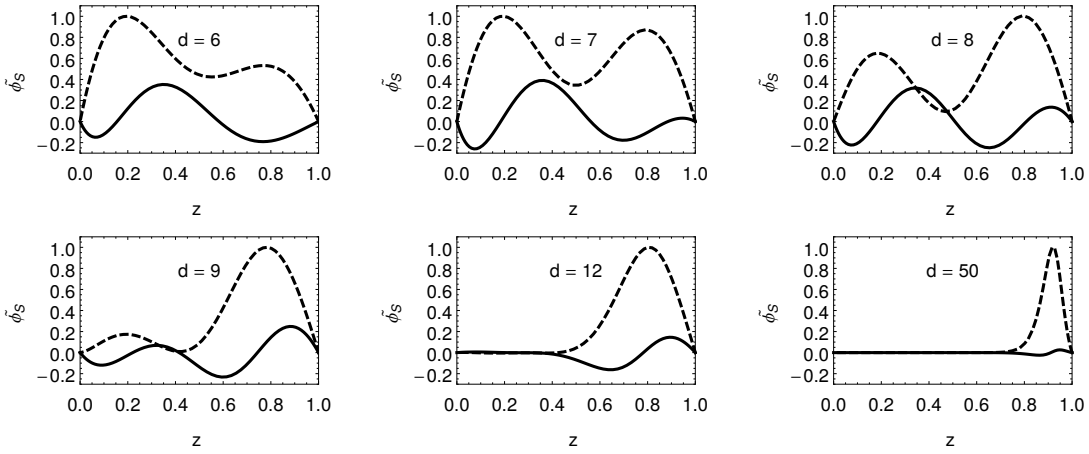

Figure 3.8: **Schwarzschild**. The real (dashed) and imaginary (dotted) parts of the scalar gauge invariant wavefunctions $\widetilde{\phi}_S$ for $\widetilde{\ell}_S = 2$. As the dimension is increased, the wavefunctions become localized near the horizon.

The presence of the saturating modes connects nicely to recent observations concerning unstable perturbations of rotating BHs in higher dimensions. Before turning to the rotating case, a comment is in order concerning overtones. For a given spherical harmonic there are an infinite number of QNM frequencies. These are typically indexed by an integer n, called the overtone number. The name suggests that n might correspond to the number of zeros of a function, but actually the indexing is defined so that n sorts the frequencies by increasing $-\mathrm{Im}(\omega)$, with $n = 0$ corresponding to the smallest value (see, for example the review article [10]). We have observed that as d increases many of the QNM's cross. For example, in Fig. 3.3 the overtone number changes as one moves along the curves. Since in this section we were primarily interested in how the frequencies varied with d, we did

not consider the overtone number. For a given value of d, the overtone number is a very useful concept, and it remains so even in the expansion around $d = \infty$ done in Ref. [44]. Interestingly, they found that the saturating modes had only a single overtone–that is, for a given spherical harmonic there is only a single saturating mode.

3.4 Cohomogeneity-1 Myers-Perry black holes

As discussed in Sec. 3.2.2, when all the angular momenta are equal and non-zero for an odd dimensional Myers-Perry BH, there is a dramatic enhancement of the symmetry and the equations of motion of linearized gravitational perturbations can be reduced to systems of ODE's. As in the Schwarzschild case, the gravitational perturbations can be classified into three sectors–scalar, vector, and tensor, according to how the metric perturbation transforms under the isometries of the $\mathbb{CP}^N$ base space. The tensor sector is the simplest, where just as in the Schwarzschild case the linearized Einstein equations reduce to a single Schrödinger equation. We shall not consider tensor perturbations here, as they were studied in [30], and no instabilities were found. The study of scalar modes was first initiated in [23], where axisymmetric perturbations were studied, and continued in [5], where non-axisymmetric perturbations were considered. Instabilities were found for both types of perturbations, in agreement with the predictions of Emparan and Myers [20]. The axisymmetric instabilities are particularly interesting because they indicate the existence of new families of BHs with a single rotational symmetry [23], and the non-axisymmetric m-bar mode instabilities are important

because they occur for much slower rotations than the axisymmetric instabilities, and are hence the most dominant.

In this section we study scalar and vector perturbations of these BHs. We begin by reviewing the harmonic tensors needed for the separation of variables, and then discuss our numerical results.

3.4.1 Charged harmonic tensors on $\mathbb{CP}^N$

We now review charged scalar and vector harmonic tensors on $\mathbb{CP}^N$ which allow the separation of variables for linearised gravitational perturbations. Charged scalar harmonics were studied in [48], and vector harmonics in [24]. By charged harmonics we mean those tensors which are eigentensors with respect to the derivative operator

$$\hat{D}_a \equiv \hat{\nabla}_a - imA_a, \tag{3.29}$$

where $\hat{\nabla}$ is the covariant derivative on $\mathbb{CP}^N$, and A_a is again related to the Kähler form via $J = dA/2$. This is the natural derivative operator given the appearance of the Hopf fibration in the BH metric. The charge of a given harmonic is m, which we take to be an integer.

Scalar harmonics

Charged scalar harmonics are functions of the $\mathbb{CP}^N$ coordinates which satisfy

$$(\hat{D}^2 + \lambda_S)\mathbb{S} = 0. \tag{3.30}$$

Here the eigenvalue is a function of two quantized parameters, (κ, m):

$$\lambda_S = l(l+2N) - m^2, \quad l = 2\kappa + |m|, \tag{3.31}$$

where $\kappa = 0, 1, 2...$, and $m \in \mathbb{Z}$. Charged scalar-derived vectors can be obtained by differentiating,

$$\mathbb{S}_a = -\frac{1}{\sqrt{\lambda_S}} \hat{D}_a \mathbb{S}. \tag{3.32}$$

These can be further decomposed into Hermitian and anti-Hermitian parts

$$J_a{}^b \mathbb{S}_b^{\pm} = \mp i \mathbb{S}_a^{\pm}. \tag{3.33}$$

Lastly, the scalar-derived tensors are given by

$$\mathbb{S}_{ab}^{++} = \hat{D}^+_{(a}\mathbb{S}^+_{b)}, \qquad \mathbb{S}_{ab}^{--} = \hat{D}^-_{(a}\mathbb{S}^-_{b)}, \qquad \mathbb{S}_{ab}^{+-} = \hat{D}^+_{(a}\mathbb{S}^-_{b)} + \hat{D}^-_{(a}\mathbb{S}^+_{b)} - \frac{1}{2N}\hat{g}_{ab}\hat{D}\cdot\mathbb{S}. \tag{3.34}$$

Here $\hat{D}_a^{\pm}$ is the (anti-)Hermitian projection of the $\hat{D}$ operator, $\hat{D}_a^{\pm} = \frac{1}{2}\left(\delta_a{}^b \pm i J_a{}^b\right)\hat{D}_b$.

Vector harmonics

Next we consider the vector harmonics which only exist for $N \geq 2$. These are also eigenfunctions of $\hat{D}^2$ which transform as vectors in $\mathbb{CP}^N$ and which are also transverse with respect to $\hat{D}^a$:

$$(\hat{D}^2 + \lambda_V)\mathbb{V}_a = 0, \qquad \hat{D}^a \mathbb{V}_a = 0. \tag{3.35}$$

Just as the scalar-derived vectors, these may be further characterized according to their eigenvalue under the complex structure,

$$J_a{}^b \mathbb{V}_b = -i\epsilon \mathbb{V}_a, \qquad \epsilon = \pm 1. \tag{3.36}$$

The vector-derived tensors are given by

$$\mathbb{V}^{\pm}_{ab} = -\frac{1}{\sqrt{\lambda_V}} \hat{D}^{\pm}_{(a} \mathbb{V}_{b)}. \tag{3.37}$$

The eigenvalues were first computed in [24] for the uncharged case, $m = 0$,

$$\lambda_V^{(m=0)} = 4\kappa(\kappa+2) + 2(N+1)(2\kappa+3). \tag{3.38}$$

In Appendix 3.A we extend this result for non-zero m in the $N = 2$ case [10]:

$$\lambda_V^{(N=2)} = 4\kappa\left(\kappa + 3 + |2 + m\epsilon|\right) + 6|2 + m\epsilon| + 6 + 2m\epsilon. \tag{3.39}$$

3.4.2 Perturbation decomposition and equations

In order to implement the harmonic decomposition of the perturbation, it will be useful to introduce the 1-forms, e^A, where $A \in (0, 1, 2)$:

$$e^0 = \frac{p(\hat{r})^{1/2}}{h(\hat{r})^{1/2}} dt, \quad e^1 = p(\hat{r})^{-1/2} d\hat{r}, \quad e^2 = \hat{r} h(\hat{r})(d\psi + A_a dx^a - u(\hat{r}) dt). \tag{3.40}$$

[10] There a third integer appeared, $\tilde{n}$, in addition to the (κ, m). In what follows we have set $\tilde{n} = 1$ without loss of generality.

The scalar sector of metric perturbations is then

$$h_{AB} = f_{AB}\mathbb{S}, \tag{3.41}$$

$$h_{Aa} = \hat{r}(f_A^+\mathbb{S}_a^+ + f_A^-\mathbb{S}_a^-), \tag{3.42}$$

$$h_{ab} = -\frac{\hat{r}^2}{\lambda^{1/2}}(H^{++}\mathbb{S}_{ab}^{++} + H^{--}\mathbb{S}_{ab}^{--} + H^{+-}\mathbb{S}_{ab}^{+-}) + \hat{r}^2 H_L \hat{g}_{ab}\mathbb{S}, \tag{3.43}$$

and the vector sector is

$$h_{AB} = 0, \qquad h_{Aa} = \hat{r} f_A^{(V)}\mathbb{V}_a, \qquad h_{ab} = -\frac{\hat{r}^2}{\lambda^{1/2}}(H^+\mathbb{V}_{ab}^+ + H^-\mathbb{V}_{ab}^-). \tag{3.44}$$

Here the perturbation functions f_{AB}, f_A^+, etc are functions of the non-$\mathbb{CP}^N$ coordinates (r, t, ψ), analogous to the $f_{AB}^{(S)}, f_A^{(S)}$, etc functions introduced in the the Kodama-Ishibashi decomposition for perturbations of Schwarzschild reviewed in Sec. 3.3.1 [11]. Separation of the perturbation equations requires that the (t, ψ)-dependence is $e^{-i(\omega t - m\psi)}$. The value of m provides an important characterization of the perturbation. Those with $m = 0$ are axisymmetric, while those with $m \neq 0$ are non-axisymmetric.

This decomposition in terms of $\mathbb{CP}^N$ harmonic tensors parallels the one based on S^{2N+1} tensors used in the Kodama-Ishibashi formalism applied to Schwarzschild. Using this decomposition Kodama and Ishibashi constructed gauge invariant variables and were furthermore able to reduce the number of independent functions to one–the so called master variable. Unfortunately we do not know how to define a master variable for our system of equations, and will therefore impose a gauge and

[11] Note that the $\pm$ superscript indicates a (anti)-Hermitian projection when it appears on a $\mathbb{CP}^N$ harmonic, i.e. $\mathbb{S}_a^+$, and is simply a label when it appears on the perturbation functions, for example f_A^+.

solve the coupled ODE's [12]. The gauge we will work in is the traceless transverse gauge,

$$h = g^{\mu\nu}h_{\mu\nu} = 0, \quad \nabla^{\mu}h_{\mu\nu} = 0. \tag{3.45}$$

In this gauge the Einstein equations take the simple form:

$$\nabla^2 h_{\mu\nu} + 2R_{\mu\rho\nu\sigma}h^{\rho\sigma} = 0. \tag{3.46}$$

3.4.3 Numerical results

Here we present our results for the QNMs of equal angular momenta Myers-Perry (MP) BHs in odd dimensions $d \geq 5$. To discuss the results, first note that when the rotation vanishes, the Schwarzschild background has the discrete symmetry $t \to -t$; consequently the associated QNM frequencies always come in trivial pairs of $\{\omega, -\omega^*\}$. The $t \to -t$ symmetry is broken when the rotation is turned on and for each pair of angular quantum numbers $\{\kappa, m\}$ we have a pair of modes that are no longer trivially related. However since the rotating BHs we consider are stationary and axisymmetric, they have the symmetry $(t, \psi) \to (-t, -\psi)$ and thus we can focus our attention only on modes with $m \geq 0$, say. Indeed there are two family of modes for each m, one with $\mathrm{Re}(\omega) > 0$ and the other with $\mathrm{Re}(\omega) < 0$. It follows from the (t, ψ) symmetry that modes with negative azimuthal number $-m$ just trade the sign of the frequencies of the $m > 0$ modes.

Secondly, we will be primarily interested in instabilities, as they are by far

[12] Two comments are in order. Firstly, it has been shown by Kol that constraint-free gauge invariant variables can always be constructed from linearised perturbations of cohomogeneity-1 spacetimes [49]. Rather than working with these variables we find it more convenient to impose the gauge directly. Secondly, master variables have been successfully defined for these EAM-MP BHs in the special case of $d = 5$ by using a decomposition different from ours [25].

the most important perturbations. By definition (see the discussion at the end of Sec. 3.3.2 above) unstable modes have lower overtone than stable modes. Therefore we will mostly be interested in the lowest (unstable) overtone.

Lastly, the numerical methods used are the same as in Sec. 3.3, but adjusted to allow for coupled ODE's rather than a single ODE. Once again a compactified radial coordinate $\hat{r} = r_+/z$ is used, and the grid is Chebyshev, as before. Here we omit a detailed description of the boundary conditions. They are still determined by the physical condition of being ingoing at the horizon and outgoing at infinity, but the exact form they take depends on the perturbation sector, the dimension, and the $\mathbb{CP}^N$ quantum numbers. The reason for the perhaps unexpected dependence on these last two quantities is due to the fact that for certain dimensions and quantum numbers various $\mathbb{CP}^N$ harmonics vanish. For example, in $N = 1$, $\mathbb{S}^{+-} = 0$ and in all N, $\mathbb{S}^{++} = 0$ for $\kappa = 1$, $m > 0$. We refer the interested reader to Ref. [23] for a discussion of boundary conditions that can easily be adapted to specific cases.

Scalar modes

The scalar sector of perturbations is again the most complicated, involving the largest number of perturbation functions. Recall that charged scalar harmonics on $\mathbb{CP}^N$ are characterized by two integers, (κ, m). Axisymmetric modes ($m = 0$) were first studied in [23] where it was found that the $(2, 0)$ mode was ultraspinning unstable for odd $d \geq 7$ (see footnote 2). Ref. [5] studied scalar perturbations for $m \neq 0$ where a bar-mode instability was found for the $(0, m)$ mode for $m \geq 2$.

Ref. [23] first found the axisymmetric, ultraspinning instability by studying

the related problem of the Gregory-Laflamme instability for these rotating BHs. It was expected that the instability would produce a zero mode at the threshold of instability, i.e. $\omega = 0$, and that for larger rotations it would take the form $\omega = iK(a)$, with $K(a)$ a positive an increasing function of the rotation a. The approach of [23] only allowed for the determination of ω at and above the threshold of instability. However, our methods allow us to follow this mode all the way down to zero rotation and find its Schwarzschild limit. This is shown in Fig. 3.9 in which the QNM frequency associated with the $(2, 0)$ ultraspinning instability is plotted for $d = 11$ and $d = 13$ [13]. Interestingly, we find that ω is always purely imaginary and, at zero rotation, this mode connects to a Schwarzschild vector mode with $\widetilde{\ell}_V = 3$.

Next we consider the bar-mode instability. In Fig.'s 3.10, 3.11, and 3.12 we plot the real and imaginary parts of the dominantly unstable bar-mode[14] for the $(0, m)$ mode for $m = 2, 3, 4$. The $(0, 2)$ mode is unstable for $d \geq 7$, while the $(0, 3)$ and $(0, 4)$ modes are unstable for $d \geq 9$. Of all the bar-mode instabilities found, the $(0, 2)$ mode is most unstable, i.e. it has the largest growth rate, $\mathrm{Im}(\omega)$. These bar-modes connect to Schwarzschild scalar modes with $\widetilde{\ell}_S = 2$ at zero rotation.

To conclude our investigation of the scalar sector, in Fig. 3.13 we plot the dominant QNM for the $(\kappa, m) = (1, 1)$ sector. Here we find instabilities for $d \geq 9$. These modes connect to the Schwarzschild vector mode with $\widetilde{\ell}_V = 5$ at zero rotation. Of course there are an infinite number of modes we have omitted, but

[13] We could of course study other dimensions quite easily in principle, but oddly it becomes numerically difficult to isolate this mode for smaller values of d, although it is undoubtedly present.

[14] By dominantly unstable we mean the frequency with the largest value of $\mathrm{Im}(\omega)$, considered as function of the rotation. Here we stress that as the rotation is tuned, the QNM frequencies can cross, and we are plotting the modes which attain the largest $\mathrm{Im}(\omega)$ for all a.

it's quite reasonable that the physical importance of these will be subdominant to the modes studied here. In Table 3.1 we list the critical rotations for the instabilities studied.

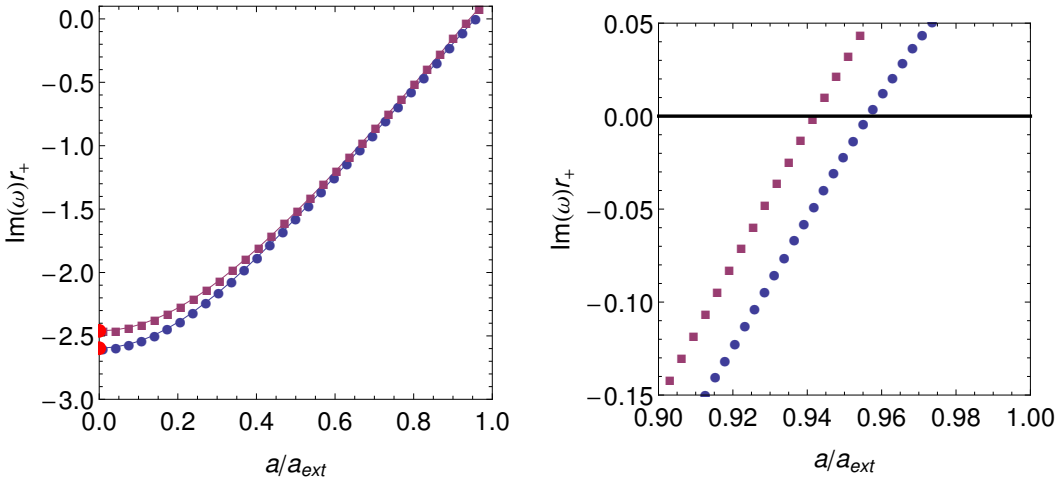

Figure 3.9: **EAM MP.** Left Panel: The purely imaginary $(2,0)$ frequency for $d = 11$ (circles) and $d = 13$ (squares). The large dots at $a = 0$ correspond to a Schwarzschild vector modes with $\tilde{\ell}_V = 3$. Right Panel: A zoomed in plot showing the modes crossing the instability threshold.

A very important quantity for non-axisymmetric modes is the so-called superradiant factor, $\varpi = \mathrm{Re}(\omega) - m\Omega_H$. The energy flux through the horizon is proportional to this factor. When it is negative, the energy flux across the horizon is negative and the perturbation is said to be *superradiant*. The first law, applied to a process that extracts the energy $\delta E = -\mathrm{Re}(\omega)$ and the angular momentum $\delta J = -m$ to the BH, yields that the change in horizon area is controlled by ϖ: $\delta A_H \propto [m\Omega_H - \mathrm{Re}(\omega)] = -\varpi$. Therefore, the second law, $\delta A_H \geq 0$, requires that any unstable mode (whose growth rate is sourced by energy and momenta ex-

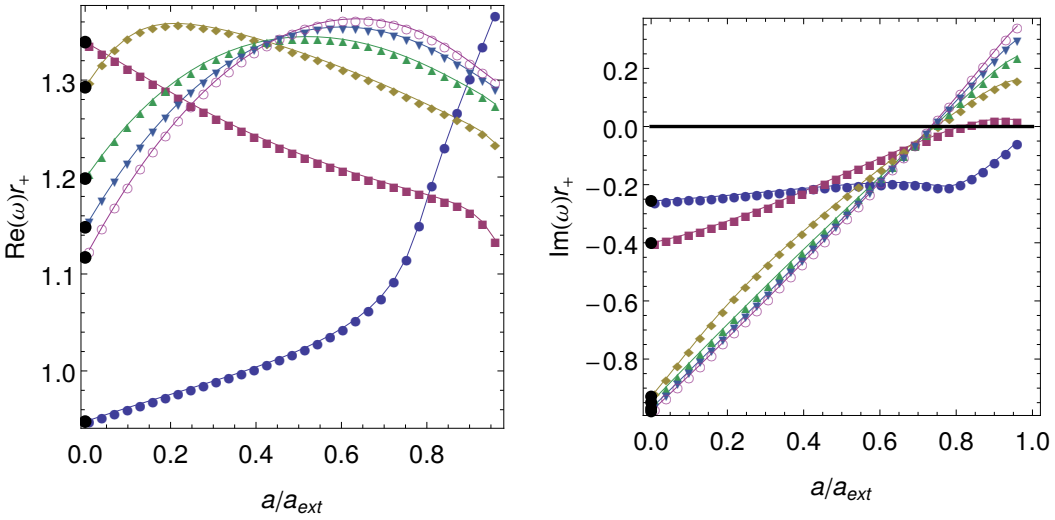

Figure 3.10: **EAM MP.** Real (left panel) and imaginary (right panel) parts of the QNM frequency for the $(0,2)$ scalar mode for $d=5$ (filled-in circles), $d=7$ (filled-in squares), $d=9$ (filled-in diamonds), $d=11$ (filled-in triangles), $d=13$ (filled-in upside-down triangles), and $d=15$ (open circles). For zero rotation the frequencies reduce to the $\ell_S=2$ scalar modes of Schwarzschild, which are depicted by large black dots. These were calculated using a separate code based on the KI master equation.

tracted from the BH) must satisfy $\varpi \leq 0$. We have explicitly checked that $\varpi < 0$ for the non-axisymmetric bar-mode instabilities we found numerically. Note that these modes have $\mathrm{Im}(\omega) > 0$ and $m \neq 0$, so in a non-linear time evolution the system will have to radiate since the associated linear mode breaks axisymmetry.

Vector modes

Since $\mathbb{CP}^N$ charged vector harmonics only exist for $N \geq 2$, vector perturbations only exist for $d \geq 7$. In order to study these perturbations, the spectrum of charged vector harmonics is needed. For $N=2$ we derived this in Appendix 3.A. For all other N, the result is only known for uncharged ($m=0$) harmonics.

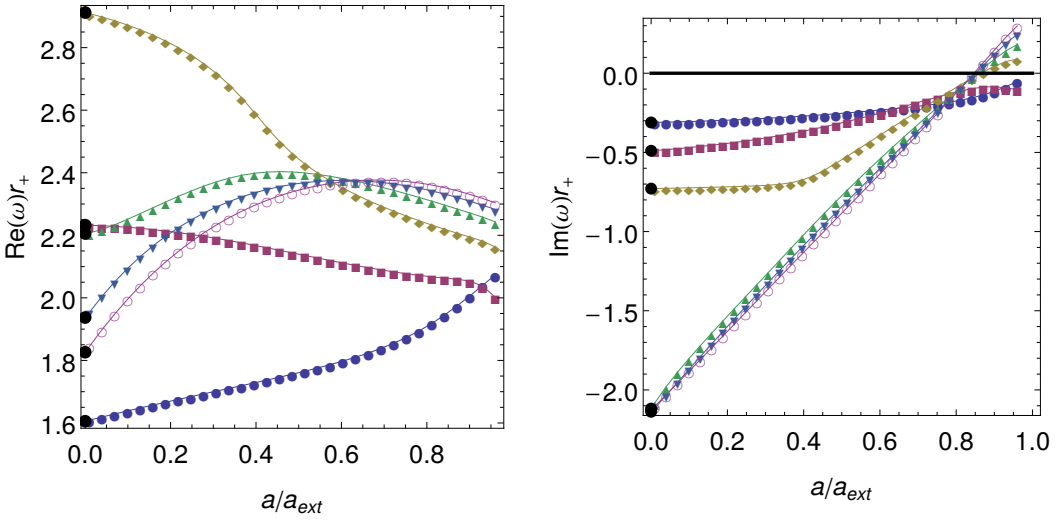

Figure 3.11: **EAM MP.** Real (left panel) and imaginary (right panel) parts of the QNM frequency for the $(0,3)$ scalar mode for $d=5$ (filled-in circles), $d=7$ (filled-in squares), $d=9$ (filled-in diamonds), $d=11$ (filled-in triangles), $d=13$ (filled-in upside-down triangles), and $d=15$ (open circles). For zero rotation the frequencies reduce to the $\ell_S=3$ scalar modes of Schwarzschild, which are depicted by large black dots. These were calculated using a separate code based on the KI master equation.

Therefore, we are able to exhaustively study vector perturbations only in $d=7$. We also studied axisymmetric perturbations for $d=9,11,13,15$. In no cases were instabilities found.

We now present our results for $d=7$. Since there are no special modes to single out, i.e. ones that become unstable, in Fig. 3.14 we plot the complex QNM frequencies for some of the $d=7$ vector modes. Here we need to be careful. Using our explicit construction of the charged vector harmonics, we can verify that for $\kappa=0$, one or both vector-derived tensors vanish (recall this also happened for the scalar perturbations). To discuss this, it is useful to introduce the parameter $\alpha=2+m\epsilon$. For $\alpha=0$, both vector-derived tensors vanish. For $\alpha>0, \epsilon=\pm 1$,

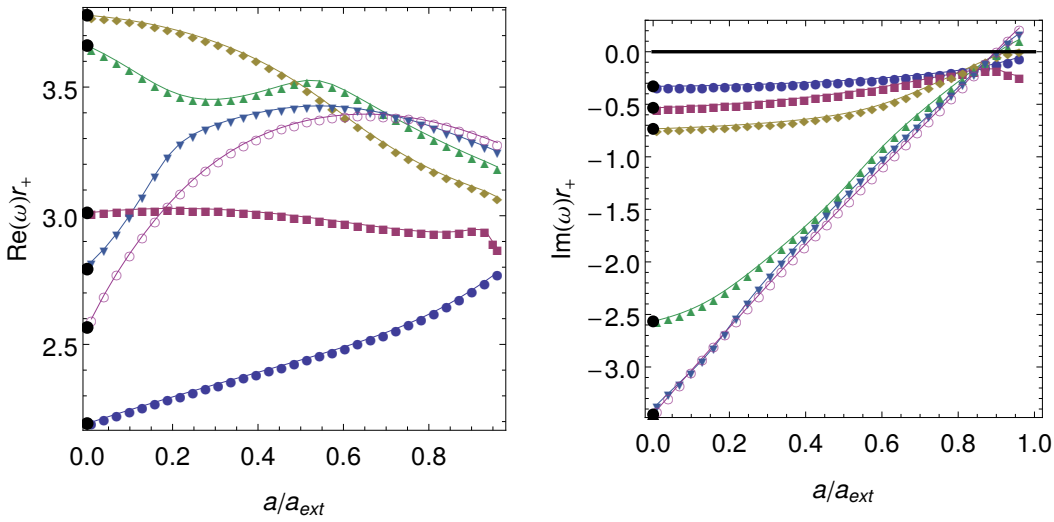

Figure 3.12: **EAM MP.** Real (left panel) and imaginary (right panel) parts of the QNM frequency for the $(0,4)$ scalar mode for $d=5$ (filled-in circles), $d=7$ (filled-in squares), $d=9$ (filled-in diamonds), $d=11$ (filled-in triangles), $d=13$ (filled-in upside-down triangles), and $d=15$ (open circles). For zero rotation the frequencies reduce to the $\widetilde{\ell}_S=4$ scalar modes of Schwarzschild, which are depicted by large black dots. These were calculated using a separate code based on the KI master equation.

$V^{\pm}=0$, and for $\alpha<0, \epsilon=\pm 1$, $V^{\mp}=0$.

3.4.4 Unstable black holes in the large-d Limit

The large range of dimensions studied in this section allows for some interesting observations concerning the large-d limit. As the dimension grows, it seems like some of the QNM frequencies are approaching limiting values. In particular, the critical rotation seems to approach a limiting value. This motivates a connection with the saturating Schwarzschild modes, discussed in Sec. 3.3. In Fig. 3.16 we plot in black both the low-lying $\widetilde{\ell}_S=2$ saturating and scaling QNM curves of

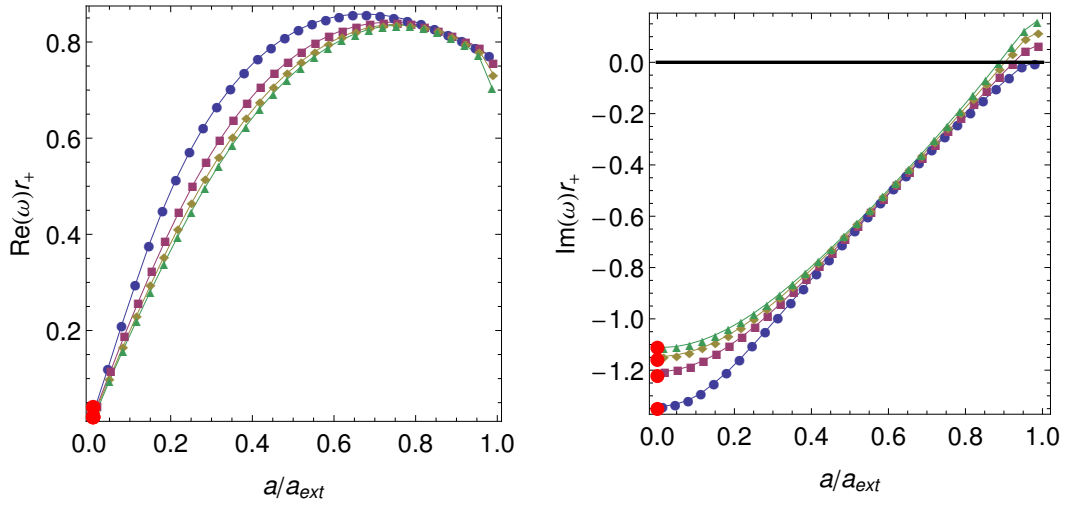

Figure 3.13: **EAM MP.** Real (left panel) and imaginary (right panel) parts of the QNM frequency for the $(1,1)$ scalar mode for $d = 7$ (circles), $d = 9$ (squares), $d = 11$ (diamonds), and $d = 13$ (triangles). For zero rotation the frequencies reduce to $\widetilde{\ell}_V = 5$ vector modes of Schwarzschild, which are depicted by red dots. These were calculated using a separate code based on the KI master equation.

the Schwarzschild solution in the complex ω plane. On top of this we also show, in color, the complex frequencies associated with the $(\kappa, m) = (0, 2)$ bar-mode instability for equal angular momenta MP BHs. For $d = 5, 7$, the MP curves connect to the scaling Schwarzschild mode but, for $d = 9, 11, 13, 15$, they connect to the saturating Schwarzschild mode. Similar results hold for the other instabilities found. In particular, the $(0, m)$ bar-modes connect to the saturating Schwarzschild scalars with $\widetilde{\ell}_S = m$, and, for large enough dimension, the $(\kappa, m) = (2, 0)$ ultraspinning mode connects to the saturating Schwarzschild vector mode with $\widetilde{\ell}_V = 3$. We expect the $(\kappa, m) = (1, 1)$ instability to connect to a saturating vector for $\widetilde{\ell}_V = 5$, but we have not verified this, since as $\widetilde{\ell}$ increases it takes larger d values to see the

d	$(2,0)$	$(0,2)$	$(0,3)$	$(0,4)$	$(1,1)$
7	0.99998	0.8109	stable	stable	stable
9	0.9979	0.7463	0.8644	0.9291	0.9252
11	0.9921	0.7413	0.8547	0.9052	0.9024
13	0.9850	0.7369	0.8504	0.9011	0.8873
15	0.9777	0.7331	0.8464	0.8973	–

Table 3.1: Critical rotation $a_c/a_{\rm ext}$ at which the instabilities set in for (κ, m) scalar sector of perturbations. $d = 5$ is linearly stable. Dashes indicate modes for which no data exists. The $(2,0)$ data is taken from [23], [24]. In the dimensions where we independently have data for the $(2,0)$ mode we agree with [23], [24] to within a few percent.

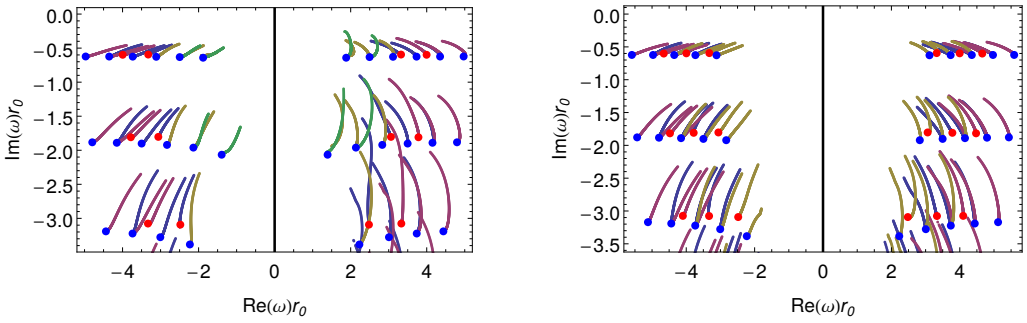

Figure 3.14: **EAM MP.** Left Panel: $\kappa = 0$ vector QNM frequencies for $(m, \epsilon) = (1,1)$ (magenta), $(2,1)$ (blue), $(1,-1)$ (yellow), $(2,-1)$ (green). Right Panel: $\kappa = 1$ vector QNM frequencies for $m = 0$ (magenta), and $(m, \epsilon) = (1,1)$ (blue), $(1,-1)$ (yellow). At zero rotation the curves connect to Schwarzschild vector modes (red dots) and tensor modes (blue dots) of various $\tilde{\ell}$ values. The first few overtones of each harmonic (labelled by (κ, m, ϵ)) are shown.

QNM begin to saturate. To summarize, it seems that in all cases we can study, the instabilities of these MP BHs, for sufficiently large d, can be connected to saturating Schwarzschild modes in the zero rotation limit.

Thus, we see that the existence of saturating modes in the Schwarzschild geometry seems to be essential to allow for instabilities of rotating BHs for arbitrarily

large-d. Indeed, if there were no such saturating modes, then an unstable mode of a large-d MP BH would necessarily start off far from the origin in the complex plane, and would need to move a large distance in order to become unstable for a finite value of the rotation. This seems particularly unlikely for the equal angular momenta case as the rotation cannot be taken arbitrarily large. Therefore, any instability of equal angular momenta MP BHs that persists for arbitrarily large-d is very likely connected to a saturating Schwarzschild mode. One of the motivations for studying the equal angular momenta case was the expectation that it might be representative of generic MP BHs which have no vanishing angular momenta. These BHs also have an upper bound on the rotations, and are likely to suffer from instabilities similar to the equal angular momenta BHs. Therefore, we conjecture that, for sufficiently large-d, all unstable modes of MP BHs with no vanishing angular momenta are connected to saturating Schwarzschild modes in the zero rotation limit.

Next, we discuss a second interesting feature of large-d unstable BHs. Above we remarked that any unstable modes must satisfy $\varpi \leq 0$. Suppose that both ϖ and $\mathrm{Im}(\omega)$ cross zero at the same critical rotation for some bar-mode instability (so with $m \neq 0$). This is a particularly interesting possibility because then we exactly have $\omega = m\Omega_H$ at the threshold of the instability, and although the perturbation breaks the t, ψ-translational symmetries, it is invariant under the horizon-generating Killing field, $K = \partial_t + \Omega_H \partial_\psi$. This is not an academic assumption since it actually happens for superradiant instabilities in the Kerr-AdS BH, and it signals the existence of a new family of BHs that are neither axisymmetric nor time independent, but are invariant under the linear combination K

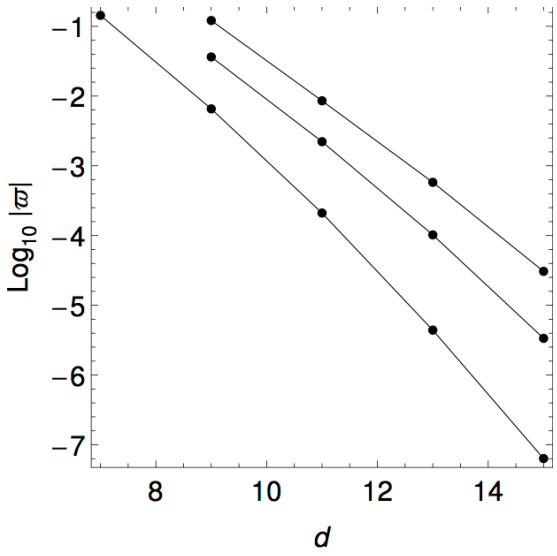

Figure 3.15: **EAM MP.** The logarithm of the absolute value of the superradiant factor for the scalar (0,2) mode (bottom curve), (0,3) mode (middle curve), and (0,4) mode (top curve), plotted as a function of d.

(see [30, 4] and references therein). It is thus interesting to investigate whether or not this is also the case for the asymptotically flat bar-mode instabilities, i.e. if $\omega = m\Omega_H$ when $\mathrm{Im}(\omega) = 0$ in the MP BHs. In Fig. 3.15 we plot $\log_{10}(-\varpi)$ at the threshold of the instability (where $\mathrm{Im}(\omega) = 0$) for the $(0, m)$ bar-modes studied [15]. Interestingly, it appears that as the dimension increases, this factor quickly goes to zero [16]. This agrees with analytic results for the large-d limit of the $m-$bar instability [44]. Thus, in analogy with the single Killing field BHs that have been conjectured to exist in AdS [4], it seems like large-d asymptotically flat BHs only approximately allow for such solutions, with the approximation becoming better as d increases.

[15] The negative of the superradiant factor is considered because by the area law one must have $\varpi \leq 0$ at the threshold.

[16] We do not observe a similar trend for the other bar-mode instability studied, the $(1, 1)$ mode. It could be that such an effect is not present for this mode, or it could be that it is, and we simply don't have data for large enough dimensions to observe it.

In Sec. 3.3 saturating QNMs of Schwarzschild were studied, and the existence of these modes supported the idea that gravity in the large-d limit still retains some very interesting features. The results of this section further support this interpretation, as we have seen that some of the most interesting physics of rotating BHs, namely linearly instabilities, survives the large-d limit.

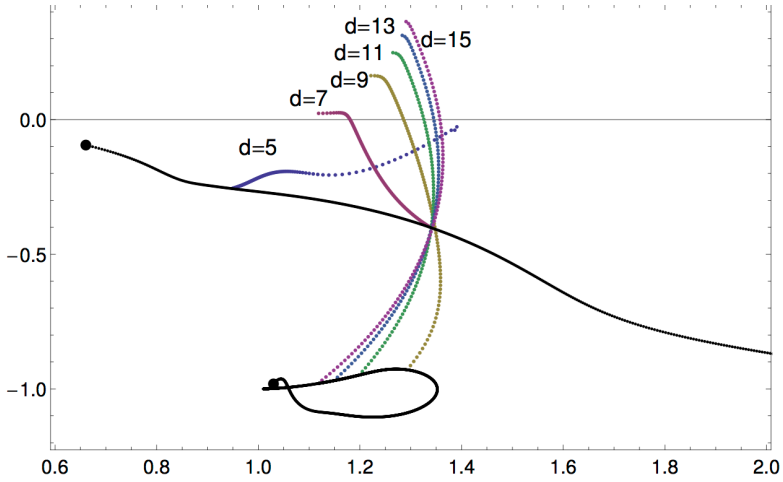

Figure 3.16: **EAM MP.** The QNM frequency ω in the complex plane for different BHs. The curves in black represent the $\widetilde{\ell}_S = 2$ Schwarzschild frequencies (the smallest d is indicated with a large dot. The dimension then increases along the curves). The top and bottom curves correspond to the scaling and saturating modes discussed in Sec. 3.3, respectively. The coloured curves correspond to the $(0, 2)$ scalar frequencies for equal angular momenta MP BHs. At zero rotation the MP frequencies agree with the Schwarzschild modes, and as the rotation increases the frequencies move upwards in the complex plane, becoming unstable for $d \geq 7$. For $d = 5, 7$, the MP curves connect to the scaling Schwarzschild mode, while for $d \geq 9$ they connect to the saturating mode.

3.5 Singly Spinning MP black holes

The singly spinning MP BH can be written as direct sum of the metrics of a 4-dimensional orbit space $g_{AB}\left(x^C\right)$, with $A, B, C = \{t, r, \widetilde{x}, \phi\}$, and spherical

fibres:

$$ds^2 = g_{\mu\nu}dx^\mu dx^\nu = g_{AB}\left(x^C\right)dx^A dx^B + R^2\left(x^C\right)d\Omega^2_{d-4}, \tag{3.47}$$

where $R = r\widetilde{x}$ and $d\Omega^2_{d-4} = \gamma_{i,j}d\hat{x}^i d\hat{x}^j$ is the line element of a unit-radius $(d-4)$-sphere (we will use small latin indices i, j to describe the coordinates on the sphere). We can decompose perturbations on this background according to how they transform under diffeomorphisms of the sphere S^{d-4}. More concretely, an arbitrary metric perturbation $h_{\mu\nu}$ can be decomposed into perturbations of scalar, transverse vector, and transverse traceless tensor types on S^{d-4}.[17] Ref. [42] studied in detail the tensor sector of perturbations. They found no instability in this sector and computed its QNM frequencies. We will have nothing to add to this tensor sector analysis. Our aim in this subsection is to study the spectrum of QNMs and instabilities in the scalar and vector sectors since this study is missing. We are particularly motivated by the fact that two known instabilities of the MP BH, namely the bar-mode [20, 28, 29] and ultraspinning [20, 26, 40] instabilities are precisely in the scalar sector of perturbations.

We briefly summarize the novel results that emerge from the study we do next. We will find the (most relevant, low-lying) scalar and vector QNMs of the singly spinning MP BH and will compute the timescale of the bar-mode instability that is present in $d \geq 6$. As a major result we find that the $d = 5$ singly spinning MP BH is linearly stable in the sense that we find no linear instability; in particular,

[17] Note that the KI formalism for the Schwarzschild BH of Section 3.3 uses the harmonic decomposition of perturbations on a S^{d-2} sphere [31], while in the singly spinning MP background of this Section we will use a harmonic decomposition with respect to S^{d-4}. To distinguish the different dimensionality of these two families of harmonics we will use a different notation, i.e. $\mathbf{S}, \mathbf{V}_{\underline{a}}, \mathbf{T}_{\underline{ab}}$ and ℓ_S, ℓ_V, ℓ_T for the decomposition on the S^{d-4} instead of the notation S, V_a, T_{ab} and $\widetilde{\ell}_S, \widetilde{\ell}_V, \widetilde{\ell}_T$ employed in the S^{d-2} decomposition.

we find that it does not have a linear bar-mode instability (a bar-mode instability was reported to be present also in the $d = 5$ BH in the time evolution study of [28, 29]).

Technically, we find convenient to introduce the dimensioneless rotational parameter α and new coordinates $\{T, y, x, x^i\}$ related to the standard coordinates $\{t, r, \widetilde{x}, x^i\}$ as

$$\alpha = a/r_+\,; \qquad t = r_+ T\,, \qquad r = \frac{r_+}{1-y^2}\,, \qquad \widetilde{x} = x\sqrt{2-x^2}, \tag{3.48}$$

where y is a compact radial coordinate, $0 \leq y \leq 1$, with horizon at $y = 0$ and asymptotic spatial infinity at $y = 1$, and the new polar coordinate x ranges between $0 \leq x \leq 1$. With these new coordinates g_{tt} and $g_{\phi\phi}$ vanish quadratically as y^2 and $(1-x^2)^2$ at the horizon and pole, respectively, as they should at a bolt. Moreover, in this coordinate frame the boundary conditions will be much simpler. In these coordinates the geometry of the singly spinning MP BH reads

$$\begin{aligned} ds^2 = {} & \frac{\Delta_y \Sigma_y}{\rho_y}\, y^2 dT^2 + \frac{4\Sigma_y}{\left(1-y^2\right)^4 \Delta_y}\, dy^2 + \frac{4\Sigma_y}{\left(2-x^2\right)\left(1-y^2\right)^2}\, dx^2 \\ & + \frac{\left(1-x^2\right)^2 \rho_y}{\left(1-y^2\right)^2 \Sigma_y} \left(d\phi - \frac{\alpha\left(1-y^2\right)^2}{\rho_y} \left(\alpha^2 \left(1-y^2\right)^2 + 1 - y^2 \Delta_y \right) dT \right)^2 \\ & + \frac{x^2\left(2-x^2\right)}{\left(1-y^2\right)^2}\, d\Omega_{d-4}^2 \end{aligned} \tag{3.49}$$

where

$$\Delta_y = \frac{(1-y^2)^2}{y^2}\frac{\Delta(y)}{r_+^2}\,, \qquad \Sigma_y = \alpha^2 x^2\left(2-x^2\right)\left(1-y^2\right)^2+1\,,$$
$$\rho_y = \left[\alpha^2\left(1-y^2\right)^2+1\right]^2 - \alpha^2\left(1-x^2\right)^2\left(1-y^2\right)^2 y^2\Delta_y\,. \tag{3.50}$$

3.5.1 Scalar QNMs ($d \geq 5$). Bar-mode and ultraspinning instabilities

Scalar perturbations of the singly spinning MP background can be expanded in terms of a basis of scalar harmonic $\mathbf{S}$ on the unit sphere S^{d-4} that solve the eigenvalue equation (see footnote 17)

$$\left(\Box_{S^{d-4}} + \lambda_S\right)\mathbf{S} = 0\,, \tag{3.51}$$

where λ_S is the eigenvalue, and $\Box = D^i D_i$ with D being the derivative defined by the metric γ_{ij} of the base space S^{d-4}. Regularity of the scalar harmonics requires

$$\lambda_S = \ell_S\left(\ell_S + d - 5\right)\,, \qquad \text{with} \quad \ell_S = 0,1,2,\cdots\,. \tag{3.52}$$

Note that the angular base space is exactly a sphere. Therefore the perturbation equations and solutions are independent of the azimuthal quantum number of the $S^{(d-4)}$. They only depend on the quantum number ℓ_S that measures the number of nodes along the polar direction of the $S^{(d-4)}$. Out of this scalar harmonic we can construct a scalar-type vector harmonic $\mathbf{S}_i$ and a traceless scalar-type tensor

harmonic $\mathbf{S}_{ij}$ as

$$\mathbf{S}_i = -\frac{1}{\sqrt{\lambda_S}} D_i \mathbf{S}\,, \qquad \mathbf{S}_{ij} = \frac{1}{\lambda_S} D_i D_j \mathbf{S} + \frac{1}{d-4}\gamma_{ij}\mathbf{S}\,. \tag{3.53}$$

Scalar perturbations are then given by

$$h_{ab} = f_{ab} e^{-i\omega t} e^{im\phi}\mathbf{S}, \quad h_{ai} = f_a e^{-i\omega t} e^{im\phi}\mathbf{S}_i, \quad h_{ij} = e^{-i\omega t} e^{im\phi}\left(H_L \gamma_{ij}\mathbf{S} + H_T \mathbf{S}_{ij}\right) \tag{3.54}$$

with f_{ab}, f_a, H_T, H_L functions of $\{r, \widetilde{x}\}$, and we used the fact that ∂_t and ∂_ϕ are Killing vector fields of the background to do a Fourier decomposition along these directions.

We will restrict our analysis to s-wave modes, i.e. modes with $\ell_S = 0$, which effectively means that we set $f_a = 0 = H_T$. This considerably reduces the computational cost of our task since we "just" have to solve a coupled PDE system of ten equations for ten variables f_{ab}, H_L; a task that is itself already hard even numerically. Moreover, the most interesting properties of the scalar perturbations, namely the bar-mode and ultraspinning instabilities, are precisely in this s-wave sector.

In the sequel we describe the procedure we find most tractable to solve the technical problem at hand. We find convenient to introduce the tetrad basis

$$\begin{aligned} e^{(1)} &= dt - \alpha\left(1-x^2\right)^2 d\phi\,, \qquad e^{(2)} = dy\,, \qquad e^{(3)} = dx\,, \\ e^{(4)} &= -\alpha\left(1-y^2\right)^2 dt + \left[1+\alpha^2\left(1-y^2\right)^2\right] d\phi\,, \qquad e^{(i)} = \hat{e}^i\,, \end{aligned} \tag{3.55}$$

where $\hat{e}^i$ are a vielbein for the metric $d\Omega^2_{(d-4)}$ of the unit-radius $(d-4)$-sphere.

This basis has a diagonal metric (with elements that are not equal to unity) and considerably simplifies the computations. The most general scalar perturbation has eleven non-vanishing tetrad components namely, $e^{-i\omega t}e^{im\phi}h_{(a)(b)}$, with $a, b = 1, 2, 3, 4$ and $h_{(i)(i)} = e^{-i\omega t}e^{im\phi}h_{(\Omega)(\Omega)}$ for $i = 5, \cdots d$. Since h is a symmetric tensor this gives a total of 11 unknown functions.

We choose to work in the traceless-transverse (TT) gauge,

$$h^{(a)}{}_{(a)} = 0\,, \qquad \nabla^{(a)}h_{(a)(b)} = 0\,. \tag{3.56}$$

In this gauge the linearised Einstein equations read

$$(\Delta_L h)_{(a)(b)} \equiv -\nabla_{(c)}\nabla^{(c)}h_{(a)(b)} - 2\,R_{(a)}{}^{(c)}{}_{(b)}{}^{(d)}h_{(c)(d)} = 0\,, \tag{3.57}$$

where Δ_L is the Lichnerowicz operator and R the Riemann tensor.

The traceless condition can immediately be used to eliminate $h_{(\Omega)(\Omega)}$ since it can be written as an algebraic relation as a function of $\{h_{(1)(1)}, h_{(2)(2)}, h_{(3)(3)}, h_{(4)(4)}\}$. The transverse conditions give algebraic relations that could be used to eliminate further variables but we find that this yields complicated equations of motion that increase the numerical error in our computations. Instead we identify the following system of PDEs

$$\begin{aligned}
&(\Delta_L h)_{(1)(3)} = 0\,, \qquad (\Delta_L h)_{(2)(2)} = 0\,, \qquad (\Delta_L h)_{(2)(3)} = 0\,,\\
&(\Delta_L h)_{(2)(4)} = 0\,, \qquad (\Delta_L h)_{(3)(3)} = 0\,, \qquad (\Delta_L h)_{(3)(4)} = 0\,,\\
&\nabla^{(a)}h_{(a)(1)} = 0\,, \qquad \nabla^{(a)}h_{(a)(2)} = 0\,, \qquad \nabla^{(a)}h_{(a)(3)} = 0\,, \quad \nabla^{(a)}h_{(a)(4)} = 0\,,
\end{aligned} \tag{3.58}$$

which give a system of 10 independent equations to solve for the 10 independent variables $h_{(a)(b)}$, with $a, b = 1, 2, 3, 4$. Note that we have explicitly checked that this system of 10 equations closes the Lichnerowicz system, i.e. that the equations (3.58) imply that the remaining equations in (3.57) are also obeyed.

Boundary conditions

To discuss the boundary conditions (BCs) on the future event horizon $\mathcal{H}^+$ we introduce the ingoing Eddington-Finkelstein (EF) coordinates $\{v, \widetilde{\phi}\}$ that are regular at $\mathcal{H}^+$

$$dT = dv - \frac{2\left(1+\alpha^2\left(1-y^2\right)^2\right)}{y\left(1-y^2\right)^2\Delta_y}\,dy\,, \qquad d\phi = d\widetilde{\phi} - \frac{2\alpha}{y\Delta_y}\,dy\,. \tag{3.59}$$

The BC at the future horizon requires that the metric components $h_{(a)(b)}$ are smooth functions of the ingoing EF coordinates $\{v, y, x, \widetilde{\phi}, x^i\}$ at $y = 0$. This requires the BCs

$$\begin{aligned}
&h_{(1)(1)}\big|_{y=0} \sim y^{-2\,i\,\frac{\omega-m\Omega_H}{4\pi T_H}} H_{11}(x)\,, \qquad h_{(1)(2)}\big|_{y=0} \sim y^{-2\,i\,\frac{\omega-m\Omega_H}{4\pi T_H}-1} H_{12}(x)\,,\\
&h_{(1)(3)}\big|_{y=0} \sim y^{-2\,i\,\frac{\omega-m\Omega_H}{4\pi T_H}} H_{13}(x)\,, \qquad h_{(1)(4)}\big|_{y=0} \sim y^{-2\,i\,\frac{\omega-m\Omega_H}{4\pi T_H}} H_{14}(x)\,,\\
&h_{(2)(2)}\big|_{y=0} \sim y^{-2\,i\,\frac{\omega-m\Omega_H}{4\pi T_H}-2} H_{22}(x)\,, \qquad h_{(2)(3)}\big|_{y=0} \sim y^{-2\,i\,\frac{\omega-m\Omega_H}{4\pi T_H}-1} H_{23}(x)\,,\\
&h_{(2)(4)}\big|_{y=0} \sim y^{-2\,i\,\frac{\omega-m\Omega_H}{4\pi T_H}-1} H_{24}(x)\,, \qquad h_{(3)(3)}\big|_{y=0} \sim y^{-2\,i\,\frac{\omega-m\Omega_H}{4\pi T_H}} H_{33}(x)\,,\\
&h_{(3)(4)}\big|_{y=0} \sim y^{-2\,i\,\frac{\omega-m\Omega_H}{4\pi T_H}-1} H_{34}(x)\,, \qquad h_{(4)(4)}\big|_{y=0} \sim y^{-2\,i\,\frac{\omega-m\Omega_H}{4\pi T_H}} H_{44}(x)
\end{aligned} \tag{3.60}$$

where $H_{ab}(x)$ are smooth functions of x.

At spatial infinity, $y \to 1$, i.e. $r \to \infty$, we demand that the perturbations

preserve the asymptotic flatness of the spacetime. This means that they must decay strictly faster than the asymptotic Minkowski background asymptotic. In this asymptotic region, the Lichnerowicz equation (3.57) reduces to $\Box h_{(a)(b)} = 0$. We would like to solve this system to find the exact decay of the asymptotic solutions. *À priori* this is a hard task since, in the spherical coordinate system we work, the non-vanishing connections in the differential operator means that we have a coupled system of 10 differential equations to solve for. However, we can make our life considerably easier and get the desired result by solving a single ODE. The procedure is the following. Consider Minkowski spacetime and the perturbation components h'_{ab} in Cartesian coordinates. In these conditions the affine connection vanishes and $\Box h'_{ab} = 0$ reduces simply to $\partial_c \partial^c h'_{ab} = 0$. A Fourier decomposition in the time direction, $h'_{ab} = e^{-i\omega t} h'_{ab}$ allows to write it as $\nabla^2 h'_{ab} = -\omega^2 h'_{ab}$. Using the spherical harmonic decomposition of the perturbation $h'_{ab} = h'_{ab}(r) Y_\ell(x)$ and writing the spatial operator in spherical coordinates this equation reads

$$\frac{1}{r^{d-2}}\,\partial_r\left(r^{d-2}\partial_r h'_{ab}\right) + \frac{\ell(\ell+d-3)}{r^{d-2}}\,h'_{ab} = -\omega^2 h'_{ab}. \tag{3.61}$$

Near spatial infinity, h'_{ab} behaves as $h'_{ab}\big|_{r\to\infty} \sim C_{in}\, r^{-\frac{d-2}{2}}\, e^{-i\omega r} + C_{out}\, r^{-\frac{d-2}{2}}\, e^{i\omega r}$ where the amplitudes $\{C_{in}, C_{out}\}$ are a function of $\{A, B\}$. Asymptotically we want outgoing waves so we impose the BC $C_{in} = 0$. We conclude that all the Cartesian components of the perturbation must decay asymptotically as $h'_{ab} \sim r^{-\frac{d-2}{2}} e^{i\omega r}$ in order to have outgoing BCs that preserve the asymptotic Minkowski structure of the spacetime. We can now apply a coordinate transformation from

Cartesian to our spherical coordinates $\{t, y, x, \phi, x_{S^{d-4}}\}$ to find the decays of $h_{(a)(b)}$ in the spherical frame. In this process we keep in mind that we are interested only in scalar perturbations so we do not consider the vector contributions here. We find that scalar perturbations with asymptotically Minkowski outgoing BCs behave as:

$$
\begin{aligned}
h_{(1)(1)}\big|_{y=1} &\sim \left(1-y^2\right)^{\frac{d-2}{2}} e^{\frac{i\omega}{1-y^2}} H_{11}(x)\,, \qquad (3.62)\\
h_{(1)(2)}\big|_{y=1} &\sim \left(1-y^2\right)^{\frac{d-2}{2}-2} e^{\frac{i\omega}{1-y^2}} H_{12}(x)\,,\\
h_{(1)(3)}\big|_{y=1} &\sim \left(1-y^2\right)^{\frac{d-2}{2}-1} e^{\frac{i\omega}{1-y^2}} H_{13}(x)\,,\\
h_{(1)(4)}\big|_{y=1} &\sim \left(1-y^2\right)^{\frac{d-2}{2}-1} e^{\frac{i\omega}{1-y^2}} H_{14}(x)\,,\\
h_{(2)(2)}\big|_{y=1} &\sim \left(1-y^2\right)^{\frac{d-2}{2}-4} e^{\frac{i\omega}{1-y^2}} H_{22}(x)\,,\\
h_{(2)(3)}\big|_{y=1} &\sim \left(1-y^2\right)^{\frac{d-2}{2}-3} e^{\frac{i\omega}{1-y^2}} H_{23}(x)\,,\\
h_{(2)(4)}\big|_{y=1} &\sim \left(1-y^2\right)^{\frac{d-2}{2}-3} e^{\frac{i\omega}{1-y^2}} H_{24}(x)\,,\\
h_{(3)(3)}\big|_{y=1} &\sim \left(1-y^2\right)^{\frac{d-2}{2}-2} e^{\frac{i\omega}{1-y^2}} H_{33}(x)\,,\\
h_{(3)(4)}\big|_{y=1} &\sim \left(1-y^2\right)^{\frac{d-2}{2}-2} e^{\frac{i\omega}{1-y^2}} H_{34}(x)\,,\\
h_{(4)(4)}\big|_{y=1} &\sim \left(1-y^2\right)^{\frac{d-2}{2}-2} e^{\frac{i\omega}{1-y^2}} H_{44}(x)\,,
\end{aligned}
$$

(3.63)

where $H_{ab}(x)$ are smooth functions of x.

To find the BCs at the equator, $x = 0$ where $g_{\Omega\Omega} \to 0$, we require that the metric perturbation $h_{ab}dx^a dx^b$ is a regular symmetric 2-tensor when expressed in coordinates where the background metric is regular. A procedure similar to the

one described in detail in Section 3.3 of [40] yields that smooth BCs at $x = 0$ require that

$$\begin{aligned} &h_{(a)(b)}\big|_{x=0} \sim x H_{ab}(y)\,, \quad \text{for} \quad (a)(b) = \{(1)(3),(2)(3),(3)(4)\}; \\ &h_{(a)(b)}\big|_{x=0} \sim H_{ab}(y), \quad \text{otherwise} \end{aligned} \tag{3.64}$$

where $H_{ab}(y)$ are smooth functions of y.

Finally we discuss the BCs that the metric perturbations must satisfy at the axis of rotation, $x = 1$, where ∂_ϕ vanishes. Near $x = 1$, a generic component of the metric behaves as $h_{(a)(b)} = (1-x)^{\beta_j} h_{(a)(b)}(y)$ for some constant β_j that generically is a function of the azimuthal quantum number m associated with the Killing field ∂_ϕ. Our task is to find the ten β_j's that yield smooth perturbations at $x = 1$. These can be determining introducing the Cartesian coordinates $\{X, Y\}$ as $\rho \equiv 1-x = \sqrt{X^2+Y^2}$ and $\phi = \text{ArcTan}\,(Y/X)$ and then requiring the absence of non-analytical or divergent contributions (e.g. of the type $\sqrt{X^2+Y^2}$ or $(X \pm i\,Y)^{-1}$) on each component of the metric perturbation in this frame. This requires the BCs at $x = 1$:

$$\begin{aligned} &h_{(1)(1)}\big|_{x=1} \sim (1-x)^m\, H_{11}(y)\,, \qquad h_{(1)(2)}\big|_{x=1} \sim (1-x)^m\, H_{12}(y)\,, \\ &h_{(1)(3)}\big|_{x=1} \sim (1-x)^{m-1}\, H_{13}(y)\,, \qquad h_{(1)(4)}\big|_{x=1} \sim (1-x)^m\, H_{14}(y)\,, \\ &h_{(2)(2)}\big|_{x=1} \sim (1-x)^m\, H_{22}(y)\,, \qquad h_{(2)(3)}\big|_{x=1} \sim (1-x)^{m-1}\, H_{23}(y)\,, \\ &h_{(2)(4)}\big|_{x=1} \sim (1-x)^m\, H_{24}(y)\,, \qquad h_{(3)(3)}\big|_{x=1} \sim (1-x)^{\beta_1}\, H_{33}(y)\,, \\ &h_{(3)(4)}\big|_{x=1} \sim (1-x)^{\beta_2}\, H_{34}(y)\,, \qquad h_{(4)(4)}\big|_{x=1} \sim (1-x)^{\beta_3}\, H_{44}(y)\,, \end{aligned} \tag{3.65}$$

where $H_{ab}(y)$ are smooth functions of y and the exponents $\beta_{1,2,3}$ depende on m and are given by

$$\begin{cases} \{\beta_1, \beta_3, \beta_3\} = \{1, 2, 3\}\,, & \text{if} \quad m = 1\,, \\ \{\beta_1, \beta_3, \beta_3\} = \{m-2, m-1, m\}\,, & \text{if} \quad m \geq 2\,, \end{cases} \tag{3.66}$$

For reasons that will be explained in Section 3.6, we will not present results for $m = 0$ scalar modes.

Numerical procedure

To solve numerically the equations of motion it is a good idea to factor out the singularities and/or leading behaviour identified in (3.60), (3.62), (3.64) (3.65) which allows to work with manifestly analytic functions. Hence we introduce the

new independent variables $q_1, \cdots, q_{10}$ defined as

$$
\begin{aligned}
h_{(1)(1)} &= (1-x)^m\, y^{-2\,i\,\frac{\omega-m\Omega_H}{4\pi T_H}}\, \left(1-y^2\right)^{\frac{d-2}{2}}\, e^{\frac{i\omega}{1-y^2}}\, q_1\,, \\
h_{(1)(2)} &= (1-x)^m\, y^{-2\,i\,\frac{\omega-m\Omega_H}{4\pi T_H}-1}\, \left(1-y^2\right)^{\frac{d-2}{2}-2}\, e^{\frac{i\omega}{1-y^2}}\, q_2,\,, \\
h_{(1)(3)} &= x\,(1-x)^{m-1}\, y^{-2\,i\,\frac{\omega-m\Omega_H}{4\pi T_H}}\, \left(1-y^2\right)^{\frac{d-2}{2}-1}\, e^{\frac{i\omega}{1-y^2}}\, q_3\,, \\
h_{(1)(4)} &= (1-x)^m\, y^{-2\,i\,\frac{\omega-m\Omega_H}{4\pi T_H}}\, \left(1-y^2\right)^{\frac{d-2}{2}-1}\, e^{\frac{i\omega}{1-y^2}}\, q_4\,, \\
h_{(2)(2)} &= (1-x)^m\, y^{-2\,i\,\frac{\omega-m\Omega_H}{4\pi T_H}-2}\, \left(1-y^2\right)^{\frac{d-2}{2}-4}\, e^{\frac{i\omega}{1-y^2}}\, q_5\,, \\
h_{(2)(3)} &= x\,(1-x)^{m-1}\, y^{-2\,i\,\frac{\omega-m\Omega_H}{4\pi T_H}-1}\, \left(1-y^2\right)^{\frac{d-2}{2}-3}\, e^{\frac{i\omega}{1-y^2}}\, q_6\,, \\
h_{(2)(4)} &= (1-x)^m\, y^{-2\,i\,\frac{\omega-m\Omega_H}{4\pi T_H}-1}\, \left(1-y^2\right)^{\frac{d-2}{2}-3}\, e^{\frac{i\omega}{1-y^2}}\, q_7\,, \\
h_{(3)(3)} &= (1-x)^{\beta_1}\, y^{-2\,i\,\frac{\omega-m\Omega_H}{4\pi T_H}}\, \left(1-y^2\right)^{\frac{d-2}{2}-2}\, e^{\frac{i\omega}{1-y^2}}\, q_8\,, \\
h_{(3)(4)} &= x\,(1-x)^{\beta_2}\, y^{-2\,i\,\frac{\omega-m\Omega_H}{4\pi T_H}-1}\, \left(1-y^2\right)^{\frac{d-2}{2}-2}\, e^{\frac{i\omega}{1-y^2}}\, q_9\,, \\
h_{(4)(4)} &= (1-x)^{\beta_3}\, y^{-2\,i\,\frac{\omega-m\Omega_H}{4\pi T_H}}\, \left(1-y^2\right)^{\frac{d-2}{2}-2}\, e^{\frac{i\omega}{1-y^2}}\, q_{10}\,.
\end{aligned}
\tag{3.67}
$$

where $\beta_{1,2,3}$ are defined in (3.66).

Introducing these new definitions in the equations of motion (3.58), and solving these equations using a standard Taylor expansion around each of the four boundaries, it is now straightforward to find the final BCs we need to impose in each of the variables $q_j(x,y)$. Namely, we find simple Robin, Neumann or Dirichlet BCs for all q_j's at the equator $x=0$, axis of rotation $x=1$ and horizon $y=0$. At the asymptotic boundary, $y=1$ some of the q_j's obey Dirichlet BCs and the others are subject to less simple Robin BCs.

The equations of motion (3.58) constitute a coupled system of ten partial differential equations that forms a quadratic eigenvalue problem in the frequency

ω, for a given mode m. To solve this eigenvalue problem, we use a pseudospectral collocation procedure to descretize our PDE system. We use a collocation grid, in the x and y directions, on Gauss-Chebyshev-Lobbato points. Alternatively, to check results and especially when we want to increase the accuracy of our results at lower computational cost, we use the novel numerical procedure introduced and described in [4] and already used in previous sections. This numerical method is based on the Newton-Raphson root-finding algorithm that searches for specific QNMs, once a seed solution is given.

As described in detail in Section 3.3, we have also written an independent code to search directly for the QNMs of the Schwarzschild BH using the Kodama-Ishibashi (KI) decomposition on a S^{d-2}[31]. These independent results are very useful to check the numerical results we get with the codes for the single spin MP BH when the rotation vanishes. Recall that the KI formalism for the Schwarzschild BH uses the harmonic decomposition of perturbations on a S^{d-2} sphere [31] (while in the our spinning case we use a harmonic decomposition with respect to S^{d-4}). There are scalar, vector and tensor KI modes specified by quantum numbers that we will denote as $\widetilde{\ell}_S, \widetilde{\ell}_V, \widetilde{\ell}_T$, respectively. Non-trivial KI perturbations are described by integer $\widetilde{\ell}_S \geq 2, \widetilde{\ell}_V \geq 2, \widetilde{\ell}_T \geq 1$. The results from the KI code will be useful also to establish the relation between the harmonic decomposition on S^{d-4}, and associated quantum numbers (ℓ_S, m), that we use in our analysis of the single spin MP BH and the KI harmonic decomposition on S^{d-2} and its quantum numbers $\widetilde{\ell}_S, \widetilde{\ell}_V, \widetilde{\ell}_T$. In Section 3.3 we were mainly interested in the large-d limit of Schwarzschild QNMs, while in the present section we will be interested in the results for $d = 5, 6, 7$.

Results

To discuss the results, first note that as for the equal angular momenta case, we may restrict our attention to modes with $m > 0$. The argument presented in Sec. 3.4.3 applies equally well here, since it only relied on the discrete symmetry $(t, \phi) \to (-t, -\phi)$ that all stationary and axisymmetric BHs possess when ϕ is the standard azimuthal coordinate. Secondly, as the modes with smallest $-\mathrm{Im}(\omega)$ (i.e. lowest overtone, see the discussion at the end of Sec. 3.3.2) are the slowest to decay, they are the most important for the time evolution, and we will therefore focus on them.

Typically, we will express our results using the dimensionless frequency ωr_+ and dimensionless rotation a/r_+. However, sometimes we will also find convenient to express our results in terms of the dimensionless quantities ωr_0 and dimensionless rotation a/r_0 where r_0 is the mass radius related to the horizon radius r_+ by

$$r_0 = r_+ \left(\frac{a^2}{r_+^2} + 1 \right)^{\frac{1}{d-3}} . \tag{3.68}$$

Finally note that we choose to present results only for $d = 5, 6, 7$ dimensions since we expect higher dimensions to have a behavior that is similar to the cases $d = 6, 7$.

Consider first the results when the rotation vanishes. The KI scalar, vector and tensor modes of the Schwarzschild BH (with lower overtone) in $d = 5, 6, 7$ are listed in Table II of [3] (see footnote 3; these agree with the $d = 5$ QNMs of [50]). Some of these KI modes will be represented by red dots in the plots of Figs 3.17-3.22 and they agree with zero rotation results of the single MP analysis.

Switching-on the rotation, consider first the scalar modes of the singly spinning MP BH with $\ell_S = 0$ and $m = 2$. There is a pair of curves (one with positive and the other with negative real part) with $(\ell_S, m) = (0, 2)$ in each spacetime dimension d. Fig. 3.17 shows these pairs of curves for $d = 5$ (green disk curves), $d = 6$ (blue square curves) and $d = 7$ (black triangle curves); these are the pairs of curves for the zero overtone solutions. The *left panel* (*right panel*) plots the real (imaginary) part of the dimensional frequency ωr_+ as a function of the dimensional rotation parameter a/r_+. When the rotation vanishes these curves coincide exactly with the KI scalar mode with $\widetilde{\ell}_S = 2$ of the Schwarzschild BH (see Table II of [3]). It is interesting to point out that, although not shown in Fig. 3.17, there are other $(\ell_S, m) = (0, 2)$ scalar modes of MP − with higher overtone and consequently with higher absolute value of the imaginary part of the frequency − that connect to even $\widetilde{\ell}_S = 4, 6, \ldots$ KI scalar QNMs, to odd $\widetilde{\ell}_V = 3, 5, \ldots$ KI vector QNMs, and to even $\widetilde{\ell}_T = 2, 4, 6, \ldots$ KI tensor QNMs when $a/r_+ \to 0$. We concentrate on the lowest-lying modes that are less damped and thus dominate the time evolution of a perturbed BH.

In Fig. 3.17 we find that there are two modes that stand out, because as the rotation increases their imaginary part goes from negative to positive. Therefore they are QNMs at low rotation but they become unstable modes after a critical rotation. These two modes are plotted in more detail in Fig. 3.18. They are the low-lying scalar modes with $(\ell_S, m) = (0, 2)$ for $d = 6$ (blue squares) and $d = 7$ (black triangles). We identify them as the linear modes that are responsible for the bar-mode instability that was first conjectured to exist by Emparan-Myers [20] and later confirmed to be indeed present in a full non-linear time evolution analysis

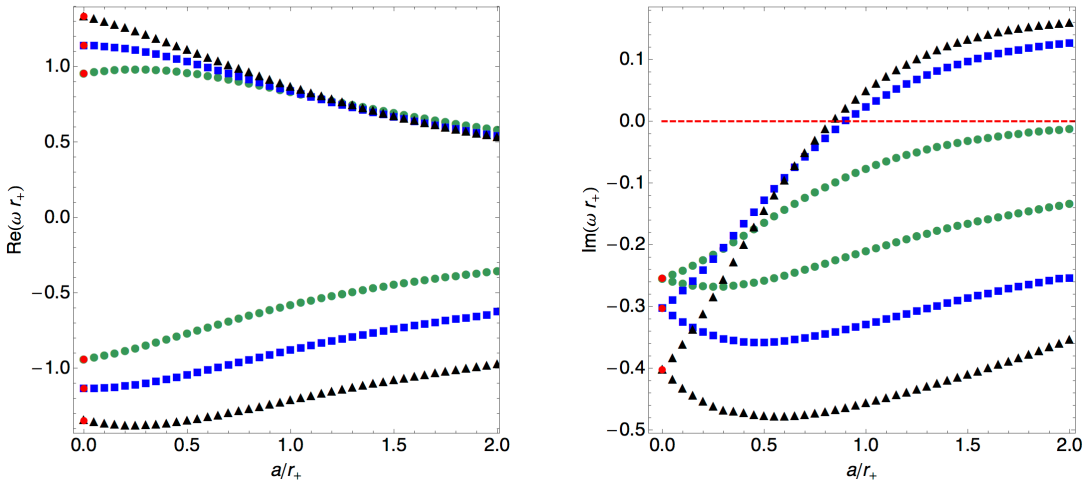

Figure 3.17: **Single MP.** Scalar modes with $(\ell_S, m) = (0, 2)$ for $d = 5$ (green disks), $d = 6$ (blue squares) and $d = 7$ (black triangles). These modes reduce to the $\widetilde{\ell}_S = 2$ KI scalar QNMs when $a/r_+ \to 0$ (pinpointed as red dots; see Table II of [3]).

of a perturbed singly spinning MP BH by Shibata-Yoshino [29]. Indeed, the critical rotation at which $\mathrm{Im}(\omega r_+) = 0$ agrees precisely with the critical rotation above which the time evolution code of Shibata-Yoshino [29] finds the bar-mode instability. The values we find for these onset critical rotations are given in Table 3.2 (to be compared with Table I of [29]).

$Bar-mode$	a_c/r_+	a_c/r_0
$d=5$	Not present	Not present
$d=6$	0.903 ± 0.002	0.740 ± 0.001
$d=7$	0.833 ± 0.002	0.730 ± 0.001

Table 3.2: Critical dimensionless rotation at which the bar-mode (linear) instability onset occurs.

In the inset plot of the *Right Panel* of Fig. 3.18 we zoom the bar-mode instability in $d = 6$ and $d = 7$ near its onset using the frequency and the rotation

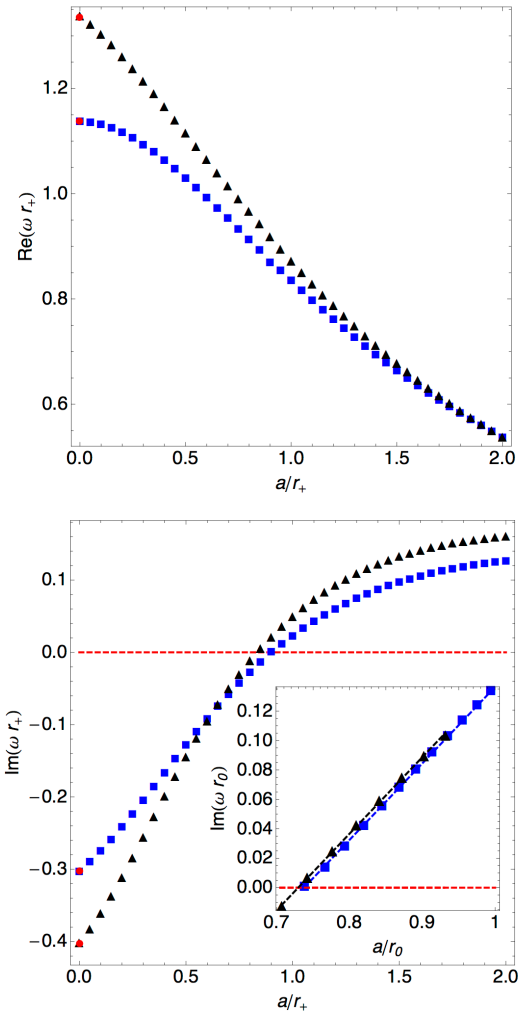

Figure 3.18: **Single MP.** bar-mode instability in $d = 6$ (blue squares) and $d = 7$ (black triangles). *Left Panel:* Real part of the frequency $\mathrm{Re}(\omega r_+)$ as a function of the dimensionless rotation a/r_+. *Right Panel:* Imaginary part of the frequency $\mathrm{Im}(\omega r_+)$ as a function of a/r_+. The inset plot in the *Right Panel* details the bar-mode instability in $d = 6$ and $d = 7$ near the onset (this time in mass radius r_0 units) and is further discussed in the text.

in mass radius units, ωr_0 and a/r_0. Both in $d = 6$ and $d = 7$ we find that near the onset the unstable mode scales as $\mathrm{Im}\,(\omega r_0) \sim C_\tau (a - a_c)/r_0$ with $C_\tau \sim 0.521$ where a_c is the critical rotation above which the instability is present. This be-

haviour agrees with the linear relation predicted by the time evolution analysis of Shibata-Yoshino (see discussion associated with equation (61) of [29]).

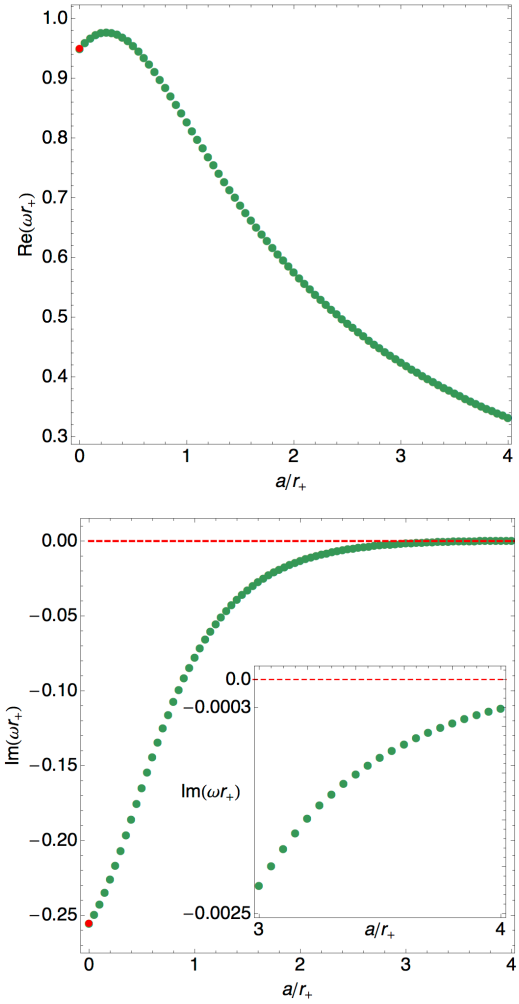

Figure 3.19: **Single MP.** Scalar modes with $(\ell_S, m) = (0, 2)$ for $d = 5$. There is no linear bar-mode instability.

Coming back to Fig. 3.17 we find that the $(\ell_S, m) = (0, 2)$ scalar mode does not become linearly unstable in $d = 5$, contrary to what happens in $d \geq 6$. To analyse this in more detail, we have followed this $(\ell_S, m) = (0, 2)$ scalar mode up to rotations $a/r_+ = 4$ using a numerical code with very high precision. The

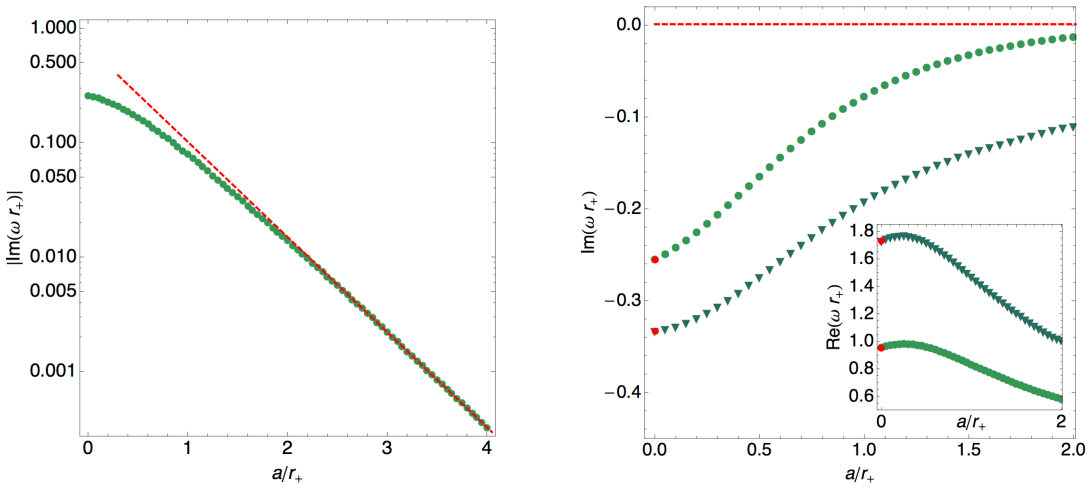

Figure 3.20: **Single MP.** *Left Panel:* Log plot for the scalar modes with $(\ell_S, m) = (0, 2)$ in $d = 5$. We find that $\mathrm{Im}\,(\omega r_+) = A_0 e^{-\gamma a/r_+}$ with $\gamma \sim 1.9$ and $A_0 \sim 0.69$. *Right Panel:* Scalar modes with $(\ell_S, m) = (0, 2)$ in $d = 5$. The green disk curve is the one already shown in Fig. 3.19 and in the left panel of this Fig. that connects to the KI scalar mode with $\widetilde{\ell}_S = 2$. The dark-green triangle curve is also a $(\ell_S, m) = (0, 2)$ but with higher overtone that connects to the KI vector mode with $\widetilde{\ell}_V = 3$ when $a/r_+ \to 0$ (see Table II of [3]).

associated results are plotted in Fig. 3.19. Clearly we find no linear bar-mode instability in $d = 5$. Actually, as shown in more detail in the log-log plot of the *left panel* of Fig. 3.20, a fit of our numerical data indicates that the imaginary part of the frequency of this modes approaches exponentially zero from below but never becomes positive. As we pointed out previously, there are other $(\ell_S, m) = (0, 2)$ scalar modes of MP (with higher radial overtone) besides the one shown in Fig. 3.19. These modes connect to the even $\widetilde{\ell}_S = 4, 6, \ldots$ KI scalar QNMs, to the odd $\widetilde{\ell}_V = 3, 5, \ldots$ KI vector QNMs, and to the even $\widetilde{\ell}_T = 2, 4, 6, \ldots$ KI tensor QNMs when $a/r_+ \to 0$, all of which have lower $\mathrm{Im}(\omega r_+)$ than the $\widetilde{\ell}_S = 2$ KI scalar QNM pinpointed as a red point in Fig. 3.19. Nevertheless, given the negative result we get for the possibility of a $d = 5$ bar-mode instability in the mode of

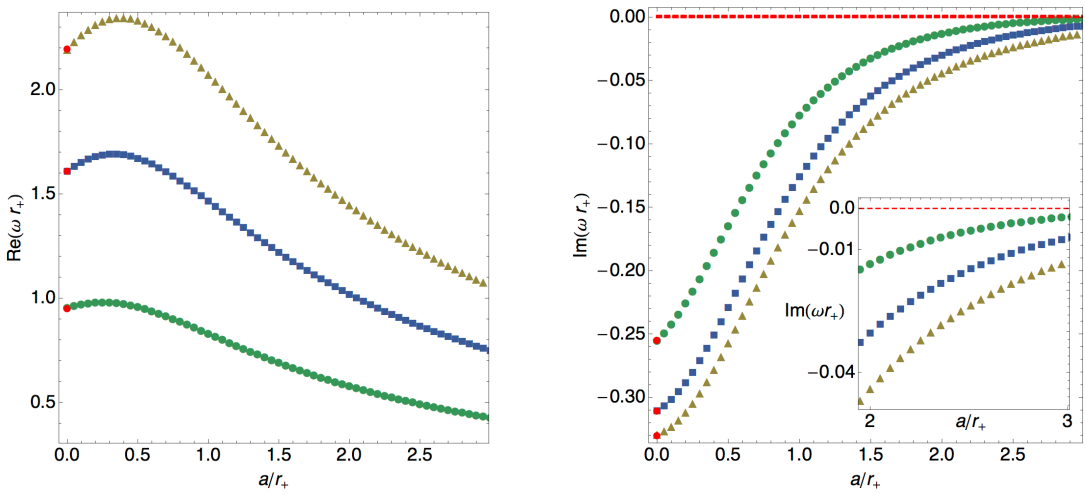

Figure 3.21: **Single MP.** Scalar modes with $(\ell, m) = (0, 2)$, $(\ell, m) = (0, 3)$ and $(\ell, m) = (0, 4)$ for $d = 5$. The $(\ell, m) = (0, 2)$ mode is the green disk curve already shown in previous plots while the $(\ell, m) = (0, 3)$ and $(\ell, m) = (0, 4)$ modes are, respectively, the blue square line and the brown triangle line which reduce to the $\widetilde{\ell}_S = 3$ and $\widetilde{\ell}_S = 4$ KI scalar modes when $a/r_+ \to 0$. The $m = 3$ and $m = 4$ scalar modes show no instability: one finds that the frequency approaches exponentially zero as the rotation grows large.

Fig. 3.19, we have done an exhaustive study of these other $(\ell_S, m) = (0, 2)$ scalar modes of MP. We find that these modes always have, for a given rotation, $\mathrm{Im}(\omega r_+)$ that is more negative than the value shown in Fig. 3.19. (A particular example illustrating this study is shown in the *right panel* of Fig. 3.20 where we look to the scalar mode that connects to the KI vector mode $\widetilde{\ell}_V = 3$ when $a/r_+ \to 0$). This in particular means that their $\mathrm{Im}(\omega r_+)$ does not become positive above a certain critical rotation and thus they are not associated to a linear bar-mode instability. We have also considered the possibility that a linear bar-mode instability could be associated to a scalar mode with $m > 2$. However we did not find such a $m \geq 3$ mode with an imaginary part of the frequency that is positive; in fact the

imaginary part of the frequency of $m \geq 3$ scalar modes is more negative than the one of the $m = 2$ scalar mode plotted in Fig. 3.19. An example that illustrates this discussion is shown in Fig. 3.21 where the blue square curve describes the low-lying scalar mode with $m = 3$ and the brown triangles describe the $m = 4$ mode; these curves (the imaginary part of the frequency) are below the $m = 2$ scalar mode curve (green disks). Finally, in our data analysis we also rule out the less conventional possibility of an unstable mode that is not connected to a QNM of the Schwarzschild BH. We conclude that the $d = 5$ singly spinning MP BH is not unstable to a linear bar-mode instability.

Concluding, we find absolutely no evidence of a linear bar-mode instability in $d = 5$. Note however that the non-linear numerical time evolution analysis of [28, 29] does find a bar-mode instability for rotations $a_c/r_+ > 1.76$ (i.e. $a_c/r_0 > 0.87$). Our linear results indicate that the $d = 5$ instability appearing in the non-linear analysis of [28, 29] has no linear origin.

We now proceed to the discussion of scalar modes of the singly spinning MP BH with $\ell_S = 0$ and $m = 1$. Again, there is a pair of curves (one with positive and the other with negative real part) with $(\ell_S, m) = (0, 1)$ in each dimension. Fig. 3.22 gives detailed data for the $(\ell_S, m) = (0, 1)$ scalar modes of the $d = 5$ case. The blue disk line reduces to the $\widetilde{\ell}_S = 3$ KI scalar mode when $a/r_+ \to 0$, while the brown square (green triangle) line connects to the $\widetilde{\ell}_V = 2$ KI vector mode ($\widetilde{\ell}_T = 3$ KI tensor mode) when $a/r_+ \to 0$. These Schwarzschild KI QNMs (see Table II of [3]) are pinpointed as red dots. For $d \geq 6$, $(\ell_S, m) = (0, 1)$ scalar QNMs behave similarly to those in $d = 5$. In particular, we checked that these modes are always stable for any dimension. Not shown in Fig. 3.22, for $d = 5$ (and $d \geq 6$) there

are other $m = 1$ scalar modes of MP with higher absolute value of the imaginary part of the frequency that connect to the odd $\widetilde{\ell}_S = 5, 7, \cdots$ KI scalar QNMs, to the even $\widetilde{\ell}_V = 4, 6, \cdots$ KI vector QNMs, and to the odd $\widetilde{\ell}_T = 5, 7, \cdots$ KI tensor QNMs.

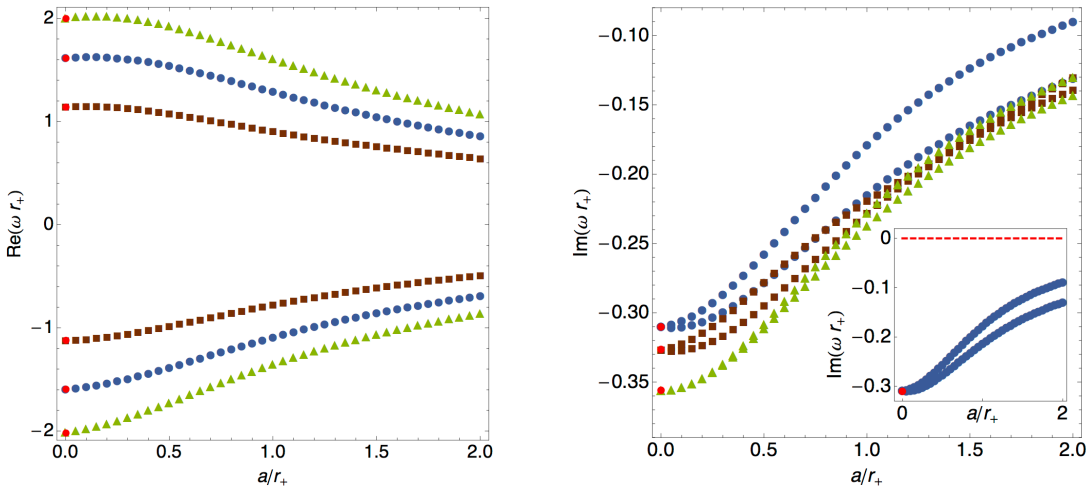

Figure 3.22: **Single MP.** Scalar modes with $(\ell, m) = (0, 1)$ for $d = 5$. The blue disk line reduces to the $\widetilde{\ell}_S = 3$ KI scalar mode when $a/r_+ \to 0$, while the brown square (green triangle) line connects to the $\widetilde{\ell}_V = 2$ KI vector mode ($\widetilde{\ell}_T = 3$ KI tensor mode) when $a/r_+ \to 0$. These Schwarzschild KI QNMs are pinpointed as red dots. For $d \geq 6$ the behaviour of the $m = 1$ QNMs has a similar behaviour. As highlighted in the inset plot of the *Right Panel* these modes are always stable, i.e. they have $\mathrm{Im}(\omega r_+) < 0$.

3.5.2 Vector QNMs ($d \geq 6$)

We now turn to the study of vector perturbations, which are out of vector harmonics $\mathbf{V}_i$

$$h_{ab} = 0\,, \qquad h_{ai} = e^{-i\omega t} e^{im\phi} h_a \mathbf{V}_i, \qquad h_{ij} = -\frac{1}{2\sqrt{\lambda_V}}\, e^{-i\omega t} e^{im\phi} h_T D_{(i}\mathbf{V}_{j)}\,, \quad (3.69)$$

where $\{h_a, h_T\}$ are functions of $(r, \widetilde{x})$, and $\mathbf{V}_i$ denotes a transverse vector harmonic on S^{d-4}:

$$D_i \mathbf{V}^i = 0, \qquad \left(D^2 + \lambda_V\right) \mathbf{V}_i = 0 \tag{3.70}$$

Regularity of the vector harmonics requires

$$\lambda = \ell_V \left(\ell_V + d - 5\right) - 1 \,, \qquad \text{with} \quad \ell_V = 1, 2, 3. \tag{3.71}$$

Harmonics with $\ell_V = 1$ are special since they are Killing vectors on S^{d-4}.

Boundary conditions and numerical approach

Like in the scalar sector, we work in the traceless-transverse (TT) gauge, and we insert the vector perturbations (3.69) into the linearised Einstein equations, $(\Delta_L h)_{ab} = 0$. The TT gauge conditions can be used to express h_T as an algebraic function of h_a and their first derivatives. We have then 4 independent variables, h_1, h_2, h_3 and h_4. The following equations,

$$(\Delta_L h)_{1\Omega} = 0 \,, \qquad (\Delta_L h)_{2\Omega} = 0 \,, \qquad (\Delta_L h)_{3\Omega} = 0 \,, \qquad (\Delta_L h)_{4\Omega} = 0 \,, \tag{3.72}$$

(where here the subscript Ω describes the azimuthal coordinate of the $S^{(d-4)}$) constitute a system of four independent equations to solve for the four independent variables h_a, and that closes the full Lichnerowicz system.

The singular or leading behaviour of the h_a's at each of the four boundaries can be determined following similar procedures to those described in the scalar sector case. Again, it is convenient to factor them out to work with manifestly analytical

functions. Therefore we introduce the new independent functions $q_1, \cdots, q_4$:

$$
\begin{aligned}
h_1 &= x^{\ell+1}\,(1-x)^m\, y^{-2\,i\,\frac{\omega-m\Omega_H}{4\pi T_H}}\,\left(1-y^2\right)^{\frac{d-2}{2}-1}\, e^{\frac{i\omega}{1-y^2}}\, q_1\,,\\
h_2 &= x^{\ell+1}\,(1-x)^m\, y^{-2\,i\,\frac{\omega-m\Omega_H}{4\pi T_H}-1}\,\left(1-y^2\right)^{\frac{d-2}{2}-3}\, e^{\frac{i\omega}{1-y^2}}\, q_2,\,,\\
h_3 &= x^{\ell}\,(1-x)^{\alpha_3}\, y^{-2\,i\,\frac{\omega-m\Omega_H}{4\pi T_H}}\,\left(1-y^2\right)^{\frac{d-2}{2}-2}\, e^{\frac{i\omega}{1-y^2}}\, q_3\,,\\
h_4 &= x^{\ell+1}\,(1-x)^{\alpha_4}\, y^{-2\,i\,\frac{\omega-m\Omega_H}{4\pi T_H}}\,\left(1-y^2\right)^{\frac{d-2}{2}-2}\, e^{\frac{i\omega}{1-y^2}}\, q_4\,,
\end{aligned}
\tag{3.73}
$$

where

$$
\begin{cases}
\{\alpha_3,\alpha_4\} = \{1,2\}\,, & \text{if} \quad m=0\,,\\
\{\alpha_3,\alpha_4\} = \{m-1,m\}\,, & \text{if} \quad m\geq 1\,,
\end{cases}
\tag{3.74}
$$

Inserting (3.73) into the equations of motion (3.72) and Taylor expanding to solve these equations around each of the four boundaries it is straightforward to find the BCs we need to impose on each of the $q_j(x,y)$. Namely, the horizon has simple Dirichlet or Neumann BCs (depending on the q_j's) and we also find very simple Robin, Neumann or Dirichlet BCs for all q_j's at the equator $x=0$ and axis of rotation $x=1$ and horizon $y=0$. At the the asymptotic boundary, $y=1$, q_2 has a Dirichlet BC while the other q_j's are subject to Robin BCs (the expressions for which are rather lengthy and so we omit their presentation here).

We solve numerically our system using the same two numerical methods that were described in the scalar sector of perturbations.

Results

Vector modes of the singly spinning MP BH exist for $d \geq 6$. As in the scalar case, in the vector sector there is also an infinite family − associated to different

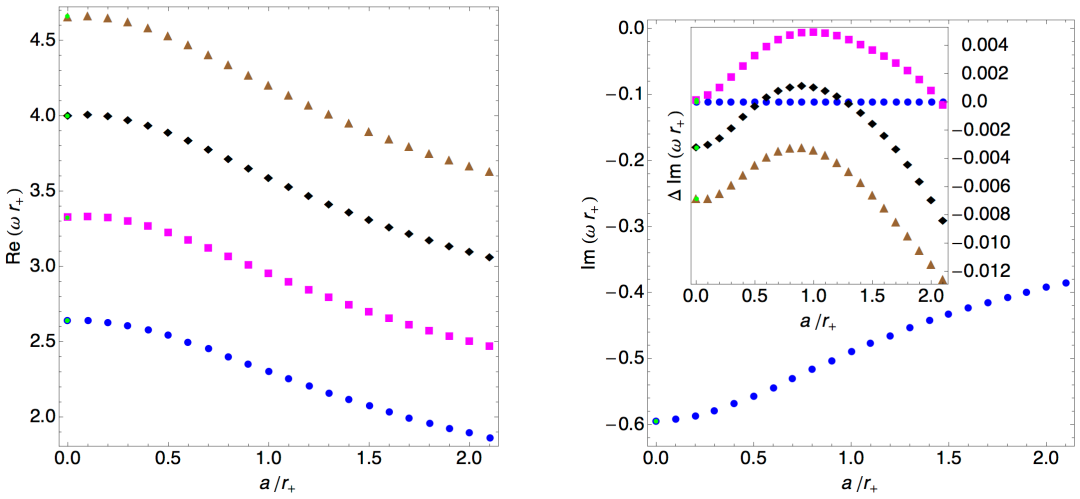

Figure 3.23: **Single MP.** Vector modes in $d = 7$ with $m = 1$ and: $\ell_V = 2$ (blue disks), $\ell_V = 3$ (magenta squares), $\ell_V = 4$ (black squares) and $\ell_V = 5$ (brown triangles). In the *Right Panel* the inset plot shows the difference between the imaginary part of the modes with respect to the $\ell_V = 2, m = 1$ mode. These MP vector modes with $m = 1$ and $\ell_V = 2, 3, 4, 5$ respectively connect to $\widetilde{\ell}_V = 3, 4, 5, 6$ KI vector QNMs when $a/r_+ \to 0$, which are pinpointed as green points.

radial overtones − of vector QNMs for each pair (ℓ_V, m) of vector modes (with $\ell_V \geq 2$ and $|m| \leq \ell_V$). We will present results only for the lowest-lying QNMs (that have smaller $|\mathrm{Im}(\omega r_+)|$). When the rotation vanishes the vector QNMs of the singly spinning MP BH reduce to certain QNMs of the Schwarzschild BH that are listed in Table II of [3] and that will be pinpointed as green dots in the plots of this subsection. They will confirm that our spinning QNMs are being correctly computed. There is a pair of curves (one with positive and the other with negative real part) for each vector mode specified by the angular quantum numbers (ℓ_V, m). For the vector modes we will show only the element of the pair that has $\mathrm{Re}(\omega r_+) > 0$, since for $m > 0$, only these can go unstable. This is a simple consequence of the area-law argument presented in Section 3.4. Quite often in the inset plots of

the imaginary part of the frequency we will present subtracted frequencies with respect to a specified reference mode to better visualise the curves, since the curves would otherwise be very close to each other.

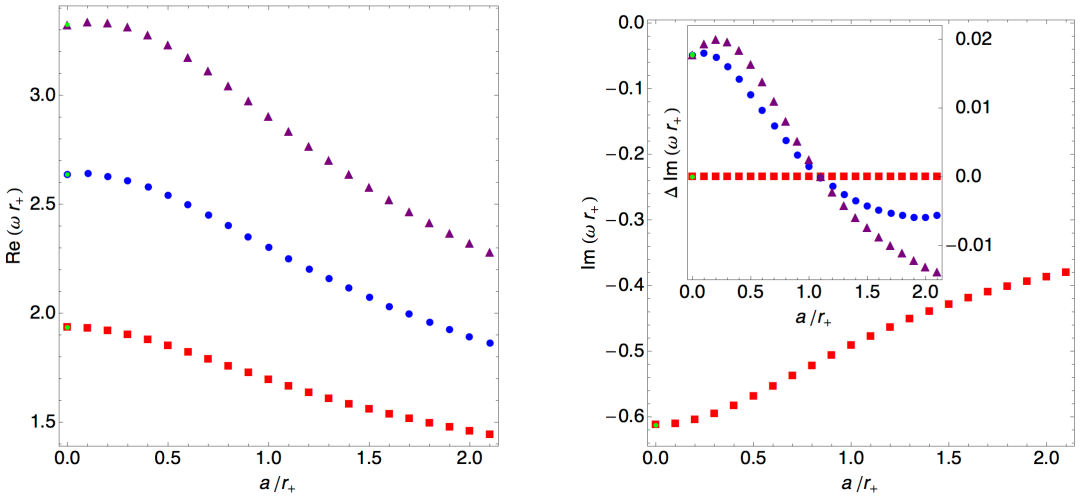

Figure 3.24: **Single MP.** Vector modes in $d = 7$ with $\ell_V = 2$ and: $m = 0$ (red squares), $m = 1$ (blue disks), $m = 2$ (purple triangles). In the *Right Panel* the inset plot shows the difference between the imaginary part of the modes with respect to the $\ell_V = 2, m = 0$ mode. These MP vector modes with $\ell_V = 2$ and $m = 0, 1, 2$ respectively connect to $\widetilde{\ell}_V = 2, 3, 4$ KI vector QNMs when $a/r_+ \to 0$, which are identified as green points.

Fig. 3.23 shows the frequencies of the $d = 7$ vector modes with fixed $m = 1$ and different ℓ_V's, namely: $\ell_V = 2$ (blue disks), $\ell_V = 3$ (magenta squares), $\ell_V = 4$ (black squares) and $\ell_V = 5$ (brown triangles). These MP vector modes with $m = 1$ and $\ell_V = 2, 3, 4, 5$, respectively connect to $\widetilde{\ell}_V = 3, 4, 5, 6$ KI vector QNMs when $a/r_+ \to 0$, which are pinpointed as green points (see Table II of [3]). We find no instability in this vector spectrum.

Fig. 3.24 fixes $\ell_V = 2$ and shows the vector modes in $d = 7$ with $m = 0$ (red squares), $m = 1$ (blue disks), $m = 2$ (purple triangles). These MP vector modes

with $\ell_V = 2$ and $m = 0, 1, 2$, respectively connect to $\widetilde{\ell}_V = 2, 3, 4$ KI vector QNMs when $a/r_+ \to 0$, which are identified as green points (see Table II of [3]). Again we find no instability in this spectrum.

Finally, to exemplify that the behaviour of the vector modes is similar for any $d \geq 6$, in Fig. 3.25 we show again the $(\ell_V, m) = (2, 1)$ and $(\ell_V, m) = (3, 1)$ vector modes in $d = 7$ but now we compare them with those with same angular quantum numbers in $d = 6$.

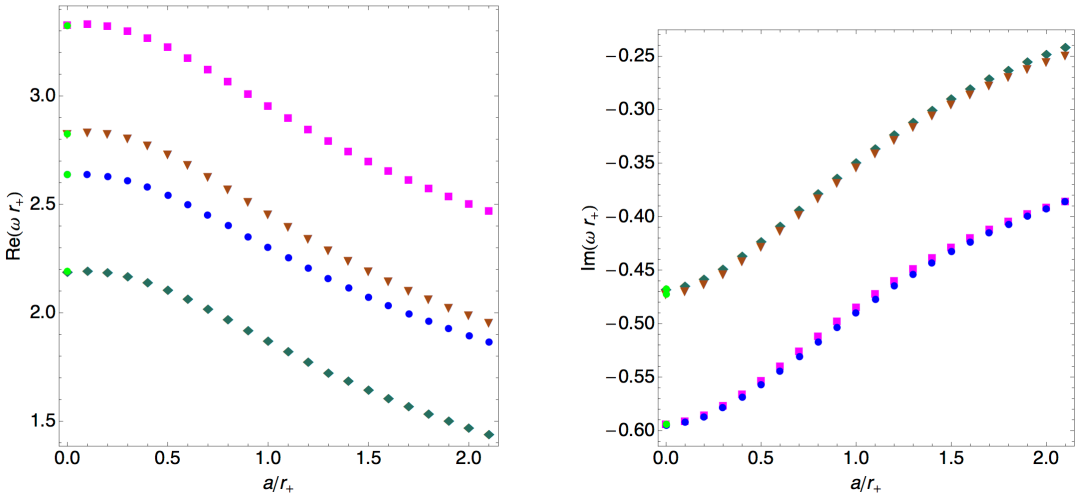

Figure 3.25: **Single MP.** Vector modes in $d = 6$ and $d = 7$ with $m = 1$ (real part in the *Left Panel* and imaginary part in the *Right Panel*). In $d = 6$ we have the green disks with $\ell_V = 2$ and the brown triangles with $\ell_V = 3$. In $d = 7$ we have the blue disks with $\ell_V = 2$ and the magenta squares with $\ell_V = 3$. These MP vector modes with $m = 1$ and $\ell_V = 2, 3$ respectively connect to $\widetilde{\ell}_V = 3, 4$ KI vector QNMs when $a/r_+ \to 0$, which are pinpointed as green points.

3.5.3 Tensor QNMs ($d \geq 7$)

Tensor perturbations of the singly spinning MP background can be expanded in terms of a basis of transverse ($\nabla_i \mathbf{T}^i_j$) and traceless ($\mathbf{T}^i_i = 0$) harmonic tensors

$\mathbf{T}_{ij}$ on the unit sphere S^{d-4} that solve $(\Box_{S^{d-4}} + \lambda_T)\,\mathbf{T}_{ij} = 0$. Regular tensor harmonics have eigenvalue $\lambda_T = \ell_T\,(\ell_T + d - 5) - 2$ with integer $\ell_T \geq 2$.

Tensor-type perturbations have the form

$$h_{ab} = 0\,, \qquad h_{ai} = 0, \qquad h_{ij} = e^{-i\omega t} e^{im\phi} H_T(r, \widetilde{x}) \mathbf{T}_{ij}\,, \tag{3.75}$$

Ref. [42] studied this tensor QNM spectrum in great detail so we do not discuss this sector of perturbations further. In particular, [42] found no instability in the tensor sector of linear perturbations.

3.6 Conclusions and Outlook

This manuscript makes a thorough study of the QNMs of the two most representative cases of asymptotically flat MP BHs as a function of the spacetime dimension d, including in the limit where all rotations are taken to zero, i.e. the Schwarzschild BH. For the latter BH, we give particular emphasis to the limit $d \to +\infty$. Also, due to the lack of symmetry of the most general MP BH, we focus on two particular classes of MP BHs: the singly spinning MP BH, and the odd-dimensional equal angular MP BH.

QNMs of the Schwarzschild BH show an interesting structure as d increases. Scalars and vector gravitational perturbations have two distinct sectors of QNMs which exhibit an universal behavior. In the first, which we denominate class I, the corresponding QNMs saturate as the spacetime dimension increases. In the second, which we coin class II, the QNMs scale with d, with (at least some of) the modes scaling as $\mathrm{Im}(\omega r_0) \propto -d^{1/2}$ and $\mathrm{Re}(\omega r_0) \propto d$. Furthermore, in class I,

our results allow us to conjecture that the imaginary part is universal, depending on ℓ only, and saturates at $\mathrm{Im}(\omega r_0) = -(\ell - 1)$, and the real part depends on the sector, being zero for vectors and non vanishing for scalars. Finally, the tensor gravitational perturbations only exhibit QNMs of class II. Each of these behaviors should be derivable from a matched asymptotic expansion, such as the one proposed in [12, 43, 32].

The structure of QNMs typical of Schwarzschild BHs, seems to persist when rotation is included. The clearest setup where this is evident, in the sense that we are able to increase d to relatively large values, occurs when we study gravitational perturbations of the equal angular momenta MP BHs. For sufficiently high d, we have shown that both the bar-mode and ultraspinning instabilities are continuously connected, as the rotation is taken to zero, to QNMs of class I. This observation could have been anticipated from the following simple argument. All unstable modes of MP BHs must, at zero rotation, reduce to Schwarzschild modes. These we have found to consist of two classes, those that saturate to finite values in the infinite-d limit, and those that scale with d. If an instability of an equal angular momenta BH connected to a class II (scaling) mode, then it would need to move a large distance in the complex ω plane as the rotation is increased a finite amount in order to turn into an instability (recall that these BHs have extremal limits). This seems unlikely, and thus it is quite natural that instabilities of these large-d MP BHs should stem from saturating Schwarzschild modes. More generally, a generic MP BH with no vanishing angular momenta also has an extremal bound and is expected to suffer from instabilities similar to the equal angular momenta case, and therefore we conjecture that, for sufficiently large d,

all instabilities of MP BHs with no vanishing angular momenta connect to class I (saturating) Schwarzschild modes at zero rotation [18]. Singly spinning MP BHs, for $d > 5$, do not have extremal limits, and the above argument does not apply. However, for large dimension, one would at least expect that the first mode to go unstable as the rotation is increased would connect to a saturating Schwarzschild mode, since these will be the lowest lying modes.

In addition to these observations concerning perturbations in the large-d limit, we have also continued the study of linear perturbations of the equal angular momenta MP BH. For the case of $d = 7$, this study is now complete as we were able to make use of our derivation of the charged vector harmonics on $\mathbb{CP}^2$ to study the vector sector of perturbations. In both cases studied, the equal angular momenta and singly spinning MP BH, only the scalar sector contains QNMs that go unstable. For axisymmetric ($m = 0$) modes, this corroborates the near-horizon analysis of [24].

One of the central results of this manuscript is the study of the linear analysis of the bar-mode instability of singly spinning MP BHs. For $d \geq 6$ our linear analysis reproduces the key results of the non-linear time evolution of [28, 29], including the slope of the growth rate as the QNMs become unstable. However, we find no evidence of a linear instability in the $d = 5$ singly spinning MP, which seems to be at odds with the results found in [28, 29]. In fact, we find that the lowest lying QNMs have an imaginary part that approaches zero exponentially

[18] After the first version of this article appeared we learned that for the specific case of equal angular momenta this conjecture has been firmly established by the results of Ref. [44]. They analytically computed the QNMs which become unstable at large rotation in the large D limit, and found that for all rotations (including zero) the frequencies are $\omega \sim \mathcal{O}(D^0)$, i.e. belonging to class I, in accord with our conjecture.

in the rotation parameter a/r_+. It would be interesting to try to understand whether this result is amenable to an analytic understanding. We leave this for future work. In $d = 5$, it seems that our results are only compatible with those found in [28, 29], if the bar-mode instability is a non-linear instability. This might well be the case, due to the aforementioned exponential approach.

An extension of our work would be to study the $m = 0$ sector of perturbations of the singly spinning MP BH, which describes the ultraspinning instability [20, 26, 40]. This would allow to compute the instability timescale, which is missing. This turns out to be a very complicated sector, due to the existence of a zero mode - namely, another MP with a slightly different angular momentum. We did not manage to use Newton's method to disentangle such perturbations, the main reason being that we don't know of a good starting seed for our iteration procedure. For the $m \neq 0$, we use the QNMs of the Schwarzschild BH as a starting point. However, for $m = 0$, and given what we observe in the equal angular momenta MP, we expect the ultraspinning mode to have zero real frequency. This means we should search for a QNM of the Schwarzschild BH with zero real part of the frequency, thus lying along the purely imaginary axis, where a branch cut exists. This makes the numerics very challenging.

The work presented in this paper can be extended in many directions. We can use our PDE methods to compute the QNMs of the Kerr-Newman BH, which is a long standing problem in Classical General Relativity. Even though there is no known mechanism to herald an instability in such system, it would be interesting to test some of the conjectures put forward in [51]. Another extension pertains the study of graybody factors of higher-dimensional asymptotically flat BHs, which is

a mild extension of our work with possible implications for LHC physics [52, 53]. Another longstanding problem that could be tackled by the methods used in this paper, is the stability of the Emparan-Reall black ring found in [37]. Recently, using indirect methods, the fat branch of the black ring solutions has been shown to be unstable [54] (see also [55] for a more heuristic argument, that leads to the same conclusion), but the stability of the thin ring remains largely unknown.

Acknowledgements

It is a pleasure to thank Roberto Emparan, Masaru Shibata, Ryotaku Suzuki, Kentaro Tanabe for enlightening discussions and for sharing their results. J.E.S.'s work is partially supported by the John Templeton Foundation. OJCD was supported in part by the ERC Starting Grant 240210 - String-QCD-BH. G.S.H was supported by NSF grant PHY12-05500. The authors thankfully acknowledge the computer resources, technical expertise and assistance provided by CENTRA/IST. Some of the computations were performed at the cluster "Baltasar-Sete-Sóis" and supported by the DyBHo-256667 ERC Starting Grant.

Appendix

3.A Spectrum of Charged Vector Harmonics on $\mathbb{CP}^2$

Here we derive the spectrum of charged vector harmonics on $\mathbb{CP}^2$. We will use the coordinates and conventions of Ref. [23], in which the metric on $\mathbb{CP}^N$ is constructed iteratively starting from the metric on $\mathbb{CP}^1 \simeq S^2$. Letting $d\Sigma_N^2$ and A_N denote the line element of the Fubini-Study metric on $\mathbb{CP}^N$ and the $U(1)$ connection, respectively, for $N = 1$ we have

$$d\Sigma_1^2 = \frac{1}{4} d\Omega_2^2 = \frac{1}{4}\left(\frac{dx^2}{1-x^2} + (1-x^2)d\phi^2\right), \qquad A_1 = \frac{x}{2}d\phi. \tag{3.76}$$

The line element and connection for general N can then be determined iteratively,

$$\begin{aligned} d\Sigma_N^2 &= \frac{dR_N^2}{\left(1+R_N^2\right)^2} + \frac{1}{4}\frac{R_N^2}{\left(1+R_N^2\right)^2}\left(d\Psi_N + 2A_{N-1}\right)^2 + \frac{R_N^2}{1+R_N^2} d\Sigma_{N-1}^2 \\ A_N &= \frac{1}{2}\frac{R_N^2}{1+R_N^2}\left(d\Psi_N + 2A_{N-1}\right). \end{aligned} \tag{3.77}$$

Charged vector harmonics are characterized by the following attributes: they are regular, transverse with respect to $\hat{D}_a = \hat{\nabla}_a - imA_a$, and eigenvectors of both $\hat{D}^2$ and the complex structure. To analyse the regularity of the vectors, it is important to understand the geometry of $\mathbb{CP}^N$ near the origin. Near $R_N = 0$, the line element takes the form

$$d\Sigma_N^2 \sim dR_N^2 + R_N^2 \left[\left(\frac{d\Psi_N}{2} + A_{N-1} \right)^2 + d\Sigma_{N-1}^2 \right], \tag{3.78}$$

which is easily seen to be $\mathbb{R}^{2N}$ once the quantity in brackets is recognized as S^{2N-1} written in terms of the Hopf fibration with the non-standard periodicity for the $U(1)$ coordinate Ψ_N. It is now relatively straightforward to introduce locally Cartesian coordinates. The form of the metric near the origin suggests that these coordinates should correspond to the embedding of $\mathbb{CP}^{N-1}$ in $\mathbb{C}^N$. For example, for $N = 2$ this is achieved by

$$z_1 = R_2 \sqrt{\frac{1-x}{2}} e^{\frac{i}{2}(\phi - \Psi_2)}, \qquad z_2 = R_2 \sqrt{\frac{1+x}{2}} e^{\frac{i}{2}(\phi + \Psi_2)}. \tag{3.79}$$

We are now in a position to derive the charged vector harmonics for the case $N = 2$. Consider the following vector,

$$\mathbb{V}_a^{(0)} dx^a = Y_2(R_2) Y_1(x) A_1 e^{i n_2 \Psi_2}. \tag{3.80}$$

This can be decomposed into hermitian and anti-hermitian parts,

$$\mathbb{V}_a = \frac{1}{2} \left(\delta_a{}^b + i\epsilon J_a{}^b \right) \mathbb{V}_b^{(0)}, \qquad \epsilon = \pm 1. \tag{3.81}$$

Requiring that this vector be transverse yields

$$Y_1(x) = x^{-1}\left(1-x^2\right)^{-n_2/(2\epsilon)}. \tag{3.82}$$

The function $Y_2(R_2)$ and the integer n_2 are constrained by the requirement of regularity. Using the above locally Cartesian coordinates, one can show that the near $R_2 = 0$ geometry reveals that $\mathbb{V}$ displays two types of pathological behaviour. First, even at finite R_2, it diverges lower-dimensional subspaces, and secondly, it diverges as R_2^{-2} near $R_2 = 0$. The first problem is resolved by the choice $n_2 = -\epsilon\tilde{n}$, with $\tilde{n} = 1, 2, ...$, and the second will be fixed by the quantization of λ_V, to which we now turn.

For the above vector, the eigenvalue equation $(\hat{D}^2 + \lambda_V)\mathbb{V}_a = 0$ reduces to a single ODE,

$$Y_2''(R_2) + \frac{Y'(R_2)}{R_2} - \frac{4\tilde{n}^2 + \left(-6 + 8\tilde{n}^2 + 2m\epsilon(2\tilde{n}-1) - \lambda_V\right)R_2^2 + (2\tilde{n}+m\epsilon)^2 R_2^4}{R_2^2(1+R_2^2)^2}. \tag{3.83}$$

It is convenient to introduce the coordinate $z^{-1} = 1 + R_N^2$ and to define a new function, $Y_2(z) = (1-z)^{\tilde{n}} z^{|2\tilde{n}+m\epsilon|/2} w(z)$, which brings the equation into hypergeometric form,

$$z(1-z)w''(z) + \big(c - (a+b-1)z\big)w'(z) - abw(z) = 0. \tag{3.84}$$

Here $c = 1 + |2\tilde{n} + m\epsilon|$, and $a + b = 1 + 2\tilde{n} + |2\tilde{n} + m\epsilon|$. Requiring that the solution is regular will fix the solution and impose a quantization condition on the eigenvalues. The general solution can be written as a sum of hypergeometric

functions with argument z. Since c is an integer, one of the two independent solutions contains factor of $\ln(z)$, which is not analytic and therefore the coefficient of this solution is set to zero. The solution is then

$$Y_2(z) = (1-z)^{\tilde{n}} z^{|2\tilde{n}+m\epsilon|/2} {}_2F_1(a,b;c;z). \tag{3.85}$$

This is regular at $z=0$ ($R_N=\infty$). To analyse the regularity near $z=1$, use the identity [56]

$$\begin{aligned} {}_2F_1(a,b;c;z) &= \frac{\Gamma(c)\Gamma(c-a-b)}{\Gamma(c-a)\Gamma(c-b)} {}_2F_1(a,b;a+b-c+1;1-z) \\ &+ \frac{\Gamma(c)\Gamma(a+b-c)}{\Gamma(a)\Gamma(b)} (1-z)^{c-a-b} {}_2F_1(c-a,c-b;c-a-b+1;1-z). \end{aligned} \tag{3.86}$$

Regularity requires that the coefficient of the second term vanish, since $c-a-b=-2\tilde{n}$. If $b=-\kappa$, where $\kappa=0,1,2,...$, then the second term will vanish and the solution will be manifestly regular at both $z=0,1$. This leads to the quantization

$$\lambda_V^{(N=2)} = 4\tilde{\kappa}(\tilde{\kappa}+5)+18-m(m+2\epsilon), \qquad \tilde{\kappa}=\kappa+(\tilde{n}-2)+|2\tilde{n}+m\epsilon|/2. \tag{3.87}$$

It is perhaps disconcerting that the spectrum depends on the three quantum numbers, $(\kappa,m,\tilde{n})$, rather than on (κ,m) as happens for the scalars, and tensors [30]. To understand the effect of $\tilde{n}$, first examine the case $m=0$. Then,

$$\lambda_V^{(N=2,m=0)} = 4\tilde{\kappa}(\tilde{\kappa}+5)+18, \qquad \tilde{\kappa}=\kappa+2(\tilde{n}-1). \tag{3.88}$$

For $\tilde{n} = 1$, the smallest possible value, this agrees with the result derived in [24]. The effect of $\tilde{n} > 1$ is simply to shift the starting value of κ from 0 to $2(\tilde{n} - 1)$. Similarly, one can show that in the charged case the allowed values of $\lambda_V^{(N=2)}$ for $\tilde{n} > 1$ are a subset of the allowed values for $\tilde{n} = 1$. Therefore, from the perspective of gravitational perturbations, $\tilde{n} = 1$ can be taken without loss of generality.

We have only succeeded in deriving the spectrum of charged vector harmonics for the case $N = 2$. The main obstacle to explicitly constructing the harmonics for larger N is finding a tensorial structure that is regular near the origin and satisfies the other criteria. It would be useful if this result could be further generalized to arbitrary N.

Part II

Gauge/Gravity Duality

Chapter 4

Introduction

This section serves as an introduction to Part II. The AdS/CFT correspondence and its generalization, the gauge/gravity duality will be briefly reviewed. There are numerous introductions to the gauge/gravity duality at varying levels of technical detail. Rather than attempting a thorough introduction to the subject, here I will take a historical perspective and review the developments leading up to Maldacena's conjecture, with the goal of explaining the extent to which gauge/gravity duality has grown beyond its string theory origin, and I will also give some insight into the current and future directions of the fields of this research.

4.1 A Brief History of String Theory Prior to 1997

The most important goal in the overlap of the fields of high energy physics and gravitation is also the oldest and the most ambitious–the search for *the* quantum

theory of gravity. This has been the outstanding desire for theoretical physicists ever since the remarkable successes of Einstein's theory of General Relativity and the quantum theories, starting with quantum mechanics and growing to include quantum field theories (QFT)'s, eventually culminating in the Standard Model. Despite the brilliant successes of these separate theories, and despite the widespread belief amongst physicists that gravity is quantized, it has proved tremendously difficult to unify these two frameworks. The two major approaches to quantum gravity are Loop Quantum Gravity and String Theory. String theory is the more developed and mature of the pair, and it is the theory I have spent the most time studying. Therefore, in this Introduction and throughout this Thesis, I will restrict my attention to either string theory or more general theories which are inspired by lessons learned using string theory.

String theory is a truly remarkable theory, and has itself undergone several transformations since its initial inception as a theory of hadrons. In order to place the work of this Thesis into context, and to introduce the AdS/CFT correspondence, here I present a very brief (and biased) history of string theory. String theory began as an attempt to explain the physics of hadrons, an attempt that was abandoned after Quantum Chromodynamics was found to be the correct description. During this initial period, a small number of physicists continued exploring the theory, discovering a number of surprises. First, it was found that the theory was only consistent in higher dimensions (26 for the bosonic string, and 10 for the superstring). If string theory is to describe our universe, then clearly these extra dimensions must be accounted for. The most common proposal is that these dimensions are curled up into tiny, un-observable spaces, as in Kaluza-Klein

theory. A second (perhaps more pleasant) surprise was that the theory required a graviton, leading to the interpretation of string theory as a quantum theory of gravity. More precisely, string theory is a theory of gravity with certain matter content. The bosonic string theory only includes bosonic degrees of freedom, but the superstring incorporates fermions as well. Fermions are a necessary ingredient in supersymmetric theories, and they serve the useful functions of helping to ensure that solutions can only have positive energy and cancelling singularities that come from quantum loops. Another reason why fermions are important is that they are a part of nature! Unfortunately, however, superstring theory incorporated chiral fermions, and such theories are generally anomalous in the sense that quantum fluctuations will spoil gauge symmetries and render the theory inconsistent. In 1984 the discovery of the Green-Schwarz mechanism [57] demonstrated that in string theory these anomalies cancelled, leading to what is now known as the First Superstring Revolution, a period of intense growth and popularity for the nascent theory.

Some important developments during this time included the development of the heterotic string theories, as well as the discovery that if the extra 6 dimensions of the superstring were curled up in a special way (i.e. as a Calabi-Yau manifold), then the resulting four dimensional theory would preserve some amount of supersymmetry [58], which is attractive from a phenomenological standpoint. Perhaps most importantly for this thesis, in 1995 D-branes were discovered to be non-perturbative objects in the theory, and moreover these solitonic objects were found to be related to the previously discovered black p-brane solutions of the supergravity theories that were the low energy limits of the various string theories

[59, 60]. This advance initiated what is now known as the Second Superstring Revolution. A fundamental insight came shortly afterwards when Ed Witten realized that the many different string theories were actually unified into one overarching theory called M-theory. [1] Witten's realization was based on *duality*, the notion that two superficially distinct and unrelated theories could actually be the same. This was a tremendous result: string theory, the most successful candidate theory of quantum gravity, had a surprising amount of uniqueness. There is just one single theory, M-theory, and the previously distinct *perturbative* string theories are interpreted as representing various corners of the solution space of this master theory. The idea of a single unique theory of quantum gravity is certainly attractive, and string theory is often praised as having "no free parameters", in contrast to the Standard Model. However, this sentiment is a bit misleading. The modern view is that although string theory has no free parameters, it has many solutions. This multitude of solutions is known as the string landscape, and indeed it is a multitude–a commonly cited number is that there are perhaps 10^{500} vacua! [2] In Part III we will have more to say about the landscape.

Another remarkable discovery relying on the concept of duality came in 1996 when Strominger and Vafa were able to show that string theory could account for the entropy of a black hole [62]. Any successful theory of quantum gravity should be able to account for the laws of black hole thermodynamics, in which

[1] The name "M-theory" has a bemusing origin: Witten has suggested that the M should stand for "magic", "mystery", or "membrane" according to taste.

[2] See [61] for a detailed analysis.

black holes are assigned a Bekenstein-Hawking entropy which is

$$S_{BH} = \frac{A_H}{4G_N}, \tag{4.1}$$

where A_H is the area of the event horizon, and G_N is Newton's gravitational constant. The equations of general relativity can be used to show that S_{BH} behaves very similarly to a thermodynamic entropy, but the interpretation as a bona fide entropy would require identifying the microstates of the hole, which would seem to require a very detailed understanding of quantum gravity. Strominger and Vafa were able to show that string theory could account for these microstates by using the fact that the system at weak coupling had a description in terms of D-branes, for which the worldvolume field theory was known. Using this field theory, they were able to count the number of microstates in a given ensemble, and miraculously, because the system they were studying was supersymmetric, the same answer held for the case of strong coupling for which the system had a description in terms of a certain black brane. The brane's area (and therefore entropy) could be calculated in a straightforward way, and the two answers matched! This served as a major achievement of string theory.

4.2 Maldacena's Conjecture and the Gauge/Gravity Duality

Building off of the growing number of connections between D-branes, their world-volume conformal field theories (CFT's), and the black p-branes of super-

gravity, Maldacena in 1997 made a startlingly bold conjecture, that Type IIB string theory in $AdS_5 \times S^5$ was dual to $\mathcal{N} = 4$ supersymmetric $SU(N)$ Yang-Mills in 4-dimensional Minkowski space, which is the conformal boundary of the 5-dimensional AdS space. The reason why this was such a bold conjecture is that the first theory is a theory of gravity in 10 dimensions and the second is a quantum field theory in one fewer dimensions. Therefore, this is a holographic duality, realizing the holographic principle of t'Hooft and Susskind. As a result of the work of Bekenstein and Hawking, it had long been understood that black holes store information holographically, that is, their entropy scales with area and not volume. It was later proposed by t'Hooft (and developed further by Susskind) that such a property should extend generally to quantum gravity, that the physics inside a certain region of spacetime should be encoded on the boundary of that region. Excitingly, this is precisely what is accomplished by the AdS/CFT duality of Maldacena!

The Maldacena duality possess another fascinating feature. The duality is a weak-strong duality, meaning that when one theory is weakly coupled, the other theory is strongly coupled. So, in particular, if the gauge theory is strongly coupled the gravitational theory is weakly coupled. It's hard to imagine the duality making sense if it were a weak-weak duality, as the degrees of freedom of both theories are well understood and are clearly not in correspondence with one another. Moreover, the weak-strong nature of the duality allows it to be extremely useful. It is hard to calculate many properties of strongly-coupled field theories, and the AdS/CFT duality therefore provides us with a new tool with which to study these theories. It can also work the other way, providing a non-perturbative definition of

quantum gravity (with certain boundary conditions). Additionally, it has opened up surprising connections between previously disparate ideas. For example, black holes in AdS are dual to thermal states in the dual field theory. This remarkable fact implies that black holes in a rather unusual background spacetime from the point of view of our actual universe can be used to understand properties not of astrophysical systems, but of the kind of strongly coupled field theories which might govern a superconductor constructed in a laboratory.

Maldacena's conjecture has never been rigorously proven, (and there is no reason to hope for such a proof anytime soon, as rigorous mathematical results in even comparatively well-understood quantum field theories are very difficult to obtain), however it has passed a remarkable number of tests, and has had a lasting and tremendous impact on on the fields of high energy physics and gravitation. Since the initial AdS_5/CFT_4 conjecture using Type IIB string theory, other AdS/CFT correspondences have been discovered within string theory. Moreover, there are plenty of examples where the duality differs significantly from the original correspondence. For example, there are dualities with non-AdS boundary conditions, which can correspond to dual field theories lacking a UV fixed point (as in Klebanov-Strassler [63]), or to field theories on non-trivial boundary manifolds, for example a boundary Schwarzschild black hole [64]. Through this manner, one may obtain a wide variety of AdS/CFT-like dualities, and as a result many researchers prefer the umbrella term "gauge/gravity duality".

There are even attempts to expand the gauge/gravity duality beyond string theory. After all, although string theory is the most understood and well studied theory of quantum gravity, there is no reason to believe that *all* theories

of quantum gravity are string theories. Also, the original motivations for the gauge/gravity duality such as the thermodynamic properties of black holes and the arguments of t'Hooft and Susskind should hold generally for any theory of quantum gravity. Additionally, all the known dualities "derived" in string theory come along with extra dimensions, as in the S^5 of the original $AdS_5 \times S^5$. There has been much progress in understanding gauge/gravity duality without string theory and without the extra dimensions in the case of $D = 3$. For AdS_3, Brown and Henneaux [65] showed independently of string theory or any other UV completion of gravity that the asymptotic symmetry group of the spacetime is that of a 2D conformal field theory. There have been various conjectures as to the precise dual field theory, for example [66]. Along these lines of extending the gauge/gravity duality beyond string theory, there is an argument due to Marolf that any gravititational theory is in some sense holographic, at least perturbatively around certain backgrounds [67]. Thus it could well be that the original Maldacena duality of Type IIB string theory and developments inspired by it will eventually lead to a general understanding of quantum gravity. This is a very intriguing possibility, although one that will not be pursued further in this Thesis.

Much current research concerns potential real world applications of the gauge/gravity duality. Many important and not entirely well-understood condensed matter systems are governed by strongly coupled field theories. If the duality could be exploited to find a gravitational dual to these systems, then certain quantities that would be hard to calculate or study in the field theory might become more tractable in the dual description. A rather famous and close-to-home application of this is the holographic superconductor by Hartnoll, Herzog, and Horowitz [68].

Although it is often said that black holes "have no hair", this is simply not true (as Gary likes to say, regarding the non-linear stability of AdS). In asymptotically flat contexts, there are a number of ways for a black hole to have hair, but they are a bit exotic, for example a black hole can have non-abelian Yang-Mills hair. In asymptotically AdS spaces, black holes can even have $U(1)$ hair, as Gubser first noticed [69]. Expanding on this result, working in the theory of Einstein gravity with a negative cosmological constant, a $U(1)$ Maxwell field, and a charged massive scalar field (i.e. not string theory), the above authors constructed asymptotically AdS black hole solutions with static, charged scalar hair. This theory does not have a precise and well understood dual field theory at the level of the original $AdS_5 \times S^5$ duality, for example, but there are a few approaches one could take. Firstly, one might regard this theory as capturing the crucial ingredients of the system of interest, and worry later about embedding it in a higher dimensional string theory duality. This was indeed later shown to be possible, see for example [**?**]. Secondly, one could imagine working in the sort of expanded notion gauge/gravity duality discussed above, without worrying about the UV completion. This last approach is somewhat similar in spirit to Landau-Ginzburg theory.

Supposing that a dual field theory exists, Hartnoll et al showed that according to the standard AdS/CFT dictionary, the field theory dual to the charged black holes was in a superconducting state! Since this initial work, there have been hundreds of papers expanding upon this simplified model of holographic superconductivity, and in fact the use of the gauge/gravity duality to model real-world condensed matter phenomena is by now a well-established sub-field, which goes

by the name of AdS/CMT (CMT for condensed matter theory). Along these lines, in Sec. 5 a study will be presented which investigates an enlargement of the program initiated by Horowitz, Herzog, and Hartnoll to encompass a particular model of superconductivity which has eluded a complete theoretical description thus far–high-Tc superconductors. A spin-2 or d-wave order parameter is widely believed to be crucial for achieving high-Tc superconductivity, and we investigate a novel way of incorporating such an order parameter in models of holographic superconductivity.

In most of the gauge/gravity dualities, AdS space plays a prominent role. Therefore, it is good to have a thorough understanding of classical gravity in asymptotically AdS spacetimes, as gravity is a universal ingredient in the dualities. Asymptotically stationary black holes are a particularly important class of spacetimes to consider, as they are dual to field theories at finite temperature. When the black holes are rotating, they may exhibit the interesting phenomenon of superradiance, just like their asymptotically flat counterparts. Superradiance is the phenomenon in which a wave may scatter off a rotating black hole and with the reflected wave carrying away more energy and angular momentum then it started with. This naturally causes the black hole to lose mass and to slow down. In AdS, the boundary conditions force this reflected wave to reflect off the boundary, causing the superradiant scattering to repeat. Therefore, there is a feedback look, and an instability may develop. In Sec. 6 we will present a study which investigated these superradiant instabilities in an attempt to understand thermalization in conformal fluids.

Chapter 5

Spin-2 Condensates and the AdS Soliton Geon

5.1 Introduction

A geon is a classical solution to the vacuum Einstein equations representing a localized and non-dispersing lump of gravitational energy held together by its own gravitational attraction. Geons were originally conjectured to exist by Wheeler, and the first serious attempt to construct them was made by Brill and Hartle [70]. Their geon, however, has only a finite lifetime; at late times the gravitational waves comprising the geon will break free and disperse. This is a common feature of asymptotically flat geons [71]. The tendency of geons to disperse can be remedied with a negative cosmological constant, as anti-de Sitter (AdS) space acts like a confining box. Perturbative geons in global AdS in four dimensions have been recently constructed in [72]. This provides strong evidence that associated with

every individual linearized graviton mode in global AdS, there is a one parameter family of exact nonsingular geons[1].

One should be able to construct geons starting with gravitational perturbations of any locally asymptotically AdS ground state. In particular, one can start with the AdS soliton [74, 75], which has seen several applications in gauge/gravity duality. It was originally introduced to describe the ground state of a confining gauge theory [74], but in more recent condensed matter applications it has been used to construct the gravitational dual of an insulator/superconductor quantum phase transition [76, 77]. In this note we perturbatively construct a class of geons starting with the five-dimensional AdS soliton.

Although the geons we find are interesting in their own right, perhaps the most intriguing aspect of these solutions is the potential connection with a d-wave superconductor. The possibility of obtaining a gravitational dual of a d-wave superconductor is exciting because this is what is seen in the high-T_c cuprates. While the original holographic superconductor exhibited an s-wave order parameter [68], and later a model with a p-wave order parameter was constructed in [78], the d-wave case remains elusive. The major obstacle to building a d-wave superconductor is that there is no known consistent action for a charged, massive, spin-2 field minimally coupled to gravity. Various authors [79, 80] have worked with incomplete actions and found d-wave superconducting condensates, but as of yet no consistent holographic model has been found.

An alternative approach towards constructing a d-wave holographic superconductor is to study metric perturbations in Kaluza-Klein theory. Upon dimen-

[1]This is not true for generic perturbations of AdS containing superpositions of modes [72, 73].

sional reduction, gravitons carrying momentum along a compact direction become charged under a gauge group that corresponds to the isometry group of the internal manifold. Kaluza-Klein gravity therefore provides a natural framework to find a consistent theory of charged spin-2 fields coupled to gravity. We will explore the feasibility of this approach using the geons we construct[2].

The AdS soliton is a particularly interesting background to consider because in addition to the $U(1)$ gauge field coming from the dimensional reduction along its S^1, the linearized metric perturbations may be decomposed into scalar, vector, and tensor types, corresponding to s, p, and d-wave excitations in the boundary theory. The Kaluza-Klein approach applied to the AdS soliton thus provides the exciting possibility of being able to describe a range of qualitatively different superconductors using just pure gravity. Unfortunately, we find that d-wave superconductors are not described by the perturbative geons we construct because the condensates are never thermodynamically preferred. This result is in contrast to the one obtained when one puts a Maxwell field and charged scalar field in the soliton background (rather than obtain them by Kaluza-Klein reduction). In that case, there is a continuous phase transition which turns on the scalar field as one increases the chemical potential. We discuss a likely explanation for the different behavior.

This paper is organized as follows. In section two the linearized metric perturbations of the AdS soliton are reviewed and the perturbative construction of the geons is described. In section three holographic superconductors based on the AdS

[2]During this work we learned that the Kaluza-Klein approach to d-wave superconductivity is also being studied by Kim et al [81], who consider dimensionally reduced supergravity in 10 and 11 dimensions.

soliton background are briefly reviewed, and the possibility that the dimensionally reduced geons could describe d-wave superconductors is considered.

5.2 Geons Built from the AdS Soliton

5.2.1 Linearized Metric Perturbations

We study five-dimensional gravity described by the simple action

$$S = \int d^5x\sqrt{-g}\Big(R + \frac{12}{L^2}\Big), \tag{5.1}$$

where we have set $16\pi G = 1$. The AdS soliton is a solution of the above action with line element

$$ds^2 = \frac{L^2}{r^2 f(r)}dr^2 + \frac{r^2}{L^2}\Big(f(r)d\tilde{y}^2 + \sum_{\mu,\nu=0}^{2}\eta_{\mu\nu}dx^\mu dx^\nu\Big), \qquad f(r) = 1 - \Big(\frac{r_0}{r}\Big)^4. \tag{5.2}$$

This solution can be obtained from the planar black hole via a double Wick rotation. The geometry smoothly caps off at $r = r_0$ if the $\tilde{y}$-coordinate is chosen to be periodic with period $\pi L^2/r_0$. The conformal boundary is the direct product of three-dimensional Minkowski spacetime with a circle, $\mathbb{M}^3 \times S^1$.

Throughout this paper we work in perturbation theory around the background of the AdS soliton. For this purpose an expansion parameter ϵ is introduced and the metric is expanded as

$$g_{AB}(\epsilon) = \sum_{i=0}^{\infty}\epsilon^i g_{AB}^{(i)}, \tag{5.3}$$

where $g^{(0)}_{AB}$ is the AdS soliton metric. Since the Einstein equations will need to be solved numerically, it will be useful to work with a compactified radial coordinate and to scale the dimensionful constants out of the metric. The background line element then becomes

$$g^{(0)}_{AB}dx^A dx^B = \frac{1}{z^2}\left[\frac{dz^2}{(1-z^4)} + \frac{1}{4}(1-z^4)dy^2 - dt^2 + dx_1^2 + dx_2^2\right]. \tag{5.4}$$

The circle coordinate has been rescaled so that $y \sim y + 2\pi$. The radial coordinate takes values in the range $z \in [0, 1]$. The conformal boundary is at $z = 0$ and the tip is located at $z = 1$.

Next, we briefly review linearized metric perturbations of the AdS soliton background. A comprehensive treatment may be found in [82]. The perturbations are decomposed into scalar, vector, and tensor types according to their transformation properties under the $SO(1, 2)$ Lorentz symmetry of the soliton. We shall focus on tensor perturbations, which can be parametrized as

$$g^{(1)}_{AB} = \varepsilon_{AB}\frac{H(z)}{z^2}\cos(qy - \omega t). \tag{5.5}$$

Here $q \in \mathbb{Z}$ and ε_{AB} is a polarization tensor. In five-dimensions, there are two independent polarizations,

$$\varepsilon_{x_1x_2} = 1, \qquad \text{all other components zero,} \tag{5.6}$$

$$\varepsilon_{x_1x_1} = -\varepsilon_{x_2x_2} = 1, \qquad \text{all other components zero.} \tag{5.7}$$

With the above ansatz for the metric perturbation, the Einstein equations reduce to a single second order ODE for the function $H(z)$. Requiring that the perturbation be regular at the tip and normalizable at the boundary yields a Sturm-Liouville eigenvalue problem. Solutions only exist for a discrete set of frequencies $\omega \in \mathbb{R}$. These solutions are the normal modes and the ω are the normal mode frequencies. The tensor perturbations may therefore be characterized by two integers, the radial overtone number and the momentum q.

The perturbation breaks some, but not all, of the symmetries of the background. Translational invariance in the t and y directions is broken, but the perturbation remains invariant under the helical Killing field $K = \partial_t + (\omega/q)\partial_y$. Since $\omega > 2q$, this Killing field is timelike near the tip and spacelike near the boundary. The perturbation also remains invariant under translations in the x_1, x_2 directions and under the combined discrete operations of $t \to -t$ and $y \to -y$.

5.2.2 Perturbative Construction of Geons

We now extend the study of the previous section to higher orders in perturbation theory. We will call the resulting metrics geons as they are solutions describing nonlinear, non-dispersing concentrations of gravitational waves. The structure of the perturbative construction is very similar to Gubser's study of the non-uniform black string [83]. For every distinct linear perturbation there should exist a corresponding one-parameter family of geons, $g_{AB}(\epsilon)$, with symmetries similar to those of the linearized mode. The expansion parameter will be chosen so that the momentum of the geon is $P = \epsilon^2 V_2$, where V_2 is the coordinate volume

of the x_1-x_2 plane, although other choices are also possible. The metric ansatz is

$$ds^2 = \frac{1}{z^2}\left[Ady^2+Bdz^2+Cdt^2+D(dx_1^2+dx_2^2)+Edtdy+Fdzdt+Gdzdy+Hdx_1dx_2\right]. \tag{5.8}$$

This ansatz corresponds to a geon seeded by a tensor perturbation with polarization (5.6). Here A through H are functions of the coordinates z, t, and y, as well as the expansion parameter ϵ. Periodicity of the circle coordinate implies that the y-dependence of these functions will be organized into a Fourier series, while the existence of the helical Killing vector implies that the functions will depend on y and t only through the combination $(qy - \omega t)$. Thus the expansions for A through E take the form

$$A(z, y, t, \epsilon) = \sum_{n=0}^{\infty} A_{2n}(z, \epsilon) \cos\Big(2n(qy - \omega t)\Big), \tag{5.9}$$

while the expansions for F and G take the form

$$F(z, y, t, \epsilon) = \sum_{n=1}^{\infty} F_{2n}(z, \epsilon) \sin\Big(2n(qy - \omega t)\Big). \tag{5.10}$$

Whether a given metric function is written as a sum of sines or cosines is determined by requiring that the line element be invariant under the discrete symmetry $(y, t) \to (-y, -t)$. The amplitude of each Fourier mode may also be expanded in powers of ϵ. The expansions for A_{2n} through G_{2n} take the form

$$A_{2n}(z, \epsilon) = \sum_{i=0}^{\infty} \epsilon^{2n+2i} A_{2n}^{(2i)}(z). \tag{5.11}$$

The structure of the perturbative equations dictates that only even Fourier modes and even powers of ϵ appear in the above expansions. The function H differs from functions A through G because it seeds the geon. It is expanded in odd Fourier modes and in odd powers of ϵ,

$$H(z,y,t,\epsilon) = \sum_{n=0}^{\infty} H_{2n+1}(z,\epsilon)\cos\Big((2n+1)(qy-\omega t)\Big), \tag{5.12}$$
$$H_{2n+1}(z,\epsilon) = \sum_{i=0}^{\infty} \epsilon^{2n+2i+1} H_{2n+1}^{(2i)}(z).$$

Note that although an infinite number of Fourier modes will be needed to describe the solution, the higher modes only enter at higher orders in perturbation theory.

When constructing geons in global AdS, there was a potential problem due to resonances. Since all the normal mode frequencies were integer multiples of the lowest one, there were resonances at higher orders in the perturbative construction which threatened to introduce growing modes into the solution. It was found however, that this could be avoided by letting ω depend on ϵ, provided one starts with individual graviton modes [72].

The normal mode frequencies in the AdS soliton are not integer multiples of each other, so there are no exact resonances. Nevertheless ω still depends on ϵ for the following reason: recall that for the linearized perturbation, the value of ω was determined by requiring that $H(z)$ be regular at the tip and normalizable at the boundary. This linear perturbation then seeds the nonlinear geon, and is relabelled $H_1^{(0)}(z)$. At second order, the background geometry is altered, and at third order, the original seed Fourier mode is corrected because the function $H_1^{(2)}(z)$ is turned on. The original value for ω does not allow $H_1^{(2)}(z)$ to be both

regular and normalizable, therefore ω must also be corrected. These corrections will be determined from odd orders in perturbation theory, but the corrections to ω will be in even powers of ϵ,

$$\omega(\epsilon) = \sum_{i=0}^{\infty} \epsilon^{2i} \omega_{2i}. \tag{5.13}$$

The geon is not invariant under the action of the vectors ∂_t or ∂_y individually, but these are asymptotic Killing vectors and therefore the geon will carry the corresponding conserved charges of energy and momentum. These charges also have an expansion in even powers of ϵ,

$$E(\epsilon) = \sum_{i=0}^{\infty} \epsilon^{2i} E_{2i}, \qquad P(\epsilon) = \sum_{i=0}^{\infty} \epsilon^{2i} P_{2i}. \tag{5.14}$$

In the above expansions, ϵ appears as a formal expansion parameter. In order to relate the expansion parameter to a physical quantity, we define ϵ to make $P(\epsilon) = \epsilon^2 V_2$.

At each order in perturbation theory the Einstein equations reduce to a set of coupled ODE's. The first order equations are homogeneous, while all the higher order equations have inhomogeneous source terms consisting of powers of the lower order functions and their derivatives. We choose boundary conditions that enforce regularity at the tip and leave the boundary metric unchanged. We also fix the periodicity of the circle to be 2π.

We numerically solved the perturbative hierarchy of Einstein's equations to third order. The energy and momentum were obtained using the AdS stress tensor formalism of Ref. [84]. We find that the geon has larger energy than the

background, $E_2 > 0$, in accord with the positive energy conjecture [75]. As a numerical check, we verified that the solutions obey the first law of thermodynamics to $\mathcal{O}(\epsilon^4)$. Since there are no horizons (and hence no entropy) and the solution is invariant under $\partial_t + \omega/q\ \partial_y$, this is simply [85]

$$dE = \frac{\omega}{q} dP. \tag{5.15}$$

We also checked that the boundary stress tensor is traceless. Odd-dimensional asymptotically locally AdS spacetimes may have a conformal anomaly, but not when the boundary is Ricci flat, as it is for these geons. Since there are no exact resonances, there should be no obstructions to extending the perturbative solution to all orders and constructing a one parameter family of exact solutions for each linearized mode.

For later reference, we now consider how the frequency changes with the Kaluza-Klein excitation q: $\omega(q) = \omega_0(q) + \omega_2(q)\epsilon^2 + \mathcal{O}(\epsilon^4)$. For large q, one finds $\omega_0 \to 2q$. This is a simple consequence of the fact that as $q \to \infty$, the support of the first order normal mode becomes both squeezed (in the coordinate z) and pushed further away from the tip (see Fig. 1). For arbitrarily large q, the normal mode is effectively localized on the boundary, and so its equation of motion becomes that of a massless scalar field on $\mathbb{M}^3 \times S^1$. This leads to the dispersion relation $\omega_0 = 2q$. The factor of 2 arises from the fact that the y coordinate has been rescaled to make its period 2π. As discussed above, the second order term in the frequency expansion, ω_2, is found by requiring that the function $H_1^{(2)}(z)$ be regular at the tip and normalizable at the boundary. The result is always nega-

tive (see Fig. 2). With our choice of expansion parameter, $P = \epsilon^2 V_2$, the second order change asymptotes to 0 as $q \to \infty$. This is simply a reflection of the fact that as q gets larger, the amplitude of the linearized perturbation must decrease to maintain a fixed P. Thus the second order backreaction becomes smaller and hence there is a smaller change in the frequency. The fact that $\omega_2 < 0$ will play an important role in the next section. The global AdS geons also had $\omega_2 < 0$ [72].

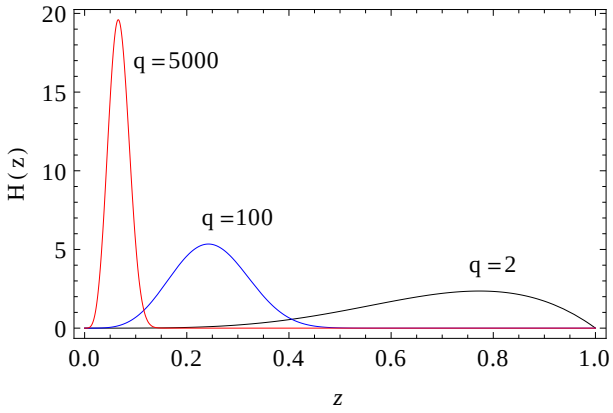

Figure 5.1: The linearized tensor perturbation for three different choices of q. As q increases the function becomes squeezed and pushed towards $z = 0$. These functions correspond to the lowest overtone number, and have been normalized so that the area under the curve is 1.

5.3 Geons and Holographic Superconductors

5.3.1 AdS Soliton Superconductors

In this section we briefly review the holographic superconductor in the AdS soliton background [76, 77]. This system has many features in common with the dimensionally reduced geons, and the review will be useful when we investigate the possibility that geons could model holographic superconductors. We also present

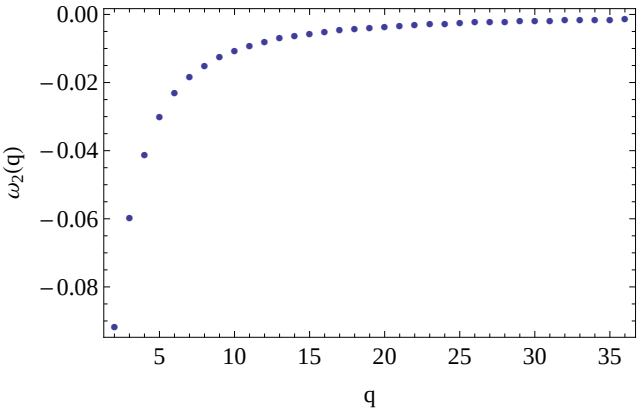

Figure 5.2: Plot of the second order change in frequency, $\omega_2(q)$. For all q studied, $\omega_2 < 0$. Normalization is fixed so that $P = \epsilon^2 V_2$ is constant.

a simple characterization of the superconducting phase transition and show that it is *not* caused by a linear instability towards scalar condensation.

Consider the Einstein-Maxwell-scalar theory defined by the following action

$$S = \int d^5x\sqrt{-g}\Big(R + \frac{12}{L^2} - \frac{1}{4}F^2 - |(\nabla - iqA)\Psi|^2 - m^2|\Psi|^2\Big). \tag{5.16}$$

The possibility that this theory could describe a $T = 0$ insulator/superconductor phase transition in the background geometry of the AdS soliton was first considered in Ref. [76]. They worked in the probe limit in which the backreaction of the metric is neglected but the nonlinearities of the Maxwell and scalar fields is preserved. A superconducting phase transition was found to occur as the chemical potential μ was increased from zero to some critical value, μ_c. Then [77] considered the full backreaction and found the complete phase diagram. Both groups either explicitly or implicitly considered the following ansatz for the matter fields

$$A = \phi(r)dt, \qquad \Psi = \psi(r)e^{-i\omega t}. \tag{5.17}$$

As a result of gauge invariance, the equations of motion are invariant under the transformation $\phi \to \phi + C$, $\omega \to \omega - qC$, where C is a constant. In both papers C was chosen to set $\omega = 0$. Since the chemical potential is defined to be the leading term in the near-boundary expansion of the gauge field, $\phi = \mu - \rho/2r^2 + \mathcal{O}(r^{-4})$, this corresponds to a choice of chemical potential.

The critical chemical potential found in the probe limit in Ref. [76] simply corresponds to the smallest normal mode frequency of a charged scalar field in the AdS soliton background (divided by the charge q). To see this, consider the system in the probe limit right at the critical point, $\phi = \mu_c$. The Maxwell field is pure gauge, and the scalar field is negligibly small, so the equations of motion reduce to a single linear ODE for the static scalar field $\Psi = \psi(r)$. By using the above symmetry this field configuration can be transformed to $\phi = 0$, $\Psi = \psi(r)\exp(-iq\mu_c t)$. The ϕ equation of motion is trivially satisfied, and the ψ equation is identical to that determining the normal modes, except with $\omega \to q\mu_c$. So the determination of μ_c is equivalent to the problem of finding the normal mode frequencies of a scalar field in the AdS soliton background. This connection between the critical chemical potentials and the normal mode frequencies was first discussed in [86].

There is a crucial difference between the superconducting phase in the AdS soliton background and the original holographic superconductor based on the Schwarzschild AdS solution [68]. In the latter case, below a critical temperature, the black hole becomes unstable to forming charged scalar hair. In the AdS soliton there is no instability for any value of the chemical potential. Instead, the insulator/superconductor phase transition reflects which configuration has lower

free energy and hence dominates a grand canonical ensemble. If there were an unstable linearized mode growing exponentially in time for some $\phi = \mu > \mu_c$, then the above shift symmetry could be used to set $\phi = 0$ at the cost of shifting the real part of ω. This shift would not affect the exponentially growing behaviour of the mode, so it would therefore be an unstable perturbation of the AdS soliton. But it is known that the AdS soliton is stable to linearized perturbations of both the metric and a free massless scalar field [75, 82]. So such a growing linearized mode cannot exist, and the appearance of a new branch of static solutions (the superconducting condensates) is not related to any linear instability.

5.3.2 Holographic Dual of the Geons

We now investigate the possibility that the dimensional reduction of the geons could model a holographic superconductor. Recall the standard Kaluza-Klein reduction of a five dimensional metric with a $U(1)$ symmetry. One can write the metric in the form

$$ds^2 = g_{AB}dx^A dx^B = \phi^2(dy + A_a dx^a)^2 + \frac{1}{\phi}g^{(4)}_{ab}dx^a dx^b, \tag{5.18}$$

where $x^a = (r, x^\mu)$ and the functions depend on the x^a coordinates only. This parametrization leads to a four-dimensional Einstein-Maxwell-dilaton theory in the Einstein frame. The off-diagonal part of the metric, A_a, is interpreted as a Maxwell field. Five-dimensional coordinate transformations of the form $y \to y + \lambda(x)$ correspond to four-dimensional gauge transformations, $A_a(x) \to A_a(x) + \partial_a\lambda(x)$.

The AdS soliton can, of course, be written in the above form[3] with $A_a = 0$. A simple five-dimensional coordinate transformation $y \to y + \mu t$ generates a nonzero gauge field $A_t = \mu$. If there is a phase transition to forming the geon at a critical value $\mu = \mu_c$, then near μ_c the amplitude of the geon will be small and it can be approximated by the leading $\mathcal{O}(\epsilon)$ correction to the metric (5.5). When $\mu = \omega/q$ (where ω is the frequency of the linearized graviton mode) the dimensional reduction of this mode corresponds to a static, charged spin-2 field. In the dual boundary theory, this corresponds to turning on a charged spin-2 condensate $\langle O_{x_1 x_2} \rangle$. Since the AdS soliton is stable to linearized metric perturbations, the appearance of this new branch of static solutions is analogous to turning on the superconducting condensate in Ref.'s [76, 77]; in neither case is the condensation the result of a linearized instability.

The key question is whether the condensate has lower free energy than the original state with no condensate. To compute this, one needs to construct the geon to higher order as we have done in the previous section. Consider the five-dimensional theory in the zero temperature grand canonical ensemble. The relevant free energy functional is the Gibbs free energy, which, in the absence of any black hole horizons or true five-dimensional Maxwell fields, takes the form $G = E - (\omega/q)P$. Making use of the first law (5.15), the Gibbs free energy obeys

$$dG = -\frac{P}{q} d\omega = -\frac{2P_2\omega_2}{q}(1 + \mathcal{O}(\epsilon^2))V_2\epsilon^3 d\epsilon. \tag{5.19}$$

Since $P_2 > 0$, the sign of the free energy depends on the sign of ω_2, which we have

[3]The four dimensional Einstein metric will be singular at the location of the tip and is not asymptotically AdS. However in terms of applications to gauge/gravity duality, both of these problems can be resolved by applying holography directly to the five dimensional solution [87].

found is always negative (see Fig. 2). Therefore, at least in perturbation theory, the geon will always have a larger free energy than the AdS soliton. Since the free energy is unaffected by dimensional reduction, we conclude that the spin-2 condensate will also have a larger free energy than the field theory state with no condensate. This result spoils the hope that the perturbative geon could model a d-wave superconductor.

What is the key difference between this case and the earlier result that there is a phase transition when the Maxwell field and charged scalar field are added to the five dimensional action? The most likely explanation is that when a charged scalar is added, one can increase the charge q keeping the mass fixed, while in the Kaluza-Klein case, increasing q also increases the effective mass in the four dimensional theory. Indeed, it was shown in [77] that for $m^2 = -15/4$ and $q = 1$ the free energy increases when the scalar turns on. It decreases only for larger q (with the same m). However, even for $q = 1$, it turns out that as the amplitude of the scalar field increases, the change in free energy eventually becomes negative and there is a first order phase transition [77].

It remains possible that the exact geon solutions will behave like the $q = 1$ charged scalar. However, even if the change in free energy eventually becomes negative, the condensate will not be pure spin-2. From the structure of the perturbative Einstein equations, it is clear that the first order seed perturbation $H_1^{(0)}(z)$ sources an infinite number of higher Fourier modes, and that the higher order perturbations are complicated combinations of scalar, vector, and tensor modes. Therefore, the corresponding state in the dual field theory is a nonlinear combination of spin-0, 1, and 2 condensates of various charges. This is conve-

niently described in terms of $\langle T_{\mu\nu} \rangle$. Since the metric is the only nonzero bulk field in five dimensions, the only dual operator with a nonzero expectation value is the (traceless) stress tensor. The Maxwell field on the boundary arises from Kaluza-Klein reduction of the (fixed) boundary metric.

To summarize, we have perturbatively constructed a class of geons in the background geometry of the AdS soliton to third order. We only considered geons seeded by tensor perturbations; vector and scalar perturbations would lead to different classes of geons. These solutions have an exact helical Killing vector $K = \partial_t + (\omega/q)\partial_y$. We considered the dimensional reduction of the geons and found some features suggestive of d-wave superconductors. However, these geons do not provide a gravitational dual of a continuous phase transition to a superconductor.

We have also seen that the previously studied phase transition in the AdS soliton is not the result of a linear instability. The dimensionally reduced spin-2 condensate we construct is also not the result of a linear instability. Perhaps the Kaluza-Klein approach towards holographic superconductivity would be more successful if the gravitational background became linearly unstable to a metric perturbation as some control parameter is varied. This possibility deserves further investigation.

Acknowledgements

We would like thank J. Santos and B. Way for useful discussions. We are especially grateful to J. Santos for suggesting this project. This work was supported in part by NSF grant PHY12-05500.

Chapter 6

Holographic thermalization, quasinormal modes and superradiance in Kerr-AdS

6.1 Introduction and summary

The behavior of perturbed black holes (BHs) in asymptotically anti de-Sitter (AAdS) spacetimes is of central importance in both current fundamental and practical research endeavors. Since these spacetimes contain a timelike boundary, exploring such behavior requires taking into account the role of boundary conditions. Of particular relevance are physically motivated conditions implying the absence of dissipation at infinity. This introduces new features and challenges in the analysis of fluctuations in AAdS scenarios: generic perturbations "bounce back" off infinity and come back to interact, in the core region of AdS

or with the black hole, in finite time. Such interaction dissipates the quasinormal modes (QNMs) only at the horizon and can trigger superradiant instabilities at the linear level, and even induce other nonlinear phenomena. Additionally, BHs in AAdS play a central role in the formulation and applications of the AdS/CFT correspondence. This correspondence [88, 89] provides a remarkable framework for studying certain strongly coupled gauge theories in d dimensions by mapping them to weakly coupled quantum gravitational systems in $d+1$ dimensions. In a certain limit (namely in the large 't Hooft coupling and planar limit), quantum gravity in the bulk reduces to classical general relativity. Within this holographic framework, a black hole is dual to a thermal state and the question of thermalization in the boundary gauge theory translates, in the gravitational bulk, to understanding the "return to equilibrium" behavior of perturbed black holes [90, 91, 92, 93, 94, 95, 96, 97].

Here, we will be interested in the original gauge/gravity duality, namely the $\mathrm{AdS}_{d+1}/\mathrm{CFT}_d$ correspondence (for the $d = 3, 4$ cases for which Super-Yang-Mills theory is dual to string theory on $AdS_4 \times S^7$ and $AdS_5 \times S^5$, respectively). Moreover, we are particularly interested in systems with a rotating chemical potential. This requires looking to CFTs formulated on a sphere (since a rotational shift is a pure gauge transformation on a plane), i.e. for bulk solutions that asymptote to global AdS (which is conformal to the static Einstein Universe $R_t \times S^{d-1}$). Henceforward, when we refer to AAdS spacetimes it is implicitly assumed that we mean global AdS (although some of the discussions are also valid for planar AdS i.e. the Poincaré patch of AdS that asymptotes to $R_t \times R^{d-1}$). We will often use the notation $D = d + 1$ for the bulk spacetime dimension; Greek indices denote

the bulk dimensions while Latin indices describe boundary coordinates.

Certainly, important headways on thermalization can be made by studying the behavior of perturbed black hole spacetimes at a linearized level. Naturally, the applicability of such analysis depends on the strength of the perturbation off the stationary black hole and the behavior obtained can hint of possible instabilities [98, 99, 100, 101].

The analog problem in asymptotically flat spacetimes is, to a large degree, understood. The approach to equilibrium depends sensitively on the character of the perturbation: massless fields (scalar, vector or tensor type) die off through their quasinormal modes (QNMs), with a time dependence of the form $e^{-i\omega t}$ with $\mathrm{Im}(\omega) < 0$ (for a review see [10])[1]. Massive fields on the other hand, have a much richer phenomenology, tied to the fact that they can be trapped inside a cavity with size of the order of the Compton wavelength. This trapping causes the field to decay much slower, or can even become unstable for large black hole rotation (see [102] and references therein). The linear behavior of massive fields around rotating black holes is not fully understood yet (and certainly not the nonlinear regime), but it is akin to that of massless fields in AAdS backgrounds in that both can develop trapping potentials. However, an important difference is that the height of the potential barrier is unbounded in the AdS case while it is finite for a massive scalar in a flat background.

Accurate expressions for the QNMs for generic black holes in the asymptotically flat case are known for both static and stationary black holes (see the re-

[1]Exceptions exist however, as QNMs do not constitute a basis for perturbations, nevertheless cases where QNMs are known to fail to describe the solution in linearized perturbative regimes are either finely-tuned or, like tails, arise after a QNM epoch can be identified).

view [10]); remarkably this is not the case in the AdS background as they are not known for the Kerr-AdS BH. This status of affairs is, at first sight, surprising given the central role they play in holographic dualities as well as in studies of AAdS black hole stability.

It is thus worth discussing in detail the reason for this gap in our knowledge. Since an AAdS spacetime is a non-globally hyperbolic spacetime (i.e., spatial infinity is a timelike boundary in the Carter-Penrose diagram and thus null rays can reach it in finite time), in order to predict the future time evolution of the system we need to give not only initial data but also to specify the choice of boundary conditions (BCs). At the inner boundary (origin or horizon) regularity fixes the BC. However, at the asymptotic boundary this choice is *à priori* arbitrary, being fixed by a physical motivation. From a pure gravitational perspective it is often stated in the literature that one is interested in "reflecting BCs" which suggests the idea that we want vanishing flux of energy and angular momentum across the asymptotic boundary. On the other hand, in the context of the AdS/CFT duality we typically want to choose BCs that preserve the asymptotic boundary (conformal) metric. Next, and in Appendix 6.A, we emphasize that these two perspectives require exactly the very same BCs. Formally, the discussion of the asymptotic BCs is more clear if we write the total metric (background plus perturbations, if present) in Fefferman-Graham coordinates (this frame is defined such that $g_{zz} = L^2/z^2$ and $g_{zb} = 0$, where z is the radial distance with boundary at $z = 0$, and x^b are the coordinates on the boundary), and looking at its boundary expansion (see [103] and references therein). For odd boundary dimension d this

reads[2]

$$ds^2 = \frac{L^2}{z^2}\left[dz^2 + g_{ab}(z,x)dx^a dx^b\right] ,$$
$$g_{ab}\big|_{z\to 0} = g^{(0)}_{ab}(x) + \cdots + z^d g^{(d)}_{ab}(x) + \cdots \qquad \text{with} \quad \langle T_{ab}(x)\rangle \equiv \frac{d}{16\pi G_N} g^{(d)}_{ab}(x) \tag{6.1}$$

where $g^{(0)}(x)$ and $g^{(d)}(x)$ are the two integration "constants" of the expansion; the first dots include only even powers of z (smaller than d) and depend only on $g^{(0)}$ (thus being the same for *any* solution that asymptotes to global AdS_d) while the second dots depend on the two independent terms $g^{(0)}, g^{(d)}$ (we will fix Newton's constant as $G_N \equiv 1$). Within the AdS/CFT duality we are (typically) interested in Dirichlet BCs that do not deform the conformal metric $g^{(0)}$. Indeed, this defines the gravitational background where the CFT is formulated and we want to keep it fixed; in our case this is the static Einstein Universe. Stated in other words, we allow perturbations in the bulk that only deform the expectation value of holographic stress tensor $\langle T_{ab}(x)\rangle$ (that specifies and describes the boundary CFT) [3] but that preserve the asymptotic structure of the original background that we perturb.[4] As discussed in Appendix 6.A these BCs do not allow asymptotic dissipation of energy or angular momentum. In other words, everything that hits the asymptotic boundary is reflected back to the bulk core allowing for a non-trivial interplay between the asymptotic and inner (e.g. horizon) boundaries. We have

[2]For even d, the asymptotic expansion (6.1) contains also a logarithmic term $z^d \log z^2 \tilde{g}^{(d)}_{ab}$ and the holographic stress tensor has an extra contribution proportional to the conformal anomalies of the boundary CFT [103]. These details are not essential for the present discussion.

[3]Note that $g^{(d)}$ is an integration "constant" but not a free function; it is fixed solving the Einstein equation in the bulk subject to regular BCs at the horizon or radial origin.

[4]Other BCs that might be called asymptotically globally AdS (and that promote the boundary graviton to a dynamical field) were proposed in [104]. However, they turn out to lead to ghosts (modes with negative kinetic energy) and thus make the energy unbounded below [105].

now growing evidence that these conditions favour the development of instabilities. For instance, it has been shown recently that even arbitrarily small perturbations can trigger black hole formation in global AdS [73, 72], indicating that global AdS is nonlinearly unstable to a weak perturbative turbulent mechanism (note however the existence of "islands" of stability [106, 107, 108]). Additionally, it has recently been shown that turbulent behavior [5] (akin to the one displayed by hydrodynamics) arises in long-wavelength perturbations of 3+1 Kerr-AdS [110, 111].

The BCs we need to impose to study AAdS perturbations of global AdS BHs are therefore well known. Yet, we still need to understand why the study of QNMs and superradiant instabilities of global AdS BHs is not a closed chapter. For that, we need to look to the perturbation equations. Studying linearized gravitational perturbations requires solving the linearized Einstein equations for the metric perturbation. For generic perturbations this is a coupled nonlinear system of PDEs. Solving this PDE system directly with the above BCs is a hard problem, even numerically. In certain special cases, however, drastic simplifications occur. Fortunately, and quite remarkably, in four dimensions it has been shown that if we use certain gauge invariant scalar variables we can reduce the problem of looking for the most generic perturbations of the above AAdS BHs to solving a single PDE. Moreover, using the harmonic decomposition of the system, the later reduces to solving two ODEs. This remarkable reformulation of the linearised perturbation problem is known as the Regge-Wheeler−Zerilli or Kodama-Ishisbashi formalism for perturbations of Schwarzchild BHs [112, 113, 31], and Teukolsky formalism for perturbations of Kerr BHs [114, 22]. We ask the reader to see the companion paper

[5] As well, in planar AdS backgrounds, turbulent behavior of gravity has also been uncovered for (sufficiently) long-wavelength perturbations of black holes in [109, 110].

[115] for a detailed discussion of these two formalisms and for the map relating them when the background rotation vanishes. Once the solution for the gauge invariant scalars is known a simple differential map generates the corresponding metric perturbation tensors (in a particular gauge).

At this point, to find QNMs or instability timescales of AAdS BHs we just need to take the above BCs, discussed for the metric perturbations, and translate them to get the corresponding BCs that need to be imposed on the gauge invariant scalars. On general grounds we should expect the Dirichlet BCs on the metric to translate to Robin BCs (which relate the field with its derivative) on the gauge invariant scalars. In the static background case, this dictionary was found by [96, 97]. There are two families of perturbations: scalar (also called even or polar) and vector (odd or axial) sectors. The associated QNMs of the global AdS Schwarzchild BH were then computed [96, 97, 115]: vector QNMs agree with those first computed in [116, 117, 118] (the scalar modes of [116, 117, 118] do not preserve the asymptotic AdS structure). In the stationary case, the BC map was constructed only recently in the companion paper [115]. With it at hand, we can finally compute the gravitational QNM spectrum and superradiant instability growth rates of the Kerr-AdS BH. This is one of main aims of the work here reported. (Previous work on gravitational QNMs [119] and superradiant instability of Kerr-AdS [120] imposed BCs that do not keep the boundary metric fixed). While many of the methods presented here are readily applicable to arbitrary dimensions we concentrate in dimensions $d = 3$ and $d = 4$ because of their interest for the $\mathrm{AdS}_{d+1}/\mathrm{CFT}_d$ holographic dualities.

The interest on the superradiant instability is not restricted to its growth

rate. Indeed, the onset curve of this instability (where the imaginary part of the frequency vanishes) is an exact zero mode that is invariant under the horizon-generating Killing field of Kerr-AdS. Therefore we will argue that, in a phase diagram of stationary solutions, this onset curve signals a bifurcation curve to a new family of BHs that have a single Killing vector field (KVF), i.e. that are periodic but not time dependent neither axisymmetric. A far reaching consequence of this statement is that Kerr-AdS BHs are not the only stationary BHs of Einstein-AdS gravity. These BHs can exist because they evade a main assumption of the rigidity theorems [121, 122, 123]. We will give the explicit perturbative construction of the leading order thermodynamics and properties of these BHs. These ideas were first proposed in [30] and further developed in [124, 72]. Now that we have the precise onset curve of superradiance, we have the opportunity to expand their discussion.

Another aim of the present work is to confirm that long wavelength gravitational QNM frequencies agree with the hydrodynamic relaxation timescales that we obtain when we consider the near-equilibrium and long wavelength effective description of the CFT_d. This will provide the first explicit confirmation that the match between the QNM spectrum and the CFT thermalization timescales also holds in the presence of a rotating chemical potential. Incidentally, it provides the first non-trivial confirmation that the Robin boundary conditions for the Teukolsky gauge-invariant variable derived in the companion paper [59] are indeed the ones that we must impose if we want the perturbations to preserve the conformal metric.

This work is divided as follows. Section 6.2 reviews relevant properties of $D =$

4 Kerr-AdS spacetime and the equations of motion and the BCs [115] governing the behavior of perturbations at the linear level. Section 6.3 describes the numerical methods employed to solve them. One of these numerical approaches is novel and we expect it to be of interest for other applications. Section 6.4 presents our results for the full spectrum of gravitational QNMs and superradiant instability timescales of the Kerr-AdS BH. In Section 6.5 we construct and discuss the novel single Killing vector field BHs that merge with the Kerr-AdS BH at the onset of superradiance. In section 6.6 we use the fluid/gravity duality to confirm the match between the gravitational long-wavelength QNM spectrum and the CFT_3 hydrodynamic modes even in the presence of a rotating chemical potential. Section 6.7 repeats the previous section computations and discussions but this time for the $D = 5$ rotating system that is of interest for the $\mathrm{AdS}_5/\mathrm{CFT}_4$ duality. It will also contribute to identify universal properties of systems with a rotating chemical potential. We work in a particularly clean environment where we study perturbations around the equal angular momentum Myers-Perry BH. Indeed, this background has enhanced symmetry − it only depends non-trivially on the radial direction − and its perturbations have an exact harmonic decomposition. The present study fills important gaps in our knowledge but confirms and opens some interesting questions. In Section 6.8 we discuss these open questions in what can be viewed as a roadmap in the subject from our viewpoint.

6.2 Gravitational perturbations & boundary conditions of Kerr-AdS black hole

In this section we review the basic properties of Kerr-AdS black holes and their gravitational perturbations.

6.2.1 Kerr-AdS black hole

The Kerr-AdS geometry was originally discovered by Carter in the Boyer-Lindquist coordinate system $\{T, r, \theta, \phi\}$ [125]. For our purposes, it is convenient here, to follow Chambers and Moss [126] and introduce the new time and polar coordinates $\{t, \chi\}$, which are related to the Boyer-Lindquist coordinates $\{T, \theta\}$ by

$$t = \Xi\, T\,, \qquad \chi = a\cos\theta\,, \tag{6.2}$$

where a is the rotation parameter of the solution and Ξ is to be defined in (6.4). In this coordinate system the Kerr-AdS black hole line element reads [126]

$$\begin{aligned} ds^2 = &-\frac{\Delta_r}{(r^2+\chi^2)\,\Xi^2}\left(dt - \frac{a^2-\chi^2}{a}\,d\phi\right)^2 + \frac{\Delta_\chi}{(r^2+\chi^2)\,\Xi^2}\left(dt - \frac{a^2+r^2}{a}\,d\phi\right)^2 \\ &+\frac{(r^2+\chi^2)}{\Delta_r}\,dr^2 + \frac{(r^2+\chi^2)}{\Delta_\chi}\,d\chi^2\,, \end{aligned} \tag{6.3}$$

where

$$\Delta_r = \left(a^2+r^2\right)\left(1+\frac{r^2}{L^2}\right) - 2Mr\,, \qquad \Delta_\chi = \left(a^2-\chi^2\right)\left(1-\frac{\chi^2}{L^2}\right)\,, \qquad \Xi = 1-\frac{a^2}{L^2}\,. \tag{6.4}$$

The Chambers-Moss (CM) coordinate system $\{t, r, \chi, \phi\}$ has the appealing property that the line element treats the radial r and polar χ coordinates on an almost equal footing. This property extends to the radial and angular equations describing gravitational perturbations in the Kerr-AdS background. In this frame, the horizon angular velocity and temperature are given by

$$\Omega_H = \frac{a}{r_+^2 + a^2}\,, \qquad T_H = \frac{1}{\Xi}\left[\frac{r_+}{2\pi}\left(1 + \frac{r_+^2}{L^2}\right)\frac{1}{r_+^2 + a^2} - \frac{1}{4\pi r_+}\left(1 - \frac{r_+^2}{L^2}\right)\right]. \quad (6.5)$$

The Kerr-AdS black hole obeys $R_{\mu\nu} = -3L^{-2}g_{\mu\nu}$, and asymptotically approaches global AdS space with radius of curvature L. This asymptotic structure is not manifest in (6.3), one of the reasons being that the coordinate frame $\{t, r, \chi, \phi\}$ rotates at infinity with angular velocity $\Omega_\infty = -a/(L^2\Xi)$. However, if we introduce the coordinate change

$$\begin{aligned} T &= \frac{t}{\Xi}\,, \qquad \Phi = \phi + \frac{a}{L^2}\frac{t}{\Xi}\,, \\ R &= \frac{\sqrt{L^2\left(a^2 + r^2\right) - \left(L^2 + r^2\right)\chi^2}}{L\sqrt{\Xi}}, \qquad \cos\Theta = \frac{L\sqrt{\Xi}\, r\, \chi}{a\sqrt{L^2\left(a^2 + r^2\right) - \left(L^2 + r^2\right)\chi^2}}, \end{aligned} \quad (6.6)$$

we find that as $r \to \infty$ (i.e. $R \to \infty$), the Kerr-AdS geometry (6.3) approaches

$$ds^2_{AdS} = -\left(1 + \frac{R^2}{L^2}\right)dT^2 + \frac{dR^2}{1 + \frac{R^2}{L^2}} + R^2\left(d\Theta^2 + \sin^2\Theta\, d\Phi^2\right), \quad (6.7)$$

which we recognize as the line element of global AdS. In other words, the conformal boundary of the bulk spacetime is the static Einstein universe $R_t \times S^2$: $ds^2_\partial = \lim_{R\to\infty}\frac{L^2}{R^2}\, ds^2_{AdS} = -dT^2 + d\Theta^2 + \sin^2\Theta\, d\Phi^2$. This is the boundary metric where the CFT lives in the context of the AdS_4/CFT_3 correspondence.

The ADM mass and angular momentum of the black hole are related to the mass M and rotation a parameters through $M_{ADM} = M/\Xi^2$ and $J_{ADM} = Ma/\Xi^2$, respectively [127, 128]. The horizon angular velocity and temperature relevant for the thermodynamic analysis are the ones measured with respect to the non-rotating frame at infinity [127, 128] and are given in terms of (6.5) by $T_h = \Xi\, T_H$ and $\Omega_h = \Xi\, \Omega_H + \frac{a}{L^2}$. The event horizon is located at $r = r_+$ (the largest real root of Δ_r), and it is a Killing horizon generated by the Killing vector $K = \partial_T + \Omega_h \partial_\Phi$. We discuss our results in terms of the horizon radius and rotation parameter, which uniquely determine a given Kerr-AdS black hole. The mass parameter is given in terms of these by $M = \left(r_+^2 + a^2\right)\left(r_+^2 + L^2\right)/\left(2L^2 r_+\right)$. All regular black hole solutions must obey $T_H \geq 0$ and $a/L < 1$. This translates into the following conditions for r_+/L and a/L:

$$\begin{aligned} &\frac{a}{L} \leq \frac{r_+}{L}\sqrt{\frac{L^2+3r_+^2}{L^2-r_+^2}}, \quad \text{for} \quad \frac{r_+}{L} < \frac{1}{\sqrt{3}}, \\ &\frac{a}{L} < 1, \quad \text{for} \quad \frac{r_+}{L} \geq \frac{1}{\sqrt{3}}\,. \end{aligned} \tag{6.8}$$

The first inequality is saturated for a degenerate extremal regular horizon. On the left panel Fig. 6.1, we show the allowable domain for a/L and r_+/L. Further properties of the Kerr-AdS spacetime are discussed in Appendix A of [129].

We will find it useful to parametrize the black hole in variables that are naturally related to the onset of superradiance, and that are gauge invariant. Here we

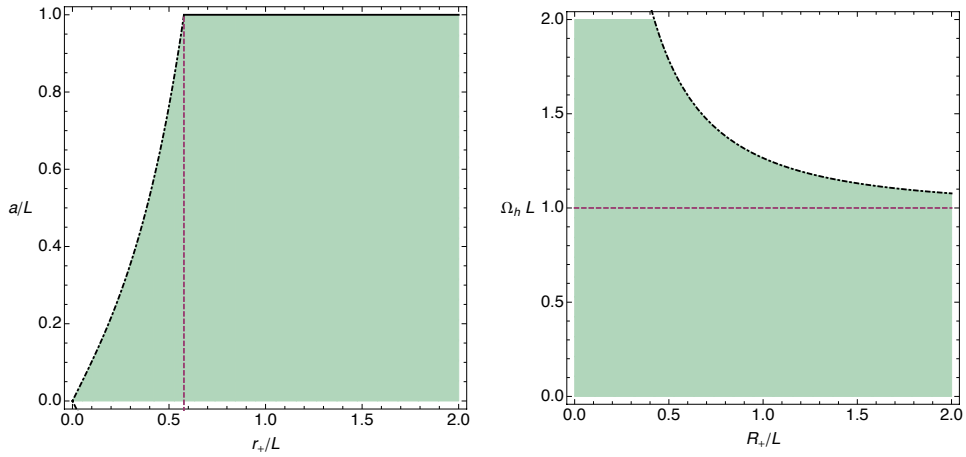

Figure 6.1: *Left panel:* Allowable region for a/L and r_+/L: the vertical dashed line is given by $r_+/L = 1/\sqrt{3}$, the dashed dotted lines indicate extremality, and the horizontal solid lines indicate $|a| = L$. *Right panel:* Allowable region for $\Omega_h L$ and R_+/L: the horizontal dashed line marks the onset of superradiance, the dashed dotted lines indicate extremality.

choose the pair (R_+, Ω_h), with R_+ given by:

$$R_+ = \frac{\sqrt{r_+^2 + a^2}}{\sqrt{\Xi}} \,. \tag{6.9}$$

Extremality is attained at

$$\left|\Omega_h^{\rm ext}\right| = \frac{1}{LR_+}\sqrt{\frac{(L^2+R_+^2)(L^2+3R_+^2)}{2L^2+3R_+^2}} \,. \tag{6.10}$$

Note that R_+ is just the square root of the area of the spatial section of the event horizon, divided by 4π, often denominated areal horizon radius. The allowed values of R_+/L and $\Omega_h L$ are depicted on the right panel of Fig. 6.1.

6.2.2 Gravitational master equation and global AdS boundary conditions

In the Newman-Penrose−Teukolsky formalism, all the information about (non-trivial) gravitational perturbations with spin $s = -2$ is encoded in the single variable $\delta\Psi_4$ which describes the perturbation of the Weyl scalar $\Psi_4 = C_{abcd}n^a\bar{m}^b n^c\bar{m}^d$. The equation of motion for this perturbation $\delta\Psi_4$ is described by the $s = -2$ Teukolsky master equation [114, 22]. Introducing the separation ansatz

$$\delta\Psi_4 = (r - i\chi)^{-2}\, e^{-i\tilde{\omega}t}\, e^{im\phi}\, R^{(-2)}_{\tilde{\omega}\ell m}(r)\, S^{(-2)}_{\tilde{\omega}\ell m}(\chi)\,, \tag{6.11}$$

the spin $s = -2$ Teukolsky master equation separates into angular and radial equations [126, 115]:

$$\partial_\chi\left(\Delta_\chi\partial_\chi S^{(-2)}_{\tilde{\omega}\ell m}\right) + \left[-\frac{\left(K_\chi + \Delta'_\chi\right)^2}{\Delta_\chi} + \left(\frac{6\chi^2}{L^2} + 4K'_\chi + \Delta''_\chi\right) + \lambda\right] S^{(-2)}_{\tilde{\omega}\ell m} = 0\,, \tag{6.12}$$

$$\partial_r\left(\Delta_r\partial_r R^{(-2)}_{\tilde{\omega}\ell m}\right) + \left[\frac{\left(K_r - i\Delta'_r\right)^2}{\Delta_r} + \left(\frac{6r^2}{L^2} + 4iK'_r + \Delta''_r\right) - \lambda\right] R^{(-2)}_{\tilde{\omega}\ell m} = 0\,, \tag{6.13}$$

where we have defined

$$K_r = \Xi\left[ma - \tilde{\omega}\left(a^2 + r^2\right)\right], \qquad K_\chi = \Xi\left[ma - \tilde{\omega}\left(a^2 - \chi^2\right)\right]. \tag{6.14}$$

The eigenfunctions $S^{(-2)}_{\tilde{\omega}\ell m}(\chi)$ are the spin-weighted $s = -2$ AdS-spheroidal harmonics. The positive integer ℓ specifies the number of zeros of the eigenfunction

along the polar direction which are given by $\ell - \max\{|m|, |s|\}$ (so the smallest ℓ is $\ell = |s| = 2$). The associated eigenvalues λ are functions of $\tilde{\omega}, \ell, m$ which can be computed numerically. Regularity imposes the constraints that $-\ell \leq m \leq \ell$ must be an integer and $\ell \geq |s|$. This equation has been studied in [115] in the limit where the rotation vanishes.

If we solve (simultaneously) the angular and radial equations, which are coupled through the two eigenvalues $\tilde{\omega}$ and λ, we get information about the most general perturbation of the Kerr-AdS black hole. In particular, the Teukolsky equation and its solution for the spin $s = +2$ perturbations, described by the variable $\delta\Psi_0 = (r - i\chi)^{-2} e^{-i\tilde{\omega}t} e^{im\phi} R^{(2)}_{\tilde{\omega}\ell m}(r) S^{(2)}_{\tilde{\omega}\ell m}(\chi)$, follow trivially from the spin $s = -2$ solution. Namely, $R^{(2)}_{\tilde{\omega}\ell m}$ is the complex conjugate of $R^{(-2)}_{\tilde{\omega}\ell m}$ and $S^{(2)}_{\tilde{\omega}\ell m}(\chi) = S^{(-2)}_{\tilde{\omega}\ell m}(-\chi)$. The later statement implies that the separation constants are such that $\lambda^{(-2)}_{\tilde{\omega}\ell m} = \lambda^{(2)}_{\tilde{\omega}\ell m} \equiv \lambda$. The only exceptions to the above are the trivial perturbations, the "$\ell = 0$" and "$\ell = 1$" modes, which shift, respectively, the mass and angular momentum of the solution along the original Kerr-AdS family, and to which the Teukolsky formalism is blind [130, 31, 35, 115].

Quasinormal modes and unstable modes of the Kerr-AdS black hole are solutions of (6.12)-(6.13) obeying physically relevant boundary conditions (BCs) [115]. At the horizon, the BCs must be such that only ingoing modes are allowed. A Frobenius analysis at this boundary gives two independent solutions,

$$R^{(-2)}_{\tilde{\omega}\ell m} \sim A_{\rm in}\,(r - r_+)^{1 - i\frac{\tilde{\omega} - m\Omega_H}{4\pi T_H}}\,[1 + \mathcal{O}\,(r - r_+)] + A_{\rm out}\,(r - r_+)^{-1 + i\frac{\tilde{\omega} - m\Omega_H}{4\pi T_H}}\,[1 + \mathcal{O}\,(r - r_+)]\,, \tag{6.15}$$

where $A_{\rm in}, A_{\rm out}$ are arbitrary amplitudes and Ω_H, T_H are the angular velocity and

temperature defined in (6.5). To impose the correct BC, we introduce the ingoing Eddington-Finkelstein coordinates $\{v, r, \chi, \widetilde{\phi}\}$, which are appropriate to extend the solution through the horizon. These are defined via

$$t = v - \Xi \int \frac{r^2 + a^2}{\Delta_r}\, dr, \qquad \phi = \widetilde{\phi} - \int \frac{a\,\Xi}{\Delta_r}\, dr\,. \tag{6.16}$$

The BC is determined by the requirement that the metric perturbation is regular in these ingoing Eddington-Finkelstein coordinates, where the metric tensor is constructed applying a differential operator to $\delta\Psi_4$ (this is known as the Hertz map; see the companion paper [115]). It follows that the metric perturbation is regular at the horizon if and only if $R(r)|_H$ behaves as $R(r)|_H \sim R_{IEF}(r)|_H\,(r - r_+)^{1 - i\frac{\tilde{\omega} - m\Omega_H}{4\pi T_H}}$ where $R_{IEF}(r)|_H$ is a smooth function [6]. Therefore, the appropriate BC at the horizon demands we set $A_{\rm out} = 0$ in (6.15):

$$R^{(-2)}_{\tilde{\omega}\ell m}\Big|_{r\to r_+} = A_{\rm in}\,(r - r_+)^{1 - i\varpi}\,[1 + \mathcal{O}\,(r - r_+)] \tag{6.17}$$

where

$$\varpi = \frac{\tilde{\omega} - m\Omega_H}{4\pi T_H}\,, \tag{6.18}$$

is what we might call the superradiant factor. Less formally, but perhaps more intuitively, when $\tilde{\omega}$ is real and non-zero we can understand this horizon BC by noting that the wave solution $e^{-i\tilde{\omega}t}\,(r - r_+)^{-i\varpi} = e^{-i\left(\tilde{\omega}t + \varpi \ln(r - r_+)\right)}$ is the one that describes ingoing modes at the horizon since r must decrease when t grows to

[6] This analysis misses the special case in which $2i\frac{\tilde{\omega} - m\Omega_H}{4\pi T_H}$ is a positive integer. For this special value, our boundary conditions still allow for outgoing modes at the horizon. However, by inspecting our numerical data we can a posteriori test if this condition is satisfied. In all our simulations, this never seems to be the case.

keep the phase constant (classically, we cannot have outgoing modes leaving the horizon).

Consider now the asymptotic boundary. A Frobenius analysis of the radial Teukolsky equation(6.13) at infinity yields the two independent asymptotic decays

$$R^{(-2)}_{\tilde{\omega}\ell m}\big|_{r\to\infty} = B^{(-2)}_{+}\,\frac{L}{r} + B^{(-2)}_{-}\,\frac{L^2}{r^2} + \mathcal{O}\left(\frac{L^3}{r^3}\right)\,, \tag{6.19}$$

for arbitrary amplitudes $B^{(-2)}_{\pm}$. We want the perturbations to preserve the asymptotic global AdS structure of the background Kerr-AdS black hole, i.e. we want the deformation to preserve the asymptotic line element (6.7). In the companion paper [115] we found that this requirement yields the following Robin BC,

$$B^{(-2)}_{-} = i\,\beta B^{(-2)}_{+}\,, \tag{6.20}$$

with two possible solutions for β, that we call $\beta_{\mathbf{s}}$ and $\beta_{\mathbf{v}}$,

$$1)\quad \beta = \beta_{\mathbf{s}} = \frac{\Lambda_0 - \sqrt{\Lambda_1}}{\Lambda_2}\,, \qquad \text{or} \tag{6.21}$$

$$2)\quad \beta = \beta_{\mathbf{v}} = \frac{\Lambda_0 + \sqrt{\Lambda_1}}{\Lambda_2}\,, \tag{6.22}$$

where we have introduced

$$\begin{aligned}
\Lambda_0 &\equiv 2a^2(\lambda-6) - 8(\lambda+1)L^4\tilde{\omega}^2\Xi^2 + 8L^6\tilde{\omega}^4\Xi^4 \\
&\quad + L^2\left[\lambda(\lambda+2) - 4\,\Xi^2 a\tilde{\omega}\left[5(m-a\tilde{\omega}) + 2a\tilde{\omega}\right]\right], \\
\Lambda_1 &\equiv 4a^4(\lambda-6)^2 + L^4\lambda^2(\lambda+2)^2 + 48(\lambda+6)a^3\Xi^2L^2\tilde{\omega}(m-a\tilde{\omega}) \\
&\quad + 8\lambda(5\lambda+6)(m-a\tilde{\omega})L^4\Xi^2 a\tilde{\omega} \\
&\quad + 4a^2L^2\Big[\lambda\left[-12 + (\lambda-4)\lambda + 24(m-a\tilde{\omega})^2\Xi^2\right] \\
&\qquad\qquad + 12\Xi^2L^2\tilde{\omega}^2\left[2\lambda + 3(m-a\tilde{\omega})^2\Xi^2\right]\Big], \\
\Lambda_2 &\equiv 4L\Xi\left[2am + L^2\tilde{\omega}\left(2+\lambda-2L^2\tilde{\omega}^2\Xi^2\right)\right].
\end{aligned} \tag{6.23}$$

Perturbations obeying the BCs (6.20)-(6.21) preserve the asymptotically global AdS behavior of the background. These are also natural BCs in the context of the AdS/CFT correspondence: they allow a non-zero expectation value for the CFT stress-energy tensor while keeping fixed the boundary metric.

The BC (6.20),(6.21) generates what we might call the "rotating sector of scalar modes", in the sense that when the rotation vanishes, these perturbations reduce continuously to the Kodama-Ishibashi scalar modes [115].[7] By a similar reasoning the BC (6.20), (6.22) selects the "rotating vector modes" of the spectrum. Having this in mind we will often use the nomenclature "scalar/vector" modes when discussing our results [115].

As discussed previously, the Chambers-Moss coordinate system $\{t, r, \chi, \phi\}$ ro-

[7]The Kodama-Ishibashi vector master equation is the Regge-Wheeler master equation for odd (also called axial) perturbations [112], and the Kodama-Ishibashi scalar master equation is the Zerilli master equation for even (also called polar) perturbations [113].

tates at infinity. However, the coordinate transformation (6.6) introduces the coordinate frame $\{T, R, \Theta, \Phi\}$ appropriate to discuss the asymptotic global AdS_4 structure of the geometry and the boundary metric where the dual CFT_3 and its hydrodynamic limit are formulated. Consider a generic linear perturbation in Kerr-AdS written in the Chambers-Moss frame $\{t, r, \chi, \phi\}$. Since ∂_t and ∂_ϕ are isometries of the background geometry we can Fourier decompose the perturbation in these directions as $e^{-i\tilde{\omega}t}\, e^{im\phi}$ as we did in (6.11). The frequency $\tilde{\omega}$ measured in the frame $\{t, r, \chi, \phi\}$ differs from the frequency measured in the frame $\{T, R, \Theta, \Phi\}$. It follows from the coordinate transformation (6.6) that they are related by

$$e^{-i\tilde{\omega}t}\, e^{im\phi} \equiv e^{-i\,\omega\, T}\, e^{im\Phi}, \qquad \text{with} \quad \omega \equiv \tilde{\omega}\,\Xi + m\frac{a}{L^2}. \tag{6.24}$$

The quantity ω can be viewed as the natural or fundamental frequency since it measures the frequency with respect to a frame that does not rotate at infinity. This is also the natural frequency measured by a CFT_3 and associated fluid rest frame observer. Therefore, although we will use the frame $\{t, r, \chi, \phi\}$ and $\tilde{\omega}$ to discuss many of our results, we choose to plot our results in terms of ω. Note that the superradiant factor defined in (6.17) can equally be written as $\varpi = \frac{\omega - m\Omega_h}{4\pi T_h}$ where the angular velocity Ω_h and temperature T_h as measured in the $\{T, R, \Theta, \Phi\}$ frame are given below (6.7).

6.3 Numerical procedures

In this section we discuss the numerical procedures applied to solve for the characteristic frequency ω and separation constant λ. We present three such methods based on: shooting, series expansion, and Newton-Raphson. The first two methods are typically used in studies of QNMs and the latter we introduce here and have found it to be the most robust when exploring limiting cases. As a powerful check, we find excellent agreement between different methods when more than one is applicable.

Shooting. The first method "shoots" for the correct answer in both the angular and radial component. Regularity of the angular eigenfunctions require that they admit the following expansion

$$S(\theta) \sim \theta^{|m-2|} \sum_{n=0} B_n^L(\tilde{\omega}, \lambda)\theta^n \,, \quad \theta \sim 0 \,, \tag{6.25}$$

$$\sim (\pi - \theta)^{|m+2|} \sum_{n=0} B_n^R(\tilde{\omega}, \lambda)(\pi - \theta)^n \,, \quad \theta \sim \pi \,, \tag{6.26}$$

at the left- and right-boundaries respectively. The coefficients B_n^L, B_n^R can be extracted from the angular equation and are functions of the frequency and the separation constant. We typically keep the first six terms in the expansion, numerically integrate the solutions towards each other where we match the logarithmic derivative at an intermediate point. We proceed identically with the radial equation, by imposing conditions (6.17) and (6.20) at the boundaries. Due to well-known divergences of QNMs at the horizon (stable modes diverge exponentially),

we use an *analytical*, series expansion close to the horizon and a similar expansion close to spatial infinity. An example notebook of how the radial equation is dealt with can be found online [10]. The method gives stable, convergent results for small black holes, but becomes less accurate for large black holes.

Series expansion. A powerful alternative is based on a series solution of the radial equation which avoids the divergent nature of QNMs at the horizon altogether by factoring the relevant terms [90, 10]. For simplicity let us focus on non-rotating BHs in this brief description, the extension to rotating BHs is straightforward. Let us start by re-expressing the boundary condition (6.20) as $-r(r/LR^{(-2)}_{\tilde{\omega}\ell m})' = i\beta R^{(-2)}_{\tilde{\omega}\ell m}$, where primes denote derivative with respect to r and all quantities are evaluated at spatial infinity. Redefine the wavefunction to $R^{(-2)}_{\tilde{\omega}\ell m} = \frac{\Delta_r}{r^5} e^{-i\omega r_*} Z(r)$, with $dr/dr_* = \Delta_r/r^2$. Then, make the variable change $z = 1/r$ and re-write the radial equation as

$$s(z)\frac{d^2Z}{dz^2} + \frac{t(z)}{z - z_\star}\frac{dZ}{dz} + \frac{u(z)}{(z - z_\star)^2} Z = 0\,, \tag{6.27}$$

and the boundary conditions as

$$Z'/L = iZ\left(\beta - L\omega\right)\,, \tag{6.28}$$

where primes now denote derivative with respect to z and $z_\star = 1/r_+$.

The idea is now to look for a series solution, $Z = a_n(z - z_\star)^n$, where the

coefficients a_n are found through the recurrence relation

$$a_n = -\frac{1}{P_n}\sum_{k=0}^{n-1}\left[k(k-1)s_{n-k} + k\,t_{n-k} + u_{n-k}\right]a_k\,, \tag{6.29}$$

where $P_n = n(n-1)s_0 + n\,t_0$ and where s, t, u have been expanded in Taylor series around the horizon. The boundary condition then translates into

$$\sum a_n(-z_\star)^n\left[1 + \frac{n}{h(i\beta - i\omega)}\right] = 0\,, \tag{6.30}$$

where β is given by either Eq. (6.21) or Eq. (6.22). Extension to rotating geometries is obtained simply by replacing ω with the corresponding superradiant factor.

Newton-Raphson. We have also developed a novel numerical procedure based on the Newton-Raphson root-finding algorithm that searches for specific quasinormal modes, once a seed solution is given. In order to proceed we first need to recast Eq. (6.12) and Eq. (6.13) in a different form. Let us introduce the following auxiliary functions:

$$R^{(-2)}_{\tilde{\omega}\ell m}(r) = \left(1 - \frac{r_+}{r}\right)^{1-i\varpi}\frac{L}{r}q_1\left(1 - \frac{r_+}{r}\right), \tag{6.31}$$

$$S^{(-2)}_{\tilde{\omega}\ell m}(\chi) = \left(1 + \frac{\chi}{a}\right)^{\left|\frac{m}{2}+1\right|}\left(\frac{\chi}{a}\right)^{\left|\frac{m}{2}-1\right|}q_2\left(1 + \frac{\chi}{a}\right), \tag{6.32}$$

where we have implicitly introduced two new compact coordinates $y = 1 - r_+/r$ and $\tilde{x} = 1 + \chi/a$, which map the problem to the unit square: $(\tilde{x}, y) \in (0,1)\times(0,1)$. The boundary conditions on the q_I simply arise from regularity, and translate into

four Robin boundary conditions at each integration boundary, i.e.

$$q_I'(0) = a_I\, q_I(0) \quad \text{and} \quad q_I'(1) = b_I\, q_I(1)\,,$$

where both a_I and b_I are constants and $I = \{1, 2\}$. For q_2, both a_2 and b_2 are determined by solving the equations of motion (6.12) off the singular points $\tilde{x} = \{0, 1\}$. q_1 on the other hand, is a little more subtle. At $y = 0$, we still get the Robin boundary conditions by solving Eq. (6.13) off $y = 0$, but the condition at $y = 1$ is obtained directly from either Eq. (6.21) or Eq. (6.22).

We are now ready to introduce the new numerical procedure that determines $\{q_1, q_2, \omega, \lambda\}$. For the sake of presentation we will only discuss below the case in which we have a single differential equation to solve. The extension to a coupled system like the one above is straightforward.

Consider the following "nonlinear Stürm-Liouville" problem in $\{\mathfrak{f}, \tilde{\lambda}\}$:

$$H(\tilde{\lambda})\mathfrak{f} = 0 \quad \text{with} \quad \mathfrak{f}'(0) = a_0\, \mathfrak{f}(0)\,, \quad \mathfrak{f}'(1) = b_0\, \mathfrak{f}(1)\,, \tag{6.33}$$

where $H(\tilde{\lambda})$ is nonlinear function in $\tilde{\lambda}$, and a linear differential operator in $\mathfrak{f}$ and both $\{a_0, b_0\}$ are constants. In many circumstances H takes the following simple form: $H(\tilde{\lambda})\mathfrak{f} = H_0\mathfrak{f} - \tilde{\lambda} H_1\mathfrak{f} - \tilde{\lambda}^2 H_2\mathfrak{f}$, where each of the H_i is a second order differential operator independent of $\tilde{\lambda}$. The former differential equation is often called a quadratic eigenvalue problem, so long as the constants $\{a_0, b_0\}$ admit a similar expansion. The method we describe below allows for any dependence in $\tilde{\lambda}$.

We discretize our Eq. (6.33) by introducing a spatial grid $\{y_i\}$, with $N + 1$

grid points. Because we are solving for manifestly analytic functions q_I, we can readily use a pseudospectral collocation discretization scheme. We choose the Gauss-Chebyshev-Lobatto grid as our collocation points. The nonlinear Stürm-Liouville problem (6.33) reduces to a nonlinear eigenvalue problem of the form:

$$H_{i,j}(\tilde{\lambda})\mathfrak{f}_j = 0 \quad \text{with} \quad D_{N+1,i}\mathfrak{f}_i = a_0\,\mathfrak{f}_{N+1}\,, \quad D_{1,i}\mathfrak{f}_i = b_0\,\mathfrak{f}_1\,, \tag{6.34}$$

where $D_{i,j}$ is a Chebyshev differentiating matrix and $H_{i,j}$ is the discretization of the operator H. We now introduce a normalization for the eigenvector $\{\mathfrak{f}_i\}$, using an auxiliary constant vector $\{v_i\}$, such that $v_i\mathfrak{f}_i = 1$. In all cases, we choose $\{v_i\}$ to have only one nonzero component, which without loss of generality we choose to be the horizon and the south pole located at $y = 0$ and $\tilde{x} = 0$, respectively.

The procedure is now clear: we promote $\tilde{\lambda}$ to be a parameter to be determined via the Newton-Raphson method. Recall that we have to solve

$$f(\mathfrak{f}_j, \tilde{\lambda}) = \left\{ \begin{array}{c} \hat{H}_{i,j}(\tilde{\lambda})\mathfrak{f}_j \\ v_i\mathfrak{f}_i - 1 \end{array} \right\} = 0\,,$$

where $\hat{H}_{i,j}$ is obtained from $H_{i,j}$ by removing its first and last lines, and substitute them by the last two conditions in Eq. (6.34). The Newton-Raphson method states that the correction to our initial guess for $(\{\mathfrak{f}_i^{(0)}\}, \tilde{\lambda}^{(0)})$ can be determined by inverting the following linear system of equations:

$$\left[\begin{array}{cc} \hat{H}_{i,j}(\tilde{\lambda}^{(0)}) & \frac{\partial \hat{H}_{i,j}}{\partial \tilde{\lambda}}\mathfrak{f}_j\Big|_{\mathfrak{f}_j=\mathfrak{f}_j^{(0)},\,\tilde{\lambda}=\tilde{\lambda}^{(0)}} \\ v_j & 0 \end{array} \right] \left[\begin{array}{c} \delta\mathfrak{f}_j \\ \delta\tilde{\lambda} \end{array} \right] = - \left[\begin{array}{c} \hat{H}_{i,j}(\tilde{\lambda}^{(0)})\mathfrak{f}_j^{(0)} \\ v_j\mathfrak{f}_j^{(0)} - 1 \end{array} \right]. \tag{6.35}$$

We then iterate this procedure until $|\delta \mathfrak{f}_j|$ and $|\delta\tilde{\lambda}|$ are below some tolerance, which in this manuscript we take to be 10^{-30}. All computations using this method were performed with octuple precision, which is particularly relevant for small black holes.

Our results have been benchmarked using previous results in the literature, specifically for scalar field perturbations of Kerr-AdS BHs [34, 120, 131]. In particular, we recover to all significant digits the numerical results reported in Ref. [131]. Furthermore, we recover all known results from gravitational perturbations of Schwarzschild-AdS BHs with the same boundary conditions [116, 132, 97, 115].

Finally, we note that an important symmetry of the relevant perturbation equations and boundary conditions for QNMs is that if (ω, λ) is a solution for a given m then $(-\omega^*, \lambda^*)$ is a solution for $-m$. As such, we will only discuss positive real part modes, with the understanding that they come in complex conjugate pairs.

6.4 QNMs and superradiance in Kerr-AdS: results

In this section we present the numerical results obtained, make contact with some analytical results, and discuss implications with the phenomena of superradiance.

6.4.1 Comparison between analytical and numerical results

The angular (6.12) and radial (6.13) equations constitute a system of ordinary differential equations coupled through the frequency $\tilde{\omega}$ and angular λ eigenvalues that cannot be solved analytically when $M, a \neq 0$. For this reason, we solve these equations using the numerical methods outlined in Section 6.3. There is however a regime where we can use a matched asymptotic expansion procedure to get an approximate analytical solution for the QNM and superradiant instability frequency spectra. This perturbative analytical computation provides useful physical insights about the system and is valuable to check our numerical results. We leave the details of this analytical construction to Appendix 6.C and present here only the main outcome of the computation and its comparison with the numerical results.

As justified in Appendix 6.C, the perturbative analytical results are valid in the regime of parameters where

$$\begin{aligned} &\frac{r_+}{L} \ll 1 \quad \Rightarrow \quad \frac{a}{L} \ll 1\,, \quad a\tilde{\omega} \ll 1\,, \quad r_+\tilde{\omega} \ll 1\,; \\ &\frac{a}{r_+} \ll 1\,. \end{aligned} \tag{6.36}$$

i.e., for Kerr-AdS black holes with small horizon radius in AdS radius units and even smaller rotation parameter, and for perturbations whose wavelength is much bigger than the black hole lengthscales.

In Appendix 6.C we find that the matched asymptotic expansion analysis indicates that the frequency spectrum is quantized by the condition (6.143), for

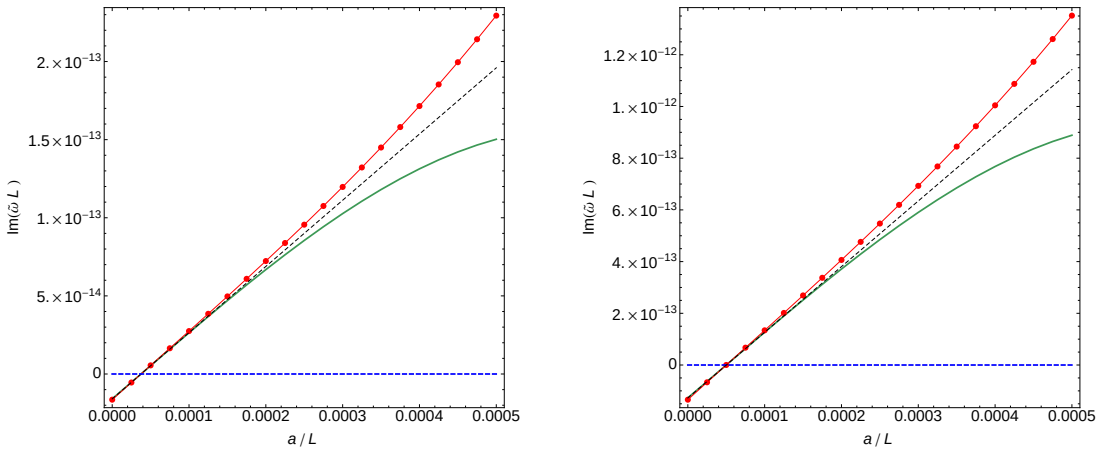

Figure 6.1: Imaginary part of the QNM frequency as a function of the rotation parameter a/L, for fixed horizon radius $r_+/L = 0.005$, for scalar (*Right Panel*) and vector modes (*Left Panel*). This is for $\ell = 2$ modes with no radial overtone. These are an example of the QNM spectrum in the regime $a/L < r_+/L \ll 1$ where the analytical matching analysis is valid and its approximated results can be used to both test our numerical code (valid in any regime), and estimate more precisely the regime of validity of the analytical approximation. The red dots are the exact results from our numerical code. The green curve is the numerical solution of the matching transcendental equation (6.37), while the dashed black curve is the approximated analytical solution (6.38) or (6.39) of (6.37). In both figures there is a critical rotation where $\mathrm{Im}(\tilde{\omega}L) = 0$ and $\mathrm{Re}(\tilde{\omega}) - m\Omega_H \simeq 0$ to within 0.01%. For lower rotations the QNMs are damped and with $\mathrm{Re}(\tilde{\omega}) - m\Omega_H > 0$, while for higher rotations we have unstable superradiant modes with $\mathrm{Re}(\tilde{\omega}) - m\Omega_H < 0$.

a generic mode with quantum numbers ℓ and m. This frequency quantization condition simplifies considerably when we choose a particular harmonic ℓ. For instance, for the lowest harmonic $\ell = 2$, the condition (6.143) reads

$$i(-1)^{L\tilde{\omega}+1}L^{-5}\left(r_+ - \frac{a}{r_+^2}\right)^5 L\tilde{\omega}\left(L^2\tilde{\omega}^2-1\right)\left(L^2\tilde{\omega}^2-4\right)\Gamma(5-2i\varpi) \\ +5400\left[\varepsilon_j + (-1)^{L\tilde{\omega}}\right]\Gamma(-2i\varpi) = 0\,, \qquad (6.37)$$

where the superradiant factor ϖ is defined in (6.18), and $\varepsilon_j = 1$ describes scalar

modes with the BC (6.138) while $\varepsilon_j = -1$ represents vector modes with the BC (6.139). We can find the frequency that solves this transcendental equation numerically using a standard root-finder routine (for instance *Mathematica*'s built-in *FindRoot* routine). Alternatively we can also provide an approximate analytic solution, still in the limit of $a/L \ll r_+/L \ll 1$, assuming that the frequency has a double expansion in the rotation and in the horizon radius, $\tilde{\omega}(a, r_+)L = \sum_{j=0}^{n} \left(\frac{a}{L}\right)^j \sum_{i=0}^{p} \tilde{\omega}_{j,i} \left(\frac{r_+}{L}\right)^i$, and solving progressively (6.37) in a series expansion in a/L and r_+/L. Here, $\tilde{\omega}_{0,0}$ is the global AdS frequency (see footnote 21). Namely, the fundamental (no radial overtone) $\ell = 2$ scalar and vector normal mode frequencies are $\tilde{\omega}^{(\mathrm{s})}_{0,0} = 3/L$ and $\tilde{\omega}^{(\mathrm{v})}_{0,0} = 4/L$, respectively. In the regime (6.36) we work in this subsection, the correction to the real part of the frequency is very small (compared with $\tilde{\omega}_{0,0}$) and (6.37) fixes the the imaginary part of the frequency for fundamental $\ell = 2$ modes to be

$$1) \quad \text{Scalar modes:} \quad \mathrm{Im}(\tilde{\omega}L) \simeq \frac{16}{15\pi}\left[-\frac{3r_+^6}{L^6} + \frac{m\,a\,r_+^4}{L^5}\left(1 + 15(5\gamma - 7)\,\frac{r_+^2}{L^2}\right)\right] + \cdots \tag{6.38}$$

$$2) \quad \text{Vector modes:} \quad \mathrm{Im}(\tilde{\omega}L) \simeq \frac{96}{15\pi}\left[-\frac{4r_+^6}{L^6} + \frac{m\,a\,r_+^4}{L^5}\left(1 + \frac{80(5\gamma - 7)}{3}\,\frac{r_+^2}{L^2}\right)\right] + \cdots \tag{6.39}$$

where $\gamma \simeq 0.577216$ is the Euler-Mascheroni constant. For both scalar and vector modes the imaginary part of the frequency starts negative for $a = 0$, consistent with the fact that QNMs of Schwarzschild-AdS are always damped. However, as a/L increases, $\mathrm{Im}(\tilde{\omega}L)$ increases. A good check of our analytical matching analysis is that we find that at the critical rotation where the crossover occurs, i.e. $\mathrm{Im}(\tilde{\omega}L) = 0$, one has $\mathrm{Re}(\tilde{\omega}) - m\Omega_H \simeq 0$ to within 0.01%. For smaller rotations one has $\mathrm{Re}(\tilde{\omega}) - m\Omega_H > 0$ and for higher rotations one has $\mathrm{Re}(\tilde{\omega}) - m\Omega_H < 0$ and

$\mathrm{Im}(\tilde{\omega}L) > 0$. Therefore, the instability which is triggered at large rotation rates has a superradiant origin since the superradiant factor becomes negative, $\varpi < 0$ precisely when the QNMs go from damped to unstable. These analytical matching results provide also a good testbed check to our numerics. Indeed we find that our analytical and numerical results have a very good agreement in the regime of validity of the matching analysis. This is demonstrated in Fig. 6.1 where we plot our numerical and analytical results for the fundamental $\ell = 2$ scalar and vector modes. As a rough reference we can take this to be $r_+/L < 5 \times 10^{-3}$ and $a/L < 10^{-4}$. (A similar analysis that lead to the results (6.37)-(6.39) can be repeated for any other harmonic starting from (6.143)).

6.4.2 Properties of superradiant unstable modes and QNMs

We are now ready to present the properties of the superradiant unstable modes and QNMs for generic solutions in the parameter space. We use the numerical methods described in Section 6.3 to find the solution of the coupled ODE angular (6.12) and radial (6.13) equations that describe the most general linear perturbation of a Kerr-AdS BH. We first present the gravitational scalar perturbations that obey the BCs (6.21), and then the gravitational vector perturbations that obey the BCs (6.22).

Consider a Kerr-AdS BH parametrized by particular values of the gauge invariant parameters $\{R_+/L, \Omega_h L\}$ described in the end of Section 6.2.1. A generic perturbation can have a frequency with negative, positive, or vanishing imaginary part. Quasinormal modes are damped, $\mathrm{Im}(\omega) < 0$, whereas unstable modes grow

exponentially in time, $\mathrm{Im}(\omega) > 0$. Thus, a particularly important set of modes, if present, are the marginal modes that define the stability boundary in a phase diagram. The marginal mode (or onset mode) curve is defined to be the locus of points in the parameter space $(R_+/L, \Omega_h L)$ for which a mode with $\mathrm{Im}(\omega) = 0$ exists. There will be a marginal mode curve for each distinct pair of wave numbers $\{\ell, m\}$ resulting in an instability. To understand the nature of this instability it is useful to look into another useful characterization of linear perturbations. It comes from considering the difference between the real part of the frequency and $m\Omega_h$, which determines the sign of the the energy and angular momentum fluxes the perturbation carries through the future horizon; see Appendix 6.A[8]. Modes with $\mathrm{Re}(\omega) > m\Omega_h$ carry positive flux through the horizon, whereas modes with $\mathrm{Re}(\omega) < m\Omega_h$ carry negative flux across the horizon, and are called superradiant. Vanishing flux at the horizon requires $\mathrm{Re}(\omega) = m\Omega_h$. We find that $\mathrm{Re}(\omega) = m\Omega_h$ whenever $\mathrm{Im}(\omega) = 0$ and that $\mathrm{Re}(\omega) < m\Omega_h$ when $\mathrm{Im}(\omega) < 0$. Therefore, unstable modes in Kerr-AdS are always associated to the superradiant instability.

As important illustrative examples, in the *left panel* of Fig. 6.2 we identify the superradiant onset curves (OC) for $\ell = m$ scalar modes (with vanishing radial overtone) in the phase diagram of Kerr-AdS BHs. The axes are given by the gauge invariant horizon radius R_+/L and the horizon angular velocity $\Omega_h L$ (for the frame that does not rotate at infinity), as previously introduced in Fig. 6.1. Regular Kerr-AdS BHs exist in the blue shaded area, starting at $\Omega_h L = 0$ and all the way up towards the black curve where extremality is attained. We identify the OC for the scalar modes with $\ell = m = 2, 3, 4, 5$. BHs that are above a

[8]Note that reflecting boundary conditions at the conformal boundary enforces the vanishing of the flux there; see Appendix 6.A

particular $\ell = m$ OC are superradiantly unstable to modes with those particular values of $\ell = m$, while BHs below a particular OC are stable to the associated modes. For completeness, in the *right panel* of Fig. 6.2 we plot the angular eigenvalue λ along the superradiant OC. Since $\mathrm{Im}(\omega) = 0$ along this OC, it follows from the mathematical structure of the coupled equations that we must also have $\mathrm{Im}(\lambda) = 0$.

The OCs have some properties that merit a detailed discussion. First, in both plots of Fig. 6.2 the large black points on the left at $R_+/L = 0$ are computed analytically and serve as additional checks for the numerical code. They describe the scalar normal mode frequencies and the associated angular eigenvalues of global AdS given by [72, 107],

$$L\,\omega_{\rm s}^{AdS} = 1 + \ell + 2p\,, \qquad \lambda = \ell(\ell+1) - 2\,, \tag{6.40}$$

where $p = 0, 1, 2, \cdots$ is the radial overtone (number of radial nodes). In more detail, to get the black points in the *left panel* of Fig. 6.2 we use the superradiant onset condition to find $\Omega_h\big|_{R_+=0} = \omega_s^{AdS}/m$ and we set $p = 0, \ell = m$, i.e.

$$L\,\Omega_h\big|_{R_+=0} = 1 + \frac{1}{m}\,, \tag{6.41}$$

Note that given a $\{\ell, m\}$ pair there is an OC for each radial overtone p, but $p > 0$ curves always lie above the $p = 0$ curve, and therefore $p = 0$ modes are the first to go unstable as the rotation is increased. For this reason only the $p = 0$ curves are plotted.

The OCs always have $\Omega_h L > 1$, monotonically approaching $\Omega_h L \to 1$ (from

above) asymptotically as $R_+/L \to \infty$, where all the scalar superradiant OCs pile up. This means that only $\Omega_h L > 1$ BHs can be unstable to superradiance, a property that was first proven in [33].

Finally, note that for small BHs (say with $R_+/L \lesssim 0.45$) as $\ell = m$ increases the corresponding superradiant OC lowers. This means that, e.g. we can have small BHs (those in the triangle-like region between the $\ell = m = 2$ and $\ell = m = 3$ curves) that are stable to $\ell = m = 2$ modes but unstable to all other $\ell = m \geq 3$ modes, or e.g. BHs that are stable to $\ell = m = 2$ and $\ell = m = 3$ but always unstable to all other $\ell = m \geq 4$ modes. However, as the areal radius grows we find that the OCs start crossing each other. For example, the $\ell = m = 2$ curve crosses the $\ell = m = 3$ curve at $R_+/L \sim 0.45$ and for higher radius it crosses the $\ell = m = 4$ and then the $\ell = m = 5$ curve. So, e.g. at $R_+/L = 1$ the $\ell = m = 2$ OC is below the three OCs $\ell = m = 3, 4, 5$. This means that at this radius we can have Kerr-BHs that are unstable to $\ell = m = 2$ modes but *not* to $\ell = m = 3, 4, 5$ modes.

At first sight, this is of course exciting as it seems to indicate that there is a region of parameter space where Kerr-BHs are unstable to $\ell = m = 2$ modes but stable to *any* other superradiant modes, with obvious consequences for the endpoint of the superradiant instability. However, this is not the case. Indeed, first notice that as $\ell = m \to \infty$ the corresponding OC still starts precisely at the point defined by (6.41). Thus, as $\ell = m$ grows large, its threshold modes are described by an OC that progressively approaches the line $\Omega_h L = 1$, becoming horizontal in the limit $\ell = m \to +\infty$. Therefore as the BH rotation is increased, the first modes that become superradiantly unstable are the $m \to \infty$ modes. The

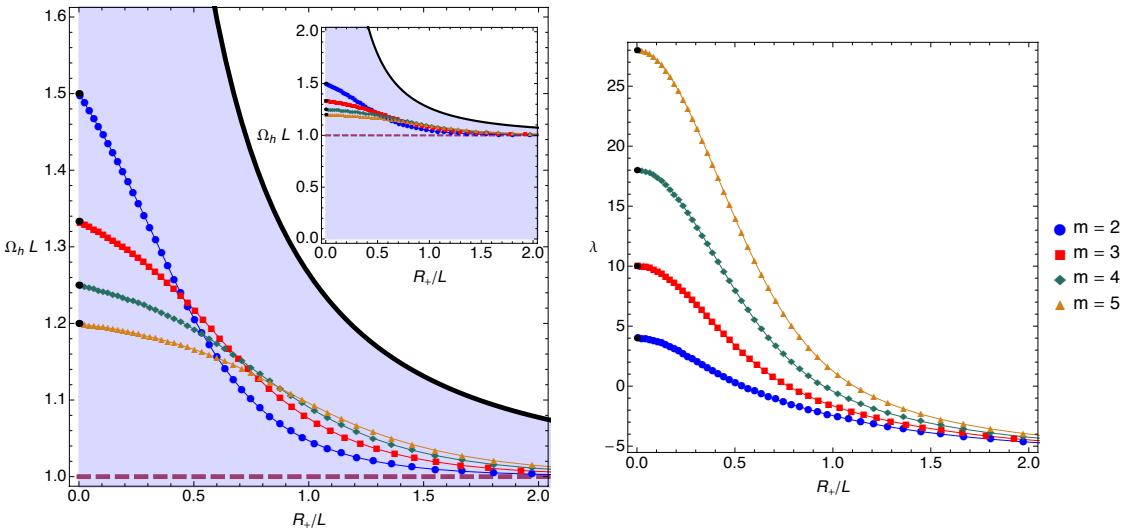

Figure 6.2: The onset of superradiance for the first $\ell = m = 2, 3, 4, 5$ *scalar* modes of the Kerr-AdS BH. The *left panel* shows the OC in the phase diagram described by the gauge invariant parameters $(R_+/L, \Omega_h L)$ (the inset plot zooms out the main plot to show an enlarged view of the parameter space). Regular Kerr-AdS BHs exist in the blue shaded area all the way up to the black curve where extremality is attained. In the *right panel* we show the value of the angular eigenvalue λ as a function of the areal radius R_+/L as we move along the OC. In both plots, the larger black points on the left with $R_+/L = 0$ are fixed by the properties (6.40) of scalar normal modes of global AdS.

conclusion that $m \to +\infty$ modes are the "first" to become unstable was first presented in the equal angular momenta Myers-Perry BHs in [30]. Furthermore, as we shall discuss later, all vector modes will be superradiantly unstable.

As stated previously, in the *left panel* of Fig. 6.2, BHs that are above a particular $\ell = m$ OC are superradiant unstable to those particular $\ell = m$ modes. That is, their perturbations have frequencies with $\mathrm{Im}(\omega) > 0$ and $\mathrm{Re}(\omega) < m\Omega$. On the other hand, BHs below a particular OC are damped and thus stable (when perturbed these BHs return to equilibrium via the emission of QNMs with $\mathrm{Im}(\omega) < 0$ and $\mathrm{Re}(\omega) > m\Omega$).

Having studied the OCs for scalar modes with $\ell = m$, we now turn to consider one particular mode throughout a region of the parameter space to gain more insight into the stability properties of these black holes. A natural mode to consider is the $\ell = m = 2$ one, as this is the mode with the largest value of the growth rate $\mathrm{Im}(\omega)$ found in our study. The imaginary and real parts of the $\ell = m = 2$ scalar mode frequencies are plotted in Fig. 6.3, and the imaginary and real part of the associated angular eigenvalues is shown in Fig. 6.4. These quantities are plotted as a function of the dimensionless horizon radius r_+/L and rotation a/L and they define a 2-dimensional surface. To extract more efficiently the relevant physics, we plot in the *right panel* of Fig. 6.3 is the real part of the superradiant factor $\mathrm{Re}(\varpi) = (\mathrm{Re}(\omega) - m\Omega_h)/(4\pi T_h)$, as introduced in (6.18). In all these plots the blue curve is the $\ell = m = 2$ OC already identified in the phase diagram of Fig. 6.2. To guide the eye (when appropriate) we draw an auxiliary plane with a grid that intersects the physical 2-dimensional surface along the OC and that has $\mathrm{Re}(\varpi) = 0$, $\mathrm{Im}(\omega) = 0$, and $\mathrm{Im}(\lambda) = 0$. We also plot some black curves at constant radius r_+/L.

In the *left panel* of Fig. 6.3, modes that are above the auxiliary plane grid are superradiant unstable modes. In the *right panel* of Fig. 6.3 and in the *left panel* of Fig. 6.4 they correspond to the surface region below the auxiliary plane grid. Finally, in the *right panel* of Fig. 6.4 these unstable modes are described by the surface region "below" the blue line. In the four plots, the superradiant unstable surface region is a 2-dimensional surface bounded by the superradiant OC (blue line) and by the extremality curve (where the black curves at constant

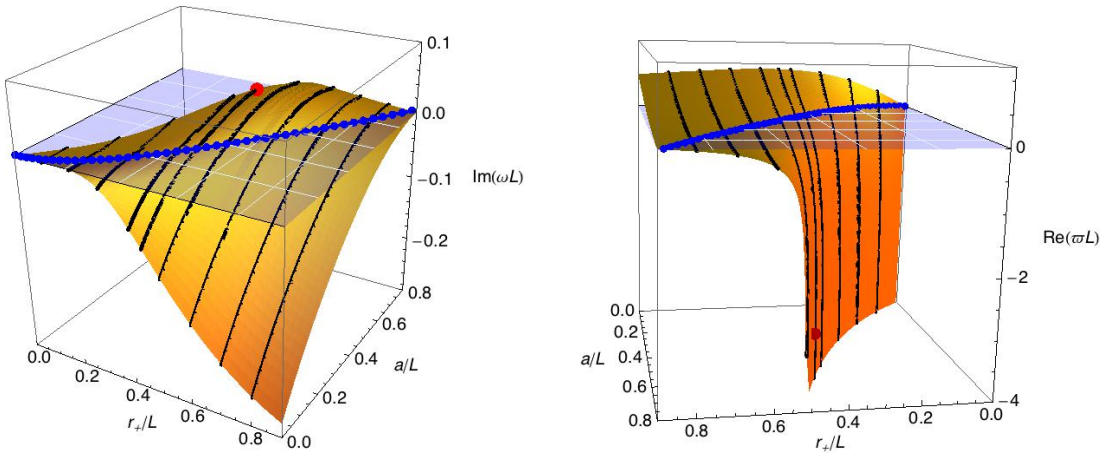

Figure 6.3: Superradiant modes and QNMs for the $\ell = m = 2$ scalar harmonic. The *left panel* plots the imaginary part $\mathrm{Im}(\omega)$ of the frequencies while the *right panel* shows the real part of the superradiant factor, i.e. $(\mathrm{Re}(\omega L) - m\Omega_h L)/(4\pi T_h)$, as a function of the horizon radius r_+/L and rotation a/L parameters. The blue curve is the superradiant OC with $\mathrm{Im}(\omega) = 0$ and $\mathrm{Re}(\varpi) = 0$. The large red point signals the Kerr-AdS BH that is most unstable to scalar superradiance described by (6.42).. The black curves have constant radius $r_+/L = 0.1; 0.2; 0.3; 0.4; 0.445; 0.5; 0.6; 0.7; 0.8$. These plots are discussed in more detail in the text.

radius end).[9] In all these plots, the surface region that starts at the blue OC that is complementary to the unstable region describes the QNMs of the Kerr-AdS BH.

An important feature of the gravitational scalar superradiant instability concerns the order of magnitude of its timescale $\tau \sim 1/\mathrm{Im}(\omega)$. Inspecting the data we find that the maximum growth rate of the instability is reached in a neighborhood of the point $\{r_+/L, a/L\}_{\max} \simeq \{0.445 \pm 0.020, 0.589 \pm 0.020\}$ where the frequency is given by $\omega L \sim 1.397 + 0.032\, i$. So, the maximum growth rate for the scalar superradiant instability and the gauge invariant properties of the BH where it is

[9]Note that in the *right panel* of Fig. 6.3 the shown surface would extend for smaller negative values of $Re(\varpi)$ but we stop it at $Re(\varpi) = -4$ for better visualization.

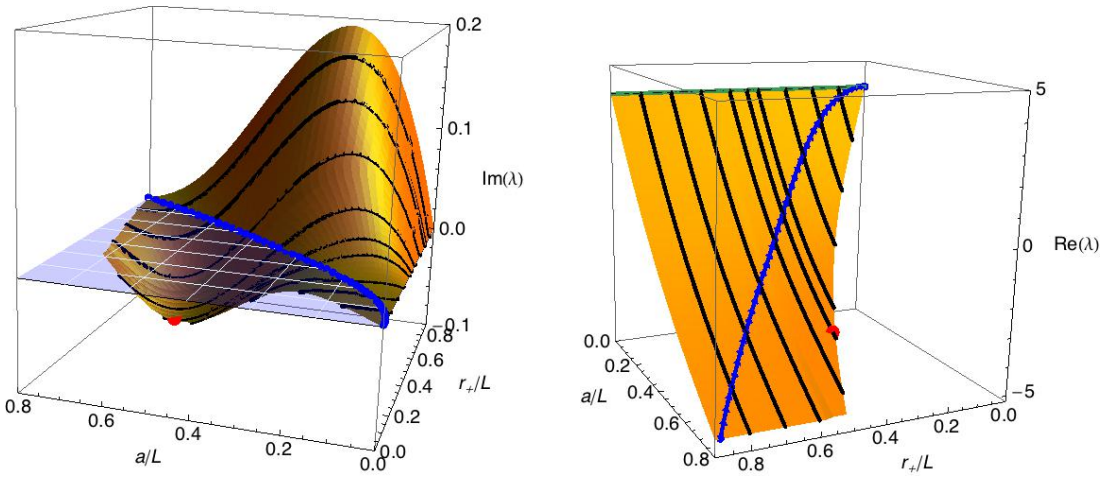

Figure 6.4: Imaginary (*left panel*) and real (*right panel*) part of the angular eigenvalues of the superradiant modes and QNMs of the $\ell = m = 2$ *scalar* harmonic whose frequencies are shown in Fig. 6.3. The color coding of the lines/points is the same as Fig. 6.3.

attained are

$$\text{Scalar:} \quad \{R_+/L, \Omega_h L\} \sim \{0.914, 1.295\}\,, \quad \text{Im}(\omega L) \sim 0.032\,, \quad \text{Re}(\varpi L) \sim -3.247\,. \tag{6.42}$$

This maximum is denoted with a large red dot in the plots of Fig. 6.3 and Fig. 6.4. Note that this maximum occurs close to extremality but not at it. In particular, if we plot the instability growth rate as a function of the rotation parameter a/L at fixed radius (e.g. $r_+/L = 0.445$), we find that, typically, starting from the onset the instability timescale first increases, reaches a maximum for a/L close to extremality, and then decreases as we approach the $T_h = 0$ Kerr-AdS BH.

Consider now the gravitational vector modes which obey the BCs (6.22). The *left panel* of Fig. 6.5 displays the phase diagram of Kerr-AdS BHs with the OCs for the $\ell = m = 2, 3, 4, 5$ vector modes displayed (again, only curves with vanishing

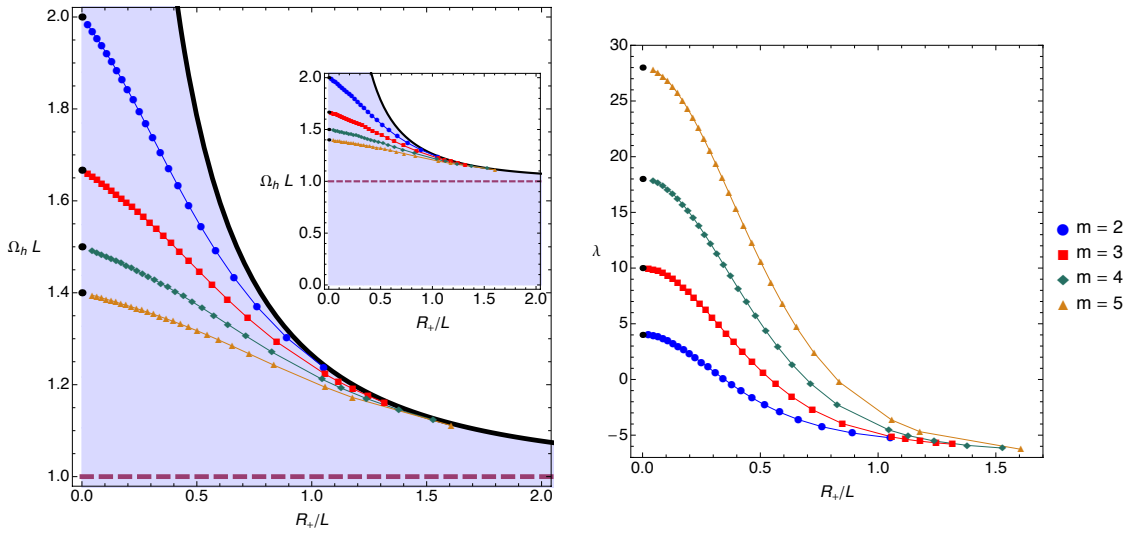

Figure 6.5: Onset of superradiance for the first $\ell = m = 2, 3, 4, 5$ *vector* modes of the Kerr-AdS BH. The *left panel* shows the OC in the $(R_+/L, \Omega_h L)$ phase diagram (the inset plot zooms out the main plot). The *right panel* shows how the angular eigenvalue λ varies with R_+/L along the OC. In both plots, the larger black points on the left with $R_+/L = 0$ are fixed by the properties (6.43) of vector normal modes of global AdS.

radial overtone are shown). As in the scalar case, BHs that are above a particular $\ell = m$ vector OC are superradiantly unstable to modes with those particular values of $\ell = m$, while BHs below a particular OC are stable to the associated modes. In the *right panel* of Fig. 6.5 we plot the angular eigenvalue λ along the OC for vector modes.

The large black points at $R_+/L = 0$, in both plots of Fig. 6.5, describe the vector normal modes of global AdS, namely [72, 107],

$$L\,\omega_{\rm v}^{AdS} = 2 + \ell + 2p \;\; (p = 0, 1, 2, \cdots)\,, \qquad \lambda = \ell(\ell+1) - 2\,. \tag{6.43}$$

Together with the superradiant onset condition (with $p = 0$ and $\ell = m$) these

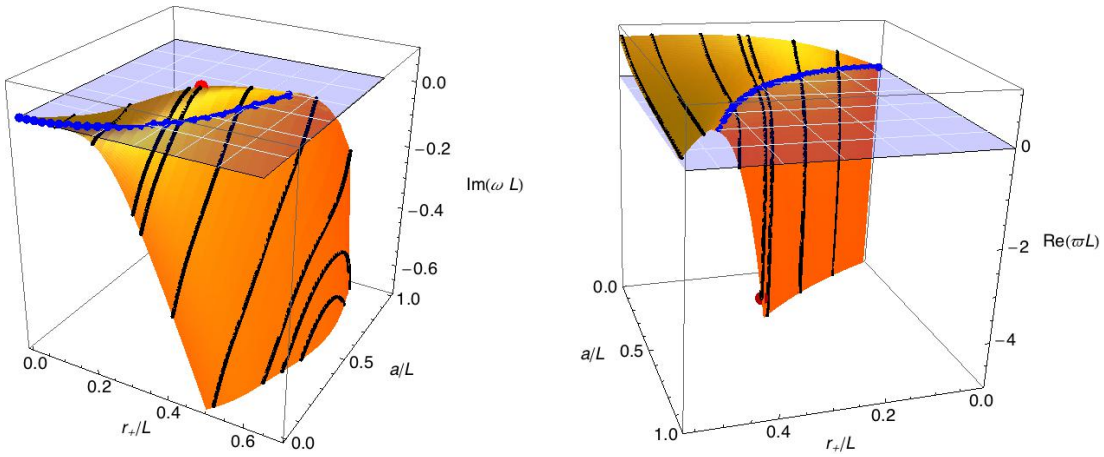

Figure 6.6: Superradiant modes and QNMs for the $\ell = m = 2$ *vector* harmonic. The *left panel* plots the imaginary part $Im(\omega)$ of the frequencies while the *right panel* shows the real part of the superradiant factor, i.e. $(Re(\omega L) - m\Omega_h L)/(4\pi T_h)$, as a function of the horizon radius r_+/L and rotation a/L parameters. The blue curve is the superradiant OC with $Im(\omega) = 0$ and $Re(\varpi) = 0$. The large red point signals the Kerr-AdS BH that is most unstable to vector superradiance described by (6.45). The black curves have constant radius $r_+/L = 0.1$; 0.2; 0.3; 0.325; 0.4; 0.5; 0.565; 0.585; 0.6 (the later two only in the *left panel*). These plot are discussed in more detail in the text.

normal modes give the black points of Fig. 6.5,

$$L\Omega_h\big|_{R_+=0} = 1 + \frac{2}{m}\,, \tag{6.44}$$

As in the scalar case, the vector OCs always have $\Omega_h L > 1$ but contrary to the scalar case, these curves always end at extremality and the OCs for different $\ell = m$ never cross each other. In particular, this means that a BH that is unstable to $\ell = m = 2$ modes must also be unstable to all $\ell = m \geq 3$ modes. As $\ell = m$ grows, the curves hit extremality at a higher areal radius R_+/L and they approach the $\Omega L = 1$ line. Modes with $m \to +\infty$ reach extremality only in the limit $R_+/L \to +\infty$.

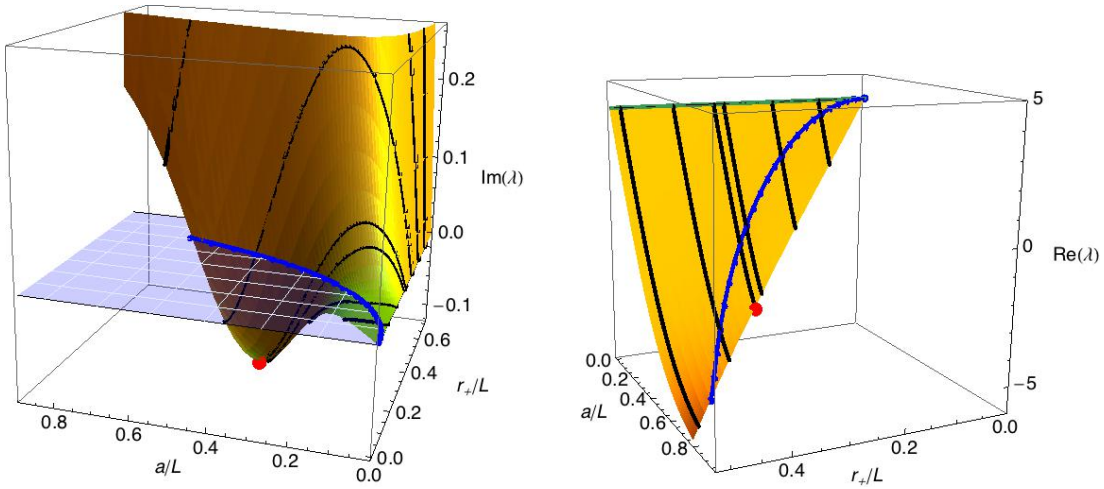

Figure 6.7: Imaginary (*left panel*) and real (*right panel*) part of the angular eigenvalues of the superradiant modes and QNMs of the $\ell = m = 2$ *vector* harmonic whose frequencies are shown in Fig. 6.6. The color coding of the lines/points is the same as Fig. 6.6.

To discuss details of the superradiant and quasinormal modes of the vector sector, we focus again our attention in the $\ell = m = 2$ case. The superradiant and QNM properties can be read from the plots of Fig. 6.6 (imaginary and real part of the frequencies) and in Fig. 6.7 (imaginary and real part of the angular eigenvalues). We use a similar color coding and visualization angle as the ones used in the scalar case. Therefore, in all these plots the blue curve is the OC already studied in Fig. 6.5; again the auxiliary plane with a grid intersects the physical 2-dimensional surface along the OC and helps visualizing the separation between unstable superradiant modes ($\mathrm{Im}(\omega) > 0$ and $\mathrm{Re}(\omega) < m\Omega$) and damped QNMs ($\mathrm{Im}(\omega) < 0$ and $\mathrm{Re}(\omega) > m\Omega$); and we plot some black curves at constant radius r_+/L. It follows that in the *left panel* of Fig. 6.6 the unstable modes are in the upper region between the blue OC and extremality, while in *right panel* they are in the lower region (that we do not show it in all its extension). The upper

region of the *left panel* of Fig. 6.7 shows the imaginary part of the eigenvalues of the QNMs (we do not show the upper surface in its full extension but its completion should be clear from the continuation of the interrupted black curves with constant $r_+/L = 0.5$ and $r_+/L = 0.6$).

In the plots of Fig. 6.6 and Fig. 6.7 the large red point signals the region where the gravitational vector superradiant instability reaches its maximum strength. This occurs for a Kerr-AdS BH with $\{r_+/L, a/L\}_{\rm max} \simeq \{0.325 \pm 0.020, 0.386 \pm 0.020\}$ where the frequency is given by $\omega L \sim 2.667 + 0.058\, i$. Stated in other words, the maximum growth rate for the vector superradiant instability and the gauge invariant properties of the BH where it is achieved are

$$\text{Vector:} \quad \{R_+/L, \Omega_h L\} \sim \{0.530, 1.687\}\,, \quad \text{Im}(\omega L) \sim 0.058\,, \quad \text{Re}(\varpi L) \sim -4.451\,. \tag{6.45}$$

In general, e.g. moving along a constant r_+/L, we find that the maximum of the vector superradiant instability is achieved much closer to extremality than in the scalar case. This property is probably related to the fact that the vector OC ends at extremality, as opposed to the scalar OC.

Comparing the properties of the maximum unstable cases (6.42) and (6.45), we see that the instability growth rate of the scalar and vector sectors is of the same order, with the maximum growth rate in the vector sector being approximately twice stronger than in the scalar sector. Moreover, the most unstable case in the vector case occurs for a Kerr-AdS BH that is smaller (i.e. with smaller gauge invariant areal radius R_+/L) but rotates faster than the Kerr-AdS BH where the scalar instability is highest.

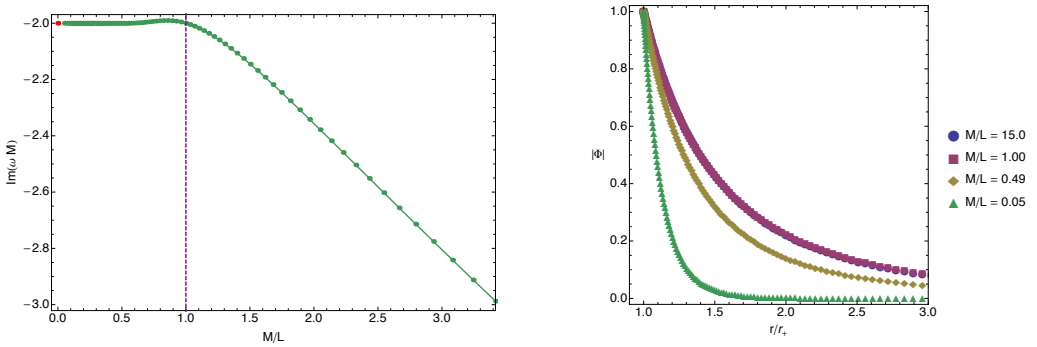

Figure 6.8: Left panel: Imaginary part of the "shear mode" as the cosmological constant is changed. The vertical purple line indicates where the Hawking-Page transition takes place. Right panel: absolute value of the vectorial Kodama Ishibashi variable in ingoing Eddington-Finkelstein coordinates.

Finally, note that the strength of the scalar or vector gravitational instabilities can can be orders of magnitude higher than the strength of the same superradiant instability sourced by a scalar field perturbation [34, 131].

6.4.3 Large AdS limit and comparison with special QNMs in asymptotically flat cases

As we will discuss in section VI, the slowly decaying QNMs in Kerr-AdS play a key role in the fluid/gravity correspondence. These modes have a particularly appealing interpretation in terms of a relativistic hydrodynamic problem naturally induced at the AdS boundary. This correspondence also indicates that rich and complex hydrodynamic phenomena have counterparts in the gravitational theory, as recently demonstrated in [110, 109, 111]. Such a remarkable, and previously unexpected, phenomena displayed by gravity in the AdS context raises the question of what analogues to hydrodynamic behavior arise in general scenarios. Studying

such question is beyond the scope of this work (for recent works related to the gravity/hydro connection in AF settings see e.g. [38, 133]); however, as we here are concerned with QNMs we can explore the connection of hydrodynamical modes in AdS with relevant ones in AF spacetimes. To this end, we examine in particular the purely-imaginary QNM mode (often called "shear mode") in the limit $r_+/L \to 0$ for the non-spinning case, see left panel of Fig. 6.8. In this limit one makes contact with its possible asymptotically flat counterpart describing QNMs of a Schwarzschild black hole. Interestingly, we find the result obtained coincides with the "algebraically special" QNM mode. Furthermore, we can look at the profile of this mode, as we change the cosmological constant. It turns out it is very localized around the horizon (becoming more and more localized as we lower the cosmological constant), perhaps indicating that the dynamics involved here does not feel the boundary in any special way, see right panel of Fig. 6.8. At this stage we stress this does not necessarily imply complex hydrodynamic phenomena has a gravitational analogue in AF cases as has been shown to be the case in the AdS case. Nevertheless this is certainly a tantalizing observation deserving further exploration.

6.5 Superradiance and black holes with a single Killing field

In the previous sections we confirmed that Kerr-AdS BHs with $\Omega_h L > 1$ are unstable to superradiance. An interesting observation is that at the onset of the superradiant instability there is an exact zero mode with $\omega = m\Omega_h$ and

$\mathrm{Im}\,\omega = 0$. This zero mode is special because it is invariant under the horizon-generating Killing field $K = \partial_T + \Omega_h \partial_\Phi$. Consequently it is regular on both the past ($\mathcal{H}^-$) and future ($\mathcal{H}^+$) horizons (generic perturbations can be made regular on the future or past horizons, but not both). In these conditions and for a given m, [30] proposed that, in a phase diagram of stationary solutions, the OC of the instability should signal a bifurcation or merger of the Kerr-AdS BH with a new family of BH solutions that are stable to superradiant modes with the given m and that preserve the same isometry of the superradiant onset mode (see also the nice discussion in [134]). That is, these new BHs have a single Killing vector field (KVF); the helical Killing field $K = \partial_T + \Omega_h \partial_\Phi$. In the context of superradiance of a *scalar field*, BHs with a similar helical single KVF that merge with the Kerr-AdS family have scalar hair orbiting around the central core. Examples of such hairy BHs were explicitly constructed perturbatively and non-linearly in [124] [10]. Given this explicit proof of existence in the scalar field case, it is natural to expect that a similar new family of single KVF BHs with "lumpy gravitational hair" merge with the Kerr-AdS BH at the OC of *gravitational* superradiance. The existence of such purely gravitational single KVF BHs was first proposed in [30] and contact between these BHs and geons was made in [72]. In this section we will give the explicit construction (omitted in [72]) that leads to the leading order thermodynamics and properties of these BHs. Perhaps the most important consequence of this study is that Kerr-AdS BHs are not the only stationary BHs of Einstein-AdS gravity [124, 72].[11]

[10] Recently, a single KVF was constructed analytically in $D = 3$ Einstein-AdS theory [134]. (In this case superradiance is absent.)

[11] The use of the word "stationary" in this context requires a comment. A solution is static if ∂_t is a KVF and the solution has the $t \to -t$ symmetry. Strickly speaking, a solution is said

We can discuss some of the main properties of the single KVF BHs [124, 72] in terms of general arguments. Recall again the main properties of superradiance in global AdS. A mode $e^{-i\omega T+im\Phi}$ can increase its amplitude by scattering off a rotating BH with angular velocity Ω_h satisfying $\omega < m\Omega_h$. In asymptotically global AdS spacetimes, the outgoing wave is reflected back onto the BH and scatters again further increasing its amplitude. This multiple amplification/reflection leads to an instability. The process decreases Ω_h and eventually results in a BH with "lumpy hair" rotating around it. Such a BH is invariant under just a single Killing field which co-rotates with the hair, $K = \partial_T + \Omega_h \partial_\Phi$. Thus, the BH is stationary (periodic) but not time symmetric nor axisymmetric. However, it does not violate the rigidity theorems [121, 122, 123]. Indeed, these theorems assume the existence of a Killing vector, typically ∂_T, that is not normal to the horizon, and prove that a second Killing field ∂_Φ must then be present. Such a BH is thus time symmetric and axisymmetric. The single KVF BHs evade the primary assumption of the rigidity theorem because in this case $K = \partial_T + \Omega_h \partial_\Phi$ is normal to the Killing horizon.

As stated previously, single KVF BHs and horizonless boson star solutions of this type with scalar hair have been constructed perturbatively as well as numerically at the full nonlinear level in [124]. Alternatively, the leading order description

to be stationary if ∂_t is still a KVF but the $t \to -t$ symmetry is no longer present. In addition, ∂_t must be timelike everywhere along the asymptotic boundary of the spacetime. The single KVF BHs discussed here and in [124, 72] certainly do not have ∂_t as a KVF. Instead, they have a helical KVF. Moreover, this KVF is not timelike everywhere at spatial infinity; indeed it is timelike in the neighbourhood of the poles but spacelike near the equator of the sphere. Nevertheless these single KVF solutions are periodic. Now, a periodic solution can be considered to fit in the intuitive notion we have of stationarity. For this reason we follow [124, 72] who proposed extending the original definition of stationarity to accommodate these novel periodic BHs as members of the stationary class of solutions.

of these BHs can also be found using a thermodynamic analysis [135, 136, 137, 124] similar to the one done below. The full nonlinear result confirms that this thermodynamic construction gives accurate leading order results [12]. For small charges the single KVF hairy BHs exist in a region of the phase diagram that is bounded by the OC of scalar superradiance and by the boson star curve.

In the purely gravitational sector of Einstein-AdS theory that we discuss here, the gravitational analogue of the horizonless boson stars are the geons constructed in [72]. Using the aforementioned thermodynamic model we will conclude that single KVF BHs exist in a region of the phase diagram that is bounded by the OC of gravitational superradiance and by the geon curve.[13]

We are ready to start the leading order thermodynamic construction of the single KVF BHs. We first review the geon and Kerr-AdS solutions, then we construct the single KVF BHs by placing a small Kerr-AdS BH on the top of a geon.

Geons are classical lumps of gravitational energy, with harmonic time dependence $e^{-i\omega T+im\Phi}$, in which the centrifugal force balances the system against gravitational collapse [72]. They are horizon-free, nonsingular, asymptotically globally AdS, and can be viewed as gravitational analogs of boson stars. Each geon is specified by ℓ, which gives the number of zeros of the solution along the polar direction, and azimuthal quantum number m. It is a one-parameter family of

[12] A similar thermodynamic model was introduced and proved to be correct, when compared with the exact non-linear results, also in the charged superradiant systems discussed in [135, 136, 137]

[13] The hairy BHs of [124] could be constructed non-linearly because they depend non-trivially only on the radial direction while the gravitational single KVF BHs we discuss here have an additional non-trivial dependence on the polar angle. It is challenging to solve the associated coupled system of PDEs and we leave its construction for future work.

solutions parametrized e.g. by its frequency. At linear order, a geon is a small perturbation around the global AdS background and its possible frequencies are given by the AdS normal modes, namely (6.40) in the scalar sector, and (6.43) in the vector sector. The energy and angular momentum of the geon are related by $E_g = \frac{\omega}{m} J_g + O(J_g^2)$; they have zero entropy $S_g = 0$ and undefined temperature, and they obey the first law of thermodynamics, $dE_g = \frac{\omega}{m} dJ_g$. [14]

Consider now the Kerr-AdS BH. For small E and J (i.e small r_+/L expansion), the leading and next-to-leading order thermodynamics of this solution is

$$E_K \simeq \frac{r_+}{2}\left(1+\frac{r_+^2}{L^2}\left(1+\Omega_h^2 L^2\right)\right)+O\left(\frac{r_+^4}{L^4}\right), \qquad J_K \simeq \frac{1}{2} r_+^3 \Omega_h + O\left(\frac{r_+^4}{L^4}\right),$$
$$S \simeq \pi r_+^2\left(1+\Omega_h^2 r_+^2\right)+O\left(\frac{r_+^5}{L^5}\right), \qquad T_h \simeq \frac{1}{4\pi r_+}\left(1+\left(3-2\Omega_h^2 L^2\right)\frac{r_+^2}{L^2}\right)+O\left(\frac{r_+^2}{L^2}\right), \tag{6.46}$$

which obeys the thermodynamic first law, $dE_K = \Omega_h\, dJ_K + T_h\, dS$, up to next-to-leading order.

We can now construct perturbatively the single KVF BH of the theory by placing a small Kerr-AdS BH at the core of the geon. The associated single KVF of the solution is inherited from the geon component of the system. To argue for the existence of this solution and to find its thermodynamic properties we can use a simple thermodynamic model where the leading order thermodynamics of the single KVF BH is modeled by a non-interacting mixture of a Kerr-AdS BH and a geon Absence of interaction between the two components of the system means that the charges E, J of the final BH are simply the sum of the charges of its individual constituents: $E = E_K + E_g$, $J = J_K + J_g$.

[14] Back-reacting to higher order each of the individual normal modes of global AdS we approach the full nonlinear geon, but we do not need this knowledge for our argument [72].

In this mixture, the Kerr-AdS component controls the entropy and the temperature of the final BH (since by definition the geon has no entropy and has undefined temperature). The single KVF BH chooses the partition of its charges between the geon and the Kerr-AdS components in such a way that the total entropy S of the system is extremized. Indeed, maximizing $S = S_K(E - E_g, J - J_g)$ with respect to J_g and using the first laws for the geon and for the Kerr-AdS, we find that the partition is such that the angular velocities of the two components are the same, $\Omega_h = \frac{\omega}{m}$, i.e. the two phases are in thermodynamic equilibrium. Actually, there is a much simpler way to derive this result. Since the geon has only one Killing field, $K = \partial_T + (\omega/m)\partial_\Phi$, and we place a Kerr-AdS BH with a Killing horizon at its centre, the geon's Killing field must coincide with the horizon generator of the single KVF BH.

The non-interacting and equilibrium conditions together with the leading order thermodynamics of the Kerr-AdS BH and of the geon yields that the final distribution of the charges among the system's constituents and the entropy and temperature of the single KVF BH are, respectively,

$$\begin{aligned} &\left\{J_g\,, E_g\right\} = \left\{J\,, \frac{\omega}{m} J\right\}\,, \quad \left\{J_K\,, E_K\right\} = \left\{0\,, E - \frac{\omega}{m}\,J\right\}\,, \\ &S = 4\pi\left(E - \frac{\omega}{m}\,J\right)^2\,, \quad T_h = \frac{1}{8\pi}\left(E - \frac{\omega}{m}\,J\right)^{-1}\,. \end{aligned} \tag{6.47}$$

So, at leading order, the geon component carries all the rotation of the system and the Kerr-AdS component stores all the entropy. By construction, these relations obey the first law of thermodynamics $dE = T_h dS + \Omega_h dJ$, up to order $\mathcal{O}(M, J)$ with $\Omega_h = \omega/m$ and ω given by (6.40) in the scalar sector, or by (6.43) in the

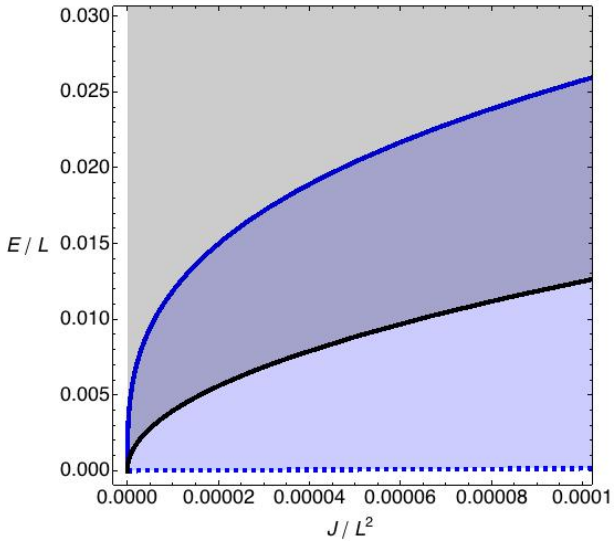

Figure 6.1: Phase diagram of global AdS stationary solutions of the $d = 4$ Einstein-AdS theory, for small E/L and J/L^2. Non-extremal Kerr-AdS BHs exist only above the extremal black line (grey region). The blue curve above the extremal line sets the onset of the gravitational superradiant instability to $\ell = m = 2$ scalar modes (already represented e.g. in Fig. 6.2). Kerr-AdS BHs below these curves are unstable to the associated $\ell = m = 2$ superradiant scalar modes. The dashed curve in the bottom represents the scalar $\ell = m = 2$ geon described by $E = \frac{\omega}{m} J$ with $\omega = \omega_{\rm s} = (1 + \ell)$ and $\ell = m = 2$ (and $p = 0$). Single Killing field BHs with $m = \ell = 2$ exist between the superradiant OC and the geon line (blue and blue/gray regions). In the blue/gray shaded region between the black and the upper blue line, Kerr-AdS and single KVF BHs coexist, i.e. we have non-uniqueness.

vector sector.

Using this simple thermodynamic model we can further predict the region in phase space where single KVF BHs should exist. A single KVF BH merges with the Kerr-AdS family at a curve that describes the onset of the m-mode superradiant instability. This occurs at an angular velocity that saturates the superradiant condition, $\omega \leq m\Omega_h$, where $\{\omega, m\}$ are the frequency and azimuthal number of the linearized geon component of the single KVF BH. (It suffices to

consider the linearized geon since the gravitational hair is very weak near the onset of the instability.) At the superradiant merger, the Kerr-AdS and single KVF BH thermodynamics coincide. Thus, we can use the Kerr-AdS BH thermodynamics (6.46) with $\Omega_h = \omega/m$ to determine the charges of the final system. In a phase diagram $\{E,\, J\}$ − see Fig. 6.1 − this determines the upper bound curve of the region where single KVF BHs exist:

$$E\big|_{merger} \simeq \frac{r_+}{2} + \frac{r_+^3}{2L^2}\left(1 + \frac{\omega^2 L^2}{m^2}\right), \qquad J\big|_{merger} \simeq \frac{1}{2}\,\frac{\omega}{m}\,r_+^3\,. \tag{6.48}$$

Moving down from this curve, the Kerr-AdS contribution weakens and the leading order thermodynamics of the system is increasingly dominated by the geon component. In the limit where $r_+ \to 0$, the lower bound curve of single KVF phase is expected to be the geon curve. This discussion is best illustrated in Fig. 6.1, where we represent the phase diagram associated to the $\ell = m = 2$ solutions of the scalar sector with frequency $\omega = \omega_{\rm s}$ given by (6.40).

Note that there is a region in the phase diagram (the blue/gray shaded region in Fig. 6.1) where the Kerr-AdS and single KVF BH families coexist, i.e. the present system provides the first example of non-uniqueness in Einstein gravity in four dimensions. The two families of BHs can have the same mass and angular momentum but different entropy.

As emphasized previously, in the scalar field superradiant system of [124], and in the charged superradiant system of [135, 137], the available full non-linear results confirm that the thermodynamic model we use also here gives the correct leading order thermodynamic properties of the system. We leave for the future

the explicit non-linear construction of the single KVF BHs.

We postpone for Sec. 6.8 the discussion of the stability properties of the single KVF BHs and the role they might have in the time evolution and endpoint of the superradiant instability of the Kerr-AdS BH.

6.6 Hydrodynamic thermalization timescales in the AdS_4/CFT_3 duality

In the context of the gauge/gravity duality, a black hole is dual to a thermal state in the holographic quantum field theory (QFT). Moreover, QNMs are fundamental entities in this correspondence since the QNM frequencies in the bulk black hole describe the thermalization or relaxation timescales in the dual QFT. This map was first proposed in [90, 91] and later it was understood and established that the QNM spectrum of a given field perturbation coincides with the poles of retarded correlation functions of the gauge theory operator that is dual to the perturbation at hand [92, 93, 94]. This was done in the framework of linear response theory appropriate for describing linearized fluctuations of any wavelength about AdS backgrounds as long as the perturbation amplitude is small. A particularly relevant family of perturbations are the lowest QNMs, i.e. those with small frequency whose wavelength is large compared to the thermal scale of the field theory. The relaxation timescales of these modes have a hydrodynamic description and can be computed studying perturbations of the Navier-Stokes equation that describes the hydrodynamic regime of the holographic QFT [94, 95, 96, 97]. These hydrodynamic modes are also captured by the fluid/gravity correspondence

which is a formal one-to-one map between Einstein's equations in AdS and non-linear hydrodynamic equations [138, 139]. It follows from a perturbation theory analysis where the small expansion parameter is the ratio of the mean free path of the theory (i.e. the thermal scale) over the typical variation wavelength of the fluid variables and gravitational field. With respect to linear response theory it has the advantage that it captures also non-linear physics but it is restricted to long wavelength physics. The two regimes therefore complement each other and intersect in a corner of the phase space corresponding to linearized long wavelength perturbations [139]. These are precisely the hydrodynamic QNMs that we want to study in this section.

A particular example of a gauge/gravity duality is the AdS_4/CFT_3 correspondence, whereby supergravity on the Kerr-AdS$\times S^7$ background is dual to a thermal conformal field theory (CFT) on the holographic boundary of the global AdS geometry. In this case the Kerr-AdS black hole is dual to a thermal state with a rotational chemical potential in the CFT_3 that is formulated on a sphere.

In this section we aim to compare the long wavelength gravitational QNMs of Kerr-AdS with the hydrodynamic relaxation timescales of the dual CFT_3. First, in Section 6.6.1 we compute the hydrodynamic modes both perturbatively and numerically and later, in Section 6.6.2, we compare them with with the long wavelength gravitational QNMs. The excellent match that we find provides a further confirmation of the holographic interpretation of the QNM spectrum, of the shear viscosity to the entropy density bound, $\eta/s = 1/(4\pi)$, and ultimately of the correspondence itself. Not less importantly, it provides the first non-trivial confirmation that the Robin boundary conditions for the Teukolsky gauge-invariant

variable derived in the companion paper [115] are indeed the ones that we must impose if we want the perturbations to preserve the asymptotic global AdS structure of the background. Indeed, had we chosen different BCs, e.g Dirichlet or Neumann BCs, and the QNM spectrum would not match the hydrodynamic timescales.

6.6.1 Hydrodynamic thermalization timescales

The conformal boundary of the Kerr-AdS geometry is the static Einstein universe $R_t \times S^2$ with line element that this time we write as

$$ds^2_\partial = h_{bc}\, dx^b dx^c = -dT^2 + L^2 d\Omega_{S^2}\,, \qquad d\Omega_{S^2} = \frac{dX^2}{1-X^2} + \left(1-X^2\right) d\Phi^2\,. \quad (6.49)$$

where X is related to the standard polar angle on the sphere introduced in (6.7) by $X = \cos\Theta$. The CFT_3 is described by an holographic stress tensor $\langle T_{bc}\rangle$ which can be found using, e.g. the formulation of Haro, Skenderis and Solodukhin [103].

We first introduce the Fefferman-Graham coordinate frame $\{T, z, X, \Phi\}$ whereby the Kerr-AdS geometry can be recast in an asymptotic expansion around the holographic boundary $z = 0$ ($r = \infty$) as

$$ds^2 = \frac{L^2}{z^2}\left[dz^2 + ds^2_\partial + \frac{z^2}{L^2}\, h_2 + \frac{z^3}{L^3}\, h_3 + \mathcal{O}(z^6)\right]\,, \quad (6.50)$$

with ds^2_∂ defined in (6.49). The coordinate transformation that takes Kerr-AdS in the Chambers-Moss frame into the FG frame is obtained as an expansion in z, with the successive terms of the expansion being fixed by requiring that $g_{zz} = L^2/z^2$ and $g_{zb} = 0$ ($b = T, X, \Phi$) at all orders. Up to the order relevant for our analysis,

this FG coordinate transformation is explicitly given by

$$
\begin{aligned}
&t = \Xi\, T\,, \qquad \phi = \Phi - \frac{a}{L^2}\, T\,,\\
&r = \sqrt{L^2 - a^2\,(1-X^2)}\left(\frac{L}{z} + \frac{z}{L}\,\frac{a^4\,(1-X^4) - L^4}{4\,[L^2 - a^2\,(1-X^2)]^2}\right.\\
&\qquad\qquad \left. + \frac{z^2}{L^2}\,\frac{\left(r_+^2 + a^2\right)\left(r_+^2 + L^2\right)}{6 r_+\,[L^2 - a^2\,(1-X^2))^{3/2}}\right) + \mathcal{O}\left(\frac{z^3}{L^3}\right),\\
&\chi = \frac{a\,L\,X}{\sqrt{L^2 - a^2\,(1-X^2)}}\left(1 + \frac{z^2}{L^2}\,\frac{a^2\,(L^2-a^2)\,(1-X^2)}{2\,[L^2 - a^2\,(1-X^2)]^2}\right) + \mathcal{O}\left(\frac{z^4}{L^4}\right).
\end{aligned}
\tag{6.51}
$$

The leading terms in these expansions are fixed by our choice of conformal frame, namely we want the normalization where $g_{TT} = -1$ and the sphere has radius L^2 in the boundary metric ds^2_∂. On the other hand the azimuthal coordinate transformation guarantees that the conformal frame does not rotate.

The holographic stress tensor can be read from the h_3 contribution of the expansion (6.50) via [103]

$$
\langle T_{bc}\rangle = \frac{3h_3}{16\pi G_4}\,, \tag{6.52}
$$

where b, c run over the boundary metric coordinates $\{T, X, \Phi\}$. This stress tensor has the form of a perfect fluid with energy density ρ, pressure p, and fluid velocity u given by

$$
\begin{aligned}
&\langle T_{bc}\rangle_{(0)} = (\rho + p) u_b u_c + p\, h_{bc}\,,\\
&\rho(0) = 2p_{(0)}, \qquad p_{(0)} = \frac{\left(r_+^2 + a^2\right)\left(r_+^2 + L^2\right)}{3 r_+\, L\, \gamma(X)^{-3}}\,,\\
&u_{(0)} = \gamma(X)\big(\partial_T - \Omega_\infty \partial_\Phi\big),\\
&\text{where} \quad \Omega_\infty = \frac{a}{L^2}, \quad \gamma(X) = \left[1 - \frac{a^2}{L^2}\left(1 - X^2\right)\right]^{-1/2}
\end{aligned}
\tag{6.53}
$$

are the angular velocity Ω_∞ of the fluid, and the ratio $\gamma^{-1} = \frac{T}{\mathcal{T}}$ between the fluid temperature T and the local temperature $\mathcal{T}$ (this gives the redshift factor relating measurements done in the laboratory and comoving frames), and $\partial_T, \partial_\Phi$ are the Killing vectors corresponding to the isometries of the boundary background (6.49),. Further, $u^2 = -1$ and the equation of state $\rho = 2p$ follows from the fact that the holographic QFT and its fluid are conformal which implies that the stress tensor is traceless. The stress tensor is conserved with respect to (6.49), $\nabla_b \langle T^{bc} \rangle = 0$, since there are no sources (e.g., scalar or Maxwell) in our system. Our bulk background is stationary and therefore the boundary fluid is also in stationary equilibrium fluid configuration with rigid roto-translational motion. Our choice for the fluid velocity definition is such that it obeys the Landau gauge condition

$$u_b \langle T^{bc} \rangle = \rho u^c \,. \tag{6.54}$$

This condition guarantees that the stress tensor components longitudinal to the velocity give the local energy density, in the local rest frame of a fluid element [140].

A generic perturbation of the stationary fluid configuration will drive the system away from equilibrium and dissipation must be included to study the evolution of the system. This dissipative contribution to the total holographic stress tensor is encoded in the term $\langle \Pi_{bc} \rangle$ (this follows from a gradient expansion of Einstein equations around AdS in the regime where the thermodynamic variation lengthscales are much larger than the thermal scale of the stationary background

[138, 139]),

$$\begin{aligned} &\langle T_{bc}\rangle = \langle T_{bc}\rangle_{(0)} + \langle \Pi_{bc}\rangle \qquad \langle \Pi_{bc}\rangle = -2\eta\sigma_{bc} \\ &\text{where} \quad \sigma^{bc} = \frac{1}{2}\left(P^{bd}\nabla_d u^c + P^{cd}\nabla_d u^b\right) - \frac{1}{2}\vartheta P^{bc} \\ &\vartheta = \nabla_c u^c\,, \qquad P^{bc} \equiv h^{bc} + u^b u^c\,, \end{aligned} \tag{6.55}$$

are the shear viscosity tensor σ^{bc}, the fluid expansion ϑ, and the is the projector P^{bc} onto the hypersurface orthogonal to u. The quantity η is the shear viscosity. Since the fluid is conformal, its stress energy tensor must be traceless (i.e. the conformal anomaly is proportional to $T_c{}^c$ and vanishes[15]). Consequently the fluid must have vanishing bulk viscosity. Also, the Landau frame condition (6.54) implies $u_a^{(0)}\Pi^{bc} = 0$ which discards a possible heat diffusion contribution to the first order dissipative stress tensor (i.e. in this frame all the dissipative contributions are orthogonal to the velocity field) [140].

We recall that a precise statement for the validity of the hydrodynamic regime of dual system can be made as follows. The mean free path of a theory is typically given by the ratio of the shear viscosity to the energy density, $\ell_{\rm mfp} \sim \frac{\eta}{\rho}$. We are working with a conformal theory so the associated fluid equation of state is $\rho = 2p$ and the viscosity to entropy bound is saturated, $\eta = s/(4\pi)$ [141]. For any fluid we also have the Euler-Gibbs relation $\rho + p = \mathcal{T}s$, where the local temperature is related to the fluid temperature (dual to the black hole temperature $T = T_h$) by the Lorentz factor. Therefore we can write $\ell_{\rm mfp} \sim \frac{\eta}{\rho} \sim \frac{3}{2}\frac{\eta}{\rho+P} \sim \frac{3}{2}\frac{\eta}{\mathcal{T}s} \sim \frac{3}{8\pi}\frac{1}{\mathcal{T}} \sim$

[15] A CFT is invariant under Weyl transformations $h_{bc} \to h_{bc}e^{-2\lambda(x)}$ which requires that its stress tensor is traceless. In a curved background the Weyl anomaly breaks in general the conformal symmetry and yields $T \propto R^2$, but this breaking occurs only at fourth order in a gradient expansion and the bulk viscosity appears at first order [140].

$\frac{3}{8\pi}\frac{\gamma^{-1}}{T_h}$. The hydrodynamic approximation is valid for when the thermodynamic quantities of the fluid and of its perturbations vary on lengthscales that are much larger than $\ell_{\rm mfp}$, namely

$$\frac{r_+}{L} \gg 1\,, \qquad \text{and} \qquad \frac{a}{L} \ll 1\,, \tag{6.56}$$

where to get the first relation we used the fact that $0 < \gamma^{-1} \leq 1$ and that the temperature scales as $T_h \sim r_+$ for large radius black holes − see (6.5) − while the second relation follows from the fact that the background pressure $p_{(0)}$ is not a constant and its gradient scales with the rotation parameter in AdS units.

According to the holographic dictionary, the fluid temperature is identified with the Hawking temperature T_h of the black hole and it follows from the previous discussion that the angular velocity of fluid $\Omega_\infty = a/L^2$ is precisely the shift in the azimuthal coordinate such that the (non-dynamical) background on which the fluid flows is static. On the other hand, the viscosity is given in terms of the horizon radius of the bulk black hole as

$$\eta = \frac{1}{3}\, L r_+^2\,. \tag{6.57}$$

This is a universal relation for any fluid that is holographically dual to a black hole of Einstein-AdS$_4$ theory. It follows from the celebrated viscosity to entropy density ratio of the theory namely $\eta = s/(4\pi)$ [141]. This is a constitutive relation that is independent of the rotation of the fluid since it follows from measuring quantities in the rest frame of the fluid. Namely we can write the entropy density as $s = S/V = S\rho_{(0)}/E = 2p_{(0)}S/E$ which yields (6.57) after using the relations

for the static black hole entropy and energy, $S = \pi r_+^2$ and $E = r_+ \left(1 + r_+^2/L^2\right)/2$, and taking the hydrodynamic limit $r_+/L \to \infty$.

The hydrodynamic equations of motion for the perturbed fluid, that will ultimately quantize the relaxation timescales of the system, follow from the conservation of the total stress tensor,

$$\nabla_b \left(\langle T^{bc} \rangle_{(0)} + \langle \Pi^{bc} \rangle \right) = 0 \,. \tag{6.58}$$

These equations can be written as a set of two family of equations, namely the relativistic continuity and Navier-Stokes equations, [16]

$$\begin{aligned} & u^c \nabla_c \rho + (\rho + p)\vartheta = 2\eta \sigma^{bc} \nabla_b u_c \,, \\ & (\rho + p) u^b \nabla_b u^c = -P^{bc} \nabla_b p + 2\eta \left(\nabla_b \sigma^{bc} - u^c \sigma^{bd} \nabla_b u_d \right) . \end{aligned} \tag{6.59}$$

To study the perturbations of these fluid equations, we use the fact that ∂_T and ∂_Φ are isometries of the background to write the most general perturbations for a conformal fluid as a sum of the following Fourier modes

$$\begin{aligned} & \rho = 2p, \qquad p = p_{(0)} + e^{-i\omega T} e^{im\Phi} \delta p(X) \,, \\ & u = u_{(0)} + \, e^{-i\omega T} e^{im\Phi} \delta u_c(X) \, dx^c . \end{aligned} \tag{6.60}$$

[16] The continuity equation follows from projecting (6.55) along the fluid velocity. Plugging it into (6.55) then yields the Navier-Stokes equation, which is the projection of (6.55) in the hypersurface orthogonal to the velocity.

The velocity normalization $u^2 = -1$ requires $u_{(0)} \cdot \delta u = 0$ i.e

$$\delta u_T = -\frac{a}{L^2}\,\delta u_\Phi \tag{6.61}$$

Plugging these fluctuations in the linearized version of the hydrodynamic equations (6.59) we get the equations of motion (EoM) that the fluid perturbations $\{\delta P, \delta u_X, \delta u_\Phi\}$ have to obey. We solve these equations exactly using numerical methods like those we use to solve the gravitational equations. In addition, to get extra physical insight and check the numerics, we also find a perturbative explicit analytical expression for the fluid quantities of interest.

To solve the linearized hydrodynamic equations using a perturbative method [135, 136, 124, 137], we assume a double expansion in the shear viscosity and in the rotation, both for the fluid perturbations introduced in (6.60), $\{Q^{(f)}(X)\} = \{Q^{(1)}, Q^{(2)}, Q^{(3)}\} \equiv \{\delta P/L, \delta u_X, \delta u_\Phi\}$, and for the perturbation frequency ω:

$$\begin{aligned} Q^{(f)}(\eta, a; X) &= \sum_{j=0}^{1} Q_j^{(f)}(a; X) \left(\frac{\eta}{L^3}\right)^j \qquad \text{and} \quad Q_j^{(f)}(a; X) = \sum_{i=0}^{p} Q_{j,i}^{(f)}(X) \left(\frac{a}{L}\right)^i, \\ \omega(\eta, a) &= \sum_{j=0}^{1} \omega_j(a) \left(\frac{\eta}{L^3}\right)^j, \qquad \text{and} \quad \omega_j(a) = \sum_{i=0}^{p} \omega_{j,i} \left(\frac{a}{L}\right)^i, \end{aligned} \tag{6.62}$$

and solve progressively (6.58) or (6.59) in a series expansion in η/L^3 and a/L. For our purpose it will be enough to go up to third order ($p = 3$) in the rotation expansion.

Inspecting the EoM at leading order $\mathcal{O}(\eta^0, a^0)$, we immediately conclude that we have to split our analysis into two family of modes, namely the scalar and vector modes. The latter have $\omega_{0,0} = 0$ and perturb the fluid velocity but not

the pressure, while the former have $\omega_{0,0} \neq 0$ and perturb all fluid variables. At this order rotation is absent and the hydrodynamic modes have an expansion in terms of the scalar $\mathbf{S}_i$ and vector $\mathbf{V}_i$ Kodama-Ishibashi harmonics (which are both related to the associated Legendre polynomials [31, 97, 115]). This is in agreement with the fact that the gravitational QNMs split also into two families as dictated by the two possible global AdS boundary conditions (6.20)-(6.22). As rotation and/or viscosity are turned on these two families naturally continue to follow different paths.

Our main goal is to find the characteristic damped oscillation frequencies of the fluid. We leave the details of our computation to Appendix 6.B and give here only its relevant outcome, namely the hydrodynamic CFT thermalization frequencies that can propagate in the CFT_3. The frequencies of the hydrodynamic scalar

modes are:[17]

$$
\begin{aligned}
\omega L|_{\mathbf{s}} = \Big[& \frac{\sqrt{\ell(\ell+1)}}{\sqrt{2}} + \frac{a}{L}\,\frac{m(\ell+2)(\ell-1)}{2\ell(\ell+1)} - \frac{a^2}{L^2}\,\frac{(\ell+2)(\ell-1)}{4\sqrt{2}(2\ell-1)(2\ell+3)[\ell(\ell+1)]^{5/2}} \\
& \times\Big(2(\ell-3)(\ell+4)\ell^2(\ell+1)^2 + 3m^2\left(6+\ell+\ell^2\right)\left(1+2\ell+2\ell^2\right)\Big) \\
& + \frac{a^3}{L^3}\,\frac{m}{2\ell^4(\ell+1)^4(2\ell-1)(2\ell+3)}\Big(\ell^2(\ell+1)^2\left(\ell^6+3\ell^5+6\ell^4+7\ell^3-53\ell^2-56\ell-48\right) \\
& + m^2\left(\ell^8+4\ell^7-6\ell^6-32\ell^5+37\ell^4+132\ell^3+224\ell^2+152\ell+48\right)\Big) + \mathcal{O}\left(\frac{a^4}{L^4}\right)\Big] \\
& + i\,\frac{\eta}{r_+^3}\,(\ell-1)(\ell+2)\Big[-\frac{1}{2} + \frac{a}{L}\,\frac{m\left(2+3\ell+3\ell^2\right)}{2\sqrt{2}[\ell(\ell+1)]^{3/2}} \\
& + \frac{a^2}{L^2}\,\frac{1}{2\ell^3(\ell+1)^3(2\ell-1)(2\ell+3)}\Big(\ell^2(\ell+1)^2\left(8+\ell+\ell^2\right)\left(3+2\ell+2\ell^2\right) \\
& - 2m^2\big[\,12+\ell(\ell+1)\left(32+14\ell+15\ell^2+2\ell^3+\ell^4\right)\big]\Big) \\
& + \frac{a^3}{L^3}\,\frac{m}{8\sqrt{2}\ell^{9/2}(\ell+1)^{9/2}(2\ell-1)(2\ell+3)(\ell-1)(\ell+2)} \\
& \times\Big\{m^2\Big(-34\ell^{10}-170\ell^9-387\ell^8-528\ell^7+164\ell^6+1626\ell^5+7009\ell^4 \\
& + 11032\ell^3+11608\ell^2+6400\ell+1680\Big) - 2\ell^2(\ell+1)^2\Big(15\ell^8+60\ell^7 \\
& + 8\ell^6-186\ell^5+113\ell^4+606\ell^3+1832\ell^2+1488\ell+864\Big)\Big\} + \mathcal{O}\left(\frac{a^4}{L^4}\right)\Big],
\end{aligned}
\tag{6.63}
$$

while the frequencies of the hydrodynamic vector modes are:

$$
\begin{aligned}
\omega L|_{\mathbf{v}} = \frac{m\,a}{L}\Big[& \frac{(\ell+2)(\ell-1)}{\ell(\ell+1)} + 4\frac{a^2}{L^2}\Big(\frac{12+\ell(\ell+1)\left(2+\ell+\ell^2\right)}{\ell^2(\ell+1)^2(2\ell-1)(2\ell+3)} \\
& - \frac{m^2\left[12+\ell(\ell+1)\left(26-2\ell+\ell^2+6\ell^3+3\ell^4\right)\right]}{\ell^4(\ell+1)^4(2\ell-1)(2\ell+3)}\Big) + \mathcal{O}\left(\frac{a^3}{L^3}\right)\Big] \\
& + i\,\frac{\eta}{r_+^3}\,(\ell-1)(\ell+2)\Big[-1 + \frac{a^2}{L^2}\Big(\frac{24+\ell(\ell+1)\left(4\ell^2+4\ell-5\right)}{\ell(\ell+1)(2\ell-1)(2\ell+3)} \\
& + \frac{8m^2\left[\ell(\ell+1)\left(\ell^4+2\ell^3+\ell^2-5\right)-3\right]}{\ell^3(\ell+1)^3(2\ell-1)(2\ell+3)}\Big) + \mathcal{O}\left(\frac{a^3}{L^3}\right)\Big].
\end{aligned}
\tag{6.64}
$$

[17] In (6.63) and (6.64) we discard terms of order $\mathcal{O}\left(\eta L^2/r_+^5\right)$.

In these expansions (and associated Figs. 6.1, 6.2 below) we assume the relation (6.57) for the viscosity. When the rotation vanishes, (6.63) and (6.64) reduce to the hydrodynamic frequencies first computed in [97].

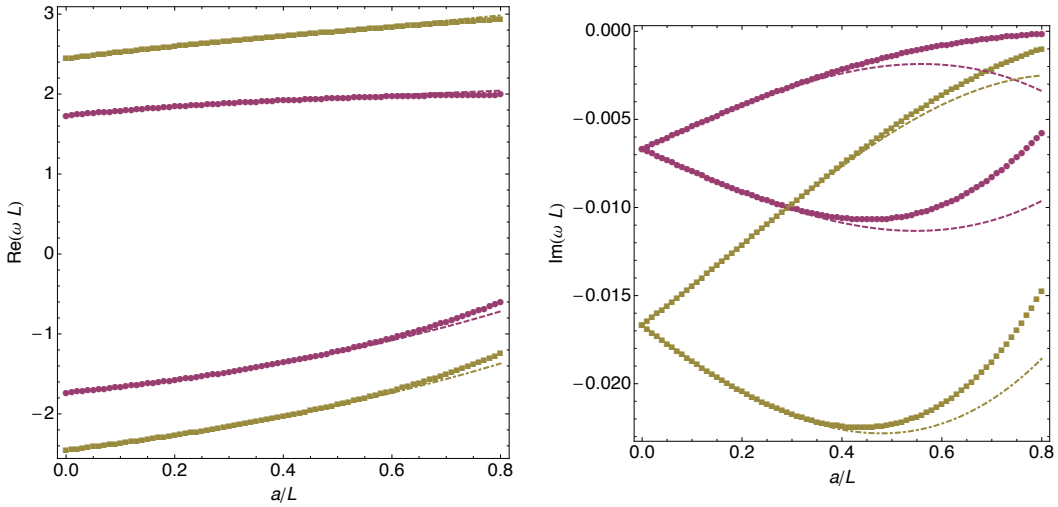

Figure 6.1: Real and Imaginary part of the frequency for the scalar hydrodynamic modes as a function of the adimensional rotation parameter. The disks (squares) are the exact numerical solutions of the hydrodynamic equations for the $\ell = m = 2$ ($\ell = m = 3$) harmonics. On the other hand the dashed line ($\ell = 2$) and the dashed-dotted line ($\ell = 3$) are the curves dictated by the perturbative analytical expression (6.63). In the right panel the upper (lower) branches of each harmonic pair describe the imaginary part of the modes with positive (negative) real part.

As illustrative examples, Figs. 6.1 and 6.2 show the regime of validity of the perturbative expressions (6.63) and (6.64) by comparing them against the exact numerical solutions of the linearized hydrodynamic equations (6.59) for the $\ell = m = 2$ and $\ell = m = 3$ harmonics in both the scalar and vector sectors. As is evident from the figures, the match is excellent in the small rotation regime as expected.

Fig. 6.1 describes the hydrodynamic scalar modes. For each harmonic ℓ there

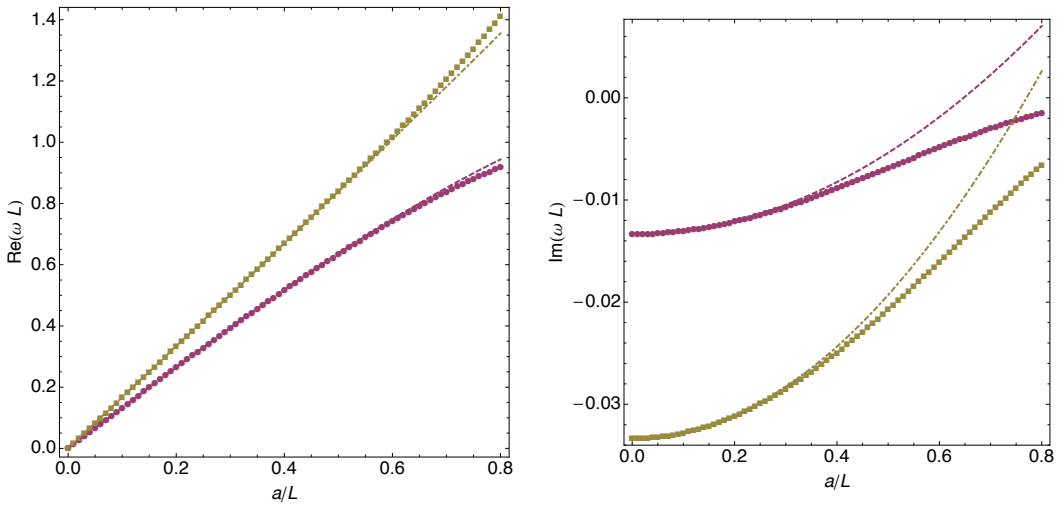

Figure 6.2: Real and Imaginary part of the frequency for the vector hydrodynamic modes as a function of the adimensional rotation parameter. The disks (squares) describe the exact numerical solution of the hydrodynamic equations for the $\ell = m = 2$ ($\ell = m = 3$) harmonics. On the other hand the dashed line ($\ell = 2$) and the dashed-dotted line ($\ell = 3$) are the curves predicted by the perturbative analytical expression (6.64).

is a pair of solutions, one with positive and the other with negative real part of the frequency. At zero rotation and only in this case, the background has the $t - \phi$ symmetry and thus the two solutions are physically the same: they form a pair $\{\omega, -\omega^*\}$ related by complex conjugation. Rotation breaks this degeneracy. Fig. 6.2 describes the hydrodynamic vector modes. These are characterized by having vanishing frequency real part when the rotation vanishes, so there is only one family of solutions for each harmonic.

6.6.2 Long wavelength QNMs and hydrodynamic modes

In the last subsection we computed analytically and numerically the hydrodynamic relaxation timescales. In this section we compare these timescales with the

long wavelength gravitational QNMs.

To perform the comparison we recall that the hydrodynamic and gravitational modes are expected to match in the regime of parameters (6.56), namely $r_+/L \gg 1$ and $a/L \ll 1$. We thus consider a Kerr-AdS black hole with radius parameter $r_+/L = 100$ to do the comparison. A measure of the deviation between the numerical hydrodynamic frequencies (call them $\omega_{\rm hydro}$) and the numerical gravitational QNM frequencies (call them ω) is given by $|1 - \omega_{\rm hydro}/\omega|$. In Fig. 6.3 we plot this deviation measure as a function of the rotation parameter a/L ($a/L < 1$ for regular black holes) for a Kerr-AdS BH with $r_+/L = 100 \gg 1$. The brown curve (disks) is for scalar modes, while the green curve (squares) is for vector modes. We see that the match between the hydrodynamic and long wavelength QNM frequencies is very good even when the rotation grows large and thus moves away from the hydrodynamic validity regime $a/L \ll 1$: for scalar (vector) modes the maximum deviation is below 10^{-4} (2×10^{-3}).

This perfect match when the rotating chemical potential is present is a further confirmation of the holographic interpretation of the QNM spectrum, of the shear viscosity to the entropy density bound, $\eta/s = 1/(4\pi)$, and ultimately of the AdS/CFT correspondence itself.

6.7 QNMs and superradiance in 5 dimensions

In this section we extend the study of thermalization, quasinormal modes, and superradiance to five dimensions. There are many motivations for doing so. Firstly, there is currently a general interest in studying gravity in higher dimen-

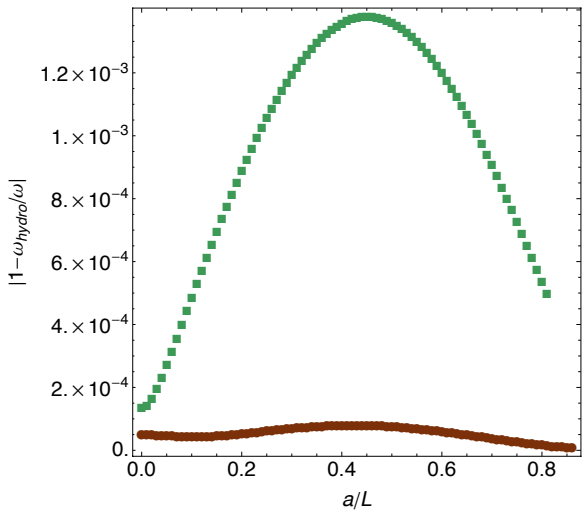

Figure 6.3: Comparison between the long wavelength gravitational QNMs and the hydrodynamic modes (for the later we use the exact numerical results) for $r_+/L = 100$. The brown (disks) curve describes the scalar modes while the green (squares) curve is for the vector modes.

sions, for a modern review see [16]. It is interesting to ask how the solutions to the Einstein equations and their properties vary with D. As the dimension increases, the types of black hole solutions increase dramatically. Some examples of the non-standard black holes possible in higher dimensions are black rings, black Saturns, and black branes. Many of these solutions challenge the intuition gained from studying four dimensions by exhibiting non-uniqueness and a variety of interesting instabilities, some of which likely lead to topology-changing transitions once quantum effects are included. In addition to this very general motivation, we shall see that superradiance in five dimensions is qualitatively very similar to four dimensional Kerr-AdS case. Thus we expect that the intuition we gain from studying superradiance in four and five dimensions will be useful for thinking about other dimensions. Additionally, because of the properties of the particular class of black holes we chose to study, certain aspects of the problem will turn out

to be more tractable than the Kerr-AdS case.

A second motivation for studying five dimensional asymptotically AdS black holes is that they play an important role in understanding strongly coupled field theories in four dimensions via gauge/gravity duality. In particular, the most well-developed example of this duality is Type IIB string theory on $\mathrm{AdS}_5 \times S^5$ spacetimes, which is dual to $\mathcal{N} = 4$ Supersymmetric Yang-Mills. The physics of five dimensional AdS black holes can thus lead to an improved understanding of this specific duality, and more generally about the physics of four dimensional field theories at finite temperature. As in the Kerr-AdS case, large black holes will be particularly interesting in this regard as they will be dual to field theories admitting a hydrodynamic description.

6.7.1 Myers-Perry−AdS black holes with equal angular momenta

The generalization of the Kerr metric to higher dimensions was found by Myers and Perry [19]. It was then further generalized to include negative cosmological constant for the case of five dimensions in [142], and then to arbitrary dimensions by [143, 47]. Although our numerical results are for five dimensions only, in the presentation that follows we will keep the dimension general whenever possible. We therefore refer to these black holes as Myers-Perry−AdS (MP-AdS) black holes.

In higher dimensions there are more planes for an object to rotate in than in four dimensions, and therefore these black holes are described by $n = \lfloor (D-1)/2 \rfloor$ angular momenta parameters. For generic choices of the angular momenta, the

symmetry of the MP-AdS black hole is $\mathbb{R} \times U(1)^n$. The first factor is due to time translations, and the n $U(1)$'s are due to the n independent planes of rotation. For certain choices of the angular momenta, this symmetry can be increased. For odd dimensions, a particularly dramatic enhancement occurs when all angular momenta are equal. In this case, the isometry becomes $\mathbb{R} \times U(1) \times SU(N+1)$, where $D = 2N + 3$. For this case, the line element becomes cohomogeneity-1, which is to say that it depends non-trivially only on the radial coordinate. This feature makes the study of linear stability particularly tractable for these black holes, as the linearized perturbation equations can be easily separated and reduced to ODE's. Therefore, in what follows, we shall restrict ourselves to odd dimensions and the equal angular momenta sector of the full parameter space.

Here we introduce the MP-AdS black holes for odd dimension $D = 2N + 3$ and with all angular momenta equal. The line element is

$$ds^2 = -f(r)^2 dt^2 + g(r)^2 dr^2 + h(r)^2 (d\psi + A_a dx^a - \Omega(r) dt)^2 + r^2 \hat{g}_{ab} dx^a dx^b, \quad (6.65)$$

with the metric functions defined as follows:

$$g(r)^2 = \Big(1 + \frac{r^2}{L^2} - \frac{r_M^{2N}}{r^{2N}} + \frac{r_M^{2N}}{r^{2N}} \frac{a^2}{L^2} + \frac{r_M^{2N} a^2}{r^{2N+2}}\Big)^{-1}, \quad h(r)^2 = r^2 \Big(1 + \frac{r_M^{2N} a^2}{r^{2N+2}}\Big), \quad (6.66)$$

$$\Omega(r) = \frac{r_M^{2N} a}{r^{2N} h(r)^2}, \quad f(r) = \frac{r}{g(r) h(r)}. \quad (6.67)$$

Here $\hat{g}_{ab}$ is the Fubini-Study metric on $\mathbb{CP}^N$. We will adopt the convention that lowercase latin indices run over $\mathbb{CP}^N$ coordinates, and that hatted tensors are

associated with this space. The Fubini-Study metric is Einstein, with the following proportionality constant

$$\hat{R}_{ab} = 2(N+1)\hat{g}_{ab}. \tag{6.68}$$

When the angular momenta are set to zero, this metric reduces to the usual Schwarzschild-AdS metric with the unit sphere written in terms of the Hopf fibration:

$$d\Omega_{2N+1}^2 = (d\psi + A_a dx^a)^2 + \hat{g}_{ab}dx^a dx^b, \tag{6.69}$$

where here A is related to the Kähler form by $2J = dA$. Constant t, r slices have the geometry of homogeneously squashed spheres, with the amount of squashing determined by $h(r)$.

The energy, angular momenta, and angular velocity of the horizon are [128]:

$$E = \frac{A_{2N+1}}{8\pi G} r_M^{2N}\Big(N + \frac{1}{2} + \frac{a^2}{2L^2}\Big), \qquad J = \frac{A_{2N+1}}{8\pi G}(N+1) r_M^{2N} a \tag{6.70}$$

$$\Omega_H = \frac{r_M^{2N} a}{r_+^{2N+2} + r_M^{2N} a^2}. \tag{6.71}$$

The horizon-generating Killing field is $K = \partial_t + \Omega_H \partial_\psi$. The physics of perturbations of this black hole will depend crucially on Ω_H. For $\Omega_H L < 1$, K is timelike everywhere outside the horizon. If $\Omega_H L > 1$, then it becomes spacelike sufficiently far away from the horizon, and in particular is spacelike at the conformal boundary. For $\Omega_H L = 1$, K is exactly null at the conformal boundary.

The metric is described by three dimensional parameters, (L, r_M, a). We will find it useful to use instead the parameters (L, r_+, Ω_H), where r_+ is the horizon

radius, to describe the solution. Note that these parameters are defined independently of the parameters that appear in the Kerr-AdS case, and also note that the boundary metric is not rotating in these coordinates.

For these equal angular momenta black holes the angular velocity cannot be arbitrarily large and must obey the extremal bound

$$\Omega_H L \leq \sqrt{1+\frac{N}{N+1}\frac{L^2}{r_+^2}}. \tag{6.72}$$

In Fig. 6.1 we plot the domain of the parameter space for the case $D = 5$. We also plot the lines $\Omega_H L = 1$ and $r_+/L = 1$. These divide the sub-extremal parameter space into four distinct regions. This division comes from the analysis of Hawking and Reall [33]. The importance of the line $\Omega_H L = 1$ is that black holes with $\Omega_H L < 1$ are expected to be stable, whereas those with $\Omega_H L > 1$ are expected to be susceptible to instabilities. Additionally, the partition function of these black holes in a grand canonical ensemble becomes ill-defined for $\Omega_H L \geq 1$, as the dual CFT will be rotating faster than the speed of light. The importance of $r_+/L = 1$ is that black holes larger than this are thermodynamically preferred over thermal, rotating AdS in the grand canonical ensemble, whereas smaller black holes are not.

6.7.2 Scalar-gravitational perturbations

We now review the problem of linear perturbations of the above metric. The decomposition we employ was first utilized in [23], where scalar-gravitational perturbations of asymptotically flat MP black holes with equal angular momenta

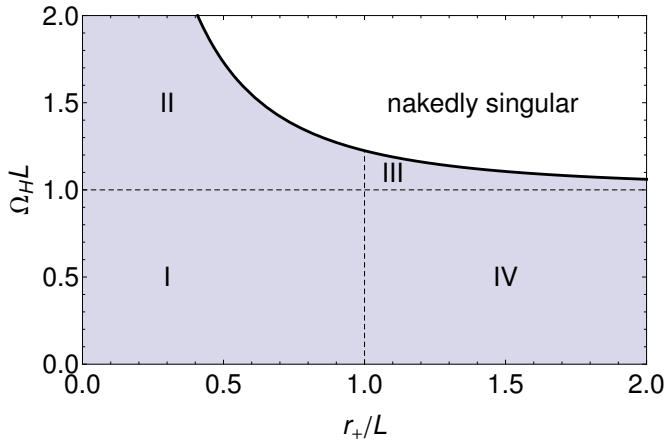

Figure 6.1: The parameter space for $5D$ equal angular momenta black holes. Below the line $\Omega_H L = 1$ the black holes are expected to be stable, and above they can potentially be unstable. Black holes to the right of the line $r_+/L = 1$ are thermodynamically preferred in the grand canonical ensemble, whereas black holes to the left are not. Note that the domain extends infinitely in both directions.

were studied. Metric perturbations may be decomposed according to how they transform under the isometries of the $\mathbb{CP}^N$ base space. There are three sectors of perturbations to consider: scalar, vector, and tensor. Tensor and scalar field perturbations of the MP-AdS black holes were studied in [30]. A major simplifying feature of five dimensions is that vector and tensor perturbations do not exist, because the associated vector and tensor harmonics do not exist on $\mathbb{CP}^1$ [30, 24]. Thus, we need only consider the scalar sector of perturbations in five dimensions. We now briefly review charged scalar harmonics on $\mathbb{CP}^N$ following [48, 23]. First, introduce a charged covariant derivative:

$$\mathcal{D}_a \equiv \hat{\nabla}_a - imA_a. \tag{6.73}$$

That this is the natural derivative operator to consider can be seen from the dimensional reduction of the fibre coordinate in the Hopf fibration. Charged scalar harmonics (with charge m) are then those functions of the $\mathbb{CP}^N$ coordinates that satisfy

$$(\mathcal{D}^2 + \lambda)\mathbb{Y} = 0. \tag{6.74}$$

Here the eigenvalue is a function of two quantized parameters, (κ, m):

$$\lambda = l(l+2N) - m^2, \quad l = 2\kappa + |m|, \tag{6.75}$$

where $\kappa = 0, 1, 2...$, and $m \in \mathbb{Z}$. Charged scalar-derived vectors can be obtained by differentiating,

$$\mathbb{Y}_a = -\frac{1}{\sqrt{\lambda}}\mathcal{D}_a\mathbb{Y}. \tag{6.76}$$

These can be further decomposed into Hermitian and anti-Hermitian parts

$$J_a^b\mathbb{Y}_b^{\pm} = \mp i\mathbb{Y}_a^{\pm}. \tag{6.77}$$

Lastly, the scalar-derived tensors are given by

$$\mathbb{Y}_{ab}^{++} = \mathcal{D}_{(a}^{+}\mathbb{Y}_{b)}^{+}, \qquad \mathbb{Y}_{ab}^{--} = \mathcal{D}_{(a}^{-}\mathbb{Y}_{b)}^{-}, \qquad \mathbb{Y}_{ab}^{+-} = \mathcal{D}_{(a}^{+}\mathbb{Y}_{b)}^{-} + \mathcal{D}_{(a}^{-}\mathbb{Y}_{b)}^{+} - \frac{1}{2N}\hat{g}_{ab}\mathcal{D}\cdot\mathbb{Y}. \tag{6.78}$$

In order to implement the harmonic decomposition of the perturbation, it will be useful to introduce the 1-forms,

$$e^0 = f(r)dt, \quad e^1 = g(r)dr, \quad e^2 = h(r)(d\psi + A_a dx^a - \Omega(r)dt). \tag{6.79}$$

The $\mathbb{CP}^N$ scalar sector of metric perturbations can then be written as

$$\begin{aligned} h_{AB} &= f_{AB}\mathbb{Y}, && (6.80)\\ h_{Aa} &= r(f_A^+\mathbb{Y}_a^+ + f_A^-\mathbb{Y}_a^-), && (6.81)\\ h_{ab} &= -\frac{r^2}{\lambda^{1/2}}(H^{++}\mathbb{Y}_{ab}^{++} + H^{--}\mathbb{Y}_{ab}^{--} + H^{+-}\mathbb{Y}_{ab}^{+-}) + r^2 H_L \hat{g}_{ab}\mathbb{Y}, && (6.82) \end{aligned}$$

where upper case latin indices run over 0,1,2, and lower case latin letters run over the $\mathbb{CP}^N$ coordinates. Adopting the traceless transverse gauge,

$$h = g^{\mu\nu}h_{\mu\nu} = 0, \quad \nabla^\mu h_{\mu\nu} = 0, \tag{6.83}$$

the linearized Einstein equations are then

$$\nabla^2 h_{\mu\nu} + 2R_{\mu\rho\nu\sigma}h^{\rho\sigma} = 0. \tag{6.84}$$

With the above parametrization, the $\mathbb{CP}^N$ dependence in the Einstein equations will separate, resulting in a system of coupled ODE's. These equations are rather lengthy, and depend non-trivially on the particular harmonic (κ, m) under consideration, and we therefore omit their presentation here. The non-trivial way in which the equations depend on the $\mathbb{CP}^N$ harmonic in question is as follows: For certain values of (κ, m), some of the harmonic tensors do not exist and therefore their coefficient functions are zero. As an example, for $N = 1$ ($D = 5$), and $m > 0$, $\mathbb{Y}_a^+ = \mathbb{Y}_{ab}^{++} = \mathbb{Y}_{ab}^{+-} = 0$, and so therefore the functions f_A^+, H^{++}, H^{+-} do not enter into the perturbation.

6.7.3 Boundary conditions

We now turn to a discussion of the boundary conditions. Boundary conditions must be supplied at the horizon and at the conformal boundary. The appropriate boundary conditions for quasinormal modes are those that correspond to an ingoing perturbation on the future horizon $\mathcal{H}^+$, and a normalizable perturbation at the boundary. For the case of asymptotically flat equal angular momenta MP black holes, the requirement of being ingoing at the horizon was translated into boundary conditions in Ref. [23]. The same method applies here, and so we omit a detailed discussion of the horizon boundary conditions.

The boundary conditions at infinity are less straightforward. Here we describe a general method for finding the boundary conditions of a normalizable gravitational perturbation of asymptotically locally AdS spacetimes. Recall that in the Kerr-AdS case the perturbation equations were reduced to a single gauge invariant equation, the Teukolsky equation. There were two steps in the process of finding the boundary conditions at infinity. First, a Frobenius expansion analysis yielded the allowed fall-off's, and then the requiring that the perturbation be normalizable fixed a certain linear combination of the two solution branches.

We wish to generalize this method to a system of n 2nd order ODE's for n functions f_i. In will be convenient to convert to a new radial coordinate, $z = 1/r$. First we demonstrate that $z = 0$ is a regular singular point of the equations. To do so, change to a new basis of functions $q_i = z^{\alpha_i} f_i$, and write the equations as

$$A_{ij}(z) z^2 \partial_z^2 q_j + B_{ij}(z) z \partial_z q_j + C_{ij}(z) q_j = 0. \tag{6.85}$$

If some choice of the α_i and overall multiplicative factors can be made such that the coefficient matrices approach finite and non-zero constant matrices in the limit $z \to 0$, then we will have demonstrated that $z = 0$ is a regular singular point of this system of equations. We do not know of an algorithmic way to determine the α's, but for the problem at hand we have demonstrated that the equations can be put into this form. Then, after changing coordinates to $\partial_t = z\partial_z$, the equations become:

$$A_{ij}(0)\partial_t^2 q_j + (B_{ij}(0) - A_{ij}(0))\partial_t q_j + C_{ij}(0)q_j = 0.$$

This is a 2nd order system of ODE's with constant coefficients, which can be solved via the standard method of writing it as a system of coupled 1st order ODE's:

$$\dot{V_a} = M_{ab}V_b \tag{6.86}$$

Where

$$V_a = \begin{bmatrix} q_i \\ \partial_t q_i \end{bmatrix}, \qquad M_{ab} = \begin{bmatrix} 0 & \mathbb{I} \\ -A(0)^{-1}.C(0) & (\mathbb{I} - A(0)^{-1}.B(0)) \end{bmatrix}, \tag{6.87}$$

and $a = 1, ..., 2n$. The generic solution (excluding possible logarithmic terms in z) is then

$$V_a = \begin{bmatrix} q_i \\ \partial_t q_i \end{bmatrix} = \sum_{b=1}^{2n} c_b \exp\Big(t\lambda_b\Big) v_a^{(b)},$$

where the $\lambda_b, v_a^{(b)}$ are the eigenvalues and vectors of M. There are $2n$ coefficients c_b, which is expected: for n 2nd order ODE's there should be $2n$ constants of integration. This is the generalization of the first step in the Frobenius method,

in which the two independent branches of a solution to an ODE around a regular singular point are determined. The next and last step is to use physical considerations to determine the c_b that correspond to the type of perturbation being studied. For normalizable metric perturbations, the boundary metric is held fixed and the boundary stress tensor is varied. For the purpose of translating this condition into choices of the constants of integration c_b, it is useful to put the full metric (background plus perturbation) into Fefferman-Graham gauge. In this gauge the metric takes the form

$$ds^2 = \frac{L^2}{z^2}(dz^2 + g_{ab}(z,x)dx^a dx^b), \tag{6.88}$$

$$g_{ab}(z,x) = g_0(x) + ... + z^d g_d(x) + z^d \log(z^2) h_d(x) + ... \tag{6.89}$$

Here $D = d + 1$ and the lower case Latin indices run over all but the radial coordinate. In order to make the perturbation normalizable we require that it only affects the terms g_d and higher in the above expansion. This corresponds to holding fixed the boundary metric and only allowing the metric perturbation to affect the expectation value of the stress tensor of the dual field theory. This requirement will fix n of the constants c_b. This method generalizes the usual Frobenius method for finding normalizable fall-off's for fields in AdS.

As an explicit example, we display the fall-off's for $D = 5$ and for the $(0, m)$ harmonic (for $m > 0$. For this mode, the non-zero perturbation functions are

$$(f_{00}, f_{01}, f_{02}, f_{11}, f_{12}, f_{22}, f_0^-, f_1^-, f_2^-, H^{--}, H_L), \tag{6.90}$$

and the gauge conditions can be used to algebraically solve for the functions

$(f_{00}, f_0^-, f_1^-, f_2^-, H^{--})$. Then a new auxiliary set of functions $q_i(r)$ can be defined which are finite and non-zero at both boundaries via:

$$
\begin{aligned}
f_{01}(r) &= \left(1-\frac{r_+}{r}\right)^{-i\alpha(\omega-m\Omega_H)-1}\left(\frac{r_+}{r}\right)^5 q_1(r) && (6.91)\\
f_{02}(r) &= \left(1-\frac{r_+}{r}\right)^{-i\alpha(\omega-m\Omega_H)-1/2}\left(\frac{r_+}{r}\right)^4 q_2(r) && (6.92)\\
f_{11}(r) &= \left(1-\frac{r_+}{r}\right)^{-i\alpha(\omega-m\Omega_H)-1}\left(\frac{r_+}{r}\right)^6 q_3(r) && (6.93)\\
f_{12}(r) &= \left(1-\frac{r_+}{r}\right)^{-i\alpha(\omega-m\Omega_H)-1/2}\left(\frac{r_+}{r}\right)^5 q_4(r) && (6.94)\\
f_{22}(r) &= \left(1-\frac{r_+}{r}\right)^{-i\alpha(\omega-m\Omega_H)}\left(\frac{r_+}{r}\right)^4 q_5(r) && (6.95)\\
H_L(r) &= \left(1-\frac{r_+}{r}\right)^{-i\alpha(\omega-m\Omega_H)}\left(\frac{r_+}{r}\right)^4 q_6(r). && (6.96)
\end{aligned}
$$

Here we have introduced the quantities

$$\alpha = \frac{h(r_+)}{r_+\Delta'(r_+)}, \qquad \Delta(r) = g(r)^{-2}. \tag{6.97}$$

Once these q_i functions are known, one can easily find the boundary conditions by expanding the equations near the endpoints.

6.7.4 Numerical results

Here we present our numerical results. We calculated scalar-gravitational QNM frequencies for the five dimensional, equal angular momenta MP-AdS black hole. The possible perturbations are parametrized by two integers (κ, m). We are particularly interested in the onset of superradiant instabilities, which was discussed earlier in Sec. 6.4.2. We remind the reader that superradiant modes are characterized by the condition $\mathrm{Re}(\omega) < m\Omega_H$, and linear instabilities by the

condition that $\mathrm{Im}(\omega) > 0$. For superradiant instabilities in AdS, these two conditions are satisfied simultaneously as the mode becomes unstable. In considering the onset of these instabilities, we will find it useful to consider the function $\Omega_{\mathrm{H,onset}}(r_+/L)$, which for a given (κ, m), is the value of the rotation such that $\omega = m\Omega_{\mathrm{H,onset}}$.

Before presenting our results on scalar perturbations, we briefly review the results for tensor perturbations [30], which exist for D odd and $D \geq 7$. There an infinite number of superradiant instabilities were found, all for $\Omega_H L > 1$. Lower m modes become unstable for larger values of the rotation, and in the limit $m \to \infty$, the critical rotation approaches $\Omega_{\mathrm{H,onset}} \to 1$. Also, $\Omega_{\mathrm{H,onset}}$ depends only very weakly on the size of the black hole, and in particular the ordering of $\Omega_{\mathrm{H,onset}}$'s for different m's is independent of the size of the black hole. For a given m the instability terminates once the black hole is taken to be sufficiently large. We will find that some scalar perturbations behave qualitatively differently than these tensor perturbations.

In Fig. 6.2 we plot the onset of the superradiant instability for $(0, m)$ modes, for a range of m. We calculated these threshold unstable modes using the Newton-Raphson method presented in Sec. 6.3. As a check on our results, it is useful to first consider small black holes. For small black holes, the onset of the instability can be very easily predicted by first setting $\omega = m\Omega_H$ for the onset of superradiance, and then also setting $\omega = \omega_{\mathrm{AdS}}$, where ω_{AdS} is the normal mode frequency of AdS. For $(0, m)$ modes, this results in

$$\Omega_{\mathrm{H,onset}} L = 1 + \frac{2}{m}, \tag{6.98}$$

Notice that for $m \to \infty$, $\Omega_{\rm H,onset} \to 1$. As the size of the black hole is increased, the onset curves for different m begin to cross. This behaviour was also observed for scalar perturbations of Kerr-AdS in Sec. 6.4.2, and is qualitatively different from the behavior of the tensor instabilities discussed above. Although the onset curves cross as the size is increased, the fact that the $m \to \infty$ instability hugs the line $\Omega_H L = 1$ indicates that the "$m = \infty$ mode will never be crossed", i.e. arbitrarily large m-modes will be the first ones to go unstable as $\Omega_H L$ is increased, even for arbitrarily large black holes. This same phenomenon occurs for scalar perturbations of Kerr-AdS, and is discussed in more detail in Sec. 6.4.2. Another difference between these scalar instabilities and the tensor ones is that, for a given m, the scalar onset curves extend for arbitrarily large black holes, whereas the tensor curves terminate. For very large black holes, we can examine the approach of the onset curve to it's limiting value of $\Omega_H L \to 1$. Interestingly, the approach is power-law, with the exponent independent of m:

$$\Omega_{\rm H,onset} L \sim 1 + \text{const}\Big(\frac{L}{r_+}\Big)^4. \tag{6.99}$$

In Fig. 6.3 we plot the onset of the superradiant instability for $(1, m)$ modes. These instabilities are evidently qualitatively different from the $(0, m)$ instabilities in that a) the onset curves do not cross, and b) for a given m, the instabilities do not persist for arbitrarily large black holes. In fact, these modes appear to be qualitatively very similar to the tensor modes on $\mathbb{CP}^N$ for $N \geq 2$.

In Fig. 6.4 we plot contour plots of the real and imaginary parts of ω for the $(0, 2)$ mode. The black dashed line corresponds to the onset mode, $\omega = m\Omega_H$,

and the black dot corresponds to the data point with the largest positive value of $\mathrm{Im}(\omega)$. This point is near the extremality bound, and lies at the end of the grid used to scan the parameter space, and so it is likely that true maximum either lies along or very near the extremality curve. This point is given by

$$(r_+/L, \Omega_H L) = (0.579, 1.548), \qquad \omega L = 2.481 + 0.039i. \tag{6.100}$$

Lastly, we remark on the importance of the onset modes, $\omega = m\Omega_H$, on the phase diagram of black hole solutions in five dimensions. In Sec. 6.5 it was discussed how threshold unstable modes with $\omega = m\Omega_H$ signified new branches of single KVF black hole solutions. We expect much of this analysis to carry over to five dimensions. It would be interesting to study these putative solutions further. Also, as in the Kerr-AdS case, the endpoint of the superradiant instability remains a very interesting open question, especially given the crossing of the onset curves observed in the $(0, m)$ scalar sector of perturbations.

6.7.5 Hydrodynamic thermalization timescales in the $\mathbf{AdS}_5/\mathbf{CFT}_4$ duality

We now turn to study the hydrodynamic QNM's of the five dimensional MP-AdS black hole. As discussed in Sec. 6.6, this serves as a powerful check on our numerics, the hydrodynamic approximation, and more generally, gauge/gravity duality itself. Compared to the Kerr-AdS case, the hydrodynamic approximation for the cohomogeneity-1 MP-AdS black holes is conceptually simpler and has a wider range of validity. Recall that in the Kerr-AdS case, the pressure was a

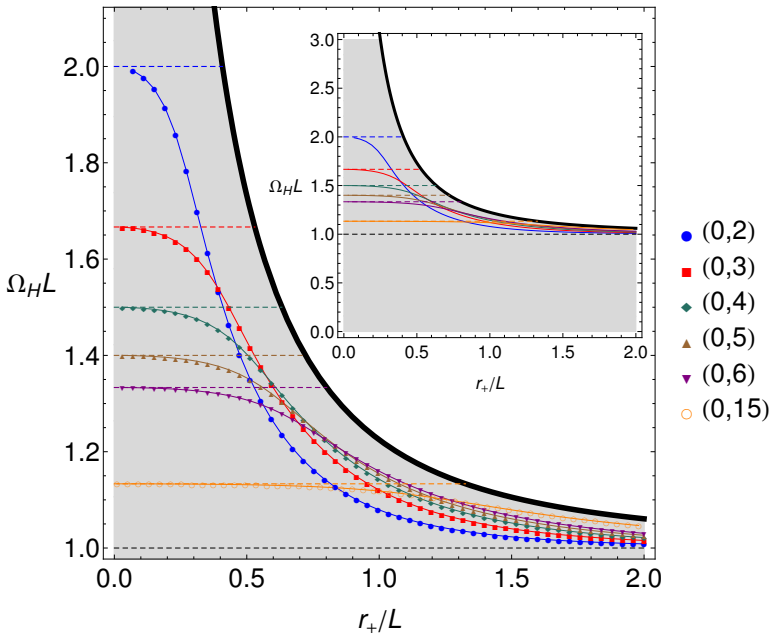

Figure 6.2: The onset of superradiance for $(0, m)$ modes. The dashed horizonal lines are the analytic prediction for small black holes, discussed above. We extend the curves past $r_+/L = 0$ to emphasize the fact that the onset curves are all monotonically decreasing. Two major features of the plot are 1) the crossing of the onset curves, and 2) that as $m \to \infty$ the onset curve approaches $\Omega_H L = 1$. Inset: a zoomed-out plot showing an enlarged view of the parameter space.

function of the angular coordinate θ, and this introduced another length scale into the approximation which limited it's domain of applicability (although the agreement turned out to be excellent even for large rotations). In contrast, the pressure for these five dimensional black holes is constant, and the approximation is valid for all rotations $\Omega_H L < 1$. As is often the case, we will find that the hydrodynamic approximation agrees excellently with our numerical for reasonably large black holes.

The general theory of hydrodynamic modes was reviewed in Sec. 6.6, and so here we only remark on the differences that occur for these five dimensional equal

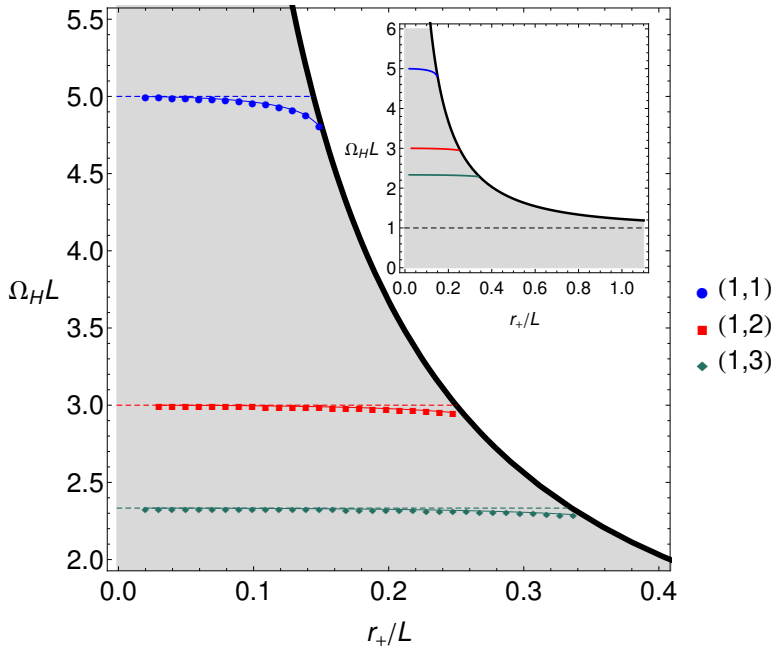

Figure 6.3: The onset of superradiance for $(1, m)$ modes. The dashed horizonal lines are the analytic prediction for small black holes, which we extend pass $r_+/L = 0$ to emphasize the fact that the onset curves are monotonically decreasing. Notice that these curves do not cross each other and terminate at finite Ω_H, in contrast to the $(0, m)$ modes. Inset: a zoomed-out plot showing an enlarged view of the parameter space. Due to numerical limitations, the onset curves do not extend all the way to $r_+/L = 0$.

angular momenta MP-AdS black holes. The boundary metric is now

$$h_{\mu\nu}dx^\mu dx^\nu = -dt^2 + L^2\Big((d\psi + A_a dx^a)^2 + \hat{g}_{ab}dx^a dx^b\Big). \tag{6.101}$$

The energy density, pressure, and fluid velocity are related to the black hole parameters via

$$\begin{aligned} &\rho = (D-2)p, \qquad p = \frac{r_M^{2N}}{2L}\Big(1 - \frac{a^2}{L^2}\Big), \\ &u_\mu dx^\mu = \Big(1 - \frac{a^2}{L^2}\Big)^{-1/2}\Big(-dt + a(d\psi + A_a dx^a)\Big). \end{aligned} \tag{6.102}$$

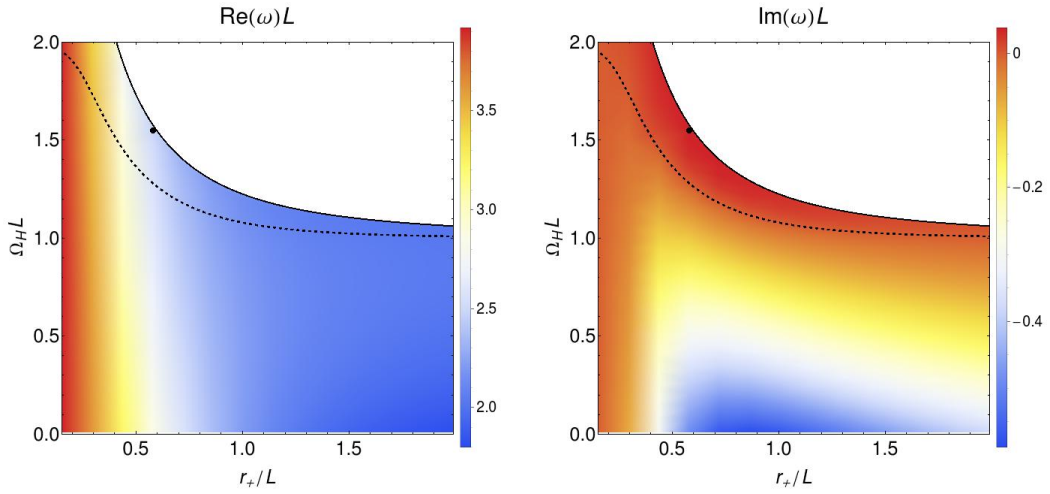

Figure 6.4: Contour plots of Re(ω) (Left plot), and Im(ω) (Right plot). Above the solid black line the black hole is nakedly singular. The dashed lines correspond to the onset of the superradiant instability, $\omega = m\Omega_H$. The isolated black dots correspond to the data point with the largest positive value of Im(ω) found in our scan of the parameter space.

We will also need to use the viscosity to entropy relation, $\eta = s/4\pi$, which in our conventions yields $\eta = r_+^3/(2L)$.

Hydrodynamic modes are obtained through perturbations of the stress tensor that are traceless and divergenceless. The $\mathbb{CP}^N$ dependence of these equations can again be separated using the charged harmonics introduced above. Since our numerical data is for scalar perturbations, we will restrict our attention to hydrodynamic scalar modes. The decomposition of the fluid variables is:

$$\delta\rho = (D-2)\delta p, \qquad \delta p = \delta\hat{p}\mathbb{Y}e^{-i(\omega t - m\psi)}, \tag{6.103}$$
$$\delta u_\mu dx^\mu = \Big((\delta u_t dt + \delta u_\psi d\psi)\mathbb{Y} + (\delta u_+ \mathbb{Y}_a^+ + \delta u_- \mathbb{Y}_a^-)dx^a\Big)e^{-i(\omega t - m\psi)}.$$

The perturbed quantities $\{\delta\hat{p}, \delta u_t, \delta u_\psi, \delta u_+ \delta u_-\}$ and ω can then be solved for by

using the conservation of the stress tensor. As the expressions are rather lengthy, and depend non-trivially on the harmonic under consideration, we omit their full presentation here. Given the difficulty of obtaining analytic predictions for black hole QNM's, we will however include the expressions in an expansion about $\Omega_H = 0$. For $D = 5$ and the $(0, m)$, harmonics (with $m \geq 2$), and to first order in both L/r_+, $\Omega_L = \Omega_H L$, the hydrodynamic modes are

$$\begin{aligned}\omega_\pm = &\left(\pm\frac{\sqrt{m(m+2)}}{\sqrt{3}} + \frac{2\left(m^2+2m-3\right)\Omega_L}{3(m+2)} + \mathcal{O}\left(\Omega_L^2\right)\right) + \\ &+ \frac{L}{r_+}\left(-\frac{1}{6}i\left(m^2+2m-3\right) \pm \frac{i\left(m^4+4m^3+3m^2-2m-6\right)\Omega_L}{2\sqrt{3m}(m+2)^{3/2}}\mathcal{O}\left(\Omega_L^2\right)\right) \\ &+ \mathcal{O}\left(L^2/r_+^2\right),\end{aligned} \tag{6.104}$$

$$\omega_0 = \left(\frac{m^2\Omega_L}{m+2} + \mathcal{O}\left(\Omega_L^2\right)\right) + \frac{L}{r_+}\left(-\frac{1}{4}im(m+4) + \mathcal{O}\left(\Omega_L^2\right)\right) + \mathcal{O}\left(L^2/r_+^2\right). \tag{6.105}$$

Next, we compare our numerical data for large black holes with the hydrodynamic approximation. In Fig.'s 6.5 and 6.6, we fix $r_+/L = 100$ and plot the analytic prediction of the hydro modes against our numerical data for two choices of $\mathbb{CP}^1$ harmonics: $(0, 2)$ and $(1, 1)$. We work to leading order in L/r_+ and find excellent agreement for all $\Omega_H L < 1$. The typical error of the hydro approximation is 10^{-4}, which is exactly what we'd expect as the next term in the expansion comes in at $\mathcal{O}(L^2/r_+^2) \sim 10^{-4}$. Although we find excellent agreement between the hydrodynamic approximation and our numerical data, the approximation fails to capture the superradiant instabilities. As mentioned earlier, all superradiant instabilities necessarily have $\Omega_H L > 1$. For these black holes, the boundary is rotating

faster than the speed of light, and the hydrodynamic approximation shouldn't be expected to be valid. So, while the hydrodynamic approximation has again proven to be an excellent approximation scheme, in this case it fails to capture the instabilities.

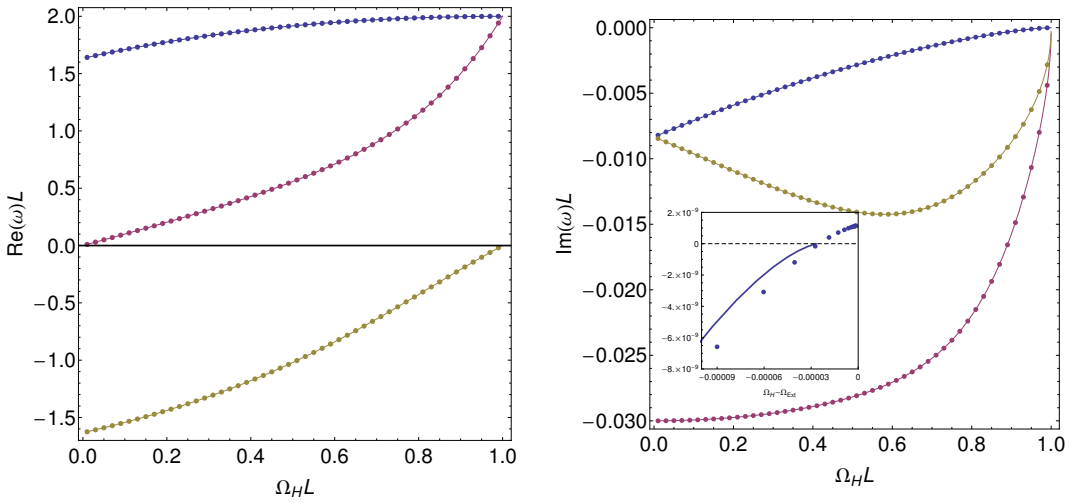

Figure 6.5: Comparision of the leading order hydrodynamic approximation for $(\kappa, m) = (0, 2)$ modes. Here $r_+/L = 100$. Right Inset: For $\Omega_H L \geq 1$ the hydrodynamic approximation breaks down, and despite the otherwise excellent agreement, fails to predict the superradiant instability.

6.8 Discussion and open problems

We studied the most general linear perturbations of the Kerr-AdS BH and of the equal angular momentum Myers-Perry-AdS BH in $D = 5$. We imposed asymptotic BCs that preserve the conformal metric [103, 115]. These BCs also guarantee that the energy and angular momentum fluxes across the asymptotic boundary vanish. Using a novel numerical approach, which we believe might also

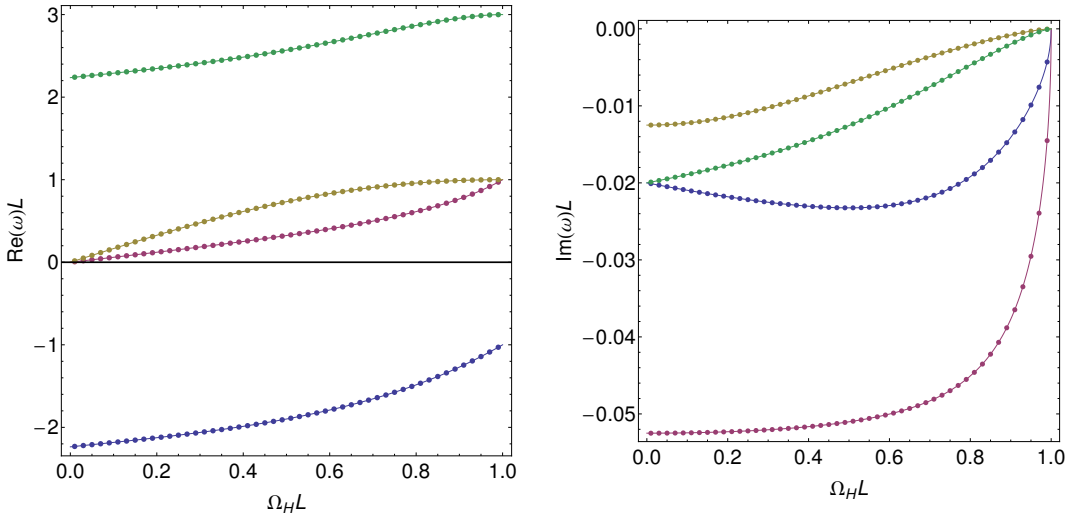

Figure 6.6: Comparision of the leading order hydrodynamic approximation for $(\kappa, m) = (1, 1)$ modes. Here $r_+/L = 100$. Once again, we find excellent agreement between our data and the hydrodynamic prediction.

be useful for other applications, we computed the QNM spectrum of these BHs and the growth rate of their instabilities. The only linear instability that we find in the $D = 4$ and $D = 5$ stationary BHs have a superradiant nature and they appear only in BHs with $\Omega_h L > 1$. We focused on these spacetimes because of their interest for AdS_4/CFT_3 and AdS_5/CFT_4 dualities formulated on the static Einstein Universe, i.e. on the sphere. Higher dimensional stationary BHs with $D \geq 6$ were not considered here but they should have novel features that might be worth investigating. Indeed, it is established that $D \geq 6$ stationary BHs are also unstable to the ultraspinning instability, whose onset was identified in [144] (this instability was first studied in asymptotically flat stationary BHs in $D \geq 6$ [20, 26, 40, 23, 27]). However, it is still an open question whether another instability that is present in $D \geq 6$ vacuum stationary BHs, namely the bar-mode

instability [20, 28, 29, 5], is present in AAdS rotating BHs.

The onset of the superradiant instability is an exact zero mode that is invariant under the horizon-generating Killing field of the Kerr-AdS (MP-AdS) BH. On the shoulders of an idea originally proposed in [30], we argued that, in a phase diagram of stationary solutions, the superradiant onset curve is a bifurcation line to a new family of BH solutions with a single Killing field that span a region that is further limited by the geon family constructed in [72]. We have constructed perturbatively the leading order thermodynamics of these novel BHs using a simple thermodynamic model [135, 136, 137, 124]. In the future, it is important to construct explicitly (numerically) these single KVF BHs and geons at full nonlinear level to confirm the ideas here discussed (in the context of scalar superradince, similar single KVF BHs and boson stars have already been constructed nonlinearly in [124]. Their properties are in agreement with the thermodynamic model we use here, in the regime of small charges). It is worth emphasizing that these single KVF BHs are periodic but not time symmetric neither axisymmetric and their existence shows that the Kerr-AdS and MP-AdS BHs are not the only stationary BHs of Einstein-AdS theory (as discussed in detail before, their existence is not in conflict with the rigidity theorems).

An interesting open question concerns the time evolution and endpoint of the superradiant instability. Before addressing this issue for rotating systems, it is useful to discuss first the situation for global AdS Reissner-Nordström BH (RN-AdS BH) with chemical potential μ that are unstable to charged superradiance. This is the case if the RN-AdS BH is scattered by a charged scalar wave with frequency ω and charge e that obeys $\omega \leq e\mu$. Here, the marginal mode with

$\omega = e\mu$ signals a bifurcation curve, in a phase diagram of static solutions, to a new family of charged BHs with scalar hair that have been explicitly constructed (perturbatively and nonlinearly) in [135, 136, 145, 137]. When they coexist, the entropy of the hairy BHs is always higher than the entropy of the RN-AdS BH with same mass and charge, for fixed e. Moreover, the hairy BHs are not unstable to superradiance since for a given mass and charge (and fixed e) the chemical potential of the hairy BH is smaller than the chemical potential of the RN-AdS BH; therefore the would-be superradiant modes of hairy BHs no longer fit inside the global AdS box. So far we have just discussed the phase diagram of solutions but said nothing about the time evolution of the original RN-AdS BH. The expectation, to be confirmed by a full time evolution, is that the endpoint of the charged superradiant instability in the RN-AdS BH is one of the hairy BHs constructed in [135, 136, 137]. This follows from the fact that for a given mass and charge (and fixed scalar charge e) the hairy BH has higher entropy and lower chemical potential than the RN-AdS BH. Therefore a time evolution towards the hairy BH is compatible with the second law of thermodynamics and the endpoint would be stable (to superradiant modes with the given fixed e). Given the properties of this charged system, and the obvious similarities with the rotating superradiant system, it is often assumed that we can use the charged system to extrapolate on evolution properties of the rotating system. However, we next argue that such an extrapolation for time evolution properties is not appropriate. To begin, notice a fundamental difference between the charged and rotating systems. The charge of the scalar field e, that enters the superradiant condition $\omega \leq e\mu$, is fixed. However, the azimuthal quantum number m, that enters the superradiant

condition $\omega \leq m\Omega_h$, is not fixed since the nonlinearities of Einstein equation will excite other m modes during a time evolution. This means that a given single KVF BH, constructed in association with a given m mode, can be at most just a metastable state but never the endpoint of the superradiant instability. This is because the single KVF BH is stable to the particular m-mode but not to other m superradiant modes that are inevitably excited in a time evolution. Therefore the endpoint of the superradiant instability in rotating BHs is not known at all and finding it is one of the most interesting open questions in BH perturbation physics. Not much can be said about it without performing the full time evolution but it is interesting to observe that, typically, stable BHs to a given m-mode are nevertheless unstable to higher m-modes. So one possibility is that the system will evolve to configurations with higher and higher m structure. Another important observation is that only BHs with angular velocity $\Omega_h L < 1$ are stable to superradiance, as first proved in [33]. So a natural expectation for the endpoint of the superradiant instability would be a (single KVF) BH with $\Omega_h L < 1$. Finding whether such a BH exists requires constructing the single KVF BHs at full nonlinear level. However, in the similar scalar superradiant system of [124], where much of the present discussion about the time evolution also applies, the single KVF BHs of the theory have been explicitly constructed nonlinearly but none of them has $\Omega_h L < 1$.

Within the gauge/gravity correspondence, black hole QNMs are dual to thermalization timescales in the dual CFT. An explicit check of this statement is possible in the regime where the CFT admits a near equilibrium, long wavelength effective hydrodynamic description. We have explicitly checked that for BHs with

radius much larger than the AdS length (and small rotations in the four dimensional case), the long wavelength gravitational QNMs of stationary BHs match the hydrodynamic relaxation timescales of the dual CFT. This confirms that the holographic interpretation of the QNM spectrum extends to systems with a rotating chemical potential. It is also a further check of the validity of the shear viscosity to the entropy density bound, $\eta/s = 1/(4\pi)$, and a non-trivial confirmation that the global AdS BCs derived in the companion paper [115] preserve the conformal boundary.

The damped QNM modes of a BH have a well defined dual CFT interpretation, but not much is known about the holographic interpretation of the superradiant instability (for discussions in this direction see[33]). From the gravity side it is clear that the superradiance instability has to do with a quenched cooling of the system, since increasing the angular momentum very rapidly, cools the system down. It would be interesting to connect this interpretation with a simple CFT model for such a phenomena, where one could perhaps understand the final state of the system. In addition, it would also be important to understand the novel holographic phases or states that are dual to the single KVF BHs and geons that appear in the superradiant context. From a different perspective, in the bulk we have discussed BHs only at the classical level. However, when quantum effects are included, Hawking radiation is also present and it is entangled with spontaneous superradiant emission. These phenomena should have a microscopic or statistical description. Within string theory, certain BHs can be described by a configuration of D-branes. In this context, Hawking radiation can be microscopically understood as the emission of a closed string off the D-branes as a result of the collision

of two open strings that are attached to the D-branes (see [146] and references therein). Similarly, superradiant emission has a microscopic description in terms of collisions of fermionic (spinning) left and right moving string excitations, and the superradiant condition $\omega \leq m\Omega_h$ follows from the Fermi-Dirac statistics for the fermionic open strings [146]. It would be interesting to extend this microscopic description to BHs (like Kerr-AdS) that do not have a D-brane description.

The properties of spheroidal wavefunctions and eigenvalues are known analytically for some time in AF spacetimes [147]. Our (numerical) analysis leaves the corresponding analytical analysis of spheroidal harmonics in AAdS unexplored, but clearly a compelling topic. Specially interesting is the extremal regime $a = L$, which might be amenable to a full analytic treatment, both in the angular eigenvalue and in the eigenfrequency.

In a similar vein, a detailed analysis of superradiance in extremal, AF and AAdS geometries is seemingly lacking. Quasinormal mode results for the extremal, AF Reissner-Nordstrom geometry uncovered an interesting symmetry between different perturbations [148] which might propagate to superradiant amplification factors and to other geometries. Note that our analysis does not apply to the extremal Kerr-AdS BH because it has a double horizon and thus our BCs are not appropriate. However, as one approaches the extremal BH, superradiance emission persists as first observed for the Kerr BH in [149]. An interesting observation is that in the AF case, when the Kerr BH is extremal and the perturbations have a frequency that saturates the superradiant bound, i.e. $\omega = m\Omega_h^{\rm ext}$, the radial Teukolsky equation has an exact solution in terms of hypergeometric functions [150]. However, for the Kerr-AdS BH we can no longer solve the radial equation

analytically, even in the above particular conditions [151]. Extremal Kerr(-AdS) BHs are also interesting because they have a near-horizon limit where a Kerr/CFT correspondence can be formulated (see e.g. [152, 151] and references therein). The study of gravitational perturbations in the Kerr(-AdS) near-horizon geometries was done in [152, 151]. It is interesting to note that all frequencies in the near-horizon geometry correspond to the single frequency $\omega = m\Omega_h^{\rm ext}$ in the original full geometry. Probably this is the reason why no signature of superradiance is found in the near-horizon geometry. It might be useful to explore further this system since its radial solutions are analytical.

We conclude this discussion section with some important general remarks concerning perturbations of AAdS spacetimes. One might wonder whether Robin boundary conditions, such as the ones used throughout this paper, lead to a well defined initial value problem for fields propagating in arbitrary asymptotically AdS backgrounds. This has been shown to be the case for the propagation of a real scalar field in [153, 100], where no assumption about the stationarity of the background or separability of the wave equation was made. The proof given there can be readily extended to complex of multi-component fields, including the gravitational perturbations discussed here. In the absence of a linear instability, one might think that linear perturbations about Kerr-AdS will decay exponentially with time, in a manner dictated by the QNM spectrum. However, it turns out that this is not the generic case, and indeed, depending on the smoothness of the initial data, the decay might be a lot slower than that. A simple argument suggest logarithmic decay: modes with very large angular momentum have a very large timescale, their growth rate can be shown (using for instance the WKB approx-

imation) to decay exponentially with increasing angular quantum number ℓ, i.e. $\tau \equiv \mathrm{Im}(\omega)^{-1} \sim \exp(\alpha\ell)$, where α is independent of ℓ. This suggests that very long timescales can be achieved if the initial data contains support in very large angular momentum quantum numbers, that is to say $\ell \sim \log\tau$. Since the initial data has to live in a Sobolev space of sufficiently high order, we conclude that $||\psi|| \sim (\log\tau)^{-p}$, where p is related to the Sobolev norm we are considering. Note that even real analytic data might not decay exponentially, this would correspond to taking the limit $p \to +\infty$, which would lead to $||\psi|| \sim \tau^{-\beta}$, for some constant β. The logarithmic behavior has been rigorously shown to be sharp in [101, 99]. Perhaps more worrying, the long time behavior of generic perturbations about black hole in global AdS might not even be related with quasinormal modes at all! In [154], it was shown, by counterexample, that quasinormal modes do not form a complete basis and that some perturbations can never be described by their dynamics. However, we should stress that in the presence of a linearly unstable mode, such as a superradiant instability, the linear spectrum of perturbations does provide an accurate description of the dynamics at early times.

Acknowledgments

It is a pleasure to thank D. Marolf and G. T. Horowitz for helpful discussions. This work was supported in part by the NRHEP 295189 FP7-PEOPLE-2011-IRSES Grant, the ANR grant 08-JCJC-0001-0, the ERC Starting Grant 240210 - String-QCD-BH, NSERC Discovery Grant (LL) and CIFAR (LL). J.E.S.'s work is partially supported by the John Templeton Foundation. V.C. acknowledges

partial financial support provided under the European Union's FP7 ERC Starting Grant "The dynamics of black holes: testing the limits of Einstein's theory" grant agreement no. DyBHo–256667. G.S.H.'s work is partially supported by the National Science Foundation under Grant No. PHY12-05500.

This research was supported in part by Perimeter Institute for Theoretical Physics. Research at Perimeter Institute is supported by the Government of Canada through Industry Canada and by the Province of Ontario through the Ministry of Economic Development & Innovation.

Appendix

6.A Fluxes across the horizon and asymptotic boundary

In this Appendix we explicitly show that the energy and angular momentum fluxes across the asymptotic boundary vanish if we impose boundary conditions (BCs) that preserve the conformal metric. We also review why the flux across the horizon is proportional to the superradiant factor.

The energy and angular momentum fluxes of gravitational perturbations are calculated using the Landau-Lifshitz "pseudotensor" whose definition we review next (see e.g. [152]). Consider metric perturbations $h_{\mu\nu}$ around a background $\bar{g}_{\mu\nu}$ up to second order in the amplitude,

$$g_{\mu\nu} = \bar{g}_{\mu\nu} + h_{\mu\nu} = \bar{g}_{\mu\nu} + h^{(1)}_{\mu\nu} + h^{(2)}_{\mu\nu} + \mathcal{O}(h^3). \tag{6.106}$$

The linearized Einstein equation reads

$$G^{(1)}_{\mu\nu}[h^{(1)}] = 0\,. \tag{6.107}$$

At second order, the Einstein equation relates terms linear in $h^{(2)}$ to terms quadratic in $h^{(1)}$:

$$G^{(1)}_{\mu\nu}[h^{(2)}] = -G^{(2)}_{\mu\nu}[h^{(1)}] \equiv 8\pi G \mathcal{T}_{\mu\nu}[h^{(1)}]\,, \tag{6.108}$$

where the RHS is quadratic in $h^{(1)}$. Written out explicitly, for generic perturbations it reads (here, we use the notation $h_{\mu\nu} \equiv h^{(1)}_{\mu\nu}$; if we choose the traceless-transverse gauge this is known as the Landau-Lifshitz "pseudotensor"):

$$\begin{aligned}
8\pi G_N \mathcal{T}_{\mu\nu} \quad = \quad & -\frac{1}{2}\Big[\frac{1}{2}\left(\nabla_\mu h_{\alpha\beta}\right)\nabla_\nu h^{\alpha\beta} + h^{\alpha\beta}\left(\nabla_\nu\nabla_\mu h_{\alpha\beta} + \nabla_\alpha\nabla_\beta h_{\mu\nu} - \nabla_\alpha\nabla_\mu h_{\nu\beta} - \nabla_\alpha\nabla_\nu h_{\mu\beta}\right) \\
& + \nabla_\alpha h^\beta{}_\mu\left(\nabla^\alpha h_{\beta\nu} - \nabla_\beta h^\alpha{}_\nu\right) - \nabla_\alpha h^{\alpha\beta}\left(\nabla_\mu h_{\beta\nu} + \nabla_\nu h_{\mu\beta} - \nabla_\beta h_{\mu\nu}\right) \\
& + \frac{1}{2}\nabla_\alpha h\left(\nabla_\mu h_{\beta\nu} + \nabla_\nu h_{\mu\beta} - \nabla_\beta h_{\mu\nu}\right)\Big] \\
& + \frac{1}{4}\bar{g}_{\mu\nu}\Big[\frac{1}{2}\left(\nabla_\gamma h_{\alpha\beta}\right)\nabla^\gamma h^{\alpha\beta} + h^{\alpha\beta}\left(\nabla_\gamma\nabla^\gamma h_{\alpha\beta} - 2\nabla_\alpha\nabla^\gamma h_{\gamma\beta}\right) - 2\left(\nabla_\alpha h^{\alpha\beta}\right)\nabla^\gamma h_{\beta\gamma} \\
& + \nabla_\alpha h^{\beta\gamma}\left(\nabla^\alpha h_{\beta\gamma} - \nabla_\beta h^\alpha{}_\gamma\right) + \frac{1}{2}\nabla_\alpha h\left(2\nabla_\beta h^{\alpha\beta} - \nabla^\alpha h\right)\Big].
\end{aligned} \tag{6.109}$$

We can now define the fluxes associated with the first order perturbation.

Let ξ be one of the Killing vector fields $\xi = \partial_t$ or $\xi = -\partial_\phi$ of (Kerr-)AdS, that are conjugate to the energy (E) and angular momentum (J) of the solution, respectively. Conservation of the "pseudotensor" $\mathcal{T}_{\mu\nu}$, $\nabla_\mu \mathcal{T}^{\mu\nu} = 0$, and the Killing equation, $\nabla_{(\mu}\xi_{\nu)} = 0$, imply that the 1-form $\mathcal{J}_\mu = -T_{\mu\nu}\xi^\nu$ is conserved, $d\star\mathcal{J} = 0$, where $\star$ is the Hodge dual. We can then define the energy or angular momentum flux across a hypersurface Σ (like the horizon or the asymptotic boundary) as

$$\Phi_\xi \equiv -\int_\Sigma \star\mathcal{J} = -\int_\Sigma dV_\Sigma\, \mathcal{T}_{\mu\nu}\xi^\mu n^\nu \tag{6.110}$$

where n^ν is the normal vector to Σ and dV_Σ is the induced volume on Σ.

Consider first the asymptotic boundary $\Sigma = \Sigma_\infty$ which is the timelike hypersurface defined by $z = 0$ (where z is the FG radial coordinate). This has unit normal $n = z/L\, dz$. As discussed in association with the FG expansion (6.1), AAdS backgrounds start differing from each other only at order $\mathcal{O}\left(g^{(d)} z^{d-2}\right)$. This in particular also implies that the most general perturbation of a global AdS background that preserves the asymptotic structure of the background has an asymptotic expansion around $z = 0$ that starts at order $\mathcal{O}\left(z^{d-2}\right)$, i.e. $h_{z\mu} = 0$ and $h_{ab} = e^{-i\omega t} e^{im\phi} f(X) z^d + \cdots$ (the Fourier decomposition in t, ϕ follows from the fact that these directions are isometries of the background). Inserting this general perturbation in the "pseudotensor" (6.109) and computing the fluxes (6.110) we find that they vanish because the integrand of the fluxes has a polynomial expansion that starts at $\mathcal{O}\left(z^d\right)$ (for both Killing fields):

$$\Phi_\xi\big|_\infty = -\int_{\Sigma_\infty} \star\mathcal{J} = 0\,. \tag{6.111}$$

That is, perturbations that preserve the conformal metric (the static Einstein Universe) have vanishing energy and angular momentum fluxes at the asymptotic boundary.

Take now the Killing horizon (null) hypersurface, $\Sigma = \Sigma_H$, defined by $r = r_+$. To find the flux across the horizon we work with the ingoing Eddington-Finkelstein coordinates $\{v, r, \chi, \widetilde{\phi}\}$, introduced in (6.16), that extend the solution through the horizon. The horizon generator is by definition normal to the horizon, i.e. $n \equiv K = \partial_v + \Omega_h \partial\widetilde{\phi}$. The metric perturbation $h_{\mu\nu} \equiv h^{(1)}_{\mu\nu}$ is constructed applying a differential operator to the Teukolsky variable $\delta\Psi_4$ (this is known as the Hertz map;

see the companion paper [115]). This yields long expressions for the components of $h_{\mu\nu}$ that are not at all illuminating. The keypoint is that inserting them in the "pseudotensor" (6.109) we find that the fluxes across the horizon are proportional to the superradiant factor (C_ξ are positive constants if $\{\omega > 0, m > 0\}$),[18]

$$\Phi_\xi\big|_H = -\int_{\Sigma_H} \star\mathcal{J} = -(\omega - m\Omega_h)C_\xi \,. \tag{6.112}$$

That is, these fluxes are negative (inwards the BH) if $\omega > m\Omega_h$ for which we perturbations are damped (QNMs); positive (outwards the BH) if $\omega < m\Omega_h$ in which case this energy and angular momentum fluxes feed the superradiant instability growth; and finally they vanish when $\omega = m\Omega_h$, i.e. at the onset of superradiance.

6.B Details of the hydrodynamic QNM computation ($D = 4$)

In this appendix we give details of the hydrodynamic computation that leads to the frequency quantization (6.63) and (6.64).

Our starting point is the double expansion (6.62) in the shear viscosity and in the rotation, both for the fluid perturbations introduced in (6.60), $\{Q^{(f)}(X)\} =$

[18]This property is universal to scalar, electromagnetic and gravitational perturbations. A massless real scalar field perturbation obeying the Klein-Gordon equation is the simplest case that illustrates the origin of the superradiant factor. Indeed, inserting a scalar perturbation $\Psi = e^{-i\omega v}e^{im\widetilde{\phi}}\Psi(r,\chi) + c.c.$ in its energy-momentum tensor $\mathcal{T}_{\mu\nu} = \partial_\mu\Psi\partial_\nu\Psi - (1/2)\,(\partial\Psi)^2$, and computing the flux vector across the horizon we find

$$-n^\mu\xi^\nu\mathcal{T}_{\mu\nu} = -n^\mu\partial_\mu\Psi\xi^\nu\partial_\nu\Psi = -(\partial_v\Psi + \Omega_h\partial_{\widetilde{\phi}}\Psi)\xi^\nu\partial_\nu\Psi = -(\omega - m\Omega_h)c_\xi\left[\mathrm{Re}(-i\Psi)\right]^2,$$

where $c_t = \omega$ and $c_{\widetilde{\phi}} = m$. We used $n \equiv K = \partial_v + \Omega_h\partial_{\widetilde{\phi}}$ and $\xi\cdot K\big|_H = 0$.

$\{Q^{(1)}, Q^{(2)}, Q^{(3)}\} \equiv \{\delta P/L, \delta u_X, \delta u_\Phi\}$, and for the perturbation frequency ω. These expansions are inserted in the hydrodynamic equations of motion (6.58) or (6.59) that are then solved progressively in a series expansion in η/L^3 and a/L. For our purpose it will be enough to go up to first order in the viscosity ($n = 1$) and up to second order in the rotation ($p = 2$) expansions. There are two families of modes, namely the scalar and the vector modes.

6.B.1 Scalar modes

Consider first the scalar modes. At leading order in the aforementioned expansion, the viscosity and rotational effects are absent, and we are interested in finding the quantities $S^{(f)}_{0,0}$ and $\omega_{0,0}$ (for scalar modes we use the notation $S^{(f)}_{j,i} \equiv Q^{(f)}_{j,i}$). In these conditions, the pressure perturbation is proportional to the Kodama-Ishibashi scalar harmonic $S(X, \Phi) \sim e^{im\Phi} P^m_\ell(X)$, where $P^m_\ell(x)$ is the associated Legendre polynomial, while the velocity perturbation is proportional to the vector derived scalar harmonics obtained by taking angular derivatives of the scalar harmonic $\mathbf{S}_i \propto D_i\mathbf{S}$ (where D_j is the covariant derivative associated to the unit radius metric on S^2). We thus have $S^{(1)}_{0,0}\, e^{im\Phi} = A_1\, e^{im\Phi} P^m_\ell(X)$, $S^{(2)}_{0,1}\, e^{im\Phi} = A_2\, e^{im\Phi} P^m_\ell(X)'$ and $S^{(3)}_{0,1}\, e^{im\Phi} = i\, m\, A_2\, e^{im\Phi} P^m_\ell(X)$, for arbitrary amplitudes A_k. Inserting these expressions in the equations of motion (EoM) we fix the ratio A_1/A_2 and quantize the frequency $\omega_{0,0}$. This yields (we introduce the

notation $z_+ = \frac{r_+}{L}$)

$$
\begin{aligned}
S^{(1)}_{0,0} &= i\, A_2\, z_+ \left(1+z_+^2\right) \frac{\sqrt{\ell(\ell+1)}}{\sqrt{2}} P^m_\ell(X), \\
S^{(2)}_{0,0} &= A_2\, P^m_\ell(X)', \\
S^{(3)}_{0,0} &= i\, m\, A_2\, P^m_\ell(X),
\end{aligned}
\tag{6.113}
$$

and $\omega_{0,0}$ that can be read from (6.63). This conclusion agrees with the static results first derived in [97].

Still at leading order in the viscosity, we now consider the first order correction introduced by the rotation. It follows from two of the EoM at this order that the perturbations $Q^{(2)}_{0,1}$ and $Q^{(3)}_{0,1}$ can be algebraically expressed as a function of $S^{(2)}_{0,1}$ and/or its derivative. Plugging these relations in the third EoM we fix the frequency correction $\omega_{0,1}$ as written in (6.63) (this is done doing the procedure exemplified below for the $\omega_{0,2}$ conribution) and the differential equation for $S^{(1)}_{0,1}$ that is left is the familiar associated Legendre equation. Altogether, the perturbation eigenfunctions at order $\mathcal{O}\left(\eta^0, a^1\right)$ are then

$$
\begin{aligned}
S^{(1)}_{0,1} &= B_0\, P^m_\ell(X), \\
S^{(2)}_{0,1} &= \frac{A_2 m z_+ \left(1+z_+^2\right)\left(\ell^2+5\ell+2\right) - 2iB_0\ell(\ell+1)}{\sqrt{2}z_+\left(1+z_+^2\right)[\ell(\ell+1)]^{3/2}} \frac{(\ell+1)X}{1-X^2} P^m_\ell(X) \\
&\quad - \frac{A_2 m z_+ \left(1+z_+^2\right)\left(\ell^2+\ell+2\right) - 2iB_0\ell(\ell+1)}{\sqrt{2}z_+\left(1+z_+^2\right)[\ell(\ell+1)]^{3/2}} \frac{(\ell+1-m)}{1-X^2} P^m_{\ell+1}(X), \\
S^{(3)}_{0,1} &= \frac{i\,A_2 z_+ \left(1+z_+^2\right)\left(m^2\left(\ell^2+\ell+2\right)+\ell(\ell+1)^2\left(X^2(\ell+4)-\ell\right)\right) - 2iB_0 m\ell(\ell+1)}{\sqrt{2}z_+\left(1+z_+^2\right)[\ell(\ell+1)]^{3/2}} P^m_\ell(X) \\
&\quad + \frac{2i\sqrt{2}A_2\ell(\ell+1)(m-\ell-1)}{[\ell(\ell+1)]^{3/2}} X P^m_{\ell+1}(X).
\end{aligned}
\tag{6.114}
$$

where B_0 is a new arbitrary amplitude that is introduced at this order.

We can improve our approximation by finding the correction up to second order in the rotation (at this point still at vanishing viscosity). This requires looking to the EoM at order $\mathcal{O}\left(\eta^0, a^2\right)$ that involve the unknown quantities $S_{0,2}^{(f)}$ and $\omega_{0,2}$. We use this case to exemplify in detail how we typically solve equations of our problem to get the perturbative frequency corrections. Two of the EoM at order $\mathcal{O}\left(\eta^0, a^2\right)$ yield two algebraically equations for $S_{0,2}^{(2)}$ and $S_{0,2}^{(3)}$ in terms of $S_{0,2}^{(1)}$ and its derivative (in addition to Legendre polynomial contributions sourced by the lower order solutions). Inserting these algebraic relations in the third EoM we get a second order ODE for $S_{0,2}^{(1)}$. Explicitly, the equations discussed in this paragraph are:

$$
\begin{aligned}
&S_{0,2}^{(1)}(X)'' - \frac{2X}{1-X^2} S_{0,2}^{(1)}(X)' - \frac{m^2 + \left(X^2-1\right)\ell(\ell+1)}{\left(1-X^2\right)^2} S_{0,2}^{(1)}(X) \\
&\quad + \frac{iA_2 z_+ \left(1+z_+^2\right)\left(5\ell^2+5\ell+16\right)}{\sqrt{2}\sqrt{\ell(\ell+1)}} X P_\ell^m(X)' \\
&\quad + \frac{iA_2 z_+ \left(1+z_+^2\right)}{2\sqrt{2}(\ell(\ell+1))^{3/2}} \frac{P_\ell^m(X)}{1-X^2}\Big[m^2\left[12+\ell(\ell+1)\left(\ell^2+\ell+4\right)\right] \\
&\qquad -\ell^2(\ell+1)^2\left[20-\left(1-X^2\right)\left(\ell^2+\ell+22\right)-4\sqrt{2}\sqrt{\ell(\ell+1)}L\omega_{0,2}\right]\Big] = 0
\end{aligned}
$$

$$
\begin{aligned}
S_{0,2}^{(2)}(X) = &-\frac{i\sqrt{2}S_{0,2}^{(1)}(X)'}{z_+\left(1+z_+^2\right)\sqrt{\ell(\ell+1)}} + P_\ell^m(X)'\left[-\frac{iB_0 m\left(\ell^2+\ell+2\right)}{z_+\left(z_+^2+1\right)\ell^2(\ell+1)^2} + A_2\left(\frac{m^2\left(\ell^2+\ell+2\right)^2}{2\ell^3(\ell+1)^3}\right.\right. \\
&\left.\left. + \frac{2\sqrt{2}X^2 z_+^2\left(\ell^2+\ell+4\right) - \sqrt{2}\left(2z_+^2+1\right)\ell(\ell+1) - 2\omega_{0,2}Lz_+^2\sqrt{\ell(\ell+1)}}{\sqrt{2}z_+^2\ell(\ell+1)}\right)\right] \\
&+ \left(\frac{A_2\left[4m^2\left(\ell^2+\ell+2\right)+\ell^2(\ell+1)^2\left(1-X^2\right)\right]}{\ell(\ell+1)} - \frac{4iB_0 m}{z_+\left(z_+^2+1\right)}\right)\frac{X P_\ell^m(X)}{\ell(\ell+1)\left(1-X^2\right)} \\
S_{0,2}^{(3)} = &\frac{\sqrt{2}mS_{0,2}^{(1)}(X)}{z_+\left(1+z_+^2\right)\sqrt{\ell(\ell+1)}} + P_\ell^m(X)\left(\frac{iA_2 m^3\left(\ell^2+\ell+2\right)^2}{2\ell^3(\ell+1)^3} + \frac{2iA_2 mX^2\left(\ell^2+\ell+4\right)}{\ell(\ell+1)}\right. \\
&\left. - \frac{iA_2 m\left(2z_+^2+1\right)}{z_+^2} - \frac{i\sqrt{2}A_2 mL\omega_{0,2}}{\sqrt{\ell(\ell+1)}} + \frac{B_0\left[m^2\left(\ell^2+\ell+2\right)+\left(X^2-1\right)\ell^2(\ell+1)^2\right]}{z_+\left(1+z_+^2\right)\ell^2(\ell+1)^2}\right) \\
&+ \frac{4iX\left(1-X^2\right)P_\ell^m(X)'}{z_+\left(1+z_+^2\right)\ell^2(\ell+1)^2}\left[A_2 m z_+\left(1+z_+^2\right)\left(\ell^2+\ell+2\right) - iB_0\ell(\ell+1)\right].
\end{aligned}
\tag{6.115}
$$

Note that the ODE for $S_{0,2}^{(1)}$ is of the form $f_1 S_{0,2}^{(1)\prime\prime} + f_2 S_{0,2}^{(1)\prime} + f_3 S_{0,2}^{(1)} + s_2 P_\ell^{m\prime} +$

$s_1 P_\ell^m = 0$, with f_k and s_k being functions of X that can be read from the first equation in (6.115). Contracting this equation with $\int dX P_\ell^m$ we can now use the properties of integration by parts. Namely, we can subtract the vanishing total divergence contribution $\int dX \partial_X \left(P_\ell^m f_1 S_{0,2}^{(1)\prime} \right)$ to the previous equation and integrate by parts the $\int dX P_\ell^m f_1 S_{0,2}^{(1)\prime\prime}$ term to rewrite the "EoM" as $\int dX P_\ell^m \left[\hat{f}_2 S_{0,2}^{(1)\prime} + f_3 Q_{0,2}^{(1)} + \hat{s}_2 P_\ell^{m\prime} + s_1 P_\ell^m \right] = 0$, where we have redefined the coefficients $f_2 \to \hat{f}_2$ and $s_2 \to \hat{s}_2$ to absorb the new contributions arising from the integration by parts. We use again a similar approach, namely we subtract the total divergence term $\int dX \partial_X \left(P_\ell^m \hat{f}_2 S_{0,2}^{(1)} \right) = 0$ and use integration by parts to get $\int dX P_\ell^m \left(\tilde{s}_2 P_\ell^{m\prime} + s_1 P_\ell^m \right) = 0$ where we made the redefinition $\hat{s} \to \tilde{s}_2$ and a would be $S_{0,2}^{(1)}$ contribution is absent since $f_3 - \hat{f}_2{}' = 0$. Subtracting the total divergence $\int dX \partial_X [\tilde{s}_2 \, (P_\ell^m)^{\,2}]$ and a third final integration by parts finally yields $\int dX P_\ell^m \hat{s}_1 P_\ell^m = 0$ with $\hat{s}_1 = \tilde{s}_2{}' + s_1$. Explicitly, this final condition is

$$\frac{A_2 z_+ \left(1+z_+^2\right)}{2\ell(\ell+1)} \Bigg\{ \left[\ell(\ell+1) \left(\ell^2+\ell+7 \right) - 48 \right] \int_{-1}^{1} dX \, X^2 \, P_\ell^m(X)^2 - \Bigg[\ell(\ell+1) \left[\ell(\ell+1) \left(4\sqrt{2}\sqrt{\ell(\ell+1)}\omega_{0,2} + \ell^2+\ell-3 \right) - 16 \right] + m^2 \left[\ell(\ell+1) \left(\ell^2+\ell+4 \right) + 12 \right] \Bigg] \frac{\int_{-1}^{1} dX \, P_\ell^m(X)^2}{\ell(\ell+1)} \Bigg\} = 0 \,. \quad (6.116)$$

To proceed we use the integrals

$$\int P_\ell^m(X) P_\ell^m(X) dX = \frac{2}{(2\ell+1)} \frac{(\ell+m)!}{(\ell-m)!}$$
$$\int X^2 P_\ell^m(X) P_\ell^m(X) dX = \frac{2\left(2\ell^2+2\ell-2m^2-1\right)}{(2\ell-1)(2\ell+1)(2\ell+3)} \frac{(\ell+m)!}{(\ell-m)!} \,, \quad (6.117)$$

to rewrite (6.116) as

$$
\begin{aligned}
0 = & \frac{A_2 z_+ \left(1+z_+^2\right)(2\ell-3)!!(\ell+m)!}{\ell^2(\ell+1)^2(2\ell+3)!!(\ell-m)!} \\
& \Big\{ 3m^2(\ell-1)(\ell+2)\left(\ell^2+\ell+6\right)\left(2\ell^2+2\ell+1\right) \\
& +2\ell^2(\ell+1)^2\Big[2\sqrt{2}\sqrt{\ell(\ell+1)}(2\ell-1)(2\ell+3)\omega_{0,2}L \\
& +(\ell+1)\ell^3+(\ell+1)\ell^2-14(\ell+1)\ell+24\Big]\Big\}.
\end{aligned}
$$

This condition finally quantizes the frequency contribution $\omega_{0,2}$ as

$$
\omega_{0,2}L = -\frac{(\ell+2)(\ell-1)\left[2(\ell-3)(\ell+4)\ell^2(\ell+1)^2+3m^2\left(6+\ell+\ell^2\right)\left(1+2\ell+2\ell^2\right)\right]}{4\sqrt{2}(2\ell-1)(2\ell+3)[\ell(\ell+1)]^{5/2}}\,. \tag{6.118}
$$

To include the effects of dissipation we now consider the linear order contribution in the viscosity, while still doing also an expansion in the (adimensional) rotation parameter, i.e. we solve the perturbative EoM at order $\mathcal{O}\left(\eta, a^0\right)$, $\mathcal{O}\left(\eta, a^1\right)$, $\mathcal{O}\left(\eta, a^2\right)$. The technical analysis proceeds in a way that is very similar to the procedure already outlined for the zero-order contribution in the viscosity so we now omit further details and just give the final results for the frequencies $\omega_{1,i}$ and for the perturbation eigenfunctions $S_{1,i}^{(f)}(X)$. At order $\mathcal{O}\left(\eta, a^0\right)$ the eigenfunctions are

$$
\begin{aligned}
S_{1,0}^{(1)} &= \left[i\frac{1}{\sqrt{2}}\,K_2\, z_+\left(1+z_+^2\right)\sqrt{\ell(\ell+1)}-\frac{1}{2}\,A_2\,(\ell+2)(\ell-1)\right]P_\ell^m(X), \\
S_{1,0}^{(2)} &= K_2\,P_\ell^m(X)', \\
S_{1,0}^{(3)} &= i\,m\,K_2\,P_\ell^m(X).
\end{aligned} \tag{6.119}
$$

where K_2 is a new arbitrary amplitude, and the frequency $\omega_{1,0}$ is written in (6.63).

At order $\mathcal{O}(\eta, a^1)$ the eigenfunctions are

$$
\begin{aligned}
S^{(1)}_{1,1} &= C_0\, P^m_\ell(X),\\
S^{(2)}_{1,1} &= \frac{iX P^m_\ell(X)}{2\sqrt{2}\left(1-X^2\right) z_+ \left(1+z_+^2\right) \ell^2(\ell+1)}\Big[4\sqrt{2}A_2 m(\ell+1)(\ell+2)(2\ell+1)\\
&\quad -\frac{2i}{z_+\left(1+z_+^2\right)}\Big(K_2 m z_+^2\left(1+z_+^2\right)^2\sqrt{\ell(\ell+1)}\left(\ell^2+5\ell+2\right)\\
&\quad -\ell(\ell+1)[\sqrt{2}B_0(\ell-1)(\ell+2)+2iC_0 z_+\left(1+z_+^2\right)\sqrt{\ell(\ell+1)}]\Big)\Big]\\
&\quad -\frac{i(\ell+1-m)P^m_{\ell+1}(X)}{2\sqrt{2}\left(1-X^2\right) z_+^2\left(1+z_+^2\right)^2\ell^2(\ell+1)^2}\Big(4\sqrt{2}A_2 m z_+\left(1+z_+^2\right)\left(5\ell^2+5\ell+2\right)\\
&\quad -2i\left[K_2 m z_+^2\left(1+z_+^2\right)^2\sqrt{\ell(\ell+1)}\left(\ell^2+\ell+2\right)-\sqrt{2}B_0(\ell-1)\ell(\ell+1)(\ell+2)\right]\\
&\quad -4C_0 z_+\left(z_+^2+1\right)[\ell(\ell+1)]^{3/2}\Big),\\
S^{(3)}_{1,1} &= \frac{P^m_\ell(X)}{2z_+^2\left(1+z_+^2\right)^2\ell^2(\ell+1)^2}\Big[-4X^2 z_+\left(1+z_+^2\right)\ell(\ell+1)^2\\
&\quad \times\left[2A_2\left(\ell^2+\ell+1\right)-i\sqrt{2}K_2 z_+\left(1+z_+^2\right)\sqrt{\ell(\ell+1)}\right]\\
&\quad -A_2 z_+\left(1+z_+^2\right)\left[4m^2\left(5\ell^2+5\ell+2\right)+\left(1-X^2\right)\ell^2(\ell+1)^2\left(\ell^2+\ell-14\right)\right]\\
&\quad +2m\ell(\ell+1)\left[\sqrt{2}C_0 z_+\left(1+z_+^2\right)\sqrt{\ell(\ell+1)}-iB_0(\ell-1)(\ell+2)\right]\\
&\quad +i\sqrt{2}K_2 z_+^2\left(1+z_+^2\right)^2\sqrt{\ell(\ell+1)}\left[m^2\left(\ell^2+\ell+2\right)-\left(1-X^2\right)\ell^2(\ell+1)^2\right]\Big]\\
&\quad +\frac{2(\ell+1-m)X\,P^m_{\ell+1}(X)}{z_+\left(1+z_+^2\right)\ell(\ell+1)}\left[2A_2\left(\ell^2+\ell+1\right)-i\sqrt{2}K_2 z_+\left(1+z_+^2\right)\sqrt{\ell(\ell+1)}\right],
\end{aligned}
\tag{6.120}
$$

where C_0 is a new arbitrary amplitude, and the frequency contribution $\omega_{1,1}$ can be found in (6.63).

Finally, to get the frequency correction at order $\mathcal{O}(\eta, a^2)$ we use again the integration by parts procedure that we already described to get the $\mathcal{O}(\eta^0, a^2)$ contribution. Going through this procedure we find the frequency $\omega_{1,2}$ that can be read from (6.63) and we omit here the associated long expressions for $S^{(f)}_{1,2}$.

The frequency contribution $\omega_{1,3}$ written in (6.63) is computed in a similar way.

6.B.2 Vector modes

Consider now the vector modes. These distinguish from the scalar modes because at leading order in the viscosity and rotation they have vanishing pressure perturbation and vanishing frequency: $V_{0,0}^{(0)} = 0$ and $\omega_{0,0} = 0$ (for scalar modes we use the notation $V_{j,i}^{(f)} \equiv Q_{j,i}^{(f)}$).. In these conditions it follows from the EoM that (as it could not be otherwise) the velocity perturbation of these modes can be expanded in terms of the Kodama-Ishisbashi vector harmonics $\mathbf{V}_i$, $i = X, \Phi$ (which can themselves be expressed as a function of the associated Legendre polynomials P_ℓ^m). Altogether, at leading order $\mathcal{O}(\eta^0, a^0)$, the vector hydrodynamic modes have eigenfunctions

$$\begin{aligned} V_{0,0}^{(1)} &= 0, \\ V_{0,0}^{(2)} &= \frac{imA_3}{1-X^2} P_\ell^m(X), \\ V_{0,0}^{(3)} &= A_3 (1-X^2) P_\ell^m(X)', \end{aligned} \tag{6.121}$$

and $\omega_{0,0} = 0$.

The EoM at $\mathcal{O}(\eta^0, a^1)$ and $\mathcal{O}(\eta^0, a^2)$ combined give the frequency corrections

$\omega_{0,1}$ and $\omega_{0,2}=0$.[19] The eigenfunctions at order $\mathcal{O}\left(\eta^0,a^1\right)$ are

$$\begin{aligned}
V_{0,1}^{(1)} &= \frac{2A_3 z_+\left(z_+^2+1\right)}{\ell(\ell+1)}\left[(\ell+1-m)P_{\ell+1}^m(X)-(\ell+1)^2 X P_\ell^m(X)\right],\\
V_{0,1}^{(2)} &= \frac{i\,mB_0}{1-X^2}P_\ell^m(X),\\
V_{0,1}^{(3)} &= -B_0\left[(\ell+1)X\,P_\ell^m(X)-(\ell+1-m)P_{\ell+1}^m(X)\right],
\end{aligned} \tag{6.122}$$

where B_0 is a new arbitrary amplitude and $\omega_{0,1}$ is given in (6.64).

To find the frequency contribution at order $\mathcal{O}\left(\eta^0,a^3\right)$ we use two of the EoM at the previous order $\mathcal{O}\left(\eta^0,a^2\right)$ to find $V_{0,2}^{(1)}$ explicitly and an algebraic relation for $V_{0,2}^{(3)}$ as a function of $V_{0,2}^{(2)}$ and its derivative. Then, one of the EoM at order $\mathcal{O}\left(\eta^0,a^3\right)$ is a second order ODE that only involves the unknown $V_{0,2}^{(2)}$ and its first and second derivatives, in addition to two source contributions proportional to the associated Legendre polynomial and its derivative. It is used to find the frequency contribution $\omega_{0,3}$ as given in (6.64), after using several integrations by parts as exemplified in the previous scalar mode treatment. The long relations associated to this discussion are omitted here.

We now consider the viscosity contributions. Using the EoM at order $\mathcal{O}\left(\eta,a^0\right)$

[19] To be more clarifying, the first order EoM determine $\omega_{0,1}=0$ but leave $V_{0,1}^{(2)}$ undetermined and $V_{0,1}^{(3)}$ is left just as a function of $V_{0,1}^{(2)}$ and its derivative. The explicit expressions for $V_{0,1}^{(2)}$ and $V_{0,1}^{(3)}$, as written in (6.122), are found only at second order where we also determine $\omega_{0,2}$. Ultimately, this technical property of the vector modes is due to the fact that the frequency contribution of rotational odd powers vanish when $\eta=0$.

and $\mathcal{O}(\eta, a^1)$ we find the eigenfunctions

$$\begin{aligned} V_{1,0}^{(1)} &= 0, \\ V_{1,0}^{(2)} &= \frac{imK_2}{1-X^2} P_\ell^m(X), \\ V_{1,0}^{(3)} &= K_2[(\ell+1-m)P_{\ell+1}^m(X) - (\ell+1)XP_\ell^m(X)], \end{aligned} \tag{6.123}$$

where K_2 is an arbitrary amplitude, and fix the frequency contribution $\omega_{1,0}$ as written in (6.64) and $\omega_{1,1} = 0$.

The EoM at order $\mathcal{O}(\eta, a^1)$ also determine $V_{1,1}^{(1)}$ and $V_{1,1}^{(3)}$ that we write below, while EoM at order $\mathcal{O}(\eta, a^2 1)$ find algebraic relations for $V_{1,2}^{(1)}$ and $V_{1,2}^{(3)}$ (that we do not write here) and a second order ODE for $V_{1,1}^{(2)}$. The relations just described are

$$\begin{aligned} V_{1,1}^{(1)} &= \frac{2K_2 z_+ \left(1+z_+^2\right)}{\ell(\ell+1)} \left[(\ell+1)^2 X P_\ell^m(X) - (\ell+1-m)P_{\ell+1}^m(X)\right], \\ V_{1,1}^{(2)}(X)'' &- \frac{6X}{1-X^2} V_{1,1}^{(2)}(X)' + \frac{(\ell-1)(\ell+2) - m^2 - (\ell-2)(\ell+3)X^2}{\left(1-X^2\right)^2} V_{1,1}^{(2)}(X) \\ &+ \frac{2A_3\left(8 - \ell(\ell+1)\left(\ell(\ell+1)\left(\ell^2+\ell-5\right)+14\right)\right)}{\left(1-X^2\right) z_+ \left(z_+^2+1\right)\ell(\ell+1)} X P_\ell^m(X)' \\ &- \frac{A_3 P_\ell^m(X)}{2\left(1-X^2\right)^2}\Big[\frac{2m^2\left(3\ell^8+12\ell^7+16\ell^6+6\ell^5-25\ell^4-46\ell^3+58\ell^2+80\ell-24\right)}{z_+\left(z_+^2+1\right)\ell(\ell+1)(2\ell-1)(2\ell+3)} \\ &\qquad - \frac{X^2\left(\ell(\ell+1)\left(\ell^2(\ell+1)^2-28\right)+32\right)}{z_+\left(z_+^2+1\right)} + \frac{(\ell-1)\ell^2(\ell+1)^2(\ell+2)}{z_+^3\left(z_+^2+1\right)} \\ &\qquad - \frac{2\ell(\ell+1)\left(-3\ell^6-9\ell^5+15\ell^3+10\ell^2+\ell+6\right)}{z_+\left(z_+^2+1\right)(2\ell-1)(2\ell+3)} + i\omega_{1,2} L\ell^2(\ell+1)^2\Big] = 0 \\ V_{1,1}^{(3)} &= \frac{i\left(1-X^2\right)}{m}\Big[\left(1-X^2\right)V_{1,1}^{(2)}(X)' - 2XV_{1,1}^{(2)}(X) \\ &\qquad + \frac{A_3(\ell-1)(\ell+2)}{z_+\left(1+z_+^2\right)}\left(4XP_\ell^m(X) - \frac{\ell^2+\ell-4}{\ell(\ell+1)}\left(1-X^2\right)P_\ell^m(X)'\right)\Big], \end{aligned} \tag{6.124}$$

We use the ODE for $V_{1,1}^{(2)}$ to determine the frequency contribution $\omega_{1,2}$, explicitly written in (6.64), after several integration by parts.

6.C QNMs and superradiance: a perturbative analytical analysis ($D = 4$)

In this appendix we give details of the perturbative matched asymptotic expansion that leads to the frequency quantization (6.37) and that we compare with the numerical results in Section 6.4.1. This perturbative approach was introduced to study perturbations of a scalar field in the Kerr black hole by Starobinsky [155], Unruh [156] and Detweiller [157], and later used successfully to study scalar and gravitational perturbations in rotating black holes in [158, 159, 34, 120, 160]. In particular, the superradiant timescales of a scalar field in the Kerr-AdS black hole computed with this method [34] were confirmed to be accurate by the numerical analysis of [131].[20]

The matched asymptotic expansion procedure allows to solve perturbatively the angular (6.12) and radial (6.13) equations, and yields an approximate analytical solution for the QNM and superradiant instability frequency spectra.

This analysis starts with the observation is that if we work in a regime of parameters where $\frac{a}{L} \ll 1$ and $a\tilde{\omega} \ll 1$ the angular equation for the spin-weighted AdS-spheroidal harmonics reduces approximately to the standard equation for the spin-weighted spherical harmonics [161, 147]. In particular it is independent of the mass parameter M and cosmological radius L, and its regular solutions can be found analytically (see e.g. [115] for a detailed construction). Here, it is important to highlight that regularity of these eigenfunctions requires that the

[20]Here we do not follow the alternative perturbative analysis of [135, 136, 124, 137] to find QNM and superradiant frequencies because, in the present system, it requires going to a high order in perturbation theory – the imaginary part of the frequency appears only at order $\mathcal{O}(r_+/L)^6$ – where the source terms make it difficult to solve analytically the equations.

angular eigenvalues and quantum numbers are quantized as

$$\lambda = (\ell-1)(\ell+2) - \frac{2m}{\ell}\,\frac{\ell^2+\ell+4}{\ell+1}\,a\tilde{\omega} + \mathcal{O}\left(a^2\tilde{\omega}^2, \frac{a^2}{L^2}\right) ,$$
$$\text{with} \quad \ell = 2,3,4,\cdots , \quad |m| \leq \ell \,, \tag{6.125}$$

where the azimuthal quantum number m is an integer, and we have introduced the quantum number ℓ with properties discussed after (6.14). This fixes the angular eigenvalue spectrum and we just need to solve now the radial equation in a regime of parameters that is consistent with the approximation where (6.125) is valid.

We follow a standard matching asymptotic expansion analysis whereby we divide the exterior spacetime of the Kerr-AdS black hole into two regions; a near-region where $r - r_+ \ll \frac{1}{\tilde{\omega}}$ and a far-region where $r - r_+ \gg r_+$. In each of these regions, some of the terms in radial equation make a sub-dominant contribution and can be consistently discarded. We will find that if we further require $\frac{r_+}{L} \ll 1$, this procedure yields an equation with an (approximate) analytical solution in both spacetime regions. The next important step is to restrict our attention to the regime $r_+\tilde{\omega} \ll 1$. In this regime, the far and near regions have an overlaping zone, $r_+ \ll r - r_+ \ll \frac{1}{\tilde{\omega}}$, where the far and near region solutions are simultaneously valid. In this matching region, we can then match/relate the set of independent parameters that are generated in each of the two regions. We will also find that if we further restrict our analysis to the regime $\frac{a}{r_+} \ll 1$, it is sufficient to work only with the the leading order contribution for the angular eigenvalues in (6.125), $\lambda \sim (\ell-1)(\ell+2)$.

The regime of validity of the matching analysis can be expressed in a much sim-

plified form. Indeed, the rotation parameter is constrained by the extremity condition $a \leq r_+\sqrt{\frac{3r_+^2+L^2}{L^2-r_+^2}}$ for $r_+ < \sqrt{3}L$ and by $a < L$ for $r_+ > \sqrt{3}L$ (see e.g. [129]). For the regime we are interested, $\frac{r_+}{L} \ll 1$, we thus have $a \leq r_+\sqrt{\frac{3r_+^2+L^2}{L^2-r_+^2}} = r_+ + \mathcal{O}(r_+^3)$. Thus $\frac{r_+}{L} \ll 1$ automatically implies $\frac{a}{L} \ll 1$. Moreover, for $\frac{r_+}{L} \ll 1$ the (real part) of the QNM frequencies of the BH do not differ much from the normal mode frequencies of global AdS that are order $\tilde{\omega}L \sim \mathcal{O}(1)$. Therefore $\frac{r_+}{L} \ll 1$ also implies $r_+\tilde{\omega} \ll 1$ and $a\tilde{\omega} \ll 1$. To sum, our analysis will be valid in the regime of parameters (6.36). We discuss the different regions separately and discuss how to match the solutions obtained next.

6.C.1 Near-region equation and regular solution at the horizon

The near-region is defined by $r - r_+ \ll \frac{1}{\tilde{\omega}}$. Introducing the wave function $\Phi = \Delta_r R^{(-2)}_{\ell\tilde{\omega}m}$, the radial equation (6.13) reads

$$\Delta_r\Phi'' - \Delta_r'\Phi' + \left(\frac{6r^2}{L^2} + 4i\,K_r' + \frac{K_r^2 - 2i\,K_r\Delta_r'}{\Delta_r} - \lambda\right)\Phi = 0\,. \tag{6.126}$$

If we further restrict to the regime $\frac{r_+}{L} \ll 1$, the cosmological constant contribution can be neglected. Specifically, in the radial equation (6.126) the following

approximations are valid

$$\begin{aligned}
&\Delta_r\big|_{r\sim r_+} \simeq r^2+a^2-2Mr+\cdots \simeq (r-r_+)(r-r_-)\,, \quad \text{with} \quad r_- \simeq \frac{a^2}{r_+}\,,\\
&\left(\frac{6r^2}{L^2}+4iK_r'\right)\big|_{r\sim r_+} \simeq \frac{6r_+^2}{L^2}-8ir_+\tilde{\omega}\left(1-\frac{a^2}{L^2}\right) \sim -8ir_+\tilde{\omega}+\cdots\,, \qquad (6.127)\\
&\frac{K_r^2-2i\,K_r\Delta_r'}{\Delta_r}\big|_{r\sim r_+} \simeq \frac{\Xi^2\left(r_+^2+a^2\right)^2(4\pi T_H)^2\,\varpi(\varpi+2i)}{\Delta_r}+8ir_+\tilde{\omega}+\cdots\\
&\qquad\qquad \simeq \frac{(r_+-r_-)^2\,\varpi(\varpi+2i)}{(r-r_+)(r-r_-)}+8ir_+\tilde{\omega}+\cdots\,,
\end{aligned}$$

where Ω_H, T_H are the angular velocity and temperature defined in (6.5), and motivated by the BC (6.17) we have introduced the superradiant factor,

$$\varpi \equiv \frac{\tilde{\omega}-m\Omega_H}{4\pi T_H} \simeq (\tilde{\omega}-m\Omega_{\rm H})\frac{r_+^2+a^2}{r_+-r_-}\,, \qquad (6.128)$$

With these near-region approximations the radial equation (6.126) is then

$$\Delta_r\Phi''(r)-\Delta_r'\Phi'(r)+\left(\frac{(r_+-r_-)^2\,\varpi(\varpi+2i)}{(r-r_+)(r-r_-)}-(\ell-1)(\ell+2)\right)\Phi(r)\simeq 0\,, \qquad (6.129)$$

where, in the approximation regime (6.36), we replaced the eigenvalue λ by its leading contribution in (6.125) (the requirement $a/r_+ \ll 1$ is fundamental here since we neglect a contribution proportional to msa/r_+ when compared with $\lambda \sim (\ell-1)(\ell+2)$). Introducing a new radial coordinate z and wavefunction F defined as

$$z=\frac{r-r_+}{r-r_-}\,, \qquad 0\le z\le 1\,; \qquad \Phi = z^{i\,\varpi}(1-z)^{\ell-1}\,F\,, \qquad (6.130)$$

the near-region radial wave equation takes the form

$$z(1-z)\partial_z^2 F + \Big[(-1+i\,2\varpi) - [1+2\ell+i\,2\varpi]\;z\Big]\partial_z F \\ -(\ell+1)\,[\ell-1+i\,2\varpi]\,F=0\,. \tag{6.131}$$

This is a standard hypergeometric equation [56], $z(1-z)\partial_z^2 F + [c-(a+b+1)z]\partial_z F - abF = 0$, whose most general solution in the neighborhood of $z=0$ is $A_{in}\, z^{1-c}F(a-c+1,b-c+1,2-c,z) + A_{out}\,F(a,b,c,z)$. Using (6.130), one finds that the most general solution of the near-region equation is therefore

$$\Phi = A_{in}\, z^{2-i\,\varpi}(1-z)^{\ell-1}F(a-c+1,b-c+1,2-c,z) \\ + A_{out}\, z^{i\,\varpi}(1-z)^{\ell-1}F(a,b,c,z)\,, \tag{6.132}$$

with

$$a=\ell-1+i\,2\varpi\,, \qquad b=\ell+1\,, \qquad c=-1+i\,2\varpi\,. \tag{6.133}$$

The first term represents an ingoing wave at the horizon $z=0$, while the second term in (6.132) represents an outgoing wave which we set to zero, $A_{out}=0$, to guarantee that no perturbations come off the horizon.

For the matching we need the large r (i.e $z\to 1$) behavior of the ingoing near-region solution. To get this, we use the $z\to 1-z$ transformation law for the

hypergeometric function [56],

$$F(a-c+1,b-c+1,2-c,z) = (1-z)^{c-a-b}\frac{\Gamma(2-c)\Gamma(a+b-c)}{\Gamma(a-c+1)\Gamma(b-c+1)}F(1-a,1-b,c-a-b+1,1-z) + \frac{\Gamma(2-c)\Gamma(c-a-b)}{\Gamma(1-a)\Gamma(1-b)}F(a-c+1,b-c+1,-c+a+b+1,1-z)\,,$$

and the property $F(a,b,c,0) = 1$. Finally, noting that when $r \to \infty$ one has $1 - z = (r_+ - r_-)/r$, one obtains the large r behavior of the near-region wave solution that is regular at the horizon,

$$\Phi \sim A_{in}\,\Gamma(3-2i\varpi)\left[\frac{(r_+-r_-)^{-\ell-2}\,\Gamma(2\ell+1)}{\Gamma(\ell+1)\Gamma(3+\ell-2i\varpi)}r^{\ell+2} + \frac{(r_+-r_-)^{\ell-1}\,\Gamma(-2\ell-1)}{\Gamma(-\ell)\Gamma(2-\ell-2i\varpi)}r^{-\ell}\right] \tag{6.134}$$

6.C.2 Far-region wave equation and global AdS solution

The far-region is defined by $r - r_+ \gg r_+$. In this region the effects induced by the black hole mass and angular momentum can be neglected to leading approximation. The far-region background where the gravitational perturbation propagate is then simply global AdS spacetime. Our approximations then yield $\Delta_r \simeq r^2\left(1+\frac{r^2}{L^2}\right)$ and, in the regime where the eigenvalue λ is given by the leading contribution in (6.125), the radial equation (6.13) boils down to

$$\partial_r\left(\Delta_r\partial_r R^{(-2)}_{\ell\tilde{\omega}m}\right) + \left[\frac{\left(\tilde{\omega}r^2+i\Delta_r'\right)^2}{\Delta_r} + 2\left(\frac{9r^2}{L^2}+1\right) - 8ir\tilde{\omega} - (\ell-1)(\ell+2)\right]R^{(-2)}_{\ell\tilde{\omega}m} \simeq 0\,. \tag{6.135}$$

This is again a hypergeometric equation in whose most general solution is

$$R^{(-2)}_{\ell\tilde{\omega}m} = \frac{L}{r}\left(\frac{L}{r}+i\right)^{\frac{1}{2}(L\tilde{\omega}-2)}\left(\frac{L}{r}-i\right)^{-\frac{1}{2}(L\tilde{\omega}+2\ell)}\Bigg[B_0\, F\left(\ell-1,\ell+1+L\tilde{\omega};2(\ell+1);\frac{2r}{r+iL}\right) + B_1(-2i)^{-(2\ell+1)}\left(\frac{L}{r}-i\right)^{2\ell+1} F\left(-\ell-2,L\tilde{\omega}-\ell;-2\ell;\frac{2r}{r+iL}\right)\Bigg] \tag{6.136}$$

where B_0, B_1 are at this point arbitrary amplitudes whose ratio will be constrained by the asymptotic global AdS BC.[21]

Asymptotically the solution decays as

$$\begin{aligned} R^{(-2)}_{\ell\tilde{\omega}m}|_{r\to\infty} \simeq\ & e^{i\frac{\pi}{2}(L\tilde{\omega}+\ell)}\times \\ & \Big\{ -i\frac{L}{r}\Big[B_0\, F(\ell-1,\ell+1+L\tilde{\omega};2(\ell+1);2) + 2^{-(2\ell+1)}B_1\, F(-\ell-2,L\tilde{\omega}-\ell;-2\ell;2)\Big] \\ & +\frac{L^2}{r^2}\Big[\frac{1}{2}\frac{B_0}{\ell+1}\Big(\Big[2\left(L^2\tilde{\omega}^2+1\right)+\ell(L\tilde{\omega}-1)-\ell^2\Big]\, F(\ell,\ell+2+L\tilde{\omega};2\ell+3;2) \\ & +\ell(\ell-1+L\tilde{\omega})\, F(\ell+1,\ell+2+L\tilde{\omega};2\ell+3;2)\Big) \\ & -2^{-(2\ell+1)}B_1\Big(L\tilde{\omega}\, F(-\ell-2,L\tilde{\omega}-\ell;-2\ell;2) \\ & -(\ell+2)\, F(-\ell-1,L\tilde{\omega}-\ell;-2\ell;2)\Big)\Big]\Big\} + O\left(\frac{L^3}{r^3}\right). \end{aligned} \tag{6.137}$$

To have an asymptotically global AdS perturbation we need to match this decay with (6.19), namely, $R^{(-2)}_{\tilde{\omega}\ell m}\big|_{r\to\infty} \sim B^{(-2)}_{+}\,\frac{L}{r} + B^{(-2)}_{-}\,\frac{L^2}{r^2} + O\left(\frac{L^3}{r^3}\right)$ and impose the BC

[21] If we were working exactly in global AdS ($a=0$ and $M=0$ everywhere) this solution would be exact and extending all the way down to the origin where regularity would require setting $B_1=0$. Then the asymptotically global AdS BC imposed below instead of constraining the ratio B_1/B_0 would instead quantize the frequencies that can propagate in global AdS. Indeed we can explicitly check that the expression for B_1/B_0 that we get when we do the procedure described below (6.139) vanishes when we insert the global AdS frequencies for scalar, $\tilde{\omega}L = 1+\ell+2p$, or vector modes, $\tilde{\omega}L = 2+\ell+2p$ (integer p is the radial overtone).

(6.20), $B_-^{(-2)} = i\,\beta B_+^{(-2)}$. In the regime we are working one has $a \simeq 0$ and the BC expressions (6.21)-(6.23) for β simplify considerably reducing to

$$1) \quad \beta = \beta_{\mathbf{s}} = -L\tilde{\omega}\left(1 + \frac{\lambda}{\lambda - 2\,(L^2\tilde{\omega}^2 - 1)}\right), \tag{6.138}$$

$$2) \quad \beta = \beta_{\mathbf{v}} = \frac{\lambda}{2L\tilde{\omega}} - L\tilde{\omega}\,, \tag{6.139}$$

for scalar and vector modes, respectively. Here, $\lambda = (\ell - 1)(\ell + 2)$. Going through this asymptotic matching we find how the amplitudes $B_0\left(B_+^{(-2)}, \beta\right)$ and $B_1\left(B_+^{(-2)}, \beta\right)$ must be related to the BC parameters $B_+^{(-2)}$ and β for the perturbation to be asymptotically global AdS.

For a later matching with the near-region solution we will need the small r behaviour of the far-region solution $\Phi = \Delta_r R_{\ell\tilde{\omega}m}^{(-2)}$ with $R_{\ell\tilde{\omega}m}^{(-2)}$ given by (6.136). This is

$$\Phi \sim B_+^{(-2)} \frac{1}{\alpha_D}\left[i\,e^{-i\,\frac{\pi}{2}(\ell + L\tilde{\omega})} L^{-\ell}(\ell+1)\,\alpha_N\, r^{\ell+2} - e^{i\,\frac{\pi}{2}(\ell - L\tilde{\omega})} L^{\ell+1}\ell\,\beta_N\, r^{1-\ell}\right], \tag{6.140}$$

where we defined

$$
\begin{aligned}
\alpha_D &= (\ell+1)(\ell+2)(\ell-L\tilde{\omega})F(-\ell-1, L\tilde{\omega}-\ell+1, 1-2\ell, 2)F(\ell-1, L\tilde{\omega}+\ell+1, 2(1+\ell), 2) \\
&\quad +\ell\, F(-\ell-2, L\tilde{\omega}-\ell, -2\ell, 2)\Big[(\ell+1)(2\ell+1)F(\ell-1, L\tilde{\omega}+\ell+1, 2(\ell+1), 2), \\
&\qquad +(\ell-1)(\ell+1+L\tilde{\omega})F(\ell, L\tilde{\omega}+\ell+2, 2\ell+3, 2)\Big], \\
\alpha_N &= \ell(\ell+2-\beta-L\tilde{\omega})F(-\ell-2, L\tilde{\omega}-\ell, -2\ell, 2) \\
&\quad +(\ell+2)(\ell-L\tilde{\omega})F(-\ell-1, L\tilde{\omega}-\ell+1, 1-2\ell, 2), \\
\beta_N &= (\ell+1)(L\tilde{\omega}+\ell-1+\beta)\, F(\ell-1, L\tilde{\omega}+\ell+1, 2(\ell+1), 2) \\
&\quad +(\ell-1)(L\tilde{\omega}+\ell+1)\, F(\ell, L\tilde{\omega}+\ell+2, 2\ell+3, 2).
\end{aligned}
\tag{6.141}
$$

6.C.3 Matching. QNM and superradiant frequencies

In the regime $r_+\tilde{\omega} \ll 1$, the near and far regions have an overlaping zone, $r_+ \ll r - r_+ \ll \frac{1}{\tilde{\omega}}$, where both are simultaneously valid. The requirement that the solutions can be matched across the overlapping zones related the amplitudes A_{in}, $B_+^{(-2)}$ and quantizes the frequency $\tilde{\omega}$. In particular, the frequencies that are allowed to propagate in the Kerr-AdS black hole are found matching the large r behavior (6.134) of the near-region solution with the small r behaviour (6.140) of the far-region solution. This yields two conditions, one following from the matching of the $r^{\ell+2}$ coefficients and the other from the matching of the $r^{1-\ell}$ coefficients. One of these constraints is used to find the ratio between the near and far region amplitudes $A_0/B_+^{(-2)}$ that is then inserted in the other constraint

to finally yield the matching condition that quantizes the frequency spectrum:[22]

$$\frac{\ell!}{(2\ell-1)!}\frac{i(\ell+1)\Gamma\left(\ell+1\right)\Gamma\left(\ell+3-2i\varpi\right)}{4L^{2\ell+1}\ell^2\Gamma\left[2(\ell+1)\right]\Gamma\left(2-\ell-2i\varpi\right)}\left(r_+-\frac{a}{r_+^2}\right)^{2\ell+1}\times$$
$$\Big[\ell(\ell+2-L\tilde{\omega}-\beta)\,F\big(-\ell-2,L\tilde{\omega}-\ell,-2\ell,2\big)$$
$$+(\ell+2)(\ell-L\tilde{\omega})\,F\big(-\ell-1,L\tilde{\omega}-\ell+1,1-2\ell,2\big)\Big]$$
$$=(\ell+1)(\ell-1+L\tilde{\omega}+\beta)\,F\big(\ell-1,L\tilde{\omega}+\ell+1,2(1+\ell),2\big)$$
$$+(\ell-1)(\ell+1+L\tilde{\omega})\,F\big(\ell,L\tilde{\omega}+\ell+2,2\ell+3,2\big), \tag{6.143}$$

where the superradiant factor ϖ was introduced in (6.18), and the asymptotic BC parameter β is given by (6.138) for scalar, and by (6.139) for vector perturbations. Recall that this expression is valid in the approximation regime (6.36).

This frequency quantization condition simplifies considerably when we choose a particular harmonic ℓ. In particular, for the lowest harmonic, $\ell=2$, it reduces to (6.37). We leave the detailed discussion of the solution of this frequency quantization condition and the comparison with the associated exact numerical results to subsection 6.4.1.

[22] To get this result, as observed in a similar context in [162], we should keep in mind that the angular eigenvalue is an integer strictly only in the limit of zero rotation. Therefore the ratio of gamma functions that appears in our computation should be taken as

$$\lim_{\epsilon\to 0}\frac{\Gamma(-\ell-\epsilon)}{\Gamma(-2\ell-2\epsilon)}=\frac{4(2\ell-1)!}{(-1)^\ell(\ell-1)!}\,, \tag{6.142}$$

after using the gamma function property $\Gamma(-n+\epsilon)\sim(-1)^n/(n!\epsilon)$, for $\epsilon\ll 1$ and integer n (assuming at the starting point that $\epsilon=0$ gives a result that differs from the correct one by a factor of 2).

Part III

Black Holes and the de Sitter Landscape of String Theory

Chapter 7

Introduction

In Part. II of this Thesis, anti-de Sitter (AdS) space played a very prominent role. Recall that AdS is the maximally symmetric Lorentz signature manifold with negative curvature. If the spacetime is analytically continued to Euclidean signature, it becomes simply hyperbolic space. The positive curvature analogue of AdS is known as de Sitter (dS) space, as it was actually the first of the two solutions to be discovered. de Sitter is the maximally symmetric Lorentz signature manifold with positive curvature, i.e. the Lorentzian version of a sphere. de Sitter also plays an extremely important role in physics and in string theory, in particular it is central to the study of cosmology. The Poincare patch line element on d-dimensional dS_d is

$$ds^2 = -dt^2 + e^{Ht} \sum_{i=1}^{d-1} dx_i^2, \tag{7.1}$$

which corresponds to a flat, exponentially expanding FRW universe. The universe experienced such exponential expansion early in its history during the inflation-

ary era. After inflation ended the universe experienced different epochs, and we are currently transitioning from an epoch in which the cosmological expansion is dominated by non-relativistic matter to an epoch where it is dominated by the mysterious dark energy. Although the true nature of the dark energy is unknown (hence the name), the effect is to produce an accelerated expansion well approximated by de Sitter space.

Therefore, if string theory is indeed a viable candidate theory of quantum gravity, it should contain de Sitter solutions, or vacua. Perhaps surprisingly, it has proven very difficult to construct such solutions in the supergravity theories that are the low energy effective field theories of the various string theories. In fact, there are no-go theorems [163, 164] which explicitly rule out such solutions as compactifications of string theory. There are various workarounds, but they all are a bit contrived and tend to not be phenomenologically attractive. [1] It should be stressed that the no-go theorems and the workaround approaches address *classical* constructions of de Sitter vacua. In this Introduction we will review the most popular construction of de Sitter vacua in string theory, the KKLT construction, as well as a recent debate surrounding the validity of this procedure. A more thorough review of both topics, as well as of inflation in string theory, can be found in [165].

[1] For example, one way to produce a de Sitter compactification with these classical sources is to allow time dependence in the internal directions.

7.1 The KKLT Construction

In [166], Kachru, Kallosh, Linde, and Trivedi (KKLT) achieved a major breakthrough in the problem of finding de Sitter vacua in string theory. A discussion of the KKLT mechanism naturally must begin with the moduli problem. In string compactifications, the size and other important properties of the internal space are controlled by a collection of scalar fields, called moduli, and these typically have potentials with flat directions. Therefore, configurations where the moduli fields take on particular constant values will be unstable to either classical perturbations or quantum fluctuations. These perturbations could be catastrophic, causing the internal space to de-compactify (which is to say that the space will not remain small in size and the full 10-dimensional manifold would not be interpreted as even approximately 4-dimensional even to low-energy observers). Therefore, in the problem of finding a bona fide string compactification, not only must a solution be found, but there should be no flat directions in the moduli potentials, so that small perturbations or fluctuations will not destroy the compactification. The problem of moduli stabilization was addressed in [167], where most, but not all, of the moduli were shown to be stabilised by the addition of fluxes in the so-called no-scale models. [2] As fluxes are the crucial ingredient in stabilizing the moduli, a short digression to explain what fluxes are is in order.

The bosonic low-energy descriptions of the various string theories are supergravity theories. The particular supergravity depends on the string theory in question [3], but a universal feature is the presence of p-form gauge fields, which

[2] These solutions were called no-scale because the modulus controlling the overall size of the internal space remained un-stabilised, that is, it had a flat potential.

[3] Recall that there are superficially 5 different superstring theories in 10 dimensions, which

are simple abelian generalizations of a Maxwell field. For example, the bosonic part of 11-dimensional supergravity is

$$2\kappa_{11}^2 S = \int d^{11}x\sqrt{-g}\Big(R - \frac{1}{2}|G_4|^2\Big) - \frac{1}{6}\int C_3 \wedge G_4 \wedge G_4. \tag{7.2}$$

Here G_4 is a 4-form field strength related to a 3-form potential via $G_4 = dC_3$. These p-form fields are generalizations of the Maxwell field, with the gauge transformation $C_3 \to C_3 + dB_2$, which leaves the field strength invariant.

The presence of the p-form fields in supergravity is intimately related to the presence of extended objects in string theory. To see the connection, take the familiar example of a point particle charged under a standard $U(1)$ Maxwell field. The particle sweeps out a one-dimensional worldline, against which the potential A_μ can be integrated. Similarly, for the case of a p-form field strength, there is a $(p-1)$-dimensional potential which couples to a $(p-1)$-dimensional worldvolume, i.e. the worldvolume of a $(p-2)$-dimensional extended object. These objects are known as branes. For each distinct p-form field present in a theory, there are two associated branes, one that couples to the field strength in the manner outlined above, known as an electric coupling, and there is a second brane which couples magnetically to the field strength. For example, in the case of M-theory above (7.2), there is an electric 2-brane known as the M2-brane which couples to G_4, and a magnetic M5-brane which couples to the Hodge dual form, $G_7 = \star G_4$.

These p-form fluxes are a universal ingredient in the various supergravity theories, and flux backgrounds or flux vacua are solutions in which these fluxes

are believed to be merely vacua of the same overarching M-theory. Included in M-theory is 11-dimensional supergravity.

are turned on to take non-zero values. An important point is that although branes serve as sources for the fluxes, just as point charges are sources for electric fields in Maxwell theory, in the flux vacua solutions there are typically no brane sources. The flux is either sourced by the boundary conditions or the Chern-Simons/transgression terms in the form equations. For example, in $D = 11$ supergravity, the Bianchi identity for the form G_4 is $dG_4 = \frac{1}{2}G_4 \wedge G_4$, which shows that a flux configuration can source itself, without the need for explicit singular sources on the right hand side.

Returning to the KKLT construction, the starting point are the no-scale flux backgrounds of [167], where most of the moduli have been stabilized by flux. In these models, the full 10 dimensional space consists of a warped product of four-dimensional Minkowski space and a 6-dimensional Calabi-Yau manifold, and they also have the property that there is a large hierarchy of scales, which is attractive from the point of view of engineering a 10-dimensional solution in which to a particular class of observers, physics appears to be 4-dimensional. The KKLT construction then is as follows. Starting from a no-scale model, they consider two sources of corrections, 1) Euclidean D3-branes, and 2) non-Abelian gauge groups arising from D7 branes wrapping 4-cycles in the Calabi-Yau. Each of these corrections have the effect that all the moduli then become stabilised, breaking the no-scale property. Moreover, the solution becomes a supersymmetric AdS vacuum. The original large hierarchy of scales allows the negative cosmological constant (or length scale of the AdS space) to be tuned parametrically small.

The next step in the KKLT construction is to add anti-D3 branes to the corrected solution. They argue that the effect of this addition will be a metastable dS

solution with small cosmological constant. Their argument relies on a very important previous calculation by Kachru, Pearson, and Verlinde (KPV) [168], which showed that anti-branes could be added to a certain flux background to produce long-lived, metastable states. A sketch of the KKLT argument is as follows: In the KPV calculation, anti-D3 branes were added to a particular flux background, known as the Klebanov-Strassler (KS) solution [63]. The KS solution contains D3-brane charge, without any D3-brane sources. The positive charge of the background naturally wants to annihilate against the added negative charge of the anti-D3 branes, but the usual annihilation channel of brane-anti-brane annihilation (an open string tachyon) is not present. What is needed is a mechanism of brane-flux annihilation. KPV worked out this annihilation process, and were able to show that, for a certain regime of parameters, annihilation proceeded through tunnelling, and that a metastable state of co-existing anti-branes and flux existed.

Then, building off of this result as well as the important fact that an example of a no-scale model can be approximated by the KS solution in a certain region, KKLT then argued that the addition of anti-branes to the corrected no-scale solution produced a metastable dS solution. The solution will contain a de Sitter factor because positive energy has been added to the solution. The difference in cosmological constant between the original AdS solution and the final dS solution comes from the positive tension of the added anti-D3 branes.

Of the two steps in the KKLT construction, correcting the no-scale solution to a supersymmetric AdS vacua and "uplifting" the AdS solution to a dS solution using anti-branes, this last step of uplifting has come under intense scrutiny in recent years. We turn now to review these criticisms, which have at times been

given the colorful name of "Scapezilla" by one of their major proponents, Iosif Bena.

7.2 A Problem with the Landscape (Scapezilla)

The KKLT construction was and is hugely influential, with the paper having over 2000 citations as of the time of the writing of this thesis. Despite this tremendous amount of work, no explicit construction exists of the metastable de Sitter solutions, or even the intermediary KPV metastable solution consisting of expanded branes in the Klebanov-Strassler solution. This perhaps startling lack of fundamental solutions is due to the fact that the solutions are not supersymmetric and break the symmetry of the background, and therefore obtaining these solutions would require solving a complicated system of coupled, non-linear PDE's. Given how hard it is to find the exact solution, and given how important the KKLT construction is to cosmological applications of string theory, it seems desirable to make progress by constructing related, simpler solutions which capture the major salient features of the desired, more complicated solutions. These simpler solutions correspond to backreacted *smeared* anti-branes added to the flux background.

Branes are extended objects, but are point like in the transverse space. For example, a $D3$-brane is extended along 3 spatial and 1 time dimensions, and is a point in the transverse 6-dimensions. Therefore, addition of a brane source charge to a given solution possessing certain symmetries will lead to a less symmetric solution in much the same way the addition of a point source would. If the

brane charge is not added at a point in the transverse space, but instead smeared out *uniformly* over an extended region, then it is possible for the symmetries to remain intact. For the case most relevant to the KKLT construction, anti-D3 branes added to the KS solution, if the anti-D3 branes are smeared uniformly over the finite-sized sphere at the tip of the deformed conifold, then the backreacted solution will remain cohomogeneity-1, that is, all the metric functions will simply be functions of a single radial coordinate.

In the Introduction of Sec. 9 the history of the construction of these smeared solutions and their relevance to the problem of backreacted anti-branes is reviewed. To summarize here, the smeared solutions all exhibited singularities which were of an unfamiliar form. Singularities play an important role in string theory. Sometimes they are an indication that a solution is unphysical, for example negative-mass Schwarzschild. At other times, they are strictly speaking unphysical, but in a much gentler sense. In fact, there is a strong connection between these rather benign singularities and the IR singularities sometimes encountered in QFT, for example, in the problem of soft photon emission amplitudes. The interpretation is that the singularity is a pointer towards non-trivial IR physics that has been missed. In contrast to the negative-mass Schwarzschild solution then, there are singular supergravity solutions for which there exist partner solutions wherein the singularity has been resolved. It can be that the resolved solution is still a valid gravity solution, or it could be that stringy corrections are required which take one outside the validity of the supergravity regime. "Bad" or unphysical singularities are those not cured by stringy effects, and in the case of negative-mass Schwarzschild, it is actually a good thing that the singularity does not get resolved.

If the negative-mass solution were physical, there would exist states of arbitrarily negative energy [169], which is clearly pathologic. This solution is unphysical, and it is handy that it is also singular–otherwise a perhaps more sophisticated or nuanced criterion than simply demanding that physically acceptable solutions be non-singular would be needed to rule out unphysical behaviour.

Given that solutions which are related to the desired anti-branes in the Klebanov-Strassler solution exhibit strange singularities, the all-important question is: are these singularities of the kind that would rule out these solutions as unphysical, or are they resolved by some mechanism? All attempts to find resolution mechanisms have failed. It could be that there does exist some resolution mechanism, and it simply has yet to be found. An indirect method for testing whether or not a singularity is physical is to see if it can be cloaked by a small black hole. This is known as the Gubser criterion [170], and all attempts to shield the above singularities behind horizons have also failed, leading most researchers, including myself, to be of the opinion that the *smeared* singularities are unphysical.

The next step is where opinions diverge, and this is very much an area under active investigation by numerous researchers. With the apparent un-physicality of the smeared solutions, some then make the leap to say that the singularities of the smeared solutions are indicative of singularities in the desired, more complicated localized solution. The conclusion that follows is then that the KKLT construction is an invalid mechanism for constructing de Sitter solutions because adding anti-branes to flux backgrounds unavoidably produces unphysical singularities. This conclusion is rather controversial. There are many reasons to believe in the validity of the anti-brane uplifting mechanism, and if the mechanism is invalid for

some reason, it would be nice to have a good insight as to where these reasons fail. Although some explanations have been offered, none have been uniformly accepted.

I am of the opinion that the singular *smeared* solutions may very well be unphysical, but that the leap taken to say that the localised solutions relevant for KKLT are unphysical is not justified, and in fact adding anti-branes is a perfectly fine uplifting mechanism. Evidence for this view comes from Sec. 9, where I show that black holes in the Klebanov-Strassler solution can be used to shield the singularities associated with localised anti-brane sources. My analysis shows that there is a crucial difference between smeared and localised branes, and if the Gubser criterion is to be believed, the existence of these black holes strongly suggests that there is in fact no obstruction to the addition of anti-branes to the Klebanov-Strassler solution, and the KKLT construction remains a valid method for constructing de Sitter vacua in string theory.

The remainder of this Part is organized as follows. In Sec. 8 a problem somewhat tangential to the above story is considered, the problem of adding black holes into a simple class of flux backgrounds which are *not* of the right form to be relevant to the above controversy. The reason for this detour is that this is in many ways a warm-up to the more difficult problem discussed above, as it is shown that black holes cannot be added to these solutions without producing singularities or introducing time dependence. Next, in 9 the problem of anti-branes in flux backgrounds is addressed, and as discussed above, it is found that black holes can shield the singularities associated with the anti-branes.

Chapter 8

A No Black Hole Theorem

8.1 Introduction

Our basic understanding of black holes includes a series of "no-hair" theorems which state that certain types of matter must vanish outside stationary black holes. Intuitively, this says that the matter either falls into the black hole or radiates out to infinity. These theorems were originally proven for linear fields, but they were thought to hold more generally. It was later realized that many types of hair are indeed possible. One class of examples consists of black holes in anti-de Sitter space. Perhaps the simplest case is a charged scalar field which can exist outside certain charged black holes [69, 68]. A large class of asymptotically flat examples involves theories that admit stationary solitons. One can often put a small stationary black hole inside the soliton without destroying it [171]. This includes solutions of Einstein-Yang-Mills theory [172, 173, 174], and monopoles of the Einstein-Yang-Mills-Higgs system [175]. (For a comprehensive review of these

solutions, see [176].) One can also put a rotating black hole inside a rotating boson stars [124, 177].

There are some cases where one cannot put a static black hole inside a static soliton. For example, if one puts a small black hole inside a static perfect fluid star it will grow and slowly consume the star. Similarly, one cannot put a static black hole inside a static boson star[1] [178]. The matter content of the soliton determines whether or not one can put a static black hole inside.

In higher dimensions, there are extended black holes such as black strings and black branes. There are also extended solitons such as flux-branes. These are higher dimensional generalizations of "Melvin's magnetic universe" [179] which describes a static, cylindrically symmetric, gravitating magnetic flux-tube. A natural question is whether one can put a static black brane inside a static flux-brane. Since there is an exact four dimensional static solution describing a Schwarzschild black hole inside Melvin's magnetic universe [180], one might expect the answer is yes. We will show that this is incorrect. If one puts a black brane inside a flux-brane, it will necessarily grow and consume the brane.

The simplest example starts with an electric flux-tube in five dimensions. As this solution does not appear to exist in the literature, we will numerically construct it in Sec. 8.4. That is, we find a static, cylindrically symmetric solution of the five-dimensional Einstein-Maxwell theory describing a self-gravitating electric flux-tube. The product of four-dimensional Schwarzschild and a line is a simple five-dimensional black string with the same symmetry as the flux-tube. Our result shows that one cannot put a thin black string inside the flux-tube and keep the

[1] A subtlety here is that although the metric is static, the scalar field has a time dependent phase and is not static itself.

solution stationary.

A much larger class of examples that have been discussed in the literature are the flux-branes of string theory [181], which are sourced by one of the higher rank forms in supergravity. We will review these solutions in Section 4. Our result implies that one cannot put a stationary black brane inside any of these flux-branes [2].

As a final application of our result, one can consider higher dimensional vacuum solutions with a $U(1)$ symmetry. Under Kaluza-Klein reduction there is a Maxwell field, and one can construct an electric flux-tube solution of the dimensionally reduced theory. Since one cannot put a stationary black string inside this flux-tube, it follows that one cannot put a black two-brane in the higher dimensional vacuum solution. At first sight, this example is more surprising than the first two. When there is nonzero flux outside the horizon, one can imagine that a stationary black hole cannot exist since the flux falls in causing the black hole to grow. But in a vacuum solution, there is no matter to fall in.

The answer to this puzzle lies in the Raychaudhuri equation applied to the null geodesic generators ℓ^a of the event horizon (in D spacetime dimensions):

$$\frac{d\theta}{d\lambda} = -\frac{1}{D-2}\theta^2 - \sigma_{ab}\sigma^{ab} - T_{ab}\ell^a\ell^b \tag{8.1}$$

where λ is an affine parameter, θ is the expansion, and σ_{ab} is the shear of the null geodesic congruence. For a stationary black hole, the left hand side must vanish. Since the theories we are interested in all satisfy the null energy condition, the

[2] It was earlier shown [182] that certain rank forms cannot exist outside static black holes which are asymptotically flat in all directions.

right hand side is the sum of three negative terms. In order for a stationary black hole to exist, each one much vanish. This is indeed possible for black holes placed inside some solitons [176], but we will see that for the flux-branes, the last term is always nonzero. In the Kaluza-Klein example where the higher dimensional solution has no matter, we will see that the shear is necessarily nonzero on the horizon causing the horizon to grow.

The outline of this paper is as follows. In the next section we prove that a uniform black brane cannot remain stationary inside a flux-brane. In section 3, we discuss the generalization to nonuniform black branes. We will prove that there cannot exist stationary black branes which are nonuniform in a compact direction and argue that similar results hold for noncompact directions also. In section 4 we discuss the flux-branes in detail, and construct some numerically. We conclude in section 5 with some open questions. The two appendices contain some technical details.

8.2 No Uniform Black Branes

Consider a theory of gravity in D dimensions coupled to a closed $(p+1)$-form field strength F_{p+1}. We will assume a general (Einstein-frame) action of the form

$$S = \int d^D x \sqrt{-g} \left[R - \frac{1}{2}(\nabla\phi)^2 - \frac{1}{2(p+1)!} e^{a\phi} F_{p+1}^2 \right] \tag{8.2}$$

Note that we have included a possible (but not required) scalar field with coupling to F_{p+1} governed by a constant a. (One can also include additional matter fields or Chern-Simons terms and they will not affect our argument.) The equations of

motion following from (8.2) are

$$R_{ab} = \tau_{ab}, \qquad d \star \left(e^{a\phi} F_{p+1}\right) = 0, \qquad \nabla^2 \phi - \frac{a e^{a\phi}}{2(p+1)!} F_{p+1}^2 = 0, \quad (8.3)$$

where τ_{ab} is the trace-reversed stress tensor $\tau_{ab} = T_{ab} - \frac{T}{D-2} g_{ab}$ given by

$$\tau_{ab} = \frac{1}{2} \nabla_a \phi \nabla_b \phi + \frac{e^{a\phi}}{2} \left[\frac{1}{p!} (F_{p+1})_{a \cdots} (F_{p+1})_b{}^{\cdots} - \frac{p}{(D-2)(p+1)!} g_{ab} F_{p+1}^2 \right]. \quad (8.4)$$

In addition, one has the constraint $dF_{p+1} = 0$. There are "flux-brane" solutions to this theory which are nonsingular solutions with at least $p+1$ (commuting) translational symmetries which include time, and F_{p+1} is nonzero when restricted to this homogeneous subspace. We will not need the detailed form of these solutions to prove our "no black hole theorem" so we delay our construction of these solutions until Sec. 8.4. In this section we rule out uniform black branes inside these flux-branes, and in the next section we will argue that similar results hold for the nonuniform case.

Theorem: Consider a "flux-brane" solution to (8.2), i.e., a nonsingular solution in which $F_{t x_1 \cdots x_p}$ is nonzero, and all fields are independent of $t, x_1, \cdots, x_p$. Then one cannot put a stationary, translationally invariant, black p-brane in the center of this flux-brane.

Proof: First note that $F_{t x_1 \cdots x_p} \equiv E$ must be constant. If it were a function of another coordinate, say r, then $dF = 0$ would require that F has a component $F_{r \cdots}$ that depends on t or one of the x_i contradicting the translation invariance. We will first rule out static black branes, and then generalize to the stationary

case. If there were a solution describing a static black p-brane in the center of this flux-brane with horizon at $r = r_0$, then $F_{tx_1\cdots x_p}F^{tx_1\cdots x_p} \to \infty$ as $r \to r_0$. To obtain a flux which is smooth on the future horizon, one can introduce $F_{rx_1\cdots x_p}(r)$ so that the t and r components of F_{p+1} combine to give $F_{vx_1\cdots x_p} = E$, where $v = t + h(r)$ is a good coordinate near the horizon. The static Killing field which is null on the horizon is now $\xi = \partial/\partial v$ (since we have not changed the radial coordinate), so the flux of energy crossing the horizon is

$$T_{bc}\xi^b\xi^c \propto e^{a\phi}(\xi^b F_{b\cdots})(\xi^c F_c{}^{\cdots}) = e^{a\phi}F_{vi\cdots j}F_v{}^{i\cdots j} \tag{8.5}$$

This cannot vanish since the right hand side is a sum of nonnegative terms with at least one positive contribution coming from $F_{vx_1\cdots x_p}$.[3] This contradicts the assumption that the black brane was static, since the Raychaudhuri equation (8.1) shows that the horizon must grow when there is an energy flux across the horizon.

This argument is easily extended to rule out stationary black branes as well. If a black brane is stationary but not static, the Killing vector which is null on the horizon takes the form

$$\xi = \partial/\partial t + v\partial/\partial x + \Omega\partial/\partial\phi \tag{8.6}$$

where x denotes some direction along the brane, i.e., a linear combination of the x_i, and ϕ denotes a rotation in the transverse space. One can first perform a boost

[3]The metric on the $x_1, \cdots, x_p$ subspace must be positive definite since the horizon is a null surface, and these coordinates denote directions along a cross section of the horizon, not along a null generator.

in the (t, x) plane to a co-moving frame $(\tilde{t}, \tilde{x})$ where the black brane is at rest. Since the flux is boost invariant, we have $F_{\tilde{t}\tilde{x}\cdots} = E$. This effectively removes the second term on the right hand side of (8.6). One can now repeat the argument above. Good coordinates near the horizon of a rotating black hole take the form $v = t + h_1(r)$, $\tilde{\phi} = \phi + h_2(r)$. The second coordinate transformation does not affect the flux, and the first is identical to the static case. So one again finds that if F_{p+1} is regular on the future horizon, there must be a nonzero flux of energy crossing this horizon causing the black hole to grow. QED

The theorem holds whether or not the black brane carries a charge. A black p-brane can carry electric charge of a $p+2$ form, or magnetic charge of a $D-(p+2)$ form. It can also carry smeared charges of lower rank forms. All these charges produce fields which are smooth on the horizon with no flux of energy crossing it. So they do not affect the above result. They cannot stop the black hole from growing.

There are various extensions of this theorem. A simple one just uses Hodge duality. Consider a solution with a magnetic q-form field $\tilde{F}$ which is nonzero. If there is a function h such that $F = h \star \tilde{F}$ satisfies the conditions of the theorem, then one cannot put a stationary black brane in such a solution.

A less trivial extension is the one mentioned in the introduction. Even if there are no form fields F in the higher dimensional theory, there can be solutions which, after dimensional reduction, have a Maxwell field satisfying the conditions of the theorem. One cannot add stationary black branes to such a solution. For

example, consider a higher dimensional vacuum solution of the form

$$ds^2 = g_{yy}(dy + Exdt)^2 + g_{tt}dt^2 + g_{xx}dx^2 + g_{ij}dz^i dz^j \tag{8.7}$$

where the metric functions are independent of t, x, y. After Kaluza-Klein reduction on y, one has a Maxwell field $F_{xt} = E$, so one cannot add a stationary black string. We will see an example of this type of solution in Sec. 8.4.

Our result certainly does not rule out the familiar planar black hole in $AdS_5 \times S^5$, even though that solution is sourced by a (self-dual) five-form. The reason is that in the usual Poincare coordinates for AdS_5, the nonzero component of the flux is $F_{trx_1x_2x_3}$. Since the radial direction is included (in which there is no translational symmetry) and a constant r surface is null at the horizon, the right hand side of (8.5) vanishes.

8.3 Generalization to Nonuniform Black Branes

We now ask what happens if we relax the assumption that the black branes are translationally invariant. It is likely that static spherical black holes can exist inside these flux-branes. Indeed, exact solutions have been constructed describing a static Schwarzschild black hole inside a magnetic flux-tube in both four [180], and higher [183] dimensions. In $D = 4$, one can dualize the magnetic flux-tube to an electric flux-tube, but this is not possible for $D > 4$. So to our knowledge exact solutions describing static spherical black holes in higher dimensional electric flux-branes have not yet been constructed, but are likely to exist.

If the horizon is extended in all p directions, it is likely that it cannot remain

stationary even if we relax the assumption that it is uniform. We will prove this when the nonuniform directions are compact, and then give an argument which applies to noncompact directions.

8.3.1 Compact case

Suppose one direction x_1 is periodically identified with period L. It is easy to rule out stationary black branes which are inhomogeneous in this compact direction. Choose a radial coordinate r such that the horizon is at constant r and x_1 is a coordinate along the horizon. Expanding $F_{tx_1\cdots x_p}$ in a Fourier series in x_1 we get

$$F_{tx_1\cdots x_p} = F^{(0)}_{tx_1\cdots x_p} + \sum_{n\neq 0} F^{(n)}_{tx_1\cdots x_p} e^{\frac{2\pi i n x_1}{L}}, \tag{8.8}$$

The coefficients, $F^{(n)}_{tx_1\cdots x_p}$ are independent of x_i, but can depend on coordinates off the brane, say r. We can similarly expand

$$F_{trx_2\cdots x_p} = F^{(0)}_{trx_2\cdots x_p} + \sum_{n\neq 0} F^{(n)}_{trx_2\cdots x_p} e^{\frac{2\pi i n x_1}{L}}, \tag{8.9}$$

where the coefficients $F^{(n)}_{trx_2\cdots x_p}$ again are independent of x_i, but can depend on r. The condition $dF_{p+1} = 0$ can also be expanded in a Fourier series and must hold mode by mode. In particular, if we look at just the zero mode, we get $\partial_r F^{(0)}_{tx_1\cdots x_p} = 0$. But $F^{(0)}_{tx_1\cdots x_p}$ must be nonzero at large distance from the brane since we are considering a flux brane. Since it is constant, we can now apply the argument in the uniform black brane case to conclude that stationary nonuniform black branes cannot exist.

This argument immediately generalizes to more than one compact direction along the brane. One can Fourier transform $F_{tx_1\cdots x_p}$ in all the compact directions. The overall zero mode must again be constant and nonzero at large distances from the black brane.

8.3.2 Noncompact case

When the black brane is inhomogeneous along a noncompact direction, the argument is more subtle. One cannot just apply a Fourier transform in x_1 and look at the $k = 0$ contribution. Since we have a constant flux at infinity, the individual $k = 0$ mode diverges. In this section we will show that inhomogeneous black strings (i.e. $p = 1$) cannot exist within a flux-tube because the horizon would thin out along the string direction at a rate so rapid that the string would pinch off. We leave for future work the general p case which we believe will yield similar results.

Let us suppose that the non-uniform black string in a flux-tube solution exists and consider the features it must possess. At a large radial distance R away from the string, there is a uniform electric field $F_{tx} = E$. This means that asymptotically the electrostatic potential grows linearly with x, $A_t = Ex$. In contrast, the horizon must be an equipotential surface $A_t = 0$ [4] independently of x, which means that the equipotential surfaces coming in from large radius cannot hit the horizon. Instead they must bunch up, producing a radial component of the electric field that grows with x (see Fig. 8.1). The radial electric field on the horizon, F_{rt},

[4]This follows either from our previous argument that if F_{tx} is nonzero on the horizon, there must be energy flux across the horizon, or simply from the fact that a nonzero A_t on the horizon would have diverging norm.

will be positive for large $x > 0$ but negative for large $x < 0$. This requires that the black string has a positive charge density for $x > 0$ and negative charge density for $x < 0$, which is similar to what happens if one puts a long conducting rod in an electric field; there is charge separation with positive charge accumulating at one end and negative charge at the other.

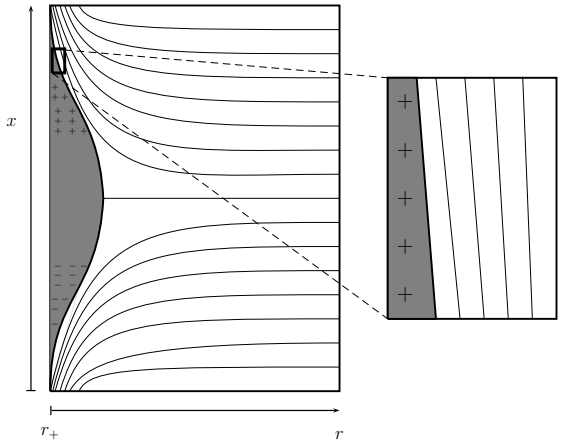

Figure 8.1: Non-uniform black string in an electric flux-tube. The black lines are equipotential surfaces. The horizon is required to be an equipotential surface with value $A_t = 0$; this forces the field lines to bunch up as $x \to \pm\infty$, which means that the black string is locally positively charged at large positive values of x, and negatively charged at large negative values of x. The string remains neutral overall, however. Inset: In the neighbourhood of some positive value of x, the non-uniform black string in a flux-tube should be approximated by a uniform charged black string with an electric field perturbation.

If the horizon indeed extends to $x = \pm\infty$ without pinching off at a finite value of x, the x-dependence of the metric should be negligible near the horizon compared with the r-dependence, as the radial electric field grows indefinitely. Then, the geometry at large x should be well described by a perturbation of a translationally invariant charged black string solution. To explore this possibility, we consider the following ansatz for the $D = d + 1$ dimensional Einstein-Maxwell

theory (8.2) with no dilaton and $p = 1$:

$$\begin{aligned} ds^2_{d+1} &= -e^{2A} H_- H_+ dt^2 + e^{2B} \left(H_-^{-\frac{2}{d-2}} dx^2 + H_-^{-1+\frac{2}{(d-3)(d-2)}} H_+^{-1} dr^2 \right) \\ &\quad + e^{2C} r^2 H_-^{\frac{2}{(d-3)(d-2)}} d\Omega^2_{d-2}, \\ A_\mu dx^\mu &= \sqrt{\frac{2(d-1)}{(d-2)}} \left(\frac{r_-}{r_+} \right)^{\frac{d-3}{2}} H_+ e^D dt. \end{aligned} \tag{8.10}$$

Here $H_\pm = 1 - (r_\pm/r)^{d-3}$ and A, B, C, D are functions of r and x. When $A = B = C = D = 0$, this is the translationally invariant electrically charged black string solution. This solution first appeared in [184] for the case $d = 4$, and the general d solution can be derived by dualising and uplifting the magnetically charged dilatonic black holes of [185, 186]. The horizon topology is $S^{d-2} \times R$ and is located at $r = r_+$, while the curvature singularity is at $r = r_-$. The extremal limit corresponds to $r_+ = r_-$ and has zero horizon area. The temperature is

$$T = \frac{(d-3)}{4\pi r_+} \left[1 - \left(\frac{r_-}{r_+} \right)^{d-3} \right]^{1-\frac{1}{(d-3)(d-2)}}. \tag{8.11}$$

To model the putative non-uniform black string in the neighbourhood of some large positive x value, we will start with this charged solution (with $A = B = C = D = 0$) and add a small electric flux along the x-direction.

A linear perturbation of the uniform charged black string can be described by:

$$\begin{aligned} A(r,x) &= \epsilon A_1(r) x, \quad B(r,x) &&= \epsilon B_1(r) x, \\ C(r,x) &= \epsilon C_1(r) x, \quad D(r,x) &&= \epsilon D_1(r) x, \end{aligned} \tag{8.12}$$

where ϵ is the small parameter controlling the perturbation and is proportional to the asymptotic value of the electric flux. Note that the perturbed gauge potential A_t vanishes on the horizon $r = r_+$ as required by regularity. Also note that all perturbations have a linear dependence on x. Typically, a perturbation about a translationally invariant solution would be expanded in modes e^{ikx}. Here we are using the fact that we expect the dominant contribution to come from small k, and have kept only the linear term[5].

The equations governing the perturbation come from linearizing the background Einstein and form equations (8.3):

$$\delta R_{ab} = \delta F_{(a|c} F_{b)}{}^{c} - \frac{1}{2} F_{ac} F_{bd} h^{cd} - \frac{1}{2(d-1)} g_{ab} F \cdot \delta F - \frac{1}{4(d-1)} h_{ab} F^2 + \frac{1}{2(d-1)} g_{ab} F_{ce} F_d{}^{e} h^{cd}, \tag{8.13}$$

$$\nabla_a \left(\delta F\right)^{ab} + \frac{1}{2} \nabla_a \left(h F^{ab}\right) - 2 \nabla_a \left(h^{c[a} F_c{}^{b]}\right) = 0. \tag{8.14}$$

There are 6 independent components of the Einstein equations and 1 independent form equation. Two equations are first order constraints: the rx-component Einstein equation is the momentum constraint and a linear combination of the diagonal components yields the Hamiltonian constraint. Using these constraints, the system can be shown to reduce to 4 ODE's, first order in A_1, C_1 and second order in B_1, D_1.

The boundary conditions we desire are such that the perturbation is regular

[5]We checked that the perturbation equations derived in this section are identical to those derived from a perturbation with an $e^{ikx}-$dependence once the limit $k \to 0$ is taken. Therefore the perturbation is both a gradient expansion as well as a perturbation in the amplitude of the asymptotic electric field (controlled by ϵ).

at the horizon and asymptotically the perturbed metric functions fall-off to zero and the Maxwell perturbation is that of a constant electric field whose magnitude is proportional by the expansion parameter ϵ [6]:

$$A_1,\, B_1,\, C_1 \to 0, \qquad D_1 \to \text{const} = 1. \tag{8.15}$$

Requiring the perturbation to be regular at the horizon translates into the Dirichlet condition $A_1(r_+) = B_1(r_+)$ as well as additional Robin boundary conditions relating functions and their derivatives at $r = r_+$. This is a boundary value problem, and to solve it numerically we first convert to a compactified coordinate and discretize using a spectral grid. It can then be converted to a simple linear algebra problem of the form $M.v = b$, with M a matrix and b, v vectors. In Fig. 8.2 we plot the solutions for the representative case of $d = 4$, $T = \sqrt{2/5}/(4\pi)$, and $r_+ = 0.632$. The solutions for other parameter values or dimensions are qualitatively similar.

It turns out that the effect of the perturbation on the horizon geometry can be understood very simply. Starting with the uniform charged solution, Eq. (8.10) with $A = B = C = D = 0$, the effect of the electric field can be taken into account by promoting the black hole parameters to be functions of x: $r_\pm = r_\pm(x)$. To see this, note that requiring that the temperature be independent of x imposes a relation between dr_+/dx and dr_-/dx. Using this condition, one can calculate dA_H/dx in terms of dr_+/dx, where A_H is the cross-sectional area of the horizon at fixed x. Returning to the linearized perturbation, one can also calculate dA_H/dx

[6] These boundary conditions correspond to the linearisation (in E) of the electric flux-brane solutions discussed later in Sec. 8.4. Although those solutions are not asymptotically flat, they are when restricted to linear order in the asymptotic value of the electric field E, which is proportional to ϵ in the current perturbative treatment. The deviations from flatness arise at $\mathcal{O}(\epsilon^2)$.

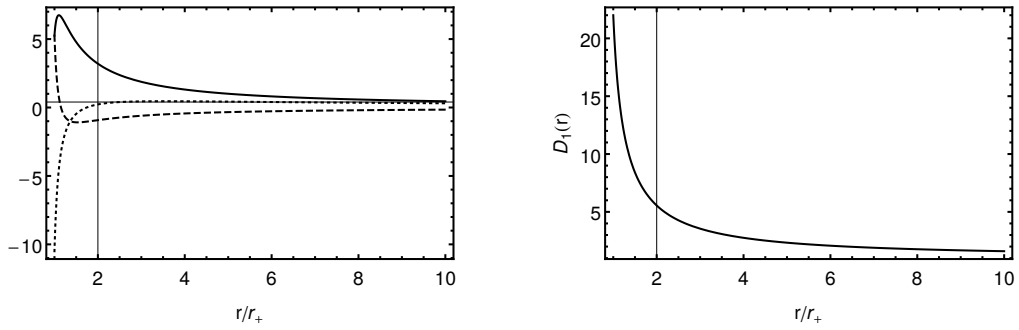

Figure 8.2: Left Panel: The numerical solution for A_1 (solid), B_1 (dashed), C_1 (dotted) for $d = 4$ and $T = \sqrt{2/5}/(4\pi)$. At the horizon, $A_1(r_+) = B_1(r_+)$, as required by regularity. Right Panel: The numerical solution for D_1 for the same dimension and temperature.

in terms of $C_1(r_+)$. Equating these two expressions yields

$$\frac{dr_+}{dx} = \left(\frac{d^2 - 5d + 5}{(d-3)(d-2)}\right) \epsilon C_1(r_+) r_+. \tag{8.16}$$

Similarly, one can calculate $dg_{xx}/dx\Big|_{r_+}$ in two different ways: first in terms of dr_+/dx, and then in terms of the perturbation $B_1(r_+)$. Equating the answers yields

$$\frac{dr_+}{dx} = -\left(\frac{d^2 - 5d + 5}{(d-3)}\right) \epsilon B_1(r_+) r_+. \tag{8.17}$$

Thus we see that if

$$C_1(r_+) + (d-2) B_1(r_+) = 0 \tag{8.18}$$

holds for our numerical solutions, then the horizon geometry is accurately modelled by the uniform charged string with the parameters r_+, r_- promoted to functions of x and subject to the constraint that $dT/dx = 0$. And indeed, we

find that this condition is satisfied for our solutions, up to a very small numerical error. Therefore, the perturbed horizon behaves exactly as the uniform charged black string made non-uniform by slowly varying parameters $r_{\pm}(x)$.

Since $C_1 < 0$, we see that as $x \to +\infty$ the horizon thins out and the electric field evaluated at the horizon increases. It seems that there are two possibilities: either the horizon radius goes to zero in finite distance, in which case one cannot place inhomogeneous non-compact black strings in flux-tubes, or the horizon continues to shrink without pinching off as x increases. This would be a new type of black hole solution, a "spiky black hole", that would look somewhat like Fig. 8.1 [7]. To investigate whether such a solution is possible, let us analyse the rate at which the perturbed horizon radius decreases with x. In Fig. 8.3, we plot $C_1(r_+)$ for $d = 4$ and fixed temperature, in this case arbitrarily chosen to be $T = \sqrt{2/5}/4\pi$. We find that $C_1(r_+)$ is always negative, and appears to be diverging as $r_+ \to 0$. The divergence is well fitted by a power law,

$$C_1(r_+) \sim -\alpha r_+^{-\beta} + \gamma, \tag{8.19}$$

with α, β, γ positive fit parameters that are in principle functions of d and T. Surprisingly, we find that $\gamma = 2$ independent of d or T, and that β is independent of T and takes on the values:

d	4	5	6	7	8	9	10	11	12	13
β	2.000	1.200	1.091	1.052	1.034	1.024	1.018	1.014	1.011	1.009

It is interesting to note that it appears that $\beta \to 1$ as $d \to \infty$. Lastly, α depends

[7] Of course, even if this solution were found to exist, quantum effects would become important since the curvature is growing large as the horizon shrinks and comes closer to the singularity at $r = r_-$.

on both d and T, but importantly is always positive. We can now use the fact that the perturbed black string is well modelled as the uniform black string with x-dependent parameters by combining Eq.'s (8.16), (8.19) to find that for small r_+

$$r_+(x)^\beta \sim c_0 - c_1 \epsilon x, \tag{8.20}$$

with c_0 a constant of integration which we take to be positive, and c_1 a positive constant. Clearly $r_+(x)$ pinches off at finite x, which is very strong evidence against the existence of these "spiky black holes". This result, together with the proofs of Sec.'s 8.2 and 8.3.1, rules out any sort of extended black string in a flux-tube.

Although we only considered the case of $p = 1$ for the non-uniform, non-compact case, it seems likely that the result holds for higher p as well. To fully answer this question one should repeat the analysis done here. The relevant uniform charged black brane solutions can be constructed in a very similar manner to (8.10), although an additional uplift would be required.

8.4 Flux-branes

In this section we construct various flux-brane solutions to (8.3). They can be described by the general ansatz

$$ds^2 = e^{2\alpha} ds^2_{p+1} + e^{2\beta} dr^2 + e^{2\gamma} ds^2_{D-p-2}, \quad F_{p+1} = E \ \mathrm{vol}(ds^2_{p+1}), \tag{8.21}$$

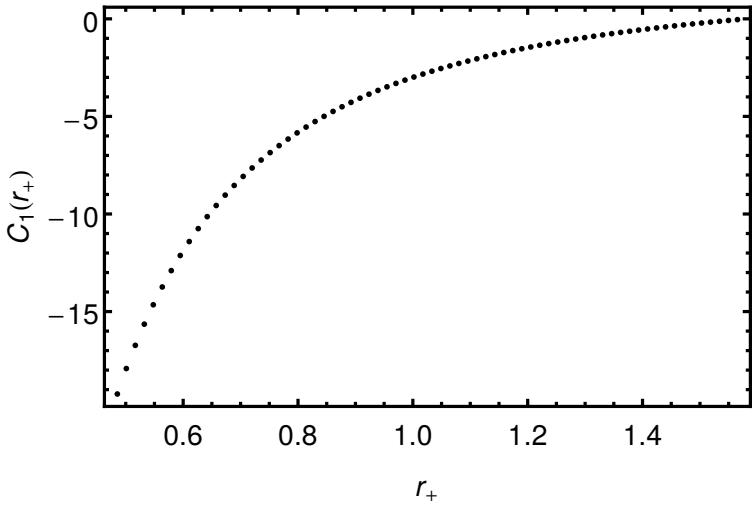

Figure 8.3: $C_1(r_+)$ for $d = 4$ and $T = \sqrt{2/5}/(4\pi)$. This data, along with Eq. (8.16), shows that the black string is tapering off as x increases. The apparent divergence as $r_+ \to 0$ indicates that the string will reach zero radius, i.e. pinch off, in finite x distance.

where α, β, γ and the dilaton ϕ are all functions of the radial coordinate only, and ds^2_{p+1}, ds^2_{D-p-2} are Einstein metrics obeying

$$ {}^{(p+1)}R^{\mu}{}_{\nu} = \lambda_{p+1}\delta^{\mu}{}_{\nu}, \quad {}^{(D-p-2)}R^{i}{}_{j} = \lambda_{D-p-2}\delta^{i}{}_{j}, \tag{8.22} $$

where λ_{p+1} and λ_{D-p-2} are constants, indices belonging to the $(p+1)$-dimensional space are labelled with Greek letters, and the indices belonging to the $(D-p-2)$-dimensional space are labelled with lowercase Latin letters starting with $i, j, ..$ Note that the form equations are already satisfied: F_{p+1} is trivially closed, and although its Hodge dual in general possess a non-trivial radial dependence, it also acquires a dr-leg, and is therefore also closed. Also note that the gauge freedom associated with the choice of radial coordinate has not been fixed yet. We will

find it convenient to work in different gauges, therefore we leave it un-fixed for now. The equations of motion for this ansatz are presented in Appendix 8.A.

8.4.1 Melvin Flux-branes

The above ansatz includes both the original four-dimensional Melvin flux-tube [179], as well as its generalization to higher dimensions and non-trivial dilaton [186][8]. The geometry of the original Melvin solution consists of the two-dimensional Lorentz invariant worldvolume of the flux-tube, the radial direction, and a transverse circle. We will call flux-branes Melvin-like if the flux-brane has the same cohomogeneity as the original four-dimensional solution. Thus we set $p+1 = D-2$ to obtain a $p = (D-3)$-dimensional flux-brane. The solution is given by:

$$\begin{aligned} ds^2 &= \Lambda^{\frac{4}{a^2(D-2)+2(D-3)}} \left(\eta_{\mu\nu} dx^\mu dx^\nu + dr^2\right) + \Lambda^{\frac{2(6-2D)}{a^2(D-2)+2(D-3)}} r^2 d\varphi^2, \\ e^{2\phi} &= \Lambda^{-\frac{4a(D-2)}{a^2(D-2)+2(D-3)}}, \qquad F_{p+1} = E \ \mathrm{vol}(\eta_{\mu\nu} dx^\mu dx^\nu), \end{aligned} \tag{8.23}$$

where Λ is given by

$$\Lambda = \left(1 + \frac{a^2(D-2)+2(D-3)}{16(D-2)} E^2 r^2\right). \tag{8.24}$$

Here we have imposed the gauge $\alpha = \beta$ which is common for these solutions. For these flux-branes of cohomogeneity-2, exact solutions can be found because the $(D-p-2)$-dimensional transverse space is simply S^1, which has no curvature.

[8] Our conventions differ from those of [186], in particular we are choosing to work with an electric $D-2 = p+1$-form as opposed to the dual magnetic 2-form.

For flux-branes of higher cohomogeneity the circle is promoted to a sphere, the curvature of which induces a coupling between the metric functions and makes the equations much harder to solve analytically [181].

Note that the magnetic dual of (8.23) involves a two-form Maxwell field. For $p = 1$ and the special value of the dilaton coupling $a = -\sqrt{2(D-1)/(D-2)}$, the action (8.2) is equivalent to pure gravity in $D+1$ dimensions (see Appendix 8.B). So for this value of a (in the dual magnetic frame), the magnetic dual of the above solution comes from dimensional reduction of a vacuum solution. In fact, it can be obtained from flat Minkowski spacetime by dimensionally reducing along a combination of a translation and a rotation in a perpendicular plane [187].

Our theorem is of limited applicability for this class of flux-branes for the following reason. Near $r = 0$, the backreaction of the flux-brane can be neglected and the spacetime looks flat. It is known that there are no vacuum black holes with horizon topology $\mathbb{R}^{D-3} \times S^1$, and so the stationary black holes excluded by the above theorem do not exist in the absence of flux.[9] In order to obtain flux-brane solutions that could in principle admit small black branes at their centre, the S^1 must be replaced with a higher dimensional sphere.

8.4.2 Higher Cohomogeneity Flux-branes

We now generalize the Melvin flux-branes to branes of higher cohomogeneity, so that the transverse space includes a sphere of dimension two or greater, while keeping the $p+1$-dimensional worldvolume to be Minkowski space. These

[9] It is possible that the non-standard asymptotics of the flux-brane geometries allow for these horizon topologies, i.e. that black branes of a large enough radius do exist in the flux-brane. Our theorem then implies that these black branes must not be stationary.

solutions have been studied before [181, 188, 189] and include the flux-brane solutions of string theory/M-theory for appropriate choices of the parameters (D, p, a): NS flux-branes correspond to $(D, p, a) = (10, 2, -1)$ and $(10, 6, 1)$; the RR flux-branes correspond $(D, a) = \left(10, \frac{4-p}{2}\right)$; and the two flux-branes of M-theory have $(D, p, a) = (11, 3, 0)$ or $(11, 6, 0)$. Here we review and extend the analysis of these solutions.

Electric Flux-tubes in $D = 5$

Perhaps the conceptually simplest generalization of the above flux-brane solutions is the case of a (non-dilatonic) electric flux-tube in $D = 5$. A flux-tube corresponds to $p = 1$, therefore our ansatz is

$$ds^2 = e^{2\alpha}\left(-dt^2 + dx^2\right) + e^{2\beta}dr^2 + e^{2\gamma}d\Omega_2^2, \qquad F_2 = E dx \wedge dt, \tag{8.25}$$

A convenient gauge choice comes from examination of the constraint equation (8.41). No derivatives of β appear, therefore if we impose a gauge by directly fixing $e^{2\gamma}$ to be a β-independent function (here we will use $e^{2\gamma} = r^2$), then the constraint can be used to algebraically solve for β and the system will reduce to a single ODE for α (it seems that the convenience of this gauge has not been appreciated before in the literature). One can scale E out of the equation since rescaling the coordinates t, x, r by λ rescales the metric by λ^2. Einstein's equation remains unchanged if we also rescale F_2 by λ. The resulting ODE for α is:

$$3z(4e^{4\alpha}+z^2)\alpha''+3(8e^{4\alpha}-5z^2)\alpha'-12z(-4e^{4\alpha}+z^2)(\alpha')^2+2z^2(6e^{4\alpha}-z^2)(\alpha')^3-4z=0, \tag{8.26}$$

where $z \equiv Er$.

We were unable to determine the general solution analytically, but a simple closed form solution does exist, and is

$$e^{2\alpha} = \sqrt{\frac{5}{6}}Er, \qquad e^{2\beta} = \frac{5}{2}, \qquad e^{2\gamma} = r^2. \tag{8.27}$$

This solution is clearly singular at $r = 0$ and hence is not of physical interest. Nevertheless, it is quite useful since it can be shown that this solution is an attractor solution for the large-r behaviour of general solutions [181]. To see this, linearise around the exact singular solution, $\alpha = \alpha_{\text{singular}} + \delta\alpha$. The solution to the linearised perturbation takes the form

$$\delta\alpha = r^{-1}\left[c_1 \sin(2\ln r) + c_2 \cos(2\ln r)\right], \tag{8.28}$$

where $c_{1,2}$ are constants of integration. For large r, the perturbation oscillates with a decaying envelope and asymptotes to the above exact singular solution, indicating that it is indeed an attractor.

The solution we are interested in is regular along the axis $r = 0$. We did not succeed in finding it analytically, but the equations can be solved numerically once the boundary conditions are supplied. The large-r behaviour is that of the attractor, and the small r behaviour is simply regularity at the origin. There will be a curvature singularity unless $e^{2\alpha} \to$ const, and $e^{2\beta} \to 1$. Expanding the equations in a power series around $r = 0$ yields

$$e^{2\alpha} = 1 + \frac{z^2}{9} + \frac{2z^4}{405} + O\left(z^6\right), \qquad e^{2\beta} = 1 + \frac{7z^2}{36} + \frac{61z^4}{6480} + O\left(z^6\right) \tag{8.29}$$

We have used the scaling symmetry of the Minkowski directions to set an overall constant to 1. The boundary condition required by regularity is then $A(0) = 1$, $A'(0) = 0$, where $A = e^{\alpha}$. In Fig. 8.1 we plot the numerical solution for this flux-tube. From the plot, the non-singular solution can be seen to asymptote to the attractor solution at large r.

This electric flux-tube is much better behaved asymptotically than the Melvin flux-branes. One can see from (8.23) that in the Melvin case, the S^1 in the transverse space shrinks to zero size as $r \to \infty$. In the current solution, the effect of the flux-tube on the asymptotic geometry is weaker, and the S^2 in the transverse space continues to grow asymptotically. However, the solution is still not asymptotically flat in the transverse directions. It is asymptotically a cone.

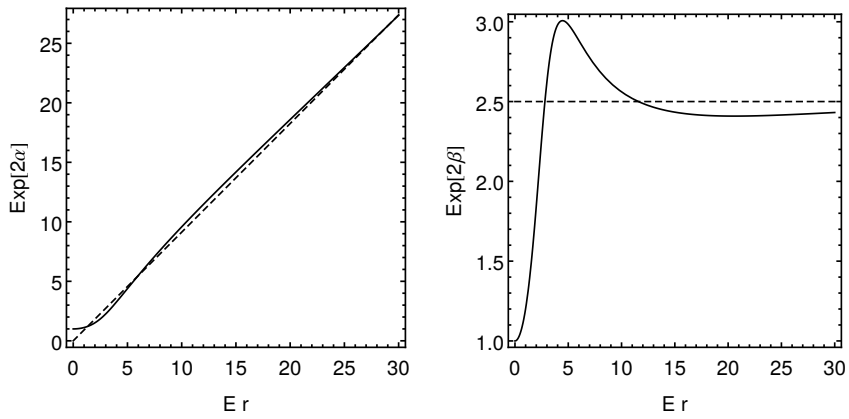

Figure 8.1: The metric functions $e^{2\alpha}$ (left panel) and $e^{2\beta}$ (right panel) for a non-dilatonic electric flux-tube in five dimensions ($D = 5$, $p = 1$, $a = 0$). The solid curves correspond to the numerical, non-singular solution, and the dotted curve corresponds to the singular attractor solution.

Applying the results of Sections 2 and 3 to this solution, we see that we cannot put a stationary black string inside the electric flux-tube. Stated intuitively, there is no way to prevent stress energy from flowing into the black string, which would

cause it to grow.

There is a simple physical interpretation of this result in terms of a stretched horizon[10]. The stretched horizon has finite electrical conductivity, so if one puts a black string along an electric field, a current will flow. Since the resistance is nonzero, the current will generate heat and cause the black string to grow. So a static black string is impossible. This is very similar to the discussion in [190] where an exact solution was found showing a black hole growing when an electric field is applied.

Kaluza-Klein flux-tube in $D = 5$

An interesting extension of this five-dimensional example is to include a dilaton, and consider it in the context of Kaluza-Klein theory. As before, we choose to impose the gauge $e^{2\gamma} = r^2$, and eliminate β using the constraint. Now the system has been reduced to two coupled ODE's in α and ϕ. As noted in Ref. [181], the dilaton equation of motion becomes a copy of the α equation of motion if we set

$$\phi = -\frac{3a}{2}\alpha. \tag{8.30}$$

Therefore the system has again been reduced to a single ODE, and the inclusion of the dilaton comes at no cost in complexity. We omit the presentation of the equation as it is rather lengthy. Once again, we find that the general solution must be solved for numerically, and that a simple, singular solution exists.

For the case $a = a_{\rm KK} = -\sqrt{8/3}$, the flux-tube can be uplifted to a vacuum solution of Einstein gravity (see Appendix 8.B). The flux-tube has been geometrized,

[10]We thank Juan Maldacena for suggesting this.

and the six-dimensional line element is now

$$ds_6^2 = e^{-3\alpha}\left(dy + Exdt\right)^2 + e^{3\alpha}\left(-dt^2 + dx^2\right) + e^{\alpha+2\beta}dr^2 + e^{\alpha+2\gamma}d\Omega_2^2. \qquad (8.31)$$

where we have chosen the gauge $A = Exdt$. While the metric (8.31) has three translational symmetries, they do not all commute. The Killing fields include $\partial/\partial t, \partial/\partial y$, and $\partial/\partial x - Et\partial/\partial y$. This is a timelike version of the Bianchi Type II symmetries of a homogeneous anisotropic cosmology. To gain some insight into this Ricci-flat solution, we can examine its large-r behaviour, which is governed by the singular attractor solution:

$$e^{2\alpha} = \left(\frac{3}{2}\right)^{1/4}(Er)^{1/2}, \qquad e^{2\beta} = \frac{27}{16}, \qquad e^{2\gamma} = r^2. \qquad (8.32)$$

Note that the KK circle is pinching off at infinity.

Since one cannot put a stationary black string in the five-dimensional flux-tube, one cannot put a stationary black two-brane in this vacuum solution. One can see this directly in six-dimensions, by deriving the following contradiction. Adding a stationary uniform black two-brane would produce a metric of the following form:

$$ds_6^2 = g_{yy}\left(dy + Exdv\right)^2 + h\left[-fdv^2 + 2dvdr\right] + g_{xx}dx^2 + r^2d\Omega \qquad (8.33)$$

where v is an ingoing null coordinate, and f vanishes at some radius r_0 denoting the horizon. The metric functions g_{xx}, g_{yy}, h depend only on r. The vector $\ell = \partial/\partial v - Ex\partial/\partial y$ is null on the horizon but it is not a Killing vector. So the six-dimensional spacetime does not have a Killing horizon. One can show that the

vector ℓ is tangent to a null geodesic, and has zero expansion, but nonzero shear. This violates the Raychaudhuri equation (8.1) and shows that the assumption of a stationary solution is inconsistent with the field equations. To see why the shear is nonzero, consider a small bundle of light rays extended in the x and y directions with thickness $\Delta x, \Delta y$. Starting at $v = v_0$, this bundle has a rectangular cross-section. Under evolution by ℓ, the rectangle gets distorted with geodesics pushed forward in the y direction by an amount proportional to x. This produces shear.

This argument is a Lorentzian version of the one given by Iizuka et al [191] who consider five dimensional black holes having Bianchi symmetry on the horizon. They show that for Bianchi types II, VI_0, or VII_0, if $\partial/\partial v - \ell$ is not a Killing field, then the shear will be nonzero and the solution cannot be stationary.

General Case

Having studied five-dimensional flux-tubes we now discuss the general case. Much of the above analysis carries over in higher dimensions. The gauge $e^{2\gamma} = r^2$ is imposed, and the constraint equation is used to algebraically solve for β. The system now only involves two coupled and undetermined functions, α and ϕ. As in the five-dimensional dilatonic flux-brane, the ϕ equation of motion becomes identical to the α equation of motion after a rescaling [181] [11]

$$\phi = -\frac{a(D-2)}{(D-p-2)}\alpha. \tag{8.34}$$

[11] As Ref. [181] worked with the Hodge dual picture, their expression is related to ours, (8.34), via $p+1 \to 10-(p+1)$.

Therefore the equations of motion for this general ansatz have been reduced to a single ODE, the presentation of which we omit as it is quite long. As before a simple analytic family of singular solutions exists:

$$e^{2\alpha} = \left[\frac{(2+a^2)(D-2)+2p(D-2)-2p^2}{4(D-2)(D-p-3)}\,(Er)^2\right]^{\frac{2(D-p-2)}{a^2(D-2)+2(1+p)(D-p-2)}}, \tag{8.35}$$

$$\begin{aligned} e^{2\beta} = {} & \frac{(a^2(D-2)(D-p-3)+2(p+1)(D-p-2)^2)}{(D-p-3)\left(a^2(D-2)+2(p+1)(D-p-2)\right)^2} \\ & \times \left(a^2(D-2)+2\left(D(p+1)-(p+1)^2-1\right)\right). \end{aligned} \tag{8.36}$$

These solutions have been noticed by numerous authors for various values of the parameters (D, p, a) [181, 188, 189]. Although clearly singular at $r = 0$, these exact solutions are still quite useful as they are often attractors for the large-r behaviour of more general solutions [181]. As before, this can be determined by linearising around the exact solution, $\alpha = \alpha_{\text{singular}} + \delta\alpha$. The solution to the linearised perturbation takes the form

$$\delta\alpha = r^{-q}\left(c_1 \sin(\nu \ln r) + c_2 \cos(\nu \ln r)\right), \tag{8.37}$$

where $c_{1,2}$ are constants of integration, and q, ν are constants depending on (D, p, a). If both $q, \nu^2 > 0$, then the perturbation oscillates with a decaying envelope and asymptotes to the above exact singular solution for large r, indicating that it is an attractor. We have checked the singular solution is an attractor for the following solutions: the two 5d flux-tubes presented above, and all of the flux-branes of string theory/M-theory with co-dimension greater than two.

The solutions we are interested in are, of course, nonsingular at the origin. We did not succeed in finding analytic non-singular solutions, but the equations can be solved numerically, just as they were in the $D = 5$ cases considered above. We therefore see that there is a large class of non-singular flux-brane solutions for which our theorem applies, including flux-branes that appear in string/M-theory. These flux-branes cannot be "blackened" without introducing time-dependence[12].

8.5 Discussion

We have shown that one cannot put stationary black branes inside flux-branes. This was rigorously established for uniform black branes or black branes that are nonuniform in compact directions. For the case of black strings inside a flux-tube, we have given numerical evidence that this result extends to the noncompact case, and we expect that it extends to all cases where the horizon is noncompact.

A translationally invariant black string (or black brane) is subject to Gregory-Laflamme instabilities. One can stabilize it by compactifying the direction it is extended along. Our result shows that even when it is stable, the black string cannot remain stationary inside a flux tube.

An interesting open question in this compactified context is the following[13]. In vacuum gravity with one direction compactified on a circle, there is a well studied black hole - black string transition in the space of static solutions (see [192] and

[12]Here a comment is in order: The flux-brane solutions are qualitatively different from the p-brane solutions of string theory. The p-branes are singular supergravity solutions that possess degrees of freedom associated with their worldvolume, whereas the flux-branes are completely non-singular (the simple family of singular solutions is not physical), and have no worldvolume degrees of freedom. Therefore, the inability to "blacken" the flux-branes carries no implications for a worldvolume theory.

[13]We thank Henriette Elvang for raising this question.

references therein). One can start with a small spherical black hole and increase its size. One obtains a continuous family of solutions in which the spherical black hole gets distorted when it approaches the size of the circle. It then makes a transition to a nonuniform black string and eventually turns into a uniform black string. Now suppose we start with an electric flux-tube wrapping the compact direction. As we argued in section 2, a small static spherical black hole should still exist. We can continuously increase the size of this black hole and it is likely that there will again be a transition to a nonuniform black string. But we have seen that the nonuniform black string cannot be static. So when does the static solution stop existing? The intuitive picture of the electric field inducing currents on the stretched horizon given in section 4.2.1 suggests that it will not be until the nonuniform black string forms.

What is the analog of this intuitive picture for higher rank forms? Can one understand the absence of static black two-branes inside F_3 flux vacua, by postulating that the stretched horizon contains strings which move when placed inside this flux? This seems likely since one can dimensionally reduce a flux p-brane along $p-1$ directions to obtain a flux-tube. We have argued that one cannot put a static black string in this flux-tube due to the existence of currents on the stretched horizon which imply the existence of charged particles. From the higher dimensional standpoint, these charged particles are charged $p-1$ branes. We should emphasize that there is no actual charged matter in the spacetime. These charged objects arise in an effective description of form fields interacting with black holes. This property of stretched horizons deserves further investigation.

Acknowledgements

It is a pleasure to thank H. Elvang, V. Hubeny, J. Maldacena, and A. Puhm for discussions. This work was supported in part by NSF grant PHY12-05500, by NSF grant PHYS-1066293 and the hospitality of the Aspen Center for Physics. It was also supported in part by JSPS KAKENHI Grants No. 26400280.

Appendix

8.A Equations of Motion

Here we present the equations of motion (8.3) for the ansatz (8.21). The form equations are already satisfied as noted above. The three independent (trace reversed) Einstein equations are

$$\begin{aligned} R^{\mu}{}_{\nu} &= \left[-\left[\alpha'' - \alpha'\beta' + (p+1)(\alpha')^2 + m\alpha'\gamma'\right] e^{-2\beta} + \lambda_{p+1} e^{-2\alpha}\right] \delta^{\mu}_{\nu}, \\ &= \tau^{\mu}{}_{\nu} = -\frac{m}{2(D-2)} E^2 e^{a\phi - 2(p+1)\alpha} \delta^{\mu}{}_{\nu}. \end{aligned} \tag{8.38}$$

$$\begin{aligned} R^{r}{}_{r} &= \left[-(p+1)\alpha'' - m\gamma'' + (p+1)\alpha'\beta' + m\beta'\gamma' - (p+1)(\alpha')^2 - m(\gamma')^2\right] e^{-2\beta} \\ &= \tau^{r}{}_{r} = \frac{1}{2} e^{-2\beta}(\phi')^2 + \frac{p}{2(D-2)} E^2 e^{a\phi - 2(p+1)\alpha}. \end{aligned} \tag{8.39}$$

$$R^i{}_j = \left[-\left[\gamma'' - \beta'\gamma' + m(\gamma')^2 + (p+1)\alpha'\gamma'\right] e^{-2\beta} + \lambda_m e^{-2\gamma}\right] \delta^i{}_j \tag{8.40}$$
$$= \tau^i{}_j = \frac{p}{2(D-2)} E^2 e^{a\phi - 2(p+1)\alpha} \delta^i{}_j.$$

where $m = D - p - 2$ and primes indicate derivatives with respect to r. A very useful linear combination of these equations is the "Hamiltonian constraint"

$$G^r{}_r = e^{-2\beta}\left[\frac{1}{2}m(m-1)(\gamma')^2 + \frac{1}{2}p(p+1)(\alpha')^2 + m(p+1)\alpha'\gamma'\right] \tag{8.41}$$
$$- \frac{m}{2}\lambda_m e^{-2\gamma} - \frac{1}{2}(p+1)\lambda_{p+1} e^{-2\alpha}$$
$$= T^r{}_r = \frac{1}{4}(\phi')^2 e^{-2\beta} + \frac{E^2}{4} e^{a\phi - 2(p+1)\alpha}.$$

Lastly, the dilaton equation of motion is

$$e^{-(p+1)\alpha - \beta - m\gamma}\partial_r\left(e^{(p+1)\alpha - \beta + m\gamma}\partial_r\phi\right) + \frac{aE^2}{2} e^{a\phi - 2(p+1)\alpha} = 0. \tag{8.42}$$

8.B Uplift of Kaluza-Klein Electric Flux-tubes

If the dilatonic coupling in (8.2) takes the special value

$$a = a_{\rm KK} = -\sqrt{\frac{2(D-1)}{(D-2)}}, \tag{8.43}$$

and $p = 1$ (so F_{p+1} is a standard Maxwell field) then a solution of the Einstein-Maxwell-dilaton theory (8.2) in D dimensions uplifts to a solution of the vacuum

Einstein equations in $D+1$ dimensions. The uplifted line element is

$$ds^2_{D+1} = e^{-\sqrt{\frac{2(D-2)}{(D-1)}}\phi}\left(dy + A_\mu dx^\mu\right)^2 + e^{\sqrt{\frac{2}{(D-2)(D-1)}}\phi} ds^2_D \tag{8.44}$$

Here A is the 1-form gauge potential related to the field strength via $F = dA$.

Chapter 9

Localised Anti-Branes in Flux Backgrounds

9.1 Introduction

There has been much recent work on the study of anti-branes in flux backgrounds.[1] This interest is historically motivated by the work of Kachru, Pearson, and Verlinde (KPV) [168] who found that a small number of anti-D3 branes placed at the tip of the Klebanov-Strassler (KS) solution [63] would expand into a metastable NS5 brane. The NS5 brane would then eventually decay via tunnelling, although its lifetime could be tuned to be parametrically long. This mechanism has led to a number of interesting applications, including the construction of de Sitter (dS) compactifications of string theory in the KKLT scenario [166], holographic duals of dynamical supersymmetry breaking [166, 194, 195], and non-

[1] For a recent review, including a comprehensive list of references, see [193].

extremal black hole microstate geometries [196, 197].

Given these varied and important applications, it is of obvious interest to construct the full backreacted NS5 brane solution and to study its properties. Unfortunately, such a solution would depend non-trivially on two coordinates, leading to a complicated non-linear PDE problem that is quite intractable. As a result, the backreaction of smeared anti-D3 branes added to the tip of the KS solution was studied instead, and unexpected singularities in the 3-form field strengths were found at the location of the anti-branes [198, 199, 200, 201, 202]. This prompted many additional investigations, the results of which all point to the fact that singularities generically arise when anti-branes are added to flux backgrounds in both string theory and M-theory [203, 204, 205, 206].[2] Importantly, these studies also found that the singularities are not artefacts of either linearisation in the anti-brane charge nor smearing.

The physical interpretation of these singularities has been the source of much debate. String theory is known to resolve many singularities in gravity. Perhaps one of the most well-known mechanisms for resolving singularities is through brane polarisation, also known as the Myers effect [207], which was shown to resolve the singularity associated with a mass deformation of $\mathcal{N} = 1^*$ $SU(N)$ supersymmetric Yang-Mills by Polchinski and Strassler (PS) [208]. Another famous example concerns the KS solution itself, which can be interpreted as the resolution of the singularity present in the Klebanov-Tseytlin [209] solution. Not all singularities are resolved by string theory however, and in fact singular solutions play an important role in constraining the theory by, for example, ruling out negative mass

[2]Here and throughout this article, by anti-brane we mean that the brane is not mutually BPS with respect to the flux background.

states [169].

The singularities associated with anti-branes in flux backgrounds throws the fate of the KPV metastable state and its many applications into doubt. Thus far, all attempts to resolve the singularities via polarisation have either failed [210, 211], or partially succeeded [212, 213], but have also indicated the presence of repulsive instabilities which might destabilize the metastable states.[3] As the backreaction of localised anti-branes in flux backgrounds has been too difficult to tackle directly, these authors cleverly extracted the polarisation potentials from the backreacted smeared solutions.

A widely held view, dubbed the Gubser criterion [170], is that if a singularity can be shielded behind a finite temperature horizon, then it is physical and resolvable by some (perhaps unknown) mechanism in string theory. According to this criterion, there is then an important relationship between the space of black brane solutions and anti-brane singularities. For a horizon to shield an anti-brane singularity the solution should asymptote to the flux background of interest, for example KS, and the horizon should carry negative charge. Thus far all attempts (including both analytic arguments and the numerical construction of solutions) to hide *smeared* anti-brane singularities behind horizons have failed, and only black branes with positive charge have been found [215, 216]. Additionally, a no-go theorem has been recently formulated which excludes non-singular solutions corresponding to anti-branes in flux backgrounds at both zero and finite

[3] An example where polarisation does resolves the singularity without any repulsive instability is [214] for the case of AdS_7 flux vacua. The polarisation relied on the curvature of the worldvolume AdS_7, and the flux backgrounds we consider here will have no curvature on the worldvolume.

temperature, regardless of smearing [206]. [4]

If the interpretation of the smeared anti-brane singularities is that they are unphysical and unable to be resolved as these many results suggest, then there are dramatic consequences for the de Sitter landscape, metastable non-SUSY field theory states, and the construction of non-extremal microstate geometries. It also raises a vexing contradiction with the original KPV calculation [168]–namely, where did this calculation go wrong? One interesting suggestion is that the probe approximation severely underestimated the amount of flux clumping caused by charge screening, and that the branes annihilate against the flux through classical time evolution [204, 217, 218].

In this work, we will provide evidence that the metastable states do in fact exist, and show that the singularity of anti-branes in flux backgrounds can be resolved. We will accomplish this by constructing, in a linear approximation, localised black branes of either sign charge in flux backgrounds that approximate the IR of KS in Type IIB string theory, and the analogous solution in M-theory, the Cvetič-Gibbons-Lü-Pope (CGLP) solution [219]. At first glance this result appears to directly contradict the no-go theorem of [206], however it has a loop-hole which our constructions make use of. The existence of these solutions demonstrates that the anti-brane singularities can be shielded behind a smooth horizon. According to the Gubser criterion then, *the anti-brane singularities are physical and are resolved by string theory.* It therefore appears that, in contrast with the title of [215], horizons can and do in fact save the landscape, once the smearing approximation

[4] It is worth noting that the inability to hide a singularity behind a horizon does not necessarily imply that the singularity is physically unacceptable. Examples of physically acceptable singular solutions that cannot support finite temperature include vacua on the Coulomb branch of $\mathcal{N} = 4$ SYM [170].

is dropped![5]

Insight into the nature of the resolution can be gained by considering the extremal limit. As the charge is made large and negative, the flux at the horizon grows without bound. In the extremal anti-brane limit, the flux is found to diverge in a way known to be resolved in certain cases by brane polarisation in a non-supersymmetric version of Polchinski-Strassler. Although we cannot directly evaluate this possibility without going to higher order in our approximation scheme, we will argue that indeed polarisation resolves the singularity. As mentioned above, this resolution mechanism was previously argued to not apply [210, 211, 212, 213], and we will therefore attempt to explain the discrepancy as a consequence of smearing. If, however, polarisation does not resolve the singularity, then either there is some new resolution mechanism yet to be discovered, or else the Gubser criterion fails and being able to shield a singularity behind a horizon is not a sufficient criterion for accepting it as physical.

The approach taken here, where the number of anti-branes is taken to be large enough that the gravity description is valid, is complementary to the recent analysis of [220], who argued that for at least a single anti-brane, the physics could be well understood from the effective field theory of the brane worldvolume theory. It therefore seems that for both a single anti-brane and many, KKLT [166] remains a valid mechanism for constructing metastable dS vacua in string theory.

This paper is organized as follows. In Sec. 9.2 we construct solutions corresponding to D3 branes at both finite and zero temperature localised in a toy flux background which approximates the IR of the KS solution. The analogous

[5]It should be emphasized that the anti-brane singularities themselves are not artefacts of smearing.

problem of anti-M2 branes in a toy background which approximates the CGLP solution of M-theory is quite similar, and all the main conclusions of the Type IIB case carry over. Accordingly, we relegate its treatment to Appendix 9.C. We close with concluding remarks in Sec. 9.3.

9.2 D3 Branes in Type IIB Flux Backgrounds

One of the major obstacles in the problem of anti-D3 branes in KS has been the complicated geometry of the deformed conifold which has discouraged attempts to study inhomogeneous or localised solutions. Therefore, in this section we will study localised D3 and anti-D3 branes in a toy flux background which approximates the IR of the KS solution. As we will argue below, this serves as an excellent approximation for the solution corresponding to branes at the tip of the KS solution. We first introduce the background and argue that it can be used to study the problem of anti-branes in KS, and then review smeared solutions before finally constructing localised solutions.

9.2.1 A Toy Model of the Klebanov-Strassler Flux Background

The Klebanov-Strassler solution [63] is the supersymmetric Type IIB supergravity solution corresponding to fractional D3 branes at the tip of the deformed conifold. Recall that the conifold is a six-dimensional Ricci-flat space which asymptotically takes the form of the cone $ds_6^2 \sim dr^2 + r^2 ds^2_{\mathbb{T}^{1,1}}$[6], and smoothly

[6]Here $\mathbb{T}^{1,1}$ is the coset space $SU(2) \times SU(2)/U(1)$.

caps off at the tip, where the geometry consists of a finite-sized S^3 and a shrinking S^2. A simple exact solution of Type IIB supergravity which serves as a toy model relevant for approximating the IR of KS is

$$\begin{aligned} ds^2 &= H^{-1/2}\left(-dt^2+dx_1^2+dx_2^2+dx_3^2\right)+H^{1/2}\left(dr_1^2+r_1^2d\Omega_2^2+\sum_{i=1}^{3}dy_i^2\right), \quad (9.1)\\ F_5 &= (1+\star)\mathcal{F}_5, \qquad \mathcal{F}_5=\varepsilon_F dH^{-1}\wedge dt\wedge dx^1\wedge dx^2\wedge dx^3,\\ G_3 &= F_3-iH_3 = m\left(dy^1\wedge dy^2\wedge dy^3-i\varepsilon_F r_1^2 dr_1\wedge d\Omega_2\right), \end{aligned}$$

with all other fields zero. The warp factor is

$$H = 1+\frac{a_0}{r_1}-\frac{m^2}{6}r_1^2. \quad (9.2)$$

The complex 3-form G_3 is (anti)-imaginary self-dual, that is $\star_6 G_3 = i\varepsilon_F G_3$, where $\star_6$ is the Hodge dual on the 6-dimensional transverse space. A solution exists for either sign of the flux, $\varepsilon_F = \pm 1$, and the constant a_0 is proportional to the number of (anti)-D3 branes smeared over the y directions, which for the purpose of approximating KS, we set to zero, $a_0 = 0$. The constant m controls the amount of flux and is analogous to the M constant in the KS solution. This solution is related via T-duality to the "massive-D6" solution of massive IIA supergravity found in [221], and was used as a toy model for KS in the context of adding smeared anti-branes to the solution by [210, 216].

That this solution approximates the IR of KS can be seen as follows. The geometry near the "tip", $r_1 \to 0$, consists of a shrinking S^2 times $\mathbb{R}^3$, which is very similar to the shrinking S^2 times S^3 geometry of the near-tip KS solution.

In both solutions F_3 near the tip is simply the volume form on the non-shrinking space, either S^3 or $\mathbb{R}^3$. Also, for each solution H_3 contains a term proportional to the volume form on the shrinking space (in the toy flux background, this is the only term present). Therefore, the IR of both solutions is seen to be quite similar–the essential difference is that one solution contains an S^3 at the tip and the other an $\mathbb{R}^3$.

In this paper we will be primarily interested in approximating the solution corresponding to anti-D3 branes localised at both the tip of the deformed conifold and at a point on the S^3. Since the branes sit at a single point, the curvature of the S^3 is negligible, and therefore the near-brane solution will be very similar to the analogous solution in the toy flux background (9.1). If the branes are blackened by turning on a small temperature, then they will no longer be localised at a single point, but for sufficiently small temperature their Schwarzschild radius will be small compared to the curvature of the S^3 and the toy flux background will remain an excellent approximation for KS in the vicinity of the branes. For the sake of constructing these solutions, it will be convenient to introduce spherical coordinates for the y^i,

$$\sum_{i=1}^{3} dy_i^2 = dr_2^2 + r_2^2 d\widetilde{\Omega}_2^2, \qquad dy^1 \wedge dy^2 \wedge dy^3 = r_2^2 dr_2 \wedge d\widetilde{\Omega}_2, \tag{9.3}$$

where $d\widetilde{\Omega}_2^2$, $d\widetilde{\Omega}_2$ are the line element and volume form for a second, distinct unit S^2.

The toy flux backgroud (9.1) has a disturbing property. For large r_1, the warp factor H is large and negative, indicating that at some point it passes through

zero. For the case of interest, $a_0 = 0$, this occurs for $r_1 = \sqrt{6}/m$. We will argue that this naked singularity and strange asymptotics are actually irrelevant for the present purpose of studying localised anti-branes in flux backgrounds. Firstly, the singularity occurs at a radius that can be taken much larger than the radius of the localised solution, and for small radii the toy flux background approximates the KS solution. Secondly, it is shown in Appendix 9.A that although the supergravity description is singular, strings are in fact well behaved and perfectly non-singular at the point $H = 0$ [7].

9.2.2 Analogue of the KPV Calculation

In this section we briefly review the KPV [168] calculation, in which a metastable NS5 brane is found to exist in the KS solution. We then repeat the analysis for the toy flux background introduced above, (9.1). Although there are important differences between the two cases, the main conclusion remains the same, namely that the probe calculation indicates that a static, expanded brane configuration should exist, strengthening the argument of the previous section that localised branes in the IR of KS are be well modelled by the analogous solution in the toy flux background.

In KPV, the potential for a probe NS5 brane carrying p units of anti-D3 charge was computed. The brane was embedded at the tip of the KS flux background as follows: it filled out the four-dimensional Minkowski space and wrapped an S^2 inside the finitely sized S^3 at the tip. Writing the line element on the S^3 as $d\chi^2 + \sin^2\chi^2 d\Omega_2^2$, the NS5 brane was localised at fixed χ, and the potential was

[7] This point was understood as a result of joint work with G. Horowitz and A. Puhm.

found in [168] to be proportional to

$$\Phi_{\rm KPV}(\chi) = \frac{1}{\pi}\left[\sqrt{b_0^4 \sin^4\chi + \left(\pi\frac{p}{M} - \chi + \frac{1}{2}\sin 2\chi\right)^2} - \chi + \frac{1}{2}\sin 2\chi\right], \qquad (9.4)$$

where $b_0^2 \approx 0.93266$, p is the anti-D3 charge, and M is the KS flux parameter. This potential is plotted in Fig. 9.1 for various values of p.

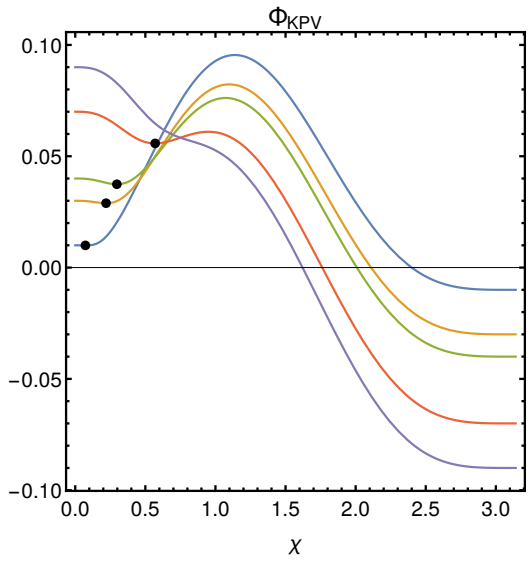

Figure 9.1: $p/M = 0.01, 0.03, 0.04, 0.07, 0.09$, from bottom to top. Metastable minima exist for $p/M \lesssim 0.08$, and are indicated by black dots.

For anti-branes ($p > 0$), the south pole $\chi = \pi$ is always the global minima. For $p/M \lesssim 0.08$ there is a second, metastable minima corresponding to a puffed-up NS5 brane. As p increases, the size of the wrapped S^2 increases from zero until a minima with a maximally-sized S^2 is attained for $p/M \simeq 0.08$. Brane flux-annihilation occurs either via tunnelling ($p/M \lesssim 0.08$) or through classical evolution by rolling down the potential hill ($p/M \gtrsim 0.08$).

For the present case of anti-branes in the toy flux background the analogous set-up would be that the branes are localised "at the tip" ($r_1 = 0$), as well as at the origin of the transverse $\mathbb{R}^3$ ($r_2 = 0$). For small enough radii of the wrapped S^2, the difference between an S^2 in S^3 or $\mathbb{R}^3$ should vanish, and the KPV potential should match the potential for the toy background. Since the KPV potential always has a minima in the limit of $p \to 0$, and in this limit the radius of the wrapped S^2 vanishes, the anti-branes at the tip of the KS solution should be excellently approximated by anti-branes at the tip of the toy flux background for p small enough (but large enough so that the gravity description is valid).

Although the potentials should agree for small radius, they will be quite different in the opposite limit of large radius. Since $\mathbb{R}^3$ is topologically trivial, the true minima corresponding to the south pole of the S^3 will not exist in the toy flux background, and in fact there should be no analogue of the KPV brane-flux annihilation mechanism where the wrapped S^2 tunnels from the metastable minima to the south pole.

Let us now turn to the calculation of the potential. The NS5 brane action is [8]

$$S = \mu_5 \int d^6\xi \left(-\det G_{||} \det\left(G_\perp + 2\pi\mathcal{F}_2\right)\right)^{1/2} + \mu_5 \int B_6. \tag{9.5}$$

Here $2\pi\mathcal{F}_2 = 2\pi F_2 - C_2$, with $F_3 = dC_2 = md\left(r_2^3/3\right) \wedge d\widetilde{\Omega}_2$, and $F_2 = (p/2)d\widetilde{\Omega}_2$ represents p units of anti-D3 charge carried by the NS5 brane worldvolume. The NS5 brane couples to B_6, where

$$\star H_3 = H_7 = dB_6 = -\frac{m\varepsilon_F}{H} d\left(\frac{r_2^3}{3}\right) \wedge d^4x \wedge d\widetilde{\Omega}_2. \tag{9.6}$$

[8] Here, and throughout this paper we set $g_s = 1$.

The potential is then found to be proportional to

$$\Phi = \frac{m^2}{\pi}\left[\sqrt{r_2^4 + \left(p\pi - \frac{mr_2^3}{3}\right)^2} - \frac{m\varepsilon_F}{3}r_2^3\right], \tag{9.7}$$

where the value of the warp factor at the tip, $H(r_1 = 0) = 1$, has been used. To compare with the KPV potential, it is useful to convert to the new flux parameter $m = \mu^{-1/2}$ and dimensionless coordinate $r_2 = \mu^{1/2}\rho$. Then for $\varepsilon_F = 1$, the behaviour of the two potentials near the tip is

$$\begin{aligned}\Phi_{\rm KPV} &\sim \frac{p}{M} - \frac{4}{3\pi}\chi^3 + \frac{b_0^4}{2\pi^2}\frac{M}{p}\chi^4 + \mathcal{O}(\chi^5), \\ \Phi &\sim \frac{p}{\mu} - \frac{2}{3\pi}\rho^3 + \frac{1}{2\pi^2}\frac{\mu}{p}\rho^4 + \mathcal{O}(\rho^7).\end{aligned} \tag{9.8}$$

There are two sources for the different coefficients. Firstly, deviations should be expected at high enough order for the simple reason that the geometries are different. Secondly, we have not taken care to ensure that the tip of the KS solution is parametrized identically to the tip of the toy flux background. The large ρ-behaviour of the toy flux background potential strongly differs from the KPV behaviour, and is

$$\Phi \sim \frac{3}{2\pi}\rho - \frac{p}{\mu} + \mathcal{O}(\rho^{-1}). \tag{9.9}$$

Since the potential is decreasing near $\rho = 0$, but increasing for large ρ, there must be a turning point at a real positive value of ρ *for all values of p!* In Fig. 9.2 this potential is plotted for $p/\mu = 1$.

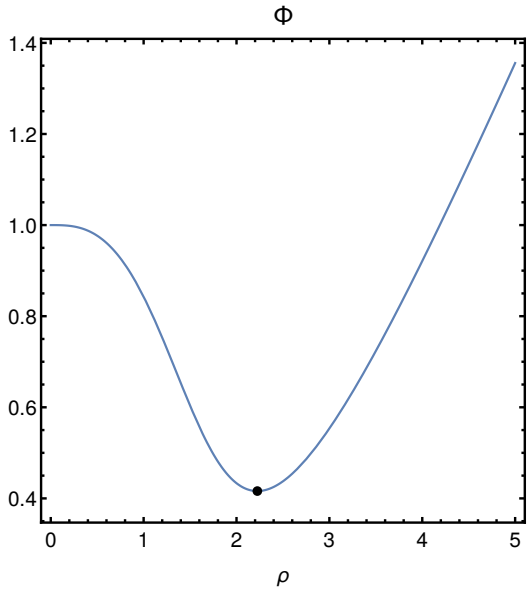

Figure 9.2: The probe potential Φ for $p/\mu = 1$. The global minima is indicated by a black dot. The key differences between the potential for the KS background and the toy flux background (9.1) are that the minima corresponding to an NS5 brane wrapping a finitely sized S^2 is 1) always present for the toy flux background, and 2) always the global minima as opposed to simply a metastable minima.

As expected, there are important global differences between the two potentials. The finite ρ-minima in the toy background always exists and is the global minima, and there is no possibility of brane-flux annihilation through either quantum tunnelling or classical evolution. However, for small p and small ρ, the KPV potential is qualitatively very similar to the potential for the toy background once the coordinates χ and ρ are identified, and a perturbatively stable, static expanded brane configuration exists in both solutions.

9.2.3 Smeared Branes

Before turning to the main focus of this paper, the construction of localised black branes in the toy flux background (9.1), we first discuss smeared solutions. In the extremal case, Ref. [210] found that the solution T-dual to smeared anti-D3 branes in the toy flux background possessed singular fluxes which were not resolved by brane polarisation. In the finite-temperature case, Ref. [216] formulated a no-go theorem excluding regular black hole solutions where the charge on the black hole is negative. These results strongly suggest that the singularity associated with *smeared* anti-branes in this flux background is simply unphysical and unable to be resolved.

In order to highlight the important differences between smeared and localised solutions, here we will approximately construct the solution corresponding to a positively charged smeared brane in the toy background. Near the brane the solution can be approximated as a linear G_3 flux perturbation of the thermal,

smeared D3 brane solution:

$$
\begin{aligned}
ds^2 &= H^{-1/2}\left(-f dt^2 + dx_1^2 + dx_2^2 + dx_3^2\right) + H^{1/2}\left(\frac{dr_1^2}{f} + r_1^2 d\Omega_2^2 + dy_1^2 + dy_2^2 + dy_3^2\right), \\
\mathcal{F}_5 &= \varepsilon_B \coth\beta\, dH^{-1} \wedge dt \wedge dx^1 \wedge dx^2 \wedge dx^3, \\
H &= 1 + \sinh^2\beta \left(\frac{r_+}{r_1}\right), \qquad f = 1 - \frac{r_+}{r_1}.
\end{aligned}
\tag{9.10}
$$

The boost parameter β characterises the charge of the brane, and we will take $\beta \geq 0$ and allow $\varepsilon_B = \pm 1$ to characterise the difference between positive and negative charge. The extremal limit is $\beta \to \infty$ while keeping $a_0 \equiv r_+ \sinh^2\beta$ fixed.

The most general ansatz for the perturbation consistent with the symmetries of the problem is

$$
G_3 = m\left(g_y dy^1 \wedge dy^2 \wedge dy^3 - i\, g_\Omega r_1^2 dr_1 \wedge d\Omega_2\right), \tag{9.11}
$$

where g_y, g_Ω are functions of r_1 only. The Bianchi constraint $dG_3 = 0$ fixes g_y to be a constant, which we choose to be $g_y = 1$. The linearised equation of motion $d \star G_3 + iG_3 \wedge F_5 = 0$ then becomes

$$
\partial_{r_1}\left(H^{-1} f g_\Omega - \varepsilon_B \coth\beta H^{-1}\right) = 0, \tag{9.12}
$$

which has the simple solution

$$
g_\Omega = f^{-1}\left(H c_0 + \varepsilon_B \coth\beta\right), \tag{9.13}
$$

with c_0 a constant of integration. First, consider the extremal case. The solution is

$$g_\Omega = c_0 \left(1 + \frac{a_0}{r_1}\right) + \varepsilon_B. \tag{9.14}$$

Regularity at the brane location requires $c_0 = 0$, in which case the flux has a definite imaginary self-duality (ISD) character: $\star_6 G_3 = i\varepsilon_B G_3$, where $\star_6$ is the Hodge operator on the transverse 6-dimensional space. Crucially, the flux is constrained to have the same self-duality sign as the brane charge. In fact, this solution just corresponds to adding ISD flux to the smeared brane solution (or AISD flux to the smeared anti-brane solution), i.e. it is simply a linearisation of the toy flux background (9.1) with the warp factor replaced by

$$H = 1 + \frac{a_0}{r} - \frac{m^2 r_1^2}{6}. \tag{9.15}$$

Suppose we took the opposite perspective and fixed the asymptotic value of the flux, rather than its behaviour near the brane source. Requiring the flux to have the opposite sign, $\star_6 G_3 = -i\varepsilon_B G_3$, fixes $c_0 = -2\varepsilon_B$, which causes the flux to diverge at $r_1 = 0$. This perturbation corresponds to the linearisation of the solution corresponding to anti-branes added to the toy flux background. These singularities were shown to not be resolved by polarisation in [210].

Next, consider the finite temperature case. Requiring regularity at the horizon fixes c_0 and the solution is simply

$$g_\Omega = \varepsilon_B \tanh \beta. \tag{9.16}$$

This perturbation corresponds to the linearisation of the positively charged smeared black brane in a flux background (which has not been constructed yet). The sign of the flux is constrained to be of the same sign as the brane charge, in agreement with the no-go theorems ruling out negative charged branes [216]. In fact, the later and more comprehensive no-go theorem of [206] correctly predicts the divergence associated with the negatively charged brane. If the constant c_0 had been taken to be any other value, including values that would yield negatively charged black branes, then the 3-form fluxes would diverge as $|H_3|^2 \sim f^{-1}$. This point will be important later.

Having reviewed the problem of smeared anti-branes in the toy background (9.1), we now turn to the central focus of this paper, the construction of localised black branes.

9.2.4 Localised Branes

Here we will construct the solution corresponding to localised D3 branes at the tip of the toy flux background (9.1) to linear order in the 3-form flux. Since the backreaction of the flux alters the asymptotics, this approximation is only valid in the vicinity of the branes. The approach we take is very similar to the one employed in [222] to approximate localised Schwarzschild black holes in the $AdS_p \times S^q$ solutions of string and M-theory.

As we are interested in finding solutions corresponding to localised D3 branes at the tip of this flux background, it will be useful to first recall the D3 brane

solution:

$$
\begin{aligned}
ds^2 &= H^{-1/2}\left(-f dt^2 + dx_1^2 + dx_2^2 + dx_3^2\right) + H^{1/2}\left(\frac{dr^2}{f} + r^2 d\Omega_5^2\right), \qquad (9.17)\\
\mathcal{F}_5 &= \varepsilon_B \coth\beta\, dH^{-1} \wedge dt \wedge dx^1 \wedge dx^2 \wedge dx^3,\\
H &= 1 + \sinh^2\beta \left(\frac{r_+}{r}\right)^4, \qquad f = 1 - \left(\frac{r_+}{r}\right)^4.
\end{aligned}
$$

As before, we will take $\beta \geq 0$ and allow $\varepsilon_B = \pm 1$ to characterise the difference between positive and negative charge. The extremal limit is $\beta \to \infty$ while keeping $r_0^2 \equiv r_+^2 \sinh\beta$ fixed. The case $\beta = 0$ corresponds to no charge at all, in which case the solution is simply $\text{Schw}_7 \times \mathbb{R}^3$. A useful coordinatization of the 5-sphere is

$$
d\Omega_5^2 = d\psi^2 + \sin^2\psi d\Omega_2^2 + \cos^2\psi d\widetilde{\Omega}_2^2, \qquad (9.18)
$$

which connects to the coordinates employed in the toy flux background (9.1) upon identifying $r_1 = r\sin\psi$, $r_2 = r\cos\psi$.

We now wish to consider a linear G_3 perturbation of the D3 brane solution. Because we wish to consider localised branes in the flux background, we will require the G_3 flux to approach the flux background form asymptotically:

$$
\begin{aligned}
\lim_{r\to\infty} G_3 &= m\left(r_2^2 dr_2 \wedge d\widetilde{\Omega}_2 - i\varepsilon_F r_1^2 dr_1 \wedge d\Omega_2\right), \qquad (9.19)\\
&= mr^2\left(\cos^2\psi\left(\cos\psi dr - r\sin\psi d\psi\right) \wedge d\widetilde{\Omega}_2 - i\varepsilon_F \sin^2\psi\left(\sin\psi dr + r\cos\psi d\psi\right) \wedge d\Omega_2\right).
\end{aligned}
$$

Using this asymptotic form as a guide, a suitable ansatz for the perturbation is

$$\begin{aligned} G_3 = & mr^2 \cos^2\psi \left(g_1 \cos\psi dr - g_2 r \sin\psi d\psi\right) \wedge d\widetilde{\Omega}_2 \\ & - i\varepsilon_F m r^2 \sin^2\psi \left(g_3 \sin\psi dr + g_4 r \cos\psi d\psi\right) \wedge d\Omega_2. \end{aligned} \tag{9.20}$$

As in [222], we find that the perturbation functions can be taken to be simply functions of r only. The Bianchi constraint $dG_3 = 0$ is satisfied for

$$g_2 = g_4, \qquad g_1 = g_3 = \frac{1}{3} r^{-2} \partial_r \left(r^3 g_4\right).$$

The linearised equation of motion $d\star G_3 + iG_3 \wedge F_5 = 0$ then reduces to the simple ODE [9]

$$r^2 f H g_4'' + \left(r^2 H f' - r^2 f H' + 7 r f H\right) g_4' + 3\left(H\left(r f' + 3f - 3\right) + r H'(\varepsilon \coth\beta - f)\right) g_4 = 0, \tag{9.21}$$

where $'$ indicates derivative with respect to r, and we have introduced $\varepsilon = \varepsilon_F \varepsilon_B$. Note that the perturbation equation only depends on the relative sign of the charge of the brane and flux background. For $\varepsilon = 1$ they are aligned, and for $\varepsilon = -1$ they are anti-aligned. We will solve this equation separately for the non-extremal and extremal cases.

[9] A similar equation was derived in [223] in the context of studying finite temperature effects in Polchinski-Strassler polarisation. They were not concerned with matching the solution to a flux background, and therefore dropped the asymptotic region (the overall constant in H).

Non-Extremal Case

Unfortunately, we were unable to find analytic solutions for the general non-extremal case, and will therefore turn to numerical methods. To facilitate the numerical evaluation, convert to the compactified coordinate $x = (r_+/r)^4$, for which the equation becomes

$$\partial_x^2 g_4 + \left(\frac{1 + x + x(3-x)\sinh^2\beta}{2x(x-1)\left(1 + x\sinh^2\beta\right)} \right) \partial_x g_4 + \left(\frac{6\varepsilon \sinh 2\beta - 3 + 3(3x-4)\sinh^2\beta}{16x(x-1)\left(1 + x\sinh^2\beta\right)} \right) g_4 = 0. \tag{9.22}$$

The boundary conditions we desire are that the perturbation approaches the form of the flux background at infinity $g_4(x = 0) = 1$, and that the perturbation be regular at the horizon. By expanding g_4 in a power series around $x = 1$, this last condition can be seen to be equivalent to

$$\left[\frac{3}{16} \left(1 - 4\,\varepsilon \tanh\beta\right) g_4 - \partial_x g_4 \right]_{x=1} = 0. \tag{9.23}$$

We solved (9.22) numerically, and in Fig. 9.3 a typical solution is plotted.

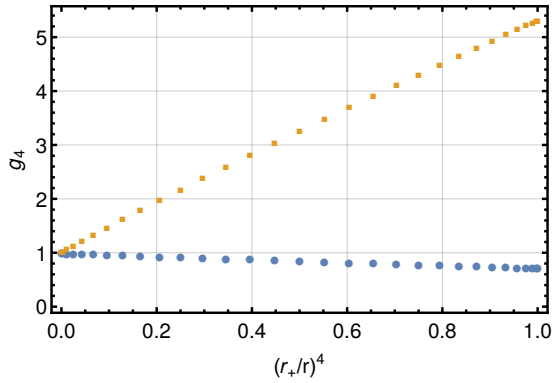

Figure 9.3: The perturbation function g_4 for $\beta = 1$ and $\varepsilon = 1$ (lower curve) and $\varepsilon = -1$ (upper curve). Note that the flux at the horizon, $(r_+/r)^4 = 1$, is significantly larger for the anti-aligned $\varepsilon = -1$ case.

We find, remarkably, that a solution exists *for both signs of the charge!* This is the central result of this paper. When the charges are anti-aligned, the flux at the horizon is significantly larger than the case when they are aligned, as might have been expected. The norm of the flux at the horizon is

$$|G_3|^2 = 6m^2 \frac{g_4(r_+)^2}{\cosh^3 \beta}. \tag{9.24}$$

In Fig. 9.4 the quantity $g_+ \equiv g_4(r_+)/\cosh^{3/2}\beta \propto |G_3|$ is plotted as a function of β for both signs of ε. For large positive charge, the flux at the horizon vanishes, while for large negative charge it grows without bound. [10]

[10]Of course, for large enough $|G_3|$ the linear approximation will break down and the backreaction will become non-negligible.

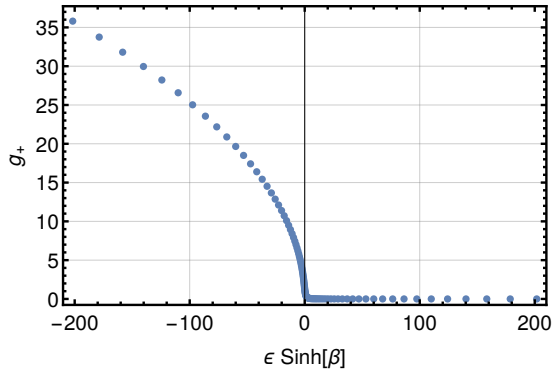

Figure 9.4: The value of the rescaled perturbation g_+ at the horizon. As extremality is approached, the flux either vanishes ($\varepsilon = 1$), or diverges ($\varepsilon = -1$). Recall that our convention is that $\beta \geq 0$ always. Fitting the data indicates that $g_+(r_+) \sim e^{\beta/2}$ as $\beta \to \infty$ for $\varepsilon = -1$, which corresponds to $g_4(r_+) \sim e^{2\beta}$.

Next, we are obliged to conduct a few checks on our calculation and to compare it with previous results. Firstly, an analytic solution can be found for the special case of $\beta = 0$:

$$g_4(x) = {}_2F_1\left(-\frac{3}{4}, \frac{1}{4}; -\frac{1}{2}; x\right) - \left(\frac{2\Gamma\left(\frac{3}{4}\right)\Gamma\left(\frac{7}{4}\right)}{\Gamma\left(\frac{1}{4}\right)^2}\right) x^{3/2}\, {}_2F_1\left(\frac{3}{4}, \frac{7}{4}; \frac{5}{2}; x\right). \quad (9.25)$$

Comparing this analytic expression against the numerical solution provides a useful check on the numerics which is passed excellently.

Secondly, as in [222], even though a static and non-singular perturbation has been found, because the flux does not vanish at the horizon it could be the case that stress-energy is flowing across the horizon and that the solution is not consistent with the Raychaudhuri equation, which requires that the energy flux across a static horizon must vanish. Letting $k^a = (\partial/\partial t)^a$ denote the null generators of the horizon, it is easy to verify that $T_{ab}k^a k^b = 0$, as F_5 is the only flux with t-legs, and is uncorrected at this order: $T_{ab}k^a k^b \propto (F_5)_{acdef}(F_5)_b{}^{cdef}k^a k^b = 0$.

As mentioned in the Introduction, this result appears to violate the recent no-go theorem of [206], and therefore some comments are in order. This theorem has a number of loop-holes. They are: (a) it could be that the boundary term does not satisfy their Eq. 4.24, (b) that $C(M_0, T)$ is not analytic [11], and (c) it could be the case that singular terms conspire to cancel. Unfortunately, due to our approximation scheme wherein the solution is only known near the branes, we cannot evaluate options (a) and (b). We will however argue that option (c) is the relevant loop-hole.

Recall the perturbation of the smeared black brane (9.13). The symmetries of the problem result in a single integration constant, which for general values lead to a singular flux $|H_3|^2 \sim f^{-1}$. Only for a particular choice of the constant do different singular terms cancel to make a regular perturbation. This cancellation of singular terms is actually standard practice in constructing hairy black hole solutions–unless the boundary conditions are chosen to make the hair regular at the horizon, the generic solution will diverge there. In the smeared case, since there is only one constant, the flux cannot be chosen to both be regular and to have the opposite orientation as the brane. In the localised case, there are fewer symmetries and therefore the flux has enough freedom to interpolate between a smooth value at the horizon and the desired value at infinity. Having two integration constants now allows both for the cancellation of singular terms at the horizon as well as for the flux to asymptote to either an ISD or AISD form far from the brane. It appears that this is how the no-go theorem is evaded.

The localised solution constructed here has important implications for the

[11] The definition of the boundary term and $C(M_0, T)$ can be found in [206].

existence of the KPV metastable state. According to the Gubser criterion the existence of a localised black brane with negative charge implies that the singularity associated with anti-D3 branes in the KS solution are physical, and can in fact be resolved by string theory. As the brane approaches the negatively charged extremal limit, the flux diverges outside the horizon, which suggests a resolution by polarisation. We will examine this possibility next.

Extremal Case

We next turn to the extremal case, for which the perturbation equation (9.21) has a very simple analytic solution:

$$\begin{aligned} (\varepsilon = 1) \qquad & g_4 = c_0 + c_1 \left(\frac{r_0^6}{r^6} + \frac{3}{5} \frac{r_0^{10}}{r^{10}} \right), \\ (\varepsilon = -1) \qquad & g_4 = c_0 \left(1 + 3 \frac{r_0^4}{r^4} \right) + c_1 \frac{r_0^6}{r^6}, \end{aligned} \tag{9.26}$$

where c_0, c_1 are integration constants. The boundary condition that $g_4(\infty) = 1$ requires $c_0 = 1$. Generically, the perturbation is singular in the IR. The norms of the 3-form fluxes are

$$\begin{aligned} (\varepsilon = 1) \qquad & |F_3|^2 \sim |H_3|^2 \sim r^{-14}, \quad c_1 \neq 0, \qquad |F_3|^2 \sim |H_3|^2 \sim r^6, \quad c_1 = 0, \\ (\varepsilon = -1) \qquad & |F_3|^2 \sim |H_3|^2 \sim r^{-6}, \quad c_1 \neq 0, \qquad |F_3|^2 \sim |H_3|^2 \sim r^{-2}, \quad c_1 = 0. \end{aligned} \tag{9.27}$$

For $\varepsilon = 1$, the norm can be made non-singular at the brane location by setting $c_1 = 0$. In fact, for this case an exact solution exists at the non-linear level corre-

sponding to extremal branes added to the flux background. This just corresponds to adding a singular harmonic source term to the warp factor H, just as in the previous section. Explicitly, the solution fits the same ansatz as the flux background (9.1), but the warp factor is now [12]

$$H = 1 + \frac{r_0^4}{r^4} - \frac{m^2 r^2 \sin^2\psi}{6}. \tag{9.28}$$

For $\varepsilon = -1$, there is no way to keep the asymptotic condition $c_0 = 1$ and to also keep the norm non-divergent. As expected from the extremal limit of the previous section, the fluxes must diverge as $r \to 0$. The interpretation of this singularity is of crucial importance for understanding the problem of anti-branes in flux backgrounds. That it can be shielded by a finite-temperature horizon implies that it can be resolved by string theory.

The obvious candidate resolution mechanism is brane polarisation. In fact, the set-up is very similar to the one considered by Polchinski-Strassler in the supersymmetric case [208]. The anti-D3 branes source an AdS_5 throat, into which the singular G_3 flux will leak. If the fluxes take the right form, polarisation will occur and the singularity will be resolved in a manner similar to the way in which Polchinski-Strassler resolves the singularity associated with a mass deformation of the $\mathcal{N} = 1^*$ theory, which we now review very briefly.

Taking both the near-brane and extremal limit of D3 brane solution (9.17)

[12] Note that the branes added here are localised. The addition of D3 branes smeared over 3 dimensions corresponds to the addition of a term $a_0/r_1 = a_0/(r\sin\psi)$, as discussed previously.

results in the line element

$$ds^2 \approx \left(\frac{r}{r_0}\right)^2 dx_\mu dx^\mu + \left(\frac{r_0}{r}\right)^2 dr^2 + r_0^2 d\Omega_5^2, \tag{9.29}$$

which is simply $AdS_5 \times S^5$. Polchinski and Strassler considered Lorentz invarance-preserving G_3 perturbations of this solution. The perturbation transforms under the transverse $SO(6)$ according to two possible representations: the **10** and the $\overline{\mathbf{10}}$. There are two solutions for each representation, each of which has a definite scaling with r, i.e. for $r \to \lambda r$, $G_3 \sim \lambda^{-\Delta} G_3$. For this very symmetric case of perturbations of AdS_5, only a single power of r is present, as opposed to the more general case where a whole power series would be expected. The possible conformal dimensions are

$$\begin{aligned} \mathbf{10}: &\qquad \Delta = 7, \qquad \Delta = -3, \\ \overline{\mathbf{10}}: &\qquad \Delta = 3, \qquad \Delta = 1. \end{aligned} \tag{9.30}$$

For $\Delta \leq 0$ the mode is regular in the IR ($r \to 0$), and for $\Delta > 0$ it diverges. Polchinski and Strassler studied the perturbation corresponding to the $\Delta = 1$ mode in the supersymmetric case and found that the singularity was cured through the physics of brane polarisation.

Returning now to the case of G_3 perturbations of the full D3 brane solution, as opposed to simply the near-horizon $AdS_5 \times S^5$, we see that for the case $\varepsilon = -1$, there are three modes present, that is, G_3 is a sum of three terms with distinct definite scalings:

$$G_3 \sim c_1 \lambda^{-3} + c_0 \left(\lambda^{-1} + \lambda^3\right). \tag{9.31}$$

The perturbation therefore contains the conformal dimensions $\Delta \in (3, 1, -3)$. Taking $c_0 \neq 0$, as required by the boundary condition that the flux approach (9.19) asymptotically forces the modes $\Delta = 1, -3$ to be turned on. The most singular $\Delta = 3$ mode can be eliminated by setting $c_1 = 0$. What remains is the non-singular $\Delta = -3$ mode, which becomes vanishingly weak and therefore negligible in the deep IR ($r \to 0$), and the $\Delta = 1$ mode, which diverges down the throat [208]. [13]

In the original Polchinski-Strassler analysis, the form of the $\Delta = 1$ mode was chosen to be supersymmetric, which allowed the polarisation potential to be determined from simply the linear G_3 flux perturbation. The present case is more complicated, as the form of the divergent $\Delta = 1$ mode can be shown to not preserve supersymmetry. In the $SO(3)$-invariant, non-supersymmetric version of Polchinski-Strassler [224], the polarisation potential depends on 3 parameters, $m_{\rm PS}, m'_{\rm PS}, \mu_{\rm PS}$, which are defined as follows. The $\Delta = 1$ G_3 perturbation can be written as

$$G_3 \propto \frac{1}{r^4}\left(T_3 - \frac{4}{3}V_3\right), \tag{9.32}$$

where T_3 and V_3 are 3-forms on the $\mathbb{R}^6$ transverse to the branes defined in [208] and reproduced in Appendix 9.B. The coefficient of the $(1, 2)$ component of T_3 is denoted $m_{\rm PS}$, while $m'_{\rm PS}$ is the coefficient of the $(3, 0)$ component. $\mu_{\rm PS}$ is a parameter that comes from the second order backreaction of the G_3 perturbation. In the supersymmetric case, $m'_{\rm PS} = \mu_{\rm PS} = 0$, and the linear flux perturbation

[13] There is a nice connection with the weaker divergence associated with setting $c_1 = 0$ for the $\varepsilon = -1$ case, and the no-go results of [206] which in the present zero temperature case imply that the 3-form fluxes must diverge as $|H_3|^2 \sim H^{1/2} \sim r^{-2}$. Unlike the finite temperature case, this divergence cannot be cured by adjusting constants to procure cancellations.

suffices to compute the polarisation potential. In the present case, the form of the $\Delta = 1$ mode of the flux is shown in Appendix 9.B to give rise to $m'_{\rm PS} = m_{\rm PS}$, and the perturbation therefore breaks all supersymmetry. In order to definitively determine whether or not polarisation resolves the singularity, the parameter $\mu_{\rm PS}$ would also need to be computed, which would require going beyond the linear approximation considered here.

Despite the lack of a definitive polarisation calculation, the finite-temperature and extremal cases together paint a compelling picture. In the extremal case of anti-branes added to the flux background, the anti-D3's source an AdS_5 throat into which the G_3 fluxes leak. It could have turned out that the most singular mode in the IR, the $\Delta = 3$ mode, was forced to be present from the requirement that the flux approach the flux background solution asymptotically, but that did not turn out the be the case. Instead, the only singular mode that leaks into the throat is the $\Delta = 1$ mode. As $r \to 0$ is approached, this mode grows until polarisation via the Myers effect likely takes over, leading to a completely non-singular, puffed-up brane configuration. The full solution corresponding to anti-branes in KS would then correspond to a gluing of the backreacted non-supersymmetric Polchinski-Strassler solution (which has yet to be explicitly constructed) to the KS geometry. This is schematically depicted in Fig. 9.5.

Our calculation in the extremal case is similar to one that appears in [225]. The existence of negatively charged black branes at finite temperature therefore strengthens the picture considered there and in [226] wherein the gravity dual of the KPV metastable state was argued to be a gluing of the polarised Polchinski-Strassler solution with the Klebanov-Strassler one. Finite temperature is seen

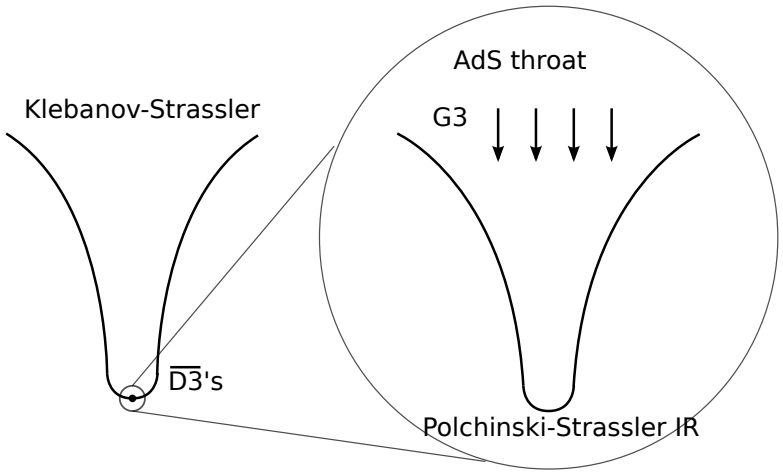

Figure 9.5: Schematic depiction of the proposed supergravity solution corresponding to anti-D3 branes in the Klebanov-Strassler solution. The solution interpolates between a Klebanov-Strassler throat asymptotically, and a mass-deformed $AdS_5 \times S^5$ throat. The $\Delta = 1$ mode of the G_3 flux grows down the throat, until it eventually induces polarisation, leading to the (as yet un–constructed) backreacted non-supersymmetric Polchinski-Strassler solution. It should be noted that each throat has a distinct radial coordinate.

to act as an IR regulator of the un-polarised singular solution. For negatively charged solutions close to extremality, one would expect that these black branes are unstable to a finite temperature version of brane polarisation as the flux is very large outside the horizon. [14]

The existence of negatively charged black branes at finite temperature provides evidence, according to the Gubser criterion, that the anti-brane singularity is resolved. The diverging form of the flux in the extremal limit strongly suggests that the appropriate resolution mechanism is brane polarisation, a conclusion at odds with previous calculations which suggested that polarisation only occurs in certain channels, and that the throat is unstable to fragmentation [210, 211, 212, 213]. Note that there is no indication of a fragmentation instability of the blackened anti-D3 brane solutions constructed here. In these works the the potentials were computed for probe branes in the solutions corresponding to *smeared* anti-branes in flux backgrounds, and it was then argued that the potential for localised anti-branes could be extracted from the smeared result. Central to the argument is the remarkable fact that in Polchinksi-Strassler the polarisation potential for branes in a mass-deformed AdS_5 throat is independent of the warp factor H. Since the potential is independent of H, the potential for a probe brane in the mass-deformed throat created by a stack of D3 branes is the same as that created by a configuration of D3-branes smeared over an S^2, a key point in the original PS analysis.

However, the smearing in the present case is much more drastic than the smearing considered in PS. For the case of anti-D3 branes added to the toy flux

[14] Finite temperature effects in the $\mathcal{N} = 1^*$ theory are treated in [223].

background (9.1), it is clear that the smearing not only alters the form of the near-brane AdS_5 throat, but also greatly restricts the form of the fluxes in the throat. In particular, it is no longer appropriate to consider general $SO(6)$ representations of G_3 perturbations, as these will generically break the symmetry imposed by smearing. It is important to note that the asymptotic form of the flux is invariant under the symmetries imposed by smearing, but the form of the flux down the throat, where polarisation would occur, is not. This fact, together with the finite temperature case where the smearing clearly constrains the form of the flux to be such that it is unable to be both regular at the horizon and asymptote to either self-duality signature, strongly suggests that smearing destroys the resolution mechanism. [15]

The calculations presented here indicate that the singularities associated with anti-D3 branes at the tip of the Klebanov-Strassler throat are resolved and that the KPV metastable state exists. In Appendix 9.C we repeat the above analysis for a toy flux background of M-theory which approximates the IR of the CGLP solution [219]. All the main results carry over, and we therefore turn to a concluding discussion.

9.3 Conclusion

In this paper we studied localised black branes in toy flux backgrounds in both string theory and M-theory. The finite temperature solution was constructed to leading order in an approximation scheme where the flux was treated perturba-

[15]It should be noted that even if smearing does indeed destroy the resolution mechanism so that the smeared solution does not capturing this crucial aspect of the localised solution, the smeared solution has been shown to pass certain non-trivial tests, see for example [227].

tively near the branes. Remarkably, black brane solutions were found to exist for either sign charge, indicating that the singularity associated with localised anti-branes can be shielded behind a smooth horizon. According to the Gubser criterion, the anti-brane singularities are then physical and resolvable by string theory.

As the charge of the black brane is taken taken to be large and negative, the flux at the horizon is seen to increase without bound. The natural resolution mechanism is therefore brane polarisation à la Polchinski-Strassler [208] or its M-theory analogue [228]. And indeed, when the extremal anti-brane limit is taken, the divergent flux is of the form known to be resolved by polarisation in the supersymmetric case. Because the matching of the AdS throat sourced by the branes with the flux background breaks supersymmetry, a non-supersymmetric version of Polchinski-Strassler [224] or its M-theory analogue is required. In order to determine the polarisation potential in the non-supersymmetric case, and to definitively address whether or not polarisation resolves the singularity, the solution will need to be extended to second order in the flux perturbation. If polarisation is indeed the correct resolution mechanism, which we view as likely, then the metastable non-SUSY states corresponding to puffed-up branes not only exist, but also possess supergravity descriptions. In the Type IIB case this corresponds to a gluing of the polarised Polchinski-Strassler solution to a Klebanov-Strassler throat.

The calculations of the current work are in tension with a number of recent results. The existence of localised black holes in the IIB flux background we considered appeared to be ruled out by the no-go theorem of [206], however we

argued that this theorem is evaded by a loop-hole. The fluxes are indeed generically singular at the horizon, but by a choice of integration constants these can be made regular in both the smeared and localised cases. The symmetry imposed by smearing is rather restrictive, and does not allow the flux at the horizon to be both regular and anti-aligned with the asymptotic value. In the less symmetric localised case, there is enough freedom to simultaneously enforce regularity at the horizon as well as to fix the orientation to be either sign asymptotically.

Additionally, previous calculations used smeared results to argue that polarisation only occurs in certain channels for the localised case, and that the AdS throats were unstable to fragmentation instabilities (the so-called tachyons), thus rendering the anti-brane singularities unphysical [210, 211, 212, 213]. However our calculation of the flux near the brane in both the extremal and non-extremal cases strongly suggests that polarisation does occur, and yields no indication of the fragmentation instability. We argued that the discrepancy could be due to the restrictive symmetry imposed by smearing. It appears that smearing destroys the resolution mechanism, a possibility in accord with existence of negatively charged anti-branes in the localised case, and the absence of them in the smeared case. If polarisation is not the resolution mechanism, then there is either some novel mechanism yet to be discovered which cures the singularity, or else the Gubser criterion as it is currently understood fails and requires revision.

Despite recent work suggesting an increasingly dire outlook for the fate of anti-branes in flux backgrounds and their many interesting applications, there are now a few distinct and complementary results which suggest that the metastable states do in fact exist as originally understood. First, there are the original polar-

isation calculations [168, 229]. Secondly, in [220] it was convincingly argued that a single brane should be non-singular and described by effective field theory. The calculations of the present work indicate that the physics of many branes is also non-singular (after they polarise, or are resolved by some new mechanism). There is no need to resort to time dependence to resolve the singularity [204, 217, 218], and there are no challenges to the de Sitter landscape or other applications of the non-SUSY metastable states.

The results of this paper suggest many avenues for future work. It is of obvious interest to go beyond the linear approximation considered here, and to construct the solutions in a systematic matched asymptotic expansion for both the extremal and non-extremal cases. In the extremal case, this would allow for a definitive answer to the question of whether polarisation resolves the singularities and results in a smooth, stable throat. It would also be very worthwhile to explore the solution space of black branes in flux backgrounds further. In addition to localised and smeared solutions, there are likely to exist inhomogeneous black branes as well. In many ways, the problem of black brane solutions in flux backgrounds seems qualitatively similar to the problem of black hole/string solutions in 5d Kaluza-Klein gravity.[16] In particular, it seems likely that there is a very interesting relationship between inhomogeneities of the black branes and charge. Additionally, the negatively charged localised black holes constructed here might themselves be unstable to a finite-temperature version of Polchinski-Strassler [223]. In a future work we plan to explore these and related issues.

[16]For a review, see [230]. Black holes in a simpler family of flux backgrounds were studied recently in [2].

Acknowledgements

Some of the ideas contained in the present work originated in a collaboration with G. Horowitz and A. Puhm, and a separate collaboration with Ó. Dias and J. Santos, and I am very grateful to them for contributing to my understanding of the problem and for their encouragement throughout this project. I also wish to thank J. Brugger, U. Danielsson, F. Gautason, D. Marolf, S. Massai, B. Michel, E. Mintun, T. Van Riet, and especially J. Polchinski for useful discussions, as well as the authors of [220] for sharing early drafts of their paper. Lastly, I wish to thank Ó. Dias, S. Fischetti, G. Horowitz, W. Kelly and J. Santos for both discussions and their comments on a draft of this paper. This work was supported by NSF grant PHY12-05500, and by funds provided by the University of California, Santa Barbara.

Appendix

9.A Strings are Well Behaved in the Toy Flux Backgrounds

In this section we show that although the toy flux backgrounds (9.1), (9.46) are certainly singular at the locus $H = 0$, strings propagating on these backgrounds are actually non-singular and completely well behaved. The work presented in this appendix is a result of joint work with G. Horowitz and A. Puhm.

Both the toy flux backgrounds considered in this paper and the KS and CGLP solutions are actually U-dual to plane-fronted waves with parallel propagation, or pp-waves for short [231]. PP-wave spacetimes are of the form

$$ds^2 = -2dudv + F(u, x_\perp)du^2 + dx_\perp^2, \tag{9.33}$$

where $dx_\perp^2$ is some Ricci-flat transverse space. The vector $\ell_a = \partial_a u$ is null and covariantly constant, and both the Riemann and Ricci curvature tensors can easily

be written in terms of ℓ and F [232]:

$$R_{abcd} = 2\ell_{[a}\partial_{b]}\partial_{[c}F\ell_{d]}, \qquad R_{ab} = -\frac{1}{2}\left(\nabla^2_\perp F\right)\ell_a\ell_b, \tag{9.34}$$

where $\nabla^2_\perp$ is the scalar Laplacian on the transverse space. Note that the u-dependence is completely arbitrary.

Because the curvature is null, all curvature invariants of pp-waves vanish, in particular the Ricci scalar. When F depends quadratically on the transverse coordinates, the spacetime is said to be an exact plane wave. If $\nabla^2_\perp F = 0$, then the plane wave is a vacuum solution, otherwise the geometry will be sourced by a stress tensor that is also purely null, $R_{ab} = T_{ab}$.

For concreteness, consider the Type IIB toy flux background (9.1). although similar comments apply to the other flux backgrounds considered here (the toy M-theory solution considered in Appendix 9.C, and the KS and CGLP solutions). This can be dualised to a Type IIB pp-wave according to the following chain of transformations [17]

$$\begin{pmatrix} D3 \\ D5 \end{pmatrix} \overset{T_{x_3}}{\longrightarrow} \begin{pmatrix} D2 \\ D4 \end{pmatrix} \overset{\uparrow x_{11}}{\longrightarrow} \begin{pmatrix} M2 \\ M5 \end{pmatrix} \overset{\downarrow x_2}{\longrightarrow} \begin{pmatrix} F1 \\ D4 \end{pmatrix} \overset{T_{x_1}}{\longrightarrow} \begin{pmatrix} P \\ D3 \end{pmatrix}, \tag{9.35}$$

where T_{x_i} indicates T-duality on the x_i-coordinate, and $\updownarrow x_i$ indicates either the M-theory uplift or reduction along x_i. The D3 charge dissolved in flux of the original solution becomes momentum while the fractional D3 brane charge (D5 branes wrapping additional two-cycles) becomes D3 charge. The resulting background is

[17] An alternative duality chain involving $T_{x_3}T_{x_2}ST_{x_1}$ results in a IIA pp-wave background.

$$ds'^2_{10} = 2\varepsilon_F dt dx_1 + H dx_1^2 + \left(dx_3^2 + dx_{11}^2 + ds_6^2\right), \tag{9.36}$$

where ds_6^2 is the 6-dimensional transverse space. The warp factor H takes the place of $F(u, x_\perp)$, and depends only on r_1 The last coordinate to be T-dualised upon, x_1, serves as the null coordinate. The Ricci tensor is

$$R_{ab} = -\frac{1}{2}\left(\nabla_6^2 H\right)\partial_a x_1 \partial_b x_1. \tag{9.37}$$

Since $\nabla_6^2 H \neq 0$, this geometry must be supported by matter. The dilaton is constant, $e^{2\Phi'} = 1$, and the only non-vanishing form field is

$$F'_5 = [F_3^0 \wedge dx_3 + H_3^0 \wedge dx_{11}] \wedge dx_1, \tag{9.38}$$

where F_3^0 and H_3^0 denote the original three-form fluxes of the toy flux background. The five-form flux is null and self-dual. The stress tensor is then

$$T_{ab} = \frac{1}{2} m^2 \partial_a x_1 \partial_b x_1. \tag{9.39}$$

An interesting feature of this duality frame is that the imaginary self-duality property of the original 3-form flux corresponds to the fact that the curvature and matter are null.

We now use the above duality chain to show that strings are perfectly well behaved in the toy flux background solution, despite the appearance of a singularity at the locus $H = 0$. The original solutions' naked singularities can be studied using the dual plane wave solutions. The physics of strings propagating on the

original solutions is dual to the physics of strings propagating on the dual plane waves, since the worldsheet theory of the strings is duality-invariant.

Recall that plane waves are a special case of pp-waves in which the F function is quadratic in the $x_\perp$ coordinates. The warp factor of the toy flux background is $H = 1 - m^2 r_1^2/6$, and so the dual solution is an exact plane wave. The fact that these simple flux backgrounds dualise to plane waves is particularly nice because plane waves have the special property in string theory that strings may be quantized exactly [232] [18] After dualising, the plane wave is completely non-singular at the locus $H = 0$. To see this, note the radius at which $H = 0$ is no longer gauge invariant; under the coordinate transformation $t = \tilde{t} + Dx^1$, with D a constant, the radius at which $H = 0$ is shifted. Therefore, whereas $H = 0$ in the original solutions corresponded to a naked singularity, the geometry is completely regular in the dual plane waves. Strings quantized on the plane wave backgrounds would not experience any singular behaviour, and therefore we can conclude that neither would they experience singular behaviour in the original flux background solutions.

[18] More precisely, because the curvatures are null, pp-waves are solutions of the supergravity equations to any order in α'. Plane waves, moreover, are solutions even non-perturbatively in α'. Additionally, pp-waves are the only non-flat spacetime to admit lightcone gauge on the string worldsheet, and for the special case of plane waves, the string equations of motion are linear and different modes decouple, allowing the string to be quantized exactly.

9.B Explicit Form of the G_3 Flux in Complex Coordinates

In this appendix we verify that the form of the G_3 perturbation considered in Sec. 9.2.4 breaks the supersymmetry of the AdS_5 throat with $m'_{\rm PS}/m_{\rm PS} = 1$.

First, introduce the complex coordinates $z^i = x^i + iy^i$, for $i = 1, 2, 3$. The metric on $\mathbb{R}^6$ is then

$$ds^2_{\mathbb{R}^6} = \sum_{i=1}^{3} dz^i d\bar{z}^i = \sum_{i=1}^{3} \left(dx_i^2 + dy_i^2\right). \tag{9.40}$$

These coordinates are related to the ones used in the perturbation of the G_3 flux for the localised case considered in Sec. 9.2.4 by

$$\sum_{i=1}^{3} dx_i^2 = dr_1^2 + r_1^2 d\Omega_2^2, \qquad \sum_{i=1}^{3} dy_i^2 = dr_2^2 + r_2^2 d\widetilde{\Omega}_2^2, \tag{9.41}$$

with $r_1 = r\sin\psi$, $r_2 = r\cos\psi$. In the anti-aligned case $\varepsilon = -1$, the flux profile was found in (9.26) to be

$$g_4 = c_0\left(1 + 3\frac{r_0^4}{r^4}\right) + c_1\frac{r_0^6}{r^6}. \tag{9.42}$$

The most singular term in the IR ($r \to 0$) can be eliminated by setting $c_1 = 0$, and the asymptotic boundary condition requires $c_0 = 1$. For this choice, the leading

term of the flux perturbation in the IR is

$$G_3 \sim m\left(\frac{r_0^4}{r^2}\right)\Big(\cos^2\psi\,(-\cos\psi dr - 3r\sin\psi d\psi)\wedge d\widetilde{\Omega}_2 + i\sin^2\psi\,(-\sin\psi dr + 3r\cos\psi d\psi)\wedge d\Omega_2\Big) + ... \tag{9.43}$$

In the notation of Polchinski-Strassler [208], the $\Delta = 1$ flux perturbation is written as $G_3 \propto r^{-4}\,(T_3 - 4V_3/3)$, where in the $SO(3)$-invariant case (in which the chiral superfields have the same mass),

$$\begin{aligned} T_3 &= m_{\rm PS}\left(dz^1\wedge d\bar{z}^2\wedge d\bar{z}^3 + d\bar{z}^1\wedge dz^2\wedge d\bar{z}^3 + d\bar{z}^1\wedge d\bar{z}^2\wedge dz^3\right) + m'_{\rm PS}dz^1\wedge dz^2\wedge dz^3, \\ V_3 &= \frac{x^q}{r^2}\left(x^m T_{qnp} + x^n T_{mqp} + x^p T_{mnq}\right). \end{aligned} \tag{9.44}$$

The parameter $m_{\rm PS}$ is therefore the coefficient of the $(1,2)$ component of T_3 and $m'_{\rm PS}$ is the coefficient of the $(3,0)$ component. For $m'_{\rm PS} \neq 0$, the perturbation breaks all supersymmetry of the AdS_5 throat. For the case at hand, (9.43) can be shown to be equivalent to

$$G_3 \sim -\frac{3i}{4}\frac{m}{m_{\rm PS}}\left(\frac{r_0^4}{r^4}\right)\left(T_3 - \frac{4}{3}V_3\right) + ..., \qquad m'_{\rm PS} = m_{\rm PS}. \tag{9.45}$$

The overall normalization is irrelevant, and can be changed by simply rescaling m. This establishes that a non-supersymmetric version of the Polchinski-Strassler analysis is needed.

9.C M2 Branes in M-theory Flux Backgrounds

The analysis of Sec. 9.2 can be repeated for M-theory. The M-theoretic version of the KS solution is the CGLP solution [219], which corresponds to fractional M2 branes at the tip of a higher dimensional version of the deformed conifold, known as the $n = 3$ Stenzel space.[19] The analogue of the KPV calculation was performed by Klebanov and Pufu (KP) [229], who found qualitatively similar results, namely that for small enough anti-M2 charge there is a metastable minima corresponding to anti-M2 branes polarised into M5 branes.

In this appendix we present a toy model of the CGLP solution. We then repeat the calculations of Sec. 9.2 and are led to exactly the same conclusions– that localised M2 brane solutions exist for any sign charge in the non-extremal case. In the extremal case, resolution by polarisation again appears likely.

9.C.1 A Toy Model of the CGLP Flux Background

A toy model relevant for approximating the IR of CGLP is

$$ds^2 = H^{-2/3}\left(-dt^2 + dx_1^2 + dx_2^2\right) + H^{1/3}\left(dr_1^2 + r_1^2 d\Omega_3^2 + \sum_{i=1}^{4} dy_i^2\right), \qquad (9.46)$$

$$G_4 = \varepsilon_F \, dH^{-1} \wedge dt \wedge dx^1 \wedge dx^2 + m\alpha_4,$$

where

$$\alpha_4 = dy^1 \wedge dy^2 \wedge dy^3 \wedge dy^4 - \varepsilon_F r_1^3 dr_1 \wedge d\Omega_3 \qquad (9.47)$$

[19] the $n = 2$ and $n = 1$ Stenzel spaces are the deformed conifold and the Eguchi-Hanson instanton, respectively.

is the (anti)-self dual magnetic part of the four-form, $\star_6\alpha_4 = -\varepsilon_F\alpha_4$, which should be thought of as analogous to the G_3 flux in the IIB case. The warp factor is

$$H = 1 + \frac{a_0}{r^2} - \frac{m^2}{8}r_1^2, \tag{9.48}$$

where, as in the IIB case, a_0 is proportional to the number of smeared M2 branes which we take to be zero and m controls the amount of flux. This solution is related via duality (reduction on x_2 followed by T-dualising the x_1 coordinate) to the plane wave solutions considered in [231]. This toy flux background also possesses a naked singularity, and the same comments as in the Type IIB case apply here as well (see Appendix 9.A).

The geometry near the tip of the $n = 3$ Stenzel space consists of a finitely-sized S^4 and a shrinking S^3. In complete analogy with the discussion in Sec. 9.2, the flux background (9.46) is seen to capture the key features of the CGLP solution, with the main difference being that the transverse S^4 is replaced with a $\mathbb{R}^4$. For the purpose of discussing M2 branes localised at both tip of the background and also at a point in this transverse space, it is useful to introduce the coordinates

$$\sum_{i=1}^{4} dy_i^2 = dr_2^2 + r_2^2 d\widetilde{\Omega}_3^2, \qquad dy^1 \wedge dy^2 \wedge dy^3 \wedge dy^4 = r_2^3 dr_2 \wedge d\widetilde{\Omega}_3, \tag{9.49}$$

where $d\widetilde{\Omega}_3^2$, $d\widetilde{\Omega}_3$ are the line elements and volume form for a second, distinct unit S^3.

In complete analogy with Sec. 9.2.2, the Klebanov-Pufu polarisation calculation can be repeated here with the same conclusion–namely that the toy flux background always possess a minima corresponding to a puffed-up 5-brane wrap-

ping an S^3 in the transverse $\mathbb{R}^4$ at the tip. This minima is the global minima, and there is no brane-flux annihilation process due to the non-compactness of the $\mathbb{R}^4$. For small anti-M2 charge, the potential is very similar to the KP potential, and the near-brane solution corresponding to localised anti-branes in the toy flux background should be identical to the analogous solution in the CGLP background.

9.C.2 Localised Branes

In this section we study localised branes in the toy M-theory flux background (9.46). As in Sec. 9.2.4, our approach is very similar to that of Ref. [222]. The thermal M2 brane solution is

$$\begin{aligned} ds^2 &= H^{-2/3}\left(-f dt^2 + dx_1^2 + dx_2^2 +\right) + H^{1/3}\left(\frac{dr^2}{f} + r^2 d\Omega_7^2\right), \qquad (9.50)\\ G_4 &= \varepsilon_B \coth\beta\, dH^{-1} \wedge dt \wedge dx^1 \wedge dx^2,\\ H &= 1 + \sinh^2\beta \left(\frac{r_+}{r}\right)^6, \qquad f = 1 - \left(\frac{r_+}{r}\right)^6, \end{aligned}$$

where as before $\beta \geq 0$ is the boost parameter and $\varepsilon_B = \pm 1$ characterises the difference between positive and negative charge. The extremal limit is $\beta \to \infty$ while keeping $r_0^3 \equiv r_+^3 \sinh\beta$ fixed. A useful coordinatization of the 7-sphere is

$$d\Omega_7^2 = d\psi^2 + \sin^2\psi d\Omega_3^2 + \cos^2\psi d\widetilde{\Omega}_3^2, \qquad (9.51)$$

which connects to the coordinates employed in the toy flux background upon identifying $r_1 = r\sin\psi$, $r_2 = r\cos\psi$.

We now wish to consider a linear magnetic G_4 perturbation of the M2 brane solution. The G_4 flux should approach the (9.46) form asymptotically:

$$\begin{aligned}\lim_{r\to\infty} G_4^{(m)} &= m\left(r_2^3 dr_2 \wedge d\widetilde{\Omega}_3 - \varepsilon_F r_1^3 dr_1 \wedge d\Omega_3\right), \\ &= mr^3\Big(\cos^3\psi\left(\cos\psi dr - r\sin\psi d\psi\right)\wedge d\widetilde{\Omega}_3 \\ &\qquad - \varepsilon_F \sin^3\psi\left(\sin\psi dr + r\cos\psi d\psi\right)\wedge d\Omega_3\Big).\end{aligned} \tag{9.52}$$

Using this asymptotic form as a guide, a useful ansatz for the perturbation is

$$\begin{aligned}\delta G_3 = {} & mr^3\cos^3\psi\left(g_1\cos\psi dr - g_2 r\sin\psi d\psi\right)\wedge d\widetilde{\Omega}_3 \\ & - \varepsilon_F mr^3\sin^3\psi\left(g_3\sin\psi dr + g_4 r\cos\psi d\psi\right)\wedge d\Omega_3,\end{aligned} \tag{9.53}$$

where again the functions $g_i = g_i(r)$. The Bianchi constraint $dG_4 = 0$ is satisfied for

$$g_2 = g_4, \qquad g_1 = g_3 = \frac{1}{4}r^{-3}\partial_r\left(r^4 g_4\right), \tag{9.54}$$

and the linearised equation of motion $d\star G_4 + \frac{1}{2}G_4\wedge G_4 = 0$ then reduces to the ODE

$$\begin{aligned}& r^2 f H g_4'' + \left(r^2 H f' - r^2 f H' + 9rfH\right)g_4' \\ & \qquad + 4\left(H\left(rf' + 4f - 4\right) + rH'\left(\varepsilon\coth\beta - f\right)\right)g_4 = 0,\end{aligned} \tag{9.55}$$

where again $\varepsilon = \varepsilon_F\varepsilon_B$. We will again consider the non-extremal and extremal cases separately.

Non-Extremal Case

As before, we were unable to find analytic solutions for the general finite temperature case, and will therefore turn to numerical methods. To facilitate the numerical evaluation, convert to the compactified coordinate $x = (r_+/r)^6$, for which the equation becomes

$$\partial_x^2 g_4 + \left(\frac{1 + 2x + x(4-x)\sinh^2\beta}{3x(x-1)\left(1 + x\sinh^2\beta\right)} \right) \partial_x g_4 + \left(\frac{3\varepsilon \sinh 2\beta - 2 + 2(2x-3)\sinh^2\beta}{9x(x-1)\left(1 + x\sinh^2\beta\right)} \right) g_4 = 0. \tag{9.56}$$

The boundary conditions we desire are that the perturbation approaches the form of the flux background at infinity $g_4(x = 0) = 1$, and that the perturbation be regular at the horizon, which requires

$$\left[\frac{2}{9}\left(1 - 3\varepsilon \tanh\beta\right) g_4 - \partial_x g_4 \right]_{x=1} = 0. \tag{9.57}$$

Once again, *a solution exists for either sign of the charge!* A typical solution is plotted in Fig. 9.C.1.

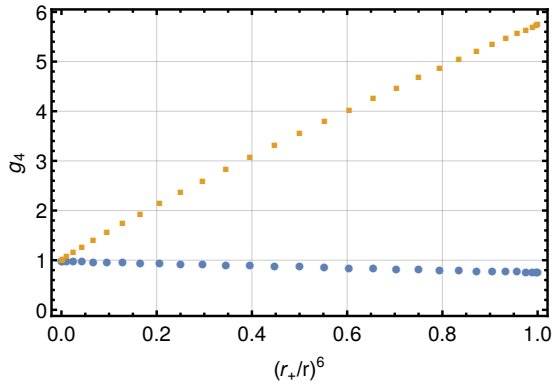

Figure 9.C.1: The perturbation function g_4 for $\beta = 1$ and $\varepsilon = 1$ (lower curve) and $\varepsilon = -1$ (upper curve).

The flux is larger at the horizon for $\varepsilon = -1$ than for $\varepsilon = 1$. The norm of the perturbation is

$$|\delta G_4|^2 = 24m^2 \frac{g_4(r_+)^2}{\cosh^{8/3}\beta}. \tag{9.58}$$

In Fig. 9.C.2 the rescaled function $g_+ \equiv g_4(r_+)/\cosh^{4/3}\beta \propto |\delta G_4|$ is plotted against β for both signs of ε. As expected, for $\varepsilon\beta \to +\infty$ the norm vanishes, and as $\varepsilon\beta \to -\infty$, the norm diverges.

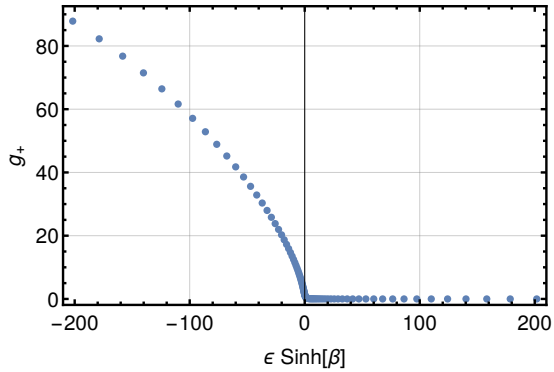

Figure 9.C.2: The value of the perturbation at the horizon. As extremality is approached, the flux either vanishes ($\varepsilon = 1$), or diverges ($\varepsilon = -1$). Recall that our convention is that $\beta \geq 0$ always. Fitting the data indicates that $g_+(r_+) \sim e^{2\beta/3}$ as $\beta \to \infty$ for $\varepsilon = -1$, which leads to the same growth as in the Type IIB case, $g_4(r_+) \sim e^{2\beta}$.

Once again, an analytic solution exists for the special case of $\beta = 0$:

$$g_4(x) = {}_2F_1\left(-\frac{2}{3}, \frac{1}{3}; -\frac{1}{3}; x\right) - \left(\frac{\Gamma\left(-\frac{1}{6}\right)\Gamma\left(\frac{2}{3}\right)}{2^{8/3}\Gamma\left(-\frac{2}{3}\right)\Gamma\left(\frac{7}{6}\right)}\right) x^{4/3}\, {}_2F_1\left(\frac{2}{3}, \frac{5}{3}; \frac{7}{3}; x\right), \tag{9.59}$$

and for $\beta = 0$ our numerics agrees with this analytic result. It is also easy to see that the perturbation is consistent with the Raychaudhuri equation, $T_{ab}k^a k^b = 0$. Unlike the Type IIB case, there is no no-go theorem excluding these solutions.

According to the discussion of Sec. 9.2.4, the ability to shield the anti-brane singularities behind a finite temperature horizon indicates that the singularities are physical and resolvable by string theory. As before, the natural resolution mechanism is polarisation. To investigate this possibility, we now turn to the extremal case.

Extremal Case

For the extremal case, the perturbation equations again have very simple analytic solutions. They are

$$\begin{aligned} (\varepsilon = 1) \qquad & g_4 = c_0 + c_1 \left(\frac{r_0^8}{r^8} + \frac{4}{7} \frac{r_0^{14}}{r^{14}} \right), \\ (\varepsilon = -1) \qquad & g_4 = c_0 \left(1 + 4 \frac{r_0^6}{r^6} \right) + c_1 \frac{r_0^8}{r^8}, \end{aligned} \tag{9.60}$$

where c_0, c_1 are integration constants. The boundary condition $g_4(\infty) = 1$ requires $c_0 = 1$. Generically, the perturbation is singular in the IR. The norms of the 3-form fluxes are

$$(\varepsilon = 1) \qquad |G_4|^2 \sim r^{-20}, \quad c_1 \neq 0, \qquad |G_4|^2 \sim r^8, \quad c_1 = 0.$$

$$(\varepsilon = -1) \qquad |G_4|^2 \sim r^{-8}, \quad c_1 \neq 0, \qquad |G_4|^2 \sim r^{-4}, \quad c_1 = 0.$$

For $\varepsilon = 1$, the norm can be made finite by setting $c_1 = 0$. As in the Type IIB case, an exact solution exists at the non-linear level corresponding to extremal branes added to the flux background.

For $\varepsilon = -1$, there is no way to keep the asymptotic condition $c_0 = 1$ and also keep the norm finite. The fluxes must diverge as $r \to 0$. To examine the possibility of the singularity being resolved by polarisation, we first recall that the M2 branes source an AdS_4 throat: taking the near-brane extremal limit of the M2 brane solution (9.50) results in the line element

$$ds^2 \approx \left(\frac{r}{r_0} \right)^4 dx_\mu dx^\mu + \left(\frac{r_0}{r} \right)^2 dr^2 + r_0^2 d\Omega_7^2. \tag{9.61}$$

After converting to a new radial coordinate $r^2 = 2r_0R$, and setting $r_0 = 2L$, this is seen to be simply $AdS_4 \times S^7$:

$$ds^2 \approx \frac{R^2}{L^2}dx_\mu dx^\mu + \frac{L^2}{R^2}dR^2 + (2L)^2 d\Omega_7^2. \tag{9.62}$$

The set-up is exactly as in the Type IIB case; the branes source an AdS throat, into which the flux leaks. Depending on the form of the fluxes, polarisation may or may not occur. The M-theory analogue of Polchinski-Strassler was worked out by Bena in [228]. For G_4 perturbations transforming under the transverse $SO(8)$, there are two possible representations, the $\mathbf{35}_\pm$, whose associated conformal dimensions are:

$$\begin{aligned} \mathbf{35}_+ : &\qquad \Delta = 5, &\qquad \Delta = -2, \\ \mathbf{35}_- : &\qquad \Delta = 2, &\qquad \Delta = 1, \end{aligned} \tag{9.63}$$

where again, $\delta G_4 \sim \lambda^{-\Delta}\delta G_4$ under the scaling of the AdS_4 coordinate $R \to \lambda R$. For $\Delta \leq 0$ the mode is regular in the IR ($R \to 0$), and for $\Delta > 0$ it diverges. Bena studied the perturbation corresponding to $\Delta = 1$ in the supersymmetric case and found that the singularity was cured through the physics of brane polarisation.

Returning now to the case of G_4 perturbations of the full M2 brane solution, we see that for the case $\varepsilon = -1$, there are three modes present, that is, δG_4 is a sum of three terms with distinct and definite scalings:

$$\delta G_4 \sim c_1\lambda^{-2} + c_0\left(\lambda^{-1} + \lambda^2\right). \tag{9.64}$$

The perturbation therefore contains the conformal dimensions $\Delta \in (2, 1, -2)$.

Taking $c_0 = 1$ as required by the boundary condition at infinity forces the $\Delta = 1, -2$ modes to be turned on. The more singular $\Delta = 2$ mode can be discarded through the boundary condition $c_1 = 0$. In the deep IR the $\Delta = -2$ mode becomes insignificant and the IR physics is dominated by the $\Delta = 1$. As in the Type IIB case, in order to definitively address whether polarisation occurs, a non-supersymmetric version of [228] will be needed, which will require the solution to be constructed to higher order.

To summarise, we find that in both Type IIB string theory and M-theory, regular localised black branes of either sign charge exist for finite temperature. According to the Gubser criterion then, the singularities should be regarded as physical, and are resolved in string theory. In the extremal case of anti-branes added to flux backgrounds the solutions are singular in a manner that is strongly suggests resolution by brane polarisation.

Bibliography

[1] G. S. Hartnett, *Localised Anti-Branes in Flux Backgrounds*, arXiv:1501.0656.

[2] G. S. Hartnett, G. T. Horowitz, and K. Maeda, *A No Black Hole Theorem*, Class.Quant.Grav. **32** (2015), no. 5 055011, [arXiv:1410.1875].

[3] . J. Dias, G. S. Hartnett, and J. E. Santos, *Quasinormal modes of asymptotically flat rotating black holes*, Class.Quant.Grav. **31** (2014), no. 24 245011, [arXiv:1402.7047].

[4] V. Cardoso, . J. Dias, G. S. Hartnett, L. Lehner, and J. E. Santos, *Holographic thermalization, quasinormal modes and superradiance in Kerr-AdS*, JHEP **1404** (2014) 183, [arXiv:1312.5323].

[5] G. S. Hartnett and J. E. Santos, *Non-Axisymmetric Instability of Rotating Black Holes in Higher Dimensions*, Phys.Rev. **D88** (2013) 041505, [arXiv:1306.4318].

[6] G. S. Hartnett and G. T. Horowitz, *Geons and Spin-2 Condensates in the AdS Soliton*, JHEP **1301** (2013) 010, [arXiv:1210.1606].

[7] N. Birrell and P. Davies, *Quantum Fields in Curved Space*, Cambridge Monogr.Math.Phys. (1982).

[8] J. Callan, Curtis G., S. B. Giddings, J. A. Harvey, and A. Strominger, *Evanescent black holes*, Phys.Rev. **D45** (1992) 1005–1009, [hep-th/9111056].

[9] R. Emparan and H. S. Reall, *A Rotating black ring solution in five-dimensions*, Phys.Rev.Lett. **88** (2002) 101101, [hep-th/0110260].

[10] E. Berti, V. Cardoso, and A. O. Starinets, *Quasinormal modes of black holes and black branes*, Class.Quant.Grav. **26** (2009) 163001, [arXiv:0905.2975].

[11] S. Aretakis, *Stability and Instability of Extreme Reissner-Nordström Black Hole Spacetimes for Linear Scalar Perturbations I*, Commun.Math.Phys. **307** (2011) 17–63, [arXiv:1110.2007].

[12] R. Emparan and K. Tanabe, *Universal quasinormal modes of large D black holes*, arXiv:1401.1957.

[13] B. Carter, *Republication of: Black hole equilibrium states part ii. general theory of stationary black hole states*, General Relativity and Gravitation **42** (2010), no. 3 653–744.

[14] H. Elvang and P. Figueras, *Black Saturn*, JHEP **0705** (2007) 050, [hep-th/0701035].

[15] H. Elvang and M. J. Rodriguez, *Bicycling Black Rings*, JHEP **0804** (2008) 045, [arXiv:0712.2425].

[16] G. T. Horowitz, *Black holes in higher dimensions*, .

[17] R. Emparan, T. Harmark, V. Niarchos, N. A. Obers, and M. J. Rodriguez, *The Phase Structure of Higher-Dimensional Black Rings and Black Holes*, JHEP **0710** (2007) 110, [arXiv:0708.2181].

[18] R. Emparan, T. Harmark, V. Niarchos, and N. A. Obers, *New Horizons for Black Holes and Branes*, JHEP **1004** (2010) 046, [arXiv:0912.2352].

[19] R. C. Myers and M. Perry, *Black Holes in Higher Dimensional Space-Times*, Annals Phys. **172** (1986) 304.

[20] R. Emparan and R. C. Myers, *Instability of ultra-spinning black holes*, JHEP **0309** (2003) 025, [hep-th/0308056].

[21] R. Gregory and R. Laflamme, *Black strings and p-branes are unstable*, Phys.Rev.Lett. **70** (1993) 2837–2840, [hep-th/9301052].

[22] S. A. Teukolsky, *Perturbations of a rotating black hole. 1. Fundamental equations for gravitational electromagnetic and neutrino field perturbations*, Astrophys.J. **185** (1973) 635–647.

[23] O. J. Dias, P. Figueras, R. Monteiro, H. S. Reall, and J. E. Santos, *An instability of higher-dimensional rotating black holes*, JHEP **1005** (2010) 076, [arXiv:1001.4527].

[24] M. Durkee and H. S. Reall, *Perturbations of near-horizon geometries and instabilities of Myers-Perry black holes*, Phys.Rev. **D83** (2011) 104044, [arXiv:1012.4805].

[25] K. Murata and J. Soda, *Stability of Five-dimensional Myers-Perry Black Holes with Equal Angular Momenta*, Prog.Theor.Phys. **120** (2008) 561–579, [arXiv:0803.1371].

[26] O. J. Dias, P. Figueras, R. Monteiro, J. E. Santos, and R. Emparan, *Instability and new phases of higher-dimensional rotating black holes*, Phys.Rev. **D80** (2009) 111701, [arXiv:0907.2248].

[27] O. J. Dias, R. Monteiro, and J. E. Santos, *Ultraspinning instability: the missing link*, JHEP **1108** (2011) 139, [arXiv:1106.4554].

[28] M. Shibata and H. Yoshino, *Nonaxisymmetric instability of rapidly rotating black hole in five dimensions*, Phys.Rev. **D81** (2010) 021501, [arXiv:0912.3606].

[29] M. Shibata and H. Yoshino, *Bar-mode instability of rapidly spinning black hole in higher dimensions: Numerical simulation in general relativity*, Phys.Rev. **D81** (2010) 104035, [arXiv:1004.4970].

[30] H. K. Kunduri, J. Lucietti, and H. S. Reall, *Gravitational perturbations of higher dimensional rotating black holes: Tensor perturbations*, Phys.Rev. **D74** (2006) 084021, [hep-th/0606076].

[31] H. Kodama and A. Ishibashi, *A Master equation for gravitational perturbations of maximally symmetric black holes in higher dimensions*, Prog.Theor.Phys. **110** (2003) 701–722, [hep-th/0305147].

[32] R. Emparan, R. Suzuki, and K. Tanabe, *The large D limit of General Relativity*, JHEP **1306** (2013) 009, [arXiv:1302.6382].

[33] S. Hawking and H. Reall, *Charged and rotating AdS black holes and their CFT duals*, Phys.Rev. **D61** (2000) 024014, [hep-th/9908109].

[34] V. Cardoso and O. J. Dias, *Small Kerr-anti-de Sitter black holes are unstable*, Phys.Rev. **D70** (2004) 084011, [hep-th/0405006].

[35] O. J. Dias and H. S. Reall, *Algebraically special perturbations of the Schwarzschild solution in higher dimensions*, Class.Quant.Grav. **30** (2013) 095003, [arXiv:1301.7068].

[36] G. T. Horowitz, Black Holes in Higher Dimensions. Cambridge University Press, Apr., 2012.

[37] R. Emparan and H. S. Reall, *A rotating black ring solution in five dimensions*, Phys. Rev. Lett. **88** (Feb, 2002) 101101.

[38] R. Emparan, T. Harmark, V. Niarchos, and N. A. Obers, *Essentials of Blackfold Dynamics*, JHEP **1003** (2010) 063, [arXiv:0910.1601].

[39] L. Lehner and F. Pretorius, *Black Strings, Low Viscosity Fluids, and Violation of Cosmic Censorship*, Phys.Rev.Lett. **105** (2010) 101102, [arXiv:1006.5960].

[40] O. J. Dias, P. Figueras, R. Monteiro, and J. E. Santos, *Ultraspinning instability of rotating black holes*, Phys.Rev. **D82** (2010) 104025, [arXiv:1006.1904].

[41] M. Durkee and H. S. Reall, *Perturbations of higher-dimensional spacetimes*, Class.Quant.Grav. **28** (2011) 035011, [arXiv:1009.0015].

[42] H. Kodama, R. Konoplya, and A. Zhidenko, *Gravitational stability of simply rotating Myers-Perry black holes: Tensorial perturbations*, Phys.Rev. **D81** (2010) 044007, [arXiv:0904.2154].

[43] R. Emparan, D. Grumiller, and K. Tanabe, *Large D gravity and low D strings*, Phys.Rev.Lett. **110** (2013) 251102, [arXiv:1303.1995].

[44] R. Emparan, R. Suzuki, and K. Tanabe, *Instability of rotating black holes: large D analysis*, arXiv:1402.6215.

[45] F. Tangherlini, *Schwarzschild field in n dimensions and the dimensionality of space problem*, Nuovo Cim. **27** (1963) 636–651.

[46] M. Godazgar, *The perturbation theory of higher dimensional spacetimes a la Teukolsky*, Class.Quant.Grav. **29** (2012) 055008, [arXiv:1110.5779].

[47] G. Gibbons, H. Lu, D. N. Page, and C. Pope, *The General Kerr-de Sitter metrics in all dimensions*, J.Geom.Phys. **53** (2005) 49–73, [hep-th/0404008].

[48] P. Hoxha, R. Martinez-Acosta, and C. Pope, *Kaluza-Klein consistency, Killing vectors, and Kahler spaces*, Class.Quant.Grav. **17** (2000) 4207–4240, [hep-th/0005172].

[49] B. Kol, *Perturbations around backgrounds with one non-homogeneous dimension*, hep-th/0609001.

[50] V. Cardoso, J. P. Lemos, and S. Yoshida, *Scalar gravitational perturbations and quasinormal modes in the five-dimensional Schwarzschild black hole*, JHEP **0312** (2003) 041, [hep-th/0311260].

[51] P. Pani, E. Berti, and L. Gualtieri, *Gravito-Electromagnetic Perturbations of Kerr-Newman Black Holes: Stability and Isospectrality in the Slow-Rotation Limit*, Phys.Rev.Lett. **110** (2013) 241103, [arXiv:1304.1160].

[52] M. Cavaglia, *Black hole and brane production in TeV gravity: A Review*, Int.J.Mod.Phys. **A18** (2003) 1843–1882, [hep-ph/0210296].

[53] P. Kanti, *Black holes in theories with large extra dimensions: A Review*, Int.J.Mod.Phys. **A19** (2004) 4899–4951, [hep-ph/0402168].

[54] P. Figueras, K. Murata, and H. S. Reall, *Black hole instabilities and local Penrose inequalities*, Class.Quant.Grav. **28** (2011) 225030, [arXiv:1107.5785].

[55] H. Elvang, R. Emparan, and A. Virmani, *Dynamics and stability of black rings*, JHEP **0612** (2006) 074, [hep-th/0608076].

[56] M. Abramowitz and I. Stegun, Handbook of Mathematical Functions. Dover, New York, fifth ed., 1964.

[57] M. B. Green and J. H. Schwarz, *Anomaly Cancellation in Supersymmetric D=10 Gauge Theory and Superstring Theory*, Phys.Lett. **B149** (1984) 117–122.

[58] P. Candelas, G. T. Horowitz, A. Strominger, and E. Witten, *Vacuum Configurations for Superstrings*, Nucl.Phys. **B258** (1985) 46–74.

[59] J. Polchinski, *Dirichlet branes and ramond-ramond charges*, Phys. Rev. Lett. **75** (Dec, 1995) 4724–4727.

[60] G. T. Horowitz and A. Strominger, *Black strings and P-branes*, Nucl.Phys. **B360** (1991) 197–209.

[61] M. R. Douglas, *The Statistics of string / M theory vacua*, JHEP **0305** (2003) 046, [hep-th/0303194].

[62] A. Strominger and C. Vafa, *Microscopic origin of the Bekenstein-Hawking entropy*, Phys.Lett. **B379** (1996) 99–104, [hep-th/9601029].

[63] I. R. Klebanov and M. J. Strassler, *Supergravity and a confining gauge theory: Duality cascades and chi SB resolution of naked singularities*, JHEP **0008** (2000) 052, [hep-th/0007191].

[64] V. E. Hubeny, D. Marolf, and M. Rangamani, *Black funnels and droplets from the AdS C-metrics*, Class.Quant.Grav. **27** (2010) 025001, [arXiv:0909.0005].

[65] J. D. Brown and M. Henneaux, *Central Charges in the Canonical Realization of Asymptotic Symmetries: An Example from Three-Dimensional Gravity*, Commun.Math.Phys. **104** (1986) 207–226.

[66] E. Witten, *Three-Dimensional Gravity Revisited*, arXiv:0706.3359.

[67] D. Marolf, *Unitarity and Holography in Gravitational Physics*, Phys.Rev. **D79** (2009) 044010, [arXiv:0808.2842].

[68] S. A. Hartnoll, C. P. Herzog, and G. T. Horowitz, *Building a Holographic Superconductor*, Phys.Rev.Lett. **101** (2008) 031601, [arXiv:0803.3295].

[69] S. S. Gubser, *Breaking an Abelian gauge symmetry near a black hole horizon*, Phys.Rev. **D78** (2008) 065034, [arXiv:0801.2977].

[70] D. R. Brill and J. B. Hartle, *Method of the Self-Consistent Field in General Relativity and its Application to the Gravitational Geon*, Phys.Rev. **135** (1964) B271–B278.

[71] J. Louko, R. B. Mann, and D. Marolf, *Geons with spin and charge*, Class.Quant.Grav. **22** (2005) 1451–1468, [gr-qc/0412012].

[72] O. J. Dias, G. T. Horowitz, and J. E. Santos, *Gravitational Turbulent Instability of Anti-de Sitter Space*, Class.Quant.Grav. **29** (2012) 194002, [arXiv:1109.1825].

[73] P. Bizon and A. Rostworowski, *On weakly turbulent instability of anti-de Sitter space*, Phys.Rev.Lett. **107** (2011) 031102, [arXiv:1104.3702].

[74] E. Witten, *Anti-de Sitter space, thermal phase transition, and confinement in gauge theories*, Adv.Theor.Math.Phys. **2** (1998) 505–532, [hep-th/9803131].

[75] G. T. Horowitz and R. C. Myers, *The AdS / CFT correspondence and a new positive energy conjecture for general relativity*, Phys.Rev. **D59** (1998) 026005, [hep-th/9808079].

[76] T. Nishioka, S. Ryu, and T. Takayanagi, *Holographic Superconductor/Insulator Transition at Zero Temperature*, JHEP **1003** (2010) 131, [arXiv:0911.0962].

[77] G. T. Horowitz and B. Way, *Complete Phase Diagrams for a Holographic Superconductor/Insulator System*, JHEP **1011** (2010) 011, [arXiv:1007.3714].

[78] S. S. Gubser and S. S. Pufu, *The Gravity dual of a p-wave superconductor*, JHEP **0811** (2008) 033, [arXiv:0805.2960].

[79] J.-W. Chen, Y.-J. Kao, D. Maity, W.-Y. Wen, and C.-P. Yeh, *Towards A Holographic Model of D-Wave Superconductors*, Phys.Rev. **D81** (2010) 106008, [arXiv:1003.2991].

[80] F. Benini, C. P. Herzog, R. Rahman, and A. Yarom, *Gauge gravity duality for d-wave superconductors: prospects and challenges*, JHEP **1011** (2010) 137, [arXiv:1007.1981].

[81] K.-Y. Kim and M. Taylor, *Holographic d-wave superconductors*, JHEP **1308** (2013) 112, [arXiv:1304.6729].

[82] N. R. Constable and R. C. Myers, *Spin two glueballs, positive energy theorems and the AdS / CFT correspondence*, JHEP **9910** (1999) 037, [hep-th/9908175].

[83] S. S. Gubser, *On nonuniform black branes*, Class.Quant.Grav. **19** (2002) 4825–4844, [hep-th/0110193].

[84] V. Balasubramanian and P. Kraus, *A Stress tensor for Anti-de Sitter gravity*, Commun.Math.Phys. **208** (1999) 413–428, [hep-th/9902121].

[85] R. M. Wald, *The First law of black hole mechanics*, gr-qc/9305022.

[86] R.-G. Cai, X. He, H.-F. Li, and H.-Q. Zhang, *Phase transitions in AdS soliton spacetime through marginally stable modes*, Phys.Rev. **D84** (2011) 046001, [arXiv:1105.5000].

[87] B. Gouteraux, J. Smolic, M. Smolic, K. Skenderis, and M. Taylor, *Holography for Einstein-Maxwell-dilaton theories from generalized dimensional reduction*, JHEP **1201** (2012) 089, [arXiv:1110.2320].

[88] J. M. Maldacena, *The Large N limit of superconformal field theories and supergravity*, Int.J.Theor.Phys. **38** (1999) 1113–1133, [hep-th/9711200].

[89] O. Aharony, S. S. Gubser, J. M. Maldacena, H. Ooguri, and Y. Oz, *Large N field theories, string theory and gravity*, Phys.Rept. **323** (2000) 183–386, [hep-th/9905111].

[90] G. T. Horowitz and V. E. Hubeny, *Quasinormal modes of AdS black holes and the approach to thermal equilibrium*, Phys.Rev. **D62** (2000) 024027, [hep-th/9909056].

[91] U. H. Danielsson, E. Keski-Vakkuri, and M. Kruczenski, *Black hole formation in AdS and thermalization on the boundary*, JHEP **0002** (2000) 039, [hep-th/9912209].

[92] D. Birmingham, I. Sachs, and S. N. Solodukhin, *Conformal field theory interpretation of black hole quasinormal modes*, Phys.Rev.Lett. **88** (2002) 151301, [hep-th/0112055].

[93] D. T. Son and A. O. Starinets, *Minkowski space correlators in AdS / CFT correspondence: Recipe and applications*, JHEP **0209** (2002) 042, [hep-th/0205051].

[94] P. K. Kovtun and A. O. Starinets, *Quasinormal modes and holography*, Phys.Rev. **D72** (2005) 086009, [hep-th/0506184].

[95] G. Policastro, D. T. Son, and A. O. Starinets, *From AdS / CFT correspondence to hydrodynamics*, JHEP **0209** (2002) 043, [hep-th/0205052].

[96] J. J. Friess, S. S. Gubser, G. Michalogiorgakis, and S. S. Pufu, *Expanding plasmas and quasinormal modes of anti-de Sitter black holes*, JHEP **0704** (2007) 080, [hep-th/0611005].

[97] G. Michalogiorgakis and S. S. Pufu, *Low-lying gravitational modes in the scalar sector of the global AdS(4) black hole*, JHEP **0702** (2007) 023, [hep-th/0612065].

[98] G. Holzegel and J. Smulevici, *Stability of Schwarzschild-AdS for the spherically symmetric Einstein-Klein-Gordon system*, Commun.Math.Phys. **317** (2013) 205–251, [arXiv:1103.3672].

[99] G. Holzegel and J. Smulevici, *Decay properties of Klein-Gordon fields on Kerr-AdS spacetimes*, Commun.Pure Appl.Math. **66** (2013) 1751–1802, [arXiv:1110.6794].

[100] G. H. Holzegel and C. M. Warnick, *Boundedness and growth for the massive wave equation on asymptotically anti-de Sitter black holes*, arXiv:1209.3308.

[101] G. Holzegel and J. Smulevici, *Quasimodes and a Lower Bound on the Uniform Energy Decay Rate for Kerr-AdS Spacetimes*, arXiv:1303.5944.

[102] V. Cardoso, *Black hole bombs and explosions: from astrophysics to particle physics*, Gen.Rel.Grav. **45** (2013) 2079–2097, [arXiv:1307.0038].

[103] S. de Haro, S. N. Solodukhin, and K. Skenderis, *Holographic reconstruction of space-time and renormalization in the AdS / CFT correspondence*, Commun.Math.Phys. **217** (2001) 595–622, [hep-th/0002230].

[104] T. Andrade and D. Marolf, *AdS/CFT beyond the unitarity bound*, JHEP **1201** (2012) 049, [arXiv:1105.6337].

[105] G. Compere and D. Marolf, *Setting the boundary free in AdS/CFT*, Class.Quant.Grav. **25** (2008) 195014, [arXiv:0805.1902].

[106] A. Buchel, S. L. Liebling, and L. Lehner, *Boson stars in AdS spacetime*, Phys.Rev. **D87** (2013), no. 12 123006, [arXiv:1304.4166].

[107] O. J. Dias, G. T. Horowitz, D. Marolf, and J. E. Santos, *On the Nonlinear Stability of Asymptotically Anti-de Sitter Solutions*, Class.Quant.Grav. **29** (2012) 235019, [arXiv:1208.5772].

[108] M. Maliborski and A. Rostworowski, *Time-Periodic Solutions in an Einstein AdSMassless-Scalar-Field System*, Phys.Rev.Lett. **111** (2013) 051102, [arXiv:1303.3186].

[109] A. Adams, P. M. Chesler, and H. Liu, *Holographic turbulence*, Phys.Rev.Lett. **112** (2014), no. 15 151602, [arXiv:1307.7267].

[110] F. Carrasco, L. Lehner, R. C. Myers, O. Reula, and A. Singh, *Turbulent flows for relativistic conformal fluids in 2+1 dimensions*, Phys.Rev. **D86** (2012) 126006, [arXiv:1210.6702].

[111] S. R. Green, F. Carrasco, and L. Lehner, *Holographic Path to the Turbulent Side of Gravity*, Phys.Rev. **X4** (2014), no. 1 011001, [arXiv:1309.7940].

[112] T. Regge and J. A. Wheeler, *Stability of a Schwarzschild singularity*, Phys.Rev. **108** (1957) 1063–1069.

[113] F. J. Zerilli, *Effective potential for even parity Regge-Wheeler gravitational perturbation equations*, Phys.Rev.Lett. **24** (1970) 737–738.

[114] S. Teukolsky, *Rotating black holes - separable wave equations for gravitational and electromagnetic perturbations*, Phys.Rev.Lett. **29** (1972) 1114–1118.

[115] . J. Dias and J. E. Santos, *Boundary Conditions for Kerr-AdS Perturbations*, JHEP **1310** (2013) 156, [arXiv:1302.1580].

[116] V. Cardoso and J. P. Lemos, *Quasinormal modes of Schwarzschild anti-de Sitter black holes: Electromagnetic and gravitational perturbations*, Phys.Rev. **D64** (2001) 084017, [gr-qc/0105103].

[117] E. Berti and K. Kokkotas, *Quasinormal modes of Reissner-Nordstrom-anti-de Sitter black holes: Scalar, electromagnetic and gravitational perturbations*, Phys.Rev. **D67** (2003) 064020, [gr-qc/0301052].

[118] J. Natario and R. Schiappa, *On the classification of asymptotic quasinormal frequencies for d-dimensional black holes and quantum gravity*, Adv.Theor.Math.Phys. **8** (2004) 1001–1131, [hep-th/0411267].

[119] M. Giammatteo and I. G. Moss, *Gravitational quasinormal modes for Kerr anti-de Sitter black holes*, Class.Quant.Grav. **22** (2005) 1803–1824, [gr-qc/0502046].

[120] V. Cardoso, O. J. Dias, and S. Yoshida, *Classical instability of Kerr-AdS black holes and the issue of final state*, Phys.Rev. **D74** (2006) 044008, [hep-th/0607162].

[121] S. Hawking, *Black holes in general relativity*, Commun.Math.Phys. **25** (1972) 152–166.

[122] S. Hollands, A. Ishibashi, and R. M. Wald, *A Higher dimensional stationary rotating black hole must be axisymmetric*, Commun.Math.Phys. **271** (2007) 699–722, [gr-qc/0605106].

[123] V. Moncrief and J. Isenberg, *Symmetries of Higher Dimensional Black Holes*, Class.Quant.Grav. **25** (2008) 195015, [arXiv:0805.1451].

[124] O. J. Dias, G. T. Horowitz, and J. E. Santos, *Black holes with only one Killing field*, JHEP **1107** (2011) 115, [arXiv:1105.4167].

[125] B. Carter, *Hamilton-Jacobi and Schrodinger separable solutions of Einstein's equations*, Commun.Math.Phys. **10** (1968) 280.

[126] C. M. Chambers and I. G. Moss, *Stability of the Cauchy horizon in Kerr-de Sitter space-times*, Class.Quant.Grav. **11** (1994) 1035–1054, [gr-qc/9404015].

[127] M. M. Caldarelli, G. Cognola, and D. Klemm, *Thermodynamics of Kerr-Newman-AdS black holes and conformal field theories*, Class.Quant.Grav. **17** (2000) 399–420, [hep-th/9908022].

[128] G. Gibbons, M. Perry, and C. Pope, *The First law of thermodynamics for Kerr-anti-de Sitter black holes*, Class.Quant.Grav. **22** (2005) 1503–1526, [hep-th/0408217].

[129] O. J. Dias, R. Monteiro, H. S. Reall, and J. E. Santos, *A Scalar field condensation instability of rotating anti-de Sitter black holes*, JHEP **1011** (2010) 036, [arXiv:1007.3745].

[130] R. M. Wald, *On perturbations of a kerr black hole*, Journal of Mathematical Physics **14** (1973), no. 10 1453–1461.

[131] N. Uchikata, S. Yoshida, and T. Futamase, *Scalar perturbations of Kerr-AdS black holes*, Phys.Rev. **D80** (2009) 084020.

[132] V. Cardoso, R. Konoplya, and J. P. Lemos, *Quasinormal frequencies of Schwarzschild black holes in anti-de Sitter space-times: A Complete study on the asymptotic behavior*, Phys.Rev. **D68** (2003) 044024, [gr-qc/0305037].

[133] L. Freidel, *Gravitational Energy, Local Holography and Non-equilibrium Thermodynamics*, Class.Quant.Grav. **32** (2015), no. 5 055005, [arXiv:1312.1538].

[134] C. Li and J. Lucietti, *Three-dimensional black holes and descendants*, Phys.Lett. **B738** (2014) 48–4, [arXiv:1312.2626].

[135] P. Basu, J. Bhattacharya, S. Bhattacharyya, R. Loganayagam, S. Minwalla, et. al., *Small Hairy Black Holes in Global AdS Spacetime*, JHEP **1010** (2010) 045, [arXiv:1003.3232].

[136] S. Bhattacharyya, S. Minwalla, and K. Papadodimas, *Small Hairy Black Holes in $AdS_5 x S^5$*, JHEP **1111** (2011) 035, [arXiv:1005.1287].

[137] O. J. Dias, P. Figueras, S. Minwalla, P. Mitra, R. Monteiro, et. al., *Hairy black holes and solitons in global AdS_5*, JHEP **1208** (2012) 117, [arXiv:1112.4447].

[138] S. Bhattacharyya, V. E. Hubeny, S. Minwalla, and M. Rangamani, *Nonlinear Fluid Dynamics from Gravity*, JHEP **0802** (2008) 045, [arXiv:0712.2456].

[139] V. E. Hubeny and M. Rangamani, *A Holographic view on physics out of equilibrium*, Adv.High Energy Phys. **2010** (2010) 297916, [arXiv:1006.3675].

[140] P. Romatschke, *Relativistic Viscous Fluid Dynamics and Non-Equilibrium Entropy*, Class.Quant.Grav. **27** (2010) 025006, [arXiv:0906.4787].

[141] G. Policastro, D. T. Son, and A. O. Starinets, *The Shear viscosity of strongly coupled N=4 supersymmetric Yang-Mills plasma*, Phys.Rev.Lett. **87** (2001) 081601, [hep-th/0104066].

[142] S. Hawking, C. Hunter, and M. Taylor, *Rotation and the AdS / CFT correspondence*, Phys.Rev. **D59** (1999) 064005, [hep-th/9811056].

[143] G. Gibbons, H. Lu, D. N. Page, and C. Pope, *Rotating black holes in higher dimensions with a cosmological constant*, Phys.Rev.Lett. **93** (2004) 171102, [hep-th/0409155].

[144] O. J. Dias, P. Figueras, R. Monteiro, and J. E. Santos, *Ultraspinning instability of anti-de Sitter black holes*, JHEP **1012** (2010) 067, [arXiv:1011.0996].

[145] S. A. Gentle, M. Rangamani, and B. Withers, *A Soliton Menagerie in AdS*, JHEP **1205** (2012) 106, [arXiv:1112.3979].

[146] O. J. Dias, R. Emparan, and A. Maccarrone, *Microscopic theory of black hole superradiance*, Phys.Rev. **D77** (2008) 064018, [arXiv:0712.0791].

[147] E. Berti, V. Cardoso, and M. Casals, *Eigenvalues and eigenfunctions of spin-weighted spheroidal harmonics in four and higher dimensions*, Phys.Rev. **D73** (2006) 024013, [gr-qc/0511111].

[148] H. Onozawa, T. Mishima, T. Okamura, and H. Ishihara, *Quasinormal modes of maximally charged black holes*, Phys.Rev. **D53** (1996) 7033–7040, [gr-qc/9603021].

[149] D. N. Page, *Particle Emission Rates from a Black Hole. 2. Massless Particles from a Rotating Hole*, Phys.Rev. **D14** (1976) 3260–3273.

[150] S. Teukolsky and W. Press, *Perturbations of a rotating black hole. III - Interaction of the hole with gravitational and electromagnet ic radiation*, Astrophys.J. **193** (1974) 443–461.

[151] O. J. Dias, J. E. Santos, and M. Stein, *Kerr-AdS and its Near-horizon Geometry: Perturbations and the Kerr/CFT Correspondence*, JHEP **1210** (2012) 182, [arXiv:1208.3322].

[152] O. J. Dias, H. S. Reall, and J. E. Santos, *Kerr-CFT and gravitational perturbations*, JHEP **0908** (2009) 101, [arXiv:0906.2380].

[153] C. Warnick, *The Massive wave equation in asymptotically AdS spacetimes*, Commun.Math.Phys. **321** (2013) 85–111, [arXiv:1202.3445].

[154] C. M. Warnick, *On quasinormal modes of asymptotically anti-de Sitter black holes*, Commun.Math.Phys. **333** (2015), no. 2 959–1035, [arXiv:1306.5760].

[155] A. Starobinskii, *Amplification of waves during reflection from a rotating black hole*, Zh. Eksp. Teor. Fiz **64** (1973) 48.

[156] W. Unruh, *Absorption Cross-Section of Small Black Holes*, Phys.Rev. **D14** (1976) 3251–3259.

[157] S. L. Detweiler, *KLEIN-GORDON EQUATION AND ROTATING BLACK HOLES*, Phys.Rev. **D22** (1980) 2323–2326.

[158] J. M. Maldacena and A. Strominger, *Universal low-energy dynamics for rotating black holes*, Phys.Rev. **D56** (1997) 4975–4983, [hep-th/9702015].

[159] V. Cardoso, O. J. Dias, J. P. Lemos, and S. Yoshida, *The Black hole bomb and superradiant instabilities*, Phys.Rev. **D70** (2004) 044039, [hep-th/0404096].

[160] O. J. Dias, *Superradiant instability of large radius doubly spinning black rings*, Phys.Rev. **D73** (2006) 124035, [hep-th/0602064].

[161] R. A. Breuer, M. P. Ryan, and S. Waller, *Some properties of spin-weighted spheroidal harmonics*, Proceedings of the Royal Society of London. A. Mathematical and Physical Sciences **358** (1977), no. 1692 71–86.

[162] P. Pani, V. Cardoso, L. Gualtieri, E. Berti, and A. Ishibashi, *Perturbations of slowly rotating black holes: massive vector fields in the Kerr metric*, Phys.Rev. **D86** (2012) 104017, [arXiv:1209.0773].

[163] G. Gibbons, *ASPECTS OF SUPERGRAVITY THEORIES*, .

[164] J. M. Maldacena and C. Nunez, *Supergravity description of field theories on curved manifolds and a no go theorem*, Int.J.Mod.Phys. **A16** (2001) 822–855, [hep-th/0007018].

[165] D. Baumann and L. McAllister, *Inflation and String Theory*, arXiv:1404.2601.

[166] S. Kachru, R. Kallosh, A. D. Linde, and S. P. Trivedi, *De Sitter vacua in string theory*, Phys.Rev. **D68** (2003) 046005, [hep-th/0301240].

[167] S. B. Giddings, S. Kachru, and J. Polchinski, *Hierarchies from fluxes in string compactifications*, Phys.Rev. **D66** (2002) 106006, [hep-th/0105097].

[168] S. Kachru, J. Pearson, and H. L. Verlinde, *Brane / flux annihilation and the string dual of a nonsupersymmetric field theory*, JHEP **0206** (2002) 021, [hep-th/0112197].

[169] G. T. Horowitz and R. C. Myers, *The value of singularities*, Gen.Rel.Grav. **27** (1995) 915–919, [gr-qc/9503062].

[170] S. S. Gubser, *Curvature singularities: The Good, the bad, and the naked*, Adv.Theor.Math.Phys. **4** (2000) 679–745, [hep-th/0002160].

[171] D. Kastor and J. H. Traschen, *Horizons inside classical lumps*, Phys.Rev. **D46** (1992) 5399–5403, [hep-th/9207070].

[172] R. Bartnik and J. Mckinnon, *Particle - Like Solutions of the Einstein Yang-Mills Equations*, Phys.Rev.Lett. **61** (1988) 141–144.

[173] M. Volkov and D. Galtsov, *NonAbelian Einstein Yang-Mills black holes*, JETP Lett. **50** (1989) 346–350.

[174] P. Bizon, *Colored black holes*, Phys.Rev.Lett. **64** (1990) 2844–2847.

[175] K.-M. Lee, V. Nair, and E. J. Weinberg, *Black holes in magnetic monopoles*, Phys.Rev. **D45** (1992) 2751–2761, [hep-th/9112008].

[176] M. S. Volkov and D. V. Gal'tsov, *Gravitating nonAbelian solitons and black holes with Yang-Mills fields*, Phys.Rept. **319** (1999) 1–83, [hep-th/9810070].

[177] C. A. R. Herdeiro and E. Radu, *Kerr black holes with scalar hair*, Phys.Rev.Lett. **112** (2014) 221101, [arXiv:1403.2757].

[178] I. Pena and D. Sudarsky, *Do collapsed boson stars result in new types of black holes?*, Class.Quant.Grav. **14** (1997) 3131–3134.

[179] M. Melvin, *Pure magnetic and electric geons*, Phys.Lett. **8** (1964) 65–70.

[180] F. J. Ernst, *Black holes in a magnetic universe*, J. Math. Phys. **17** (1976) 54.

[181] M. Gutperle and A. Strominger, *Fluxbranes in string theory*, JHEP **0106** (2001) 035, [hep-th/0104136].

[182] R. Emparan, S. Ohashi, and T. Shiromizu, *No-dipole-hair theorem for higher-dimensional static black holes*, Phys.Rev. **D82** (2010) 084032, [arXiv:1007.3847].

[183] M. Ortaggio, *Higher dimensional black holes in external magnetic fields*, JHEP **0505** (2005) 048, [gr-qc/0410048].

[184] G. T. Horowitz and K. Maeda, *Inhomogeneous near extremal black branes*, Phys.Rev. **D65** (2002) 104028, [hep-th/0201241].

[185] D. Garfinkle, G. T. Horowitz, and A. Strominger, *Charged black holes in string theory*, Phys.Rev. **D43** (1991) 3140.

[186] G. Gibbons and K.-i. Maeda, *Black Holes and Membranes in Higher Dimensional Theories with Dilaton Fields*, Nucl.Phys. **B298** (1988) 741.

[187] F. Dowker, J. P. Gauntlett, G. W. Gibbons, and G. T. Horowitz, *The Decay of magnetic fields in Kaluza-Klein theory*, Phys.Rev. **D52** (1995) 6929–6940, [hep-th/9507143].

[188] P. Saffin, *Gravitating fluxbranes*, Phys.Rev. **D64** (2001) 024014, [gr-qc/0104014].

[189] M. S. Costa, C. A. Herdeiro, and L. Cornalba, *Fluxbranes and the dielectric effect in string theory*, Nucl.Phys. **B619** (2001) 155–190, [hep-th/0105023].

[190] G. T. Horowitz, N. Iqbal, and J. E. Santos, *Simple holographic model of nonlinear conductivity*, Phys.Rev. **D88** (2013), no. 12 126002, [arXiv:1309.5088].

[191] N. Iizuka, A. Ishibashi, and K. Maeda, *Can a stationary Bianchi black brane have momentum along the direction with no translational symmetry?*, JHEP **1406** (2014) 064, [arXiv:1403.0752].

[192] M. Headrick, S. Kitchen, and T. Wiseman, *A New approach to static numerical relativity, and its application to Kaluza-Klein black holes*, Class.Quant.Grav. **27** (2010) 035002, [arXiv:0905.1822].

[193] U. Danielsson, S. Massai, and T. Van Riet, *SUSY-breaking in warped throats, to appear*, .

[194] R. Argurio, M. Bertolini, S. Franco, and S. Kachru, *Meta-stable vacua and D-branes at the conifold*, JHEP **0706** (2007) 017, [hep-th/0703236].

[195] R. Argurio, M. Bertolini, S. Franco, and S. Kachru, *Gauge/gravity duality and meta-stable dynamical supersymmetry breaking*, JHEP **0701** (2007) 083, [hep-th/0610212].

[196] I. Bena, A. Puhm, and B. Vercnocke, *Metastable Supertubes and non-extremal Black Hole Microstates*, JHEP **1204** (2012) 100, [arXiv:1109.5180].

[197] I. Bena, A. Puhm, and B. Vercnocke, *Non-extremal Black Hole Microstates: Fuzzballs of Fire or Fuzzballs of Fuzz ?*, JHEP **1212** (2012) 014, [arXiv:1208.3468].

[198] P. McGuirk, G. Shiu, and Y. Sumitomo, *Non-supersymmetric infrared perturbations to the warped deformed conifold*, Nucl.Phys. **B842** (2011) 383–413, [arXiv:0910.4581].

[199] I. Bena, M. Grana, and N. Halmagyi, *On the Existence of Meta-stable Vacua in Klebanov-Strassler*, JHEP **1009** (2010) 087, [arXiv:0912.3519].

[200] I. Bena, G. Giecold, M. Grana, N. Halmagyi, and S. Massai, *On Metastable Vacua and the Warped Deformed Conifold: Analytic Results*, Class.Quant.Grav. **30** (2013) 015003, [arXiv:1102.2403].

[201] S. Massai, *A Comment on anti-brane singularities in warped throats*, arXiv:1202.3789.

[202] I. Bena, M. Grana, S. Kuperstein, and S. Massai, *Anti-D3 Branes: Singular to the bitter end*, Phys.Rev. **D87** (2013), no. 10 106010, [arXiv:1206.6369].

[203] J. Blaback, U. H. Danielsson, D. Junghans, T. Van Riet, T. Wrase, et. al., *The problematic backreaction of SUSY-breaking branes*, JHEP **1108** (2011) 105, [arXiv:1105.4879].

[204] J. Blaback, U. H. Danielsson, D. Junghans, T. Van Riet, T. Wrase, et. al., *(Anti-)Brane backreaction beyond perturbation theory*, JHEP **1202** (2012) 025, [arXiv:1111.2605].

[205] F. F. Gautason, D. Junghans, and M. Zagermann, *Cosmological Constant, Near Brane Behavior and Singularities*, JHEP **1309** (2013) 123, [arXiv:1301.5647].

[206] J. Blaback, U. Danielsson, D. Junghans, T. Van Riet, and S. Vargas, *Localised anti-branes in non-compact throats at zero and finite T*, arXiv:1409.0534.

[207] R. C. Myers, *Dielectric branes*, JHEP **9912** (1999) 022, [hep-th/9910053].

[208] J. Polchinski and M. J. Strassler, *The String dual of a confining four-dimensional gauge theory*, hep-th/0003136.

[209] I. R. Klebanov and A. A. Tseytlin, *Gravity duals of supersymmetric SU(N) x SU(N+M) gauge theories*, Nucl.Phys. **B578** (2000) 123–138, [hep-th/0002159].

[210] I. Bena, D. Junghans, S. Kuperstein, T. Van Riet, T. Wrase, et. al., *Persistent anti-brane singularities*, JHEP **1210** (2012) 078, [arXiv:1205.1798].

[211] I. Bena, M. Grana, S. Kuperstein, and S. Massai, *Polchinski-Strassler does not uplift Klebanov-Strassler*, JHEP **1309** (2013) 142, [arXiv:1212.4828].

[212] I. Bena, M. Grana, S. Kuperstein, and S. Massai, *Tachyonic Anti-M2 Branes*, JHEP **1406** (2014) 173, [arXiv:1402.2294].

[213] I. Bena, M. Grana, S. Kuperstein, and S. Massai, *Giant Tachyons in the Landscape*, arXiv:1410.7776.

[214] D. Junghans, D. Schmidt, and M. Zagermann, *Curvature-induced Resolution of Anti-brane Singularities*, JHEP **1410** (2014) 34, [arXiv:1402.6040].

[215] I. Bena, A. Buchel, and O. J. Dias, *Horizons cannot save the Landscape*, Phys.Rev. **D87** (2013), no. 6 063012, [arXiv:1212.5162].

[216] I. Bena, J. Blaback, U. Danielsson, and T. Van Riet, *Antibranes cannot become black*, Phys.Rev. **D87** (2013), no. 10 104023, [arXiv:1301.7071].

[217] J. Blaback, U. H. Danielsson, and T. Van Riet, *Resolving anti-brane singularities through time-dependence*, JHEP **1302** (2013) 061, [arXiv:1202.1132].

[218] U. H. Danielsson and T. Van Riet, *Fatal attraction: more on decaying anti-branes*, arXiv:1410.8476.

[219] M. Cvetic, G. Gibbons, H. Lu, and C. Pope, *Ricci flat metrics, harmonic forms and brane resolutions*, Commun.Math.Phys. **232** (2003) 457–500, [hep-th/0012011].

[220] B. Michel, E. Mintun, J. Polchinski, A. Puhm, and P. Saad, *Remarks on brane and antibrane dynamics*, arXiv:1412.5702.

[221] B. Janssen, P. Meessen, and T. Ortin, *The D8-brane tied up: String and brane solutions in massive type IIA supergravity*, Phys.Lett. **B453** (1999) 229–236, [hep-th/9901078].

[222] G. T. Horowitz and V. E. Hubeny, *Note on small black holes in AdS(p) x S**q*, JHEP **0006** (2000) 031, [hep-th/0005288].

[223] D. Z. Freedman and J. A. Minahan, *Finite temperature effects in the supergravity dual of the N=1* gauge theory*, JHEP **0101** (2001) 036, [hep-th/0007250].

[224] F. Zamora, *Nonsupersymmetric SO(3) invariant deformations of N=1* vacua and their dual string theory description*, JHEP **0012** (2000) 021, [hep-th/0007082].

[225] O. DeWolfe, S. Kachru, and H. L. Verlinde, *The Giant inflaton*, JHEP **0405** (2004) 017, [hep-th/0403123].

[226] A. Dymarsky, *On gravity dual of a metastable vacuum in Klebanov-Strassler theory*, JHEP **1105** (2011) 053, [arXiv:1102.1734].

[227] A. Dymarsky and S. Massai, *Uplifting the baryonic branch: a test for backreacting anti-D3-branes*, JHEP **1411** (2014) 034, [arXiv:1310.0015].

[228] I. Bena, *The M theory dual of a three-dimensional theory with reduced supersymmetry*, Phys.Rev. **D62** (2000) 126006, [hep-th/0004142].

[229] I. R. Klebanov and S. S. Pufu, *M-Branes and Metastable States*, JHEP **1108** (2011) 035, [arXiv:1006.3587].

[230] G. T. Horowitz and T. Wiseman, *General black holes in Kaluza-Klein theory*, arXiv:1107.5563.

[231] M. Cvetic, H. Lu, and C. Pope, *Penrose limits, PP waves and deformed M2 branes*, Phys.Rev. **D69** (2004) 046003, [hep-th/0203082].

[232] G. T. Horowitz and A. R. Steif, *Strings in Strong Gravitational Fields*, Phys.Rev. **D42** (1990) 1950–1959.